Coupled Electron Proton Transfer in Biological Redox Substrates

Christopher J. Gagliardi

A dissertation submitted to the faculty of the University of North Carolina at Chapel Hill in partial fulfillment of the requirements for the degree of Doctor of Philosophy in the Department of Chemistry

Chapel Hill
2012

Approved By:

Dr. Thomas J. Meyer

Dr. H. Holden Thorp

Dr. Gary Pielak

Dr. Cynthia Schauer

Dr. Royce Murray

ABSTRACT

Christopher J. Gagliardi: Coupled Electron Proton Transfer in Biological Redox Substrates
(Under the direction of H. Holden Thorp and Thomas J. Meyer)

The amino acids tyrosine, tryptophan and cysteine are used to carryout electron transfer within enzymes and proteins. The chemistry and oxidation mechanisms vary considerably between these molecules. Proton coupled electron transfer (PCET), where electrons and protons travel in sequence, or in concert is used by these amino acids in both proteins as well as free in aqueous solution in order to minimize energy expenditure and prevent build up of high-energy intermediates. The oxidation of these amino acids by a series of metal $M(bpy)_3^{3+}$ M = Os, Fe, Ru complexes in aqueous solution at ITO electrodes as well as spectroscopically in stopped-flow mixing studies is reported. A common mechanism involving the pre-association of a base to form a hydrogen bound adduct prior to electron transfer was observed in all cases. Each of the three amino acids displayed various degrees of hydrogen bonding with bases, linked to their pK_a values (cysteine 8.2, tyrosine, 10.1 and tryptophan 16.0). Base assisted oxidation pathways occur through two competing mechanisms; either proton transfer to a base followed electron transfer (PT-ET), or concerted electron proton transfer (EPT). The kinetics of these pathways as well as additional pathways such as outer-sphere electron transfer were studied using electrochemical, and spectroscopic methods, giving rate information for each pathway as well as kinetic isotope data which provided insight into how these

molecules behave in enzymatic electron transfer reactions. We have found that for PCET reactions the driving force is the dominate factor dictating reactivity and can be influenced by both the pK_a of the proton acceptor and the oxidation potential of the $M(bpy)_3^{III/II}$ couple. This insight has provided a better understanding of how tyrosine, cysteine, and tryptophan are used to mediate biological electron transfer and allowed us to observe commonalities in redox mechanisms with respect to common bases and oxidants in biological PCET reactions.

Acknowledgements

First and foremost, thank you Holden and Dr. Meyer for taking me on as a graduate student. I knew when I told you I was a Student of Cliff's, that it may not have bode well for me, but you took a chance anyway. Holden, I would also like to specifically thank you for taking me as a student as your administrative career was taking off, I never would have imagined being the last graduate student of the Chancellor. I hope I have been able to keep science in your busy life at an interesting level. I cannot thank you enough for the guidance you have given my research and me when I needed it the most. Dr. Meyer, thank you for pushing me when I needed it, and making me question myself as a scientist. Without that kind of motivation I never would have made it to the finish line. As someone who entered graduate school as a synthetic inorganic chemist, I never would of imagined that kineticist, electrochemist and physical chemist would be the first things to come to my mind when describing my time here at UNC.

I owe an immense debt of gratitude to my Alma Mater Roger Williams University, and above all my mentor at RWU, Professor Cliff Timpson, who is also another graduate of the Meyer group. Without you I never would have found my love for chemistry. Without your mentorship, kind words, tough words and above all friendship, I never would have found myself in the position that I am in today. From someone who went from failing chemistry twice in high school, to defending a Ph.D in chemistry, I owe this to you.

I would also like to thank Chrissie Murphy, or when I met her, Chrissie Fecenko, without whose guidance and mentorship during my first two years of graduate school I never would have stuck with or even come close to understanding my projects. Your help, guidance and translation during meetings were more than I could have ever hoped for. It was more of a help than you can possibly imagine, Thank you. I would also like to thank Robert Binstead, whom without I would have been lost hopelessly trying to figure out how tryptophan oxidation worked. With your help, not only did this project move forward, but turned into a wonderful publication. Thank you so very much for all of your time and patience. I would also like to thank all of the other members of the Meyer group, especially Jonah Jurss, one of my best friends and collaborators during my time here, David Weinberg and Javier Concepcion who helped me countless times studying for my orals and for many other scientific questions and pursuits, including PCET review, which I am so thankful is over. Finally, Aaron Vannucci, probably the best lab mate someone could have, it is not easy spending countless 10-hour days back to back to someone and still have room for a friendship, thank you for yours.

Lastly, I would like to thank my family and my friends for the loving support you have given me in embarking on this endeavor, never once did I get a word of discouragement. To my wife, who was Stefanie Haas when I started graduate school, and is now Stefanie Gagliardi as I end it, your patience and comforting companionship has kept me waking up day after day to pursue knowledge. This would have been an intolerable herculean task without you by my side. Finally to my mother and father, I am sorry high school did not workout as it perhaps would have for an ideal son and student, but I hope that coming out on this end of the tunnel, you are proud of the change that I

have undergone. Thank you for your acceptance of my decisions, even if I didn't really know where I was going or why. I guess in the end, everything really works out.

And finally, for John, Henry and Clara.

Table of Contents

List of Figures

Chapter 1: Introduction to Proton-Coupled Electron Transfer

Chapter 2: Surface Activation of Electrocatalysis at Oxide Electrodes. Concerted Electron-Proton Transfer (EPT)

Chapter 3: Concerted Electron–Proton Transfer (EPT) in the Oxidation of Tryptophan with Hydroxide as a Base

Chapter 4: The Role of Concerted Electron–Proton Transfer in the Oxidation of Cysteine

List of Tables

Chapter 1: Introduction to Proton-Coupled Electron Transfer

Chapter 2: Surface Activation of Electrocatalysis at Oxide Electrodes. Concerted Electron-Proton Transfer

Chapter 3: Concerted Electron–Proton Transfer (EPT) in the Oxidation of Tryptophan with Hydroxide as a Base

Chapter 4: The Role of Concerted Electron-Proton Transfer in the Oxidation of Cysteine

List of Symbols and Abbreviations

$[TyrOH]_T$	total concentration of tyrosine
$[CysSH]_T$	total concentration of cysteine
°C	degrees Celsius
α	symmetry factor
ΔE	change in reduction potential
ΔG_{EPT}	free energy change for electron proton transfer
ΔG_{ET}	free energy change for electron transfer
ΔG_{PT}	free energy change for proton transfer
$\Delta Q_{\mu,\nu}$	change in equilibrium normal coordinate
Γ	surface coverage
Γ_o	maximum surface coverage
ε	molar absorptivity
λ	reorganizational energy
λ_{max}	maximum absorbance
μ	initial state
μM	micromolar
ν	scan rate
ν	vibrational mode
ν	final state
π	pi (3.1415926535898)
ϱ_{fc}	Frank-Condon density of states term
χ_D	mole fraction deuterium
ψ	wave function
ψ_μ	electronic wave function initial state
ψ_ν	electronic wave function final state
ϕ_μ	proton wave function initial state
ϕ_ν	proton wave function final state
ω	angular frequency
Ω	resistance
4-MeArOH	4-methylphenol

A	ampere
A	electrode area
A	absorbance
A^-/A	acceptor
A_∞	absorbance at time infinity
Abs	absorbance
ADP	adenosine diphosphate
Ag/AgCl	silver/silver chloride reference
ATP	adenosine triphosphate
B^-	base form of buffer
bpy	2,2′-bipyridine
C	coulomb
ClO_4^-	perchlorate anion
CoQ_{10}	ubiquinone
CV	cyclic voltammograms
CysSH	cysteine (protonated form)
$CysS^-$	cysteine (deprotonated anion)
$CysS^\bullet$	cysteine (deprotonated radical)
$CysS^{\bullet+}$	cysteine (protonated radical cation)
CysSH---B	cysteine (hydrogen bound base adduct)
d	distance
D^+	deuteron
D^+/D	donor
D_2O	deuterium oxide
DCl	deuterochloric acid
dmb	4,4′-dimethyl-2,2′-bipyridine
DNA	deoxyribonucleic acid
D_{op}	optical frequency dielectric constant
D_s	zero frequency dielectric constant
DPA	dipicolinic acid (pyridine-2,6-dicarboxylic acid)
E	electrode potential

e^-	electron
$E°'$	formal potential
$E_{1/2}$	midpoint potential
E_P	peak potential
EPT	electron proton Transfer
ET-PT	step-wise electron transfer followed by proton transfer
eV	electron volt
F	Faraday constant
FAD	flavin adenine dinucleotide (oxidized)
$FADH^-$	flavin adenine dinucleotide (mono protonated anion)
$FADH^{\bullet-}$	flavin adenine dinucleotide (protonated radical anion)
$FADH_2$	flavin adenine dinucleotide (reduced)
Fe	iron
FEP	fluorinated ethylene propylene
f_j	force constant
FTO	fluorine doped tin oxide
H	Hamiltonian
H^+	proton
H_{190}	histidine 190 in photosystem II
$H_2PO_4^-$	monobasic hydrogen phosphate
H_3O^+	hydronium ion
HB+	acid form of buffer
HCl	hydrochloric acid
$HClO_4$	perchloric acid
His	histidine
HPO_4^{2-}	dibasic hydrogen phosphate
i	electrode current
i_{cat}	catalytic peak current
In	indium
i_p	peak electrode current
ITO	indium doped tin oxide

K_A	acid disassociation constant
k_B	Boltzmann constant
k_D	rate constant for diffusion
k_{EPT}	electron proton transfer rate constant
KIE	kinetic isotope effect
k_{obs}	observed rate constant
k_s	heterogeneous electron transfer rate constant
LiOH	lithium hydroxide
$M_{\mu\nu}$	initial and final state mixing matrix element
M	molar
$M(bpy)_3^{III/II}$	metal tris(2,2′-bypyridine) complex, couple
MeCN	acetonitrile
M_j	reduced mass
MLCT	metal-ligand charge transfer
mM	millimolar
MS-EPT	multi-site electron proton transfer
MTHF	5,10- methylenetetrahydrofolylpolyglutamate
N	number of replicates
n	number of electrons
N_A	Avogadro's number
NAceTrp	*N*-acetyl-tryptophan
NAceTyr	*N*-acetyl-tyrosine
NaCl	sodium chloride
NAD^+	nicotinamide adenine dinucleotide (oxidized)
$NADP^+$	nicotinamide adenine dinucleotide phosphate (oxidized)
NADH	nicotinamide adenine dinucleotide (reduced)
NADPH	nicotinamide adenine dinucleotide phosphate (reduced)
NaOD	sodium deuteroxide
NaOH	sodium hydroxide
NHE	normal hydrogen electrode
AcO^-	acetate

AcOH	acetic acid
OH^-	hydroxide anion
Os	osmium
P680	photosystem II primary electron donor
P_{680^+}	oxidized form of P680
PCET	proton coupled electron transfer
pD	-Log[D^+]
pH	-Log[H^+]
P_i	inorganic phosphate
pK_a	-Log[K_a]
PMT	photomultiplier tube
PSII	photosystem II
PT-ET	stepwise proton transfer electron transfer
Q	integrated peak area of the oxidative peak
RNR	ribonucleotide reductase
Ru	ruthenium
s	second
S_j	Huang-Rhys factor
SLO	soybean lipoxygenase
SVD	singular value decomposition
T	temperature
Tris	tris base
Trp	tryptophan
TrpNH	tryptophan
$TrpN^-$	deprotonated tryptophan anion
$TrpN^\bullet$	deprotonated tryptophan radical
$TrpNH^{\bullet+}$	tryptophan radical cation
TrpNH---B	tryptophan hydrogen bound base adduct
TyrOH	tyrosine
$TyrO^-$	tyrosine anion
$TyrOH^{\bullet+}$	tyrosine radical cation

$TyrO^{\bullet}$	deprotonated tyrosine radical
TyrOH---B	tyrosine hydrogen bound base adduct
UV	ultraviolet
V	volts
V_{ET}	electron transfer matrix element
Vis	visible
$V_{\mu\nu}$	energy from initial and final state mixing
W	tryptophan amino acid residue
XRD	X-ray diffraction
Y	tyrosine amino acid residue
Y_z	tyrosine 161 in PSII

Chapter 1

Introduction to Biological Redox Substrates and Proton Coupled Electron Transfer[a]

1.1 Introduction: Almost all process, whether chemical or biological, that produce and use energy or move electrons employ proton-coupled electron transfer (PCET) as a means to do so. PCET reactions involve the coupled transfer of protons and electrons and are critical for many energy conversion processes including natural and artificial photosynthesis, catalytic water oxidation and production of molecular hydrogen as well as many enzymatic reactions. Whether it is electron transfer pathways through photosystem II to produce oxygen and carbohydrates from sunlight, water and CO_2 or in molecular water oxidation catalysts, proton-coupled electron transfer is utilized for the purpose of charge leveling in the buildup of oxidative equivalents and avoiding high energy intermediates that can be biologically damaging.

1.2 Biological Redox Cofactors: In biology, electrons are the energy currency of all living things. Shuttling these oxidative and reductive equivalents from site to site allows for living things to grow as well as defend and heal themselves. Whether this energy comes from the sun or from food, biological redox cofactors form the road upon which these redox equivalents travel, enabling essential chemical reactions.

---

[a] Reproduced in parts with permission from the American Chemical Society; Christopher J. Gagliardi, H. Holden Thorp and Thomas J. Meyer **Proton Coupled Electron Transfer: A Primer**. *J. Chem. Ed.* **2012**, *In Preparation*.

Remarkably, the number of biological electron transfer shuttles, whether membrane bound, protein based, or mobile, is relatively few given the immense diversity of life on this planet. From the smallest prokaryotic cyanobacteria, to complex life such as higher mammals, some of the same chemistry is, and to a further extent, the same redox cofactors are utilized to perform a variety of reductive and oxidative chemical reactions. Figure 1 below shows the functional groups of the most common redox cofactors.

Amino Acids:

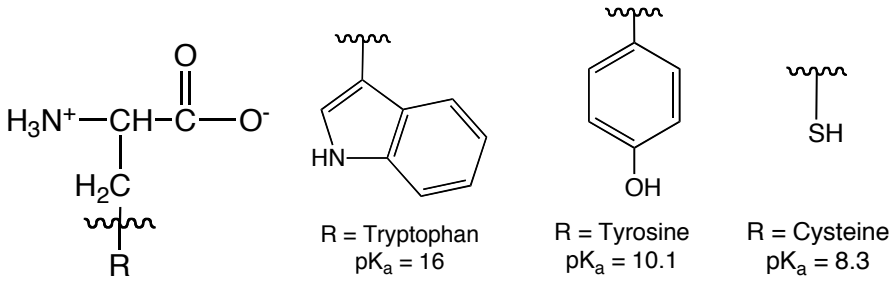

Moble Organic Cofactors:

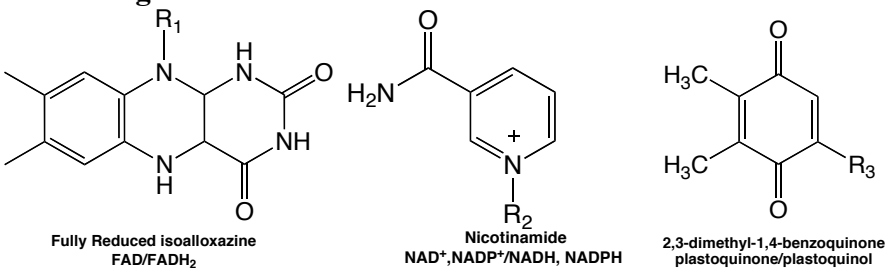

Inorganic Cofactors:

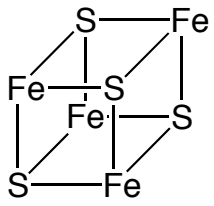

Additional Metal Ion Cofactors:

$Cu^{1+/2+}$ (azurin, cytochrome oxidase)
$Fe^{2+/3+}$ (nitrogenase, hemoglobin)
$Mn^{2+/3+}$ (PSII, arginase)
$Ni^{2+/3+}$ (Ni-Fe hydrogenase, urease)
$Mo^{4+/5+}$ (xanthene oxidase, nitrate reductase)

Figure 1. *Amino acid functional groups* (R), and pK_a values are shown with a zwitterionic backbone. Amino acids are found as electron transfer mediators within proteins. For the *mobile cofactors*, only the functional groups are shown. *Mobile organic cofactors* shuttle electrons and protons between immobile membrane bound proteins as shown in Figure 2. The *inorganic cofactors* play a large role in electron transfer reactions, with Fe-S clusters carrying out electron transfer reactions occurring in the protein subunits of mitochondrial respiration as well as other enzymes such as hydrogenases and photosystem I. In many cases, the active sites of these enzymatic reactions are metal centers, a few of which are also listed.

Proteins are folded chains of amino acids. Three of these amino acids; tyrosine, cysteine and tryptophan mediate enzymatic electron-proton transfer reactions. Photosystem II (PSII) in green plants[1-7], ribonucleotide reductase (RNR),[8-10] DNA photolyase[11,12], superoxide dismutase (SOD)[13,14] and soybean lipoxygenase (SLO)[15-18] have all been highlighted for their utility of a PCET mechanism. Within a protein, these three chemical functionalities - a phenol, an indole and a thiol - perform a wide variety of chemistry, and individually on the molecular level, demonstrate distinctive chemical behavior.[8-10,19-25] This highlights why the residues cannot be used interchangeably and why mutagenesis studies show a dramatic change in the overall functionality of a protein in the absence of even a single residue.[5-7,14]

The role of amino acids in the diverse field of biochemistry is the subject of this work and is further expanded upon below in Section 1.8. This section reviews some examples of amino acids participating in biological PCET reactions. Knowledge in this area, especially on PCET reactions involving the other mobile organic redox cofactors, is still in its adolescence. We have much to gain from further experimentation on how these other cofactors work given their biological ubiquity. A testament to this is the fact that there is a whole classification of proteins called ferredoxins, which contain iron-sulfur clusters. The mobile cofactor, ubiquinone, is named after its own biological prevalence.

All of these cofactors work in concert in biology. The next step in understanding PCET on a macroscopic scale is looking at the interfaces where the different classes of aforementioned cofactors interact. A mobile cofactor is able to pass on its redox equivalent(s) at an interface between the cofactor and the first amino acid, or iron-sulfur cluster in an electron transfer pathway. An elegant example of this can is illustrated in mitochondrial

respiration, shown in Figure 2. Oxidative phosphorylation employs two mobile electron shuttle molecules, Coenzyme Q (CoQ), otherwise known as ubiquinone, and cytochrome *c* (Cyt *c*) as well as iron-sulfur clusters and other metal centers for the transport of electrons through each subunit.

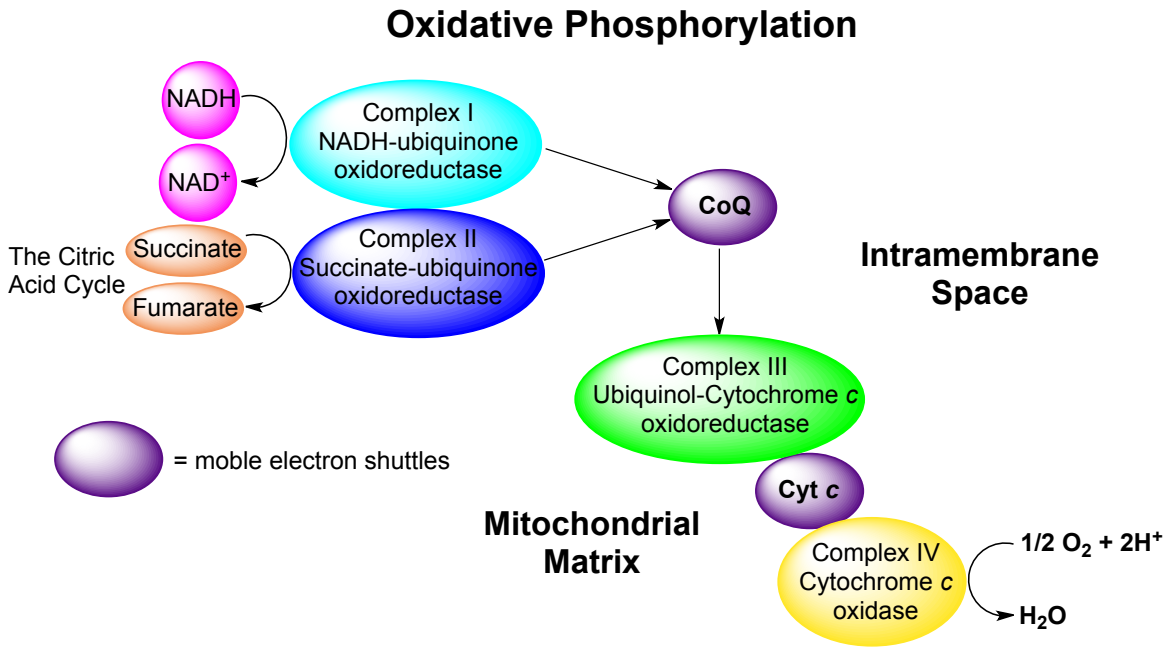

Figure 2. Oxidative phosphorylation in the cellular respiratory chain occurs in the mitochondrial membrane, and consists of over 80 peptides, five enzymatic units (ATP synthase not shown) and produces ATP from the reduction of oxygen to generate energy for cellular function.

1.3 Proton Coupled Electron Transfer: According to the broad definition, proton-coupled electron transfer encompasses any process involving the movement of both electrons and protons.[1,26,27] Within the context of this work, it will refer to a single $1e^-/1H^+$ reaction. PCET is a general classification given to a broad set of electron-proton transfer reaction mechanisms. A PCET reaction can occur through three distinct pathways:

i. Stepwise electron transfer followed by proton transfer (**ET-PT**)

ii. Stepwise proton transfer followed by electron transfer (**PT-ET**)

iii. Concerted electron proton transfer.

Within the context of concerted electron proton transfer there is another sub-set of categorical nomenclature based qualitatively on donor (D) and acceptor (A) orbitals and further defined by quantum mechanics. These are: electron proton transfer (EPT), multi-site electron proton transfer (MS-EPT), hydrogen atom transfer (HAT) and hydride transfer.

a. **EPT** e^-/H^+, different D, A orbitals, same molecule

b. **MS-EPT**, e^-/H^+, different D, A orbitals on separate molecules

c. **HAT,** e^-/H^+, same D, A orbital

d. **Hydride transfer** (simultaneous transfer of $2e^-/1H^+$)

To illustrate some key points in understanding PCET, PSII in green plants will be used as an example with the oxidation of the tyrosine (Tyr161) histidine (His190) pair (Y_z) by the reaction center, photooxidized P_{680}^+. The stepwise pathways PT-ET and ET-PT, involve initial proton or electron transfer. Initial proton transfer (PT) produces the anionic species before being oxidized to the radical and in the case of initial electron transfer (ET), the tyrosine radical cation is produced before losing its proton to become the tyrosine radical, as illustrated in Figure 3. Each of these initial stepwise products are high-energy intermediates that can become damaging even within with the polypeptide architecture of a complex set of proteins such as PSII.

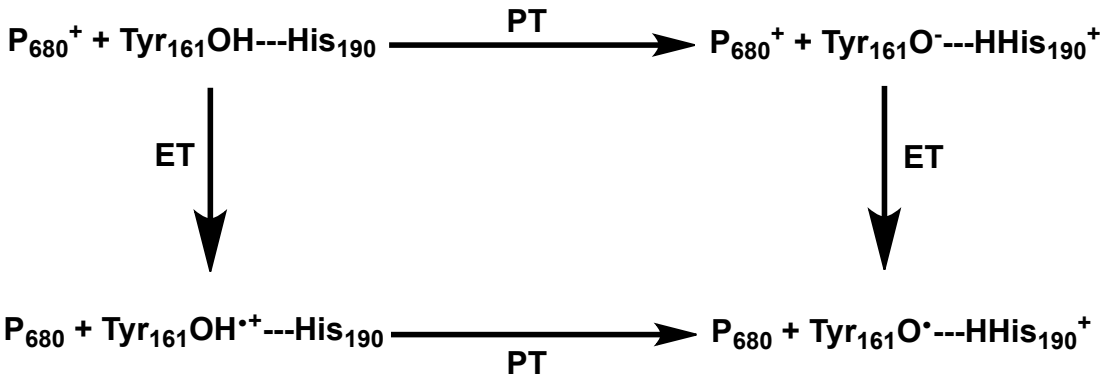

Figure 3. Simplified illustration of the stepwise ET-PT, PT-ET pathways in the oxidation of the Y_z pair in PSII.

The third mechanistic alternative for this reaction is concerted electron proton transfer (EPT), where the movement of protons and electrons is in concert and does not produce any radical cation or anionic intermediates. EPT is mechanistically more complex than either of the stepwise mechanisms because of the simultaneous transfer of two particles: the proton and electron. Thermodynamically, however, EPT conserves energy.

Within the context of PSII, the nomenclature MS-EPT is appropriate. This is because the electron and proton go to acceptors on different molecules, as illustrated in Figure 4, where the electron transfers to the photooxidised reaction center, P_{680}^{+} and the proton transfers to a nearby hydrogen bound histidine (His190).[28,29] Figure 5 illustrates the thermodynamic advantage of MS-EPT. In PSII, the concerted process is highly favored and, as suggested by Babcock and coworkers and by Krishtalik, both the formation of $Y_z^{\bullet}$ and the subsequent oxidation of the oxygen evolving complex (OEC) utilize concerted pathways in order to avoid highly energetic intermediates.[1,2,26,30-38]

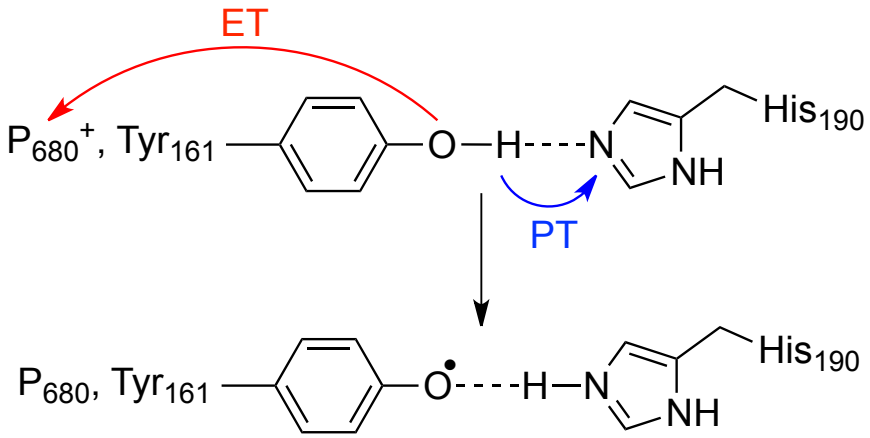

Figure 4. MS-EPT mechanism employed by the Y_z Pair in PSII. Therein the proton is transferred to the putative hydrogen bound histidine and the electron is transferred to the photooxidized PSII reaction center chlorophyll P_{680}^{+}.

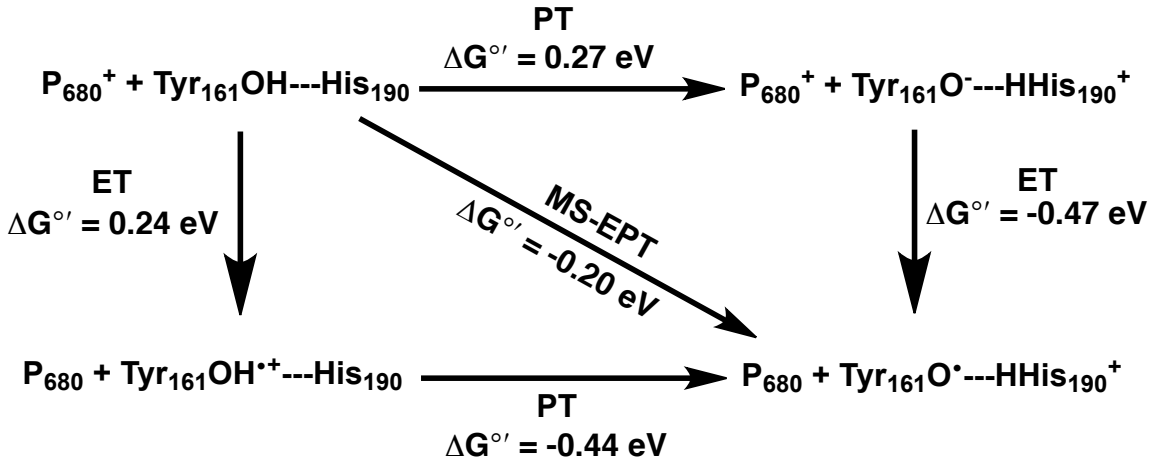

Figure 5. Square scheme for the potential PCET reactions involving oxidation of the hydrogen bound Y_z pair by the PSII reaction center chlorophyll, P_{680}^+. Either initial electron or proton transfer in the stepwise pathways is thermodynamically unfavored and produce reactive, high-energy intermediates. The initial uphill thermodynamic cost of producing these intermediates is regained upon formation of the tyrosine radical product.

The initial steps for each of the stepwise PCET mechanisms are energetically uphill. The oxidation of Y_z by P_{680}^+ by simple outer sphere electron transfer occurs with a $\Delta G°$ = +0.24 eV based on $E°'$ ($P_{680}^{+/\bullet}$) = 1.26 V (vs NHE).[36] Similarly, initial deprotonation of the Tyr161, by His190 is uphill by $\Delta G°$ = +0.27 eV based on solution values for pK_a(H^+-His) = 5.5 and pK_a(TyrOH) = 10.1. When these values are compared to the concerted reaction with electron transfer from Y_z to P_{680}^+ and proton transfer to His190 the reaction is highly favored with $\Delta G°$ = -0.20 eV.[1,26] $\Delta G°$ was calculated from $\Delta G° = F$ [($E°'$($P_{680}^{+/\bullet}$) - ($E°'$($TyrOH^{\bullet+/0}$) - 0.059(pK_a(His) - pK_a($TyrOH^{\bullet+}$)] with pK_a($TyrOH^{\bullet+}$) = -2 and $E°'$($TyrOH^{\bullet+/0}$) ~ 1.5 V. These values are only approximations to the membrane potentials and neglect free energy ($\Delta G°$) differences for the formation of the $TyrO^{\bullet}$---$^+$H-His and TyrO-H---His H-bonded complexes. The second step for each of the stepwise pathways is the difference between the $\Delta G°$ for the first step and the $\Delta G°$ for the EPT step, because it is an overall thermodynamically adiabatic process where the amount of work required to reach the final state is the same irrespective of how the work is performed.

MS-EPT and the role of energetics appear in dramatic fashion in Figure 6: (1) light absorption by an antenna apparatus sensitizes the singlet excited state of chlorophyll P_{680} (Chl_{D1}), $^1P_{680}$*; (2) $^1P_{680}$* undergoes oxidative quenching with electron transfer to pheophytin and then to quinone Q_A; (3) oxidation gives the powerful oxidant P_{680}^+ with $E°'$ ($P_{680}^{+/0}$) ~ 1.26 V; (4) water oxidation at the $CaMn_4$ cluster of the Oxygen Evolving Complex (OEC) where the oxidative activation of the OEC occurs through intervening Y_Z as an electron transfer relay; and (5) the semiquinone anion formed is further stabilized by a lateral electron transfer step to a second quinone, Q_B. Y_Z consists of a tyrosine (Tyr161) and an associated histidine, His190. Removal of His190 by mutagenesis shuts down photosynthesis. Loss of a single base is sufficient to disrupt an enormously complex apparatus with multiple linked functional elements and hundreds of thousands of atoms, highlighting the importance of the MS-EPT mechanism.

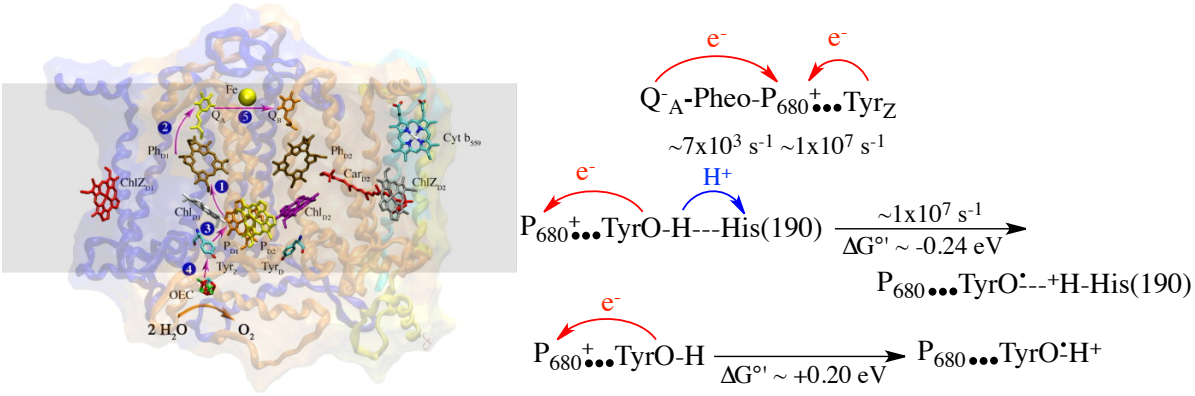

Figure 6. Structure of the Reaction Center of Photosystem II illustrating terminal chlorophyll P_{680}, pheophytin$_{D1}$, quinone acceptor Q_A, Y_Z (Tyr161-His190), the Oxygen Evolving Complex (OEC), and the sequence of electron transfer events induced by light absorption and sensitization. The critical energetic role proposed for His190 as EPT acceptor base is also shown.[3] Reproduced in part with permission from ref. 39. © 2008 Elsevier.

ET, PT, EPT, MS-EPT, HAT, and hydride transfer are all elementary steps available for carrying out PCET reactions. In general, PCET reactions occur by more than one multi-

step mechanism with a competition between mechanisms with their relative importance dictated by reaction conditions, temperature, pH and other factors.

1.4 A Short History and Nomenclature Background of PCET: In 1981 the term proton coupled electron transfer (PCET) was introduced to describe an elementary step, like electron transfer or proton transfer but in which electrons and protons transfer together. The term was coined to describe the concerted e^-/H^+ transfer process that occurs in the comproportionation reaction between $[Ru^{IV}(bpy)_2(py)(O)]^{2+}$ ($Ru^{IV}=O^{2+}$) and $[Ru^{II}(bpy)_2(py)(OH_2)]^{2+}$($Ru^{II}$-$OH_2^{2+}$) shown in Figure 7 (bpy = 2,2′-bipyridine, py = pyridine). In this reaction an electron and proton are transferred simultaneously from Ru^{II}-OH_2^{2+} to $Ru^{IV}=O^{2+}$ to give 2 equivalents of Ru^{III}-OH^{2+}.[40]

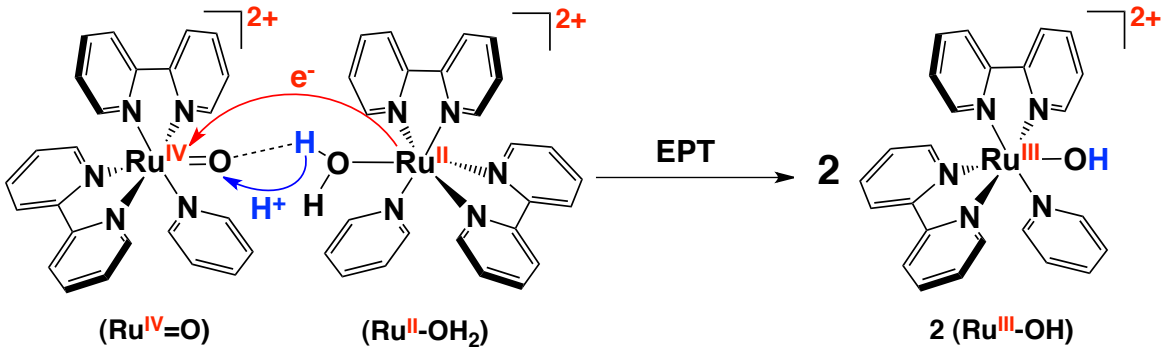

Figure 7. Comproportionation of ($Ru^{IV}=O^{2+}$) and (Ru^{II}-OH_2^{2+})

The term PCET has come to be used more broadly to describe reactions and half reactions in which both electrons and protons are transferred without regard to mechanism. Water splitting into H_2 and O_2 is a pH dependent reaction having separate PCET half reactions, one for water oxidation, eq 1, and one for proton/water reduction, (eqs 2a, b) both of which are pH dependent.

$$2\ H_2O \longrightarrow O_2 + 2\ H_2 \qquad (1)$$

$$O_2 + 4\ H^+ + 4\ e^- \longrightarrow H_2O \qquad (2a)$$

$$2\ H^+ + 2\ e^- \longrightarrow H_2 \qquad (2b)$$

Multi-electron, multi-proton PCET half reactions are universal in energy conversion and storage reactions in chemistry and biology. In biology, key half reactions for energy storage and production exploit PCET and the high-energy content in the C-H bonds of hydrocarbons, sugars, or other oxygenates by indirect reactions with oxygen at physically separated half reactions. Quintessential examples include carbohydrate formation by light driven reduction of CO_2 by water in photosynthesis and the reverse, oxidation of glucose by oxygen which releases energy in respiration. In photosynthesis, CO_2 reduction, coupled with water oxidation, occurs in a reaction that stores 29.1 eV, 1.22 eV per redox equivalent. The stored energy is released in respiration (Fig. 2) with the indirect oxidation of glucose by oxygen used to drive oxidative phosphorylation in mitochondria. This combines inorganic phosphate, P_i, and ADP to give ATP. ATP and the energy released by phosphate hydrolysis to give ADP that is used to power cells for biosynthesis, motion, and signaling.

Unfortunately, the nomenclature used to describe concerted electron-proton transfer has not been standardized, with different terms used to describe the same elementary step. Alternate terms from the literature include concerted proton-electron transfer (CPET),[41] electron transfer proton transfer (ETPT)[42] and concerted electron-proton transfer (CEP).[43] The use of EPT herein follows straightforwardly from ET to describe electron transfer and PT to describe proton transfer as fundamental elementary reactions. It is descriptive, consistent with existing terminology and, as described below, provides a systematic

nomenclature for a family of reactions that differ considerably in microscopic detail but in all of which concerted electron-proton transfer is the defining redox event.

1.5 The Difference between MS-EPT, EPT and Hydrogen Atom Transfer (HAT): Concerted proton-coupled electron transfer can be separated into three different sub-classes: multi-site electron proton transfer (MS-EPT), electron proton transfer (EPT) and hydrogen atom transfer (HAT), excluding hydride transfer because, unlike the aforementioned, it is by definition, not a $1e^-/1H^+$ reaction. The categorization of these concerted reactions is dependent on the donor-acceptor orbital nature of the reaction. EPT is categorized as a reaction that occurs between different donors or acceptors for the electron and the proton, requiring charge redistribution because of this movement. HAT on the other hand is a reaction in which the electron and proton are transferred to the same orbital, and thus does not include a large amount of charge redistribution. This definition is not quantum mechanically rigorous, however, these sub-classes can be quantitatively distinguished based upon the degree of proton non-adiabaticity, which is reflective of the charge redistribution.[44]

In EPT, the e^-/H^+ donor orbitals and e^-/H^+ acceptor orbitals interact electronically, enabling simultaneous transfer. Simultaneous means rapid relative to coupled vibrations (tens of femtoseconds) and solvent modes (~1 picosecond).[26] In EPT there is no discrete ET or PT intermediate that is thermally equilibrated with its surroundings. If there were, the underlying thermodynamics would be those of the intermediate and not those of the final EPT products. An example of differentiation between EPT and HAT is shown in Figure 8 below.

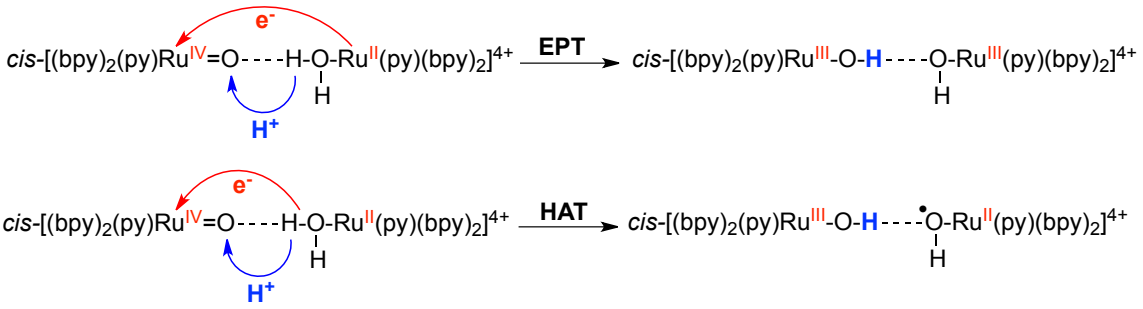

Figure 8. The difference between HAT, and EPT is the donor or acceptor orbital characteristics.

In Figures 7 and 8 EPT leads to the final, energetically stable Ru^{III}-OH^{2+} product and is thermodynamically favored with $\Delta G^{\circ\prime}$ = -0.11 eV.[40,45] For the HAT pathway, e^-/H^+ transfer occurs from a σ(O-H) orbital at Ru^{II}-OH_2^{2+} to electron ($d\pi_{Ru}$) and proton (p_O) acceptor orbitals at Ru^{IV}=O^{2+} giving Ru^{III}-OH^{2+} and the high energy (~2.1 eV) charge transfer intermediate, Ru^{II}-$O^{\bullet}$-H^{2+}. There are different qualitative explanations for the differentiation of EPT and HAT, however, a more accurate categorization comes from distinctions of adiabaticity.

There is another class of EPT reactions, multiple site electron-proton transfer (MS-EPT) as described in the context of PSII above. In MS-EPT an electron-proton donor transfers electrons and protons to spatially separated acceptors or an electron-proton acceptor accepts electrons and protons from spatially separated donors. MS-EPT is microscopically more complex than electron or proton transfer. It shares with electron transfer requirements for medium and intramolecular reorganization explained below in Section 1.6.1. However, it has the additional complexity of a coupled proton transfer.

1.5.1 The Thermodynamics of a Proton Acceptor H_2O versus Base: The rates of PCET reactions and especially concerted PCET reactions are closely tied to the tunneling proton as a result of the intrinsic nature of the reaction. As a product of this connection, it is a worthwhile exercise to explain the acid-base chemistry affecting the thermodynamics of

proton acceptors in PCET reactions. The nature of the proton acceptor is defined by its conjugate acid pK_a. For example, for $H_3O^+ \rightarrow H_2O$, the pK_a is -1.74, whereas for $H_2O \rightarrow HO^-$, the pK_a is 15.74. Similarly, for phosphate $H_2PO_4^- \rightarrow HPO_4^{2-}$ the pK_a is 7.2. The robustness of a proton acceptor in PCET can be calculated simply by the free energy equations for EPT, PT and ET in eqs 3 – 7 below. From this treatment it can be seen that water is intrinsically and microscopically a poor proton acceptor, even at its concentration of ~ 55M in neutral aqueous solution. This is well stated by Costentin and coworkers which explain that EPT oxidations involving water as a proton acceptor may compete with stepwise ET-PT reactions. However, a necessary but perhaps not sufficient, prerequisite for this to occur is that the pK_a of the reduced form of the substrate be smaller than 0, where the excess driving force has to be large enough to overcome pre-exponential and reorganizational factors that are unfavored in the concerted reaction.[46]

For EPT with PT to an associated base:

$$\Delta G_{EPT}^{\circ\prime} = -F\{E^{\circ\prime}(\text{Oxidant}^{\text{III/II}}) - E^{\circ\prime}(\text{Substrate}^{\bullet+/0})\} + 0.059\{\text{p}K_a(\text{Substrate}^{\bullet+}) - \text{p}K_a(\text{HB})\} \quad (3)$$

For EPT with PT to "water":

$$\Delta G_{EPT}^{\circ\prime} = -F\{E^{\circ\prime}(\text{Oxidant}^{\text{III/II}}) - E^{\circ\prime}(\text{Substrate}^{\bullet+/0})\} + 0.059\{\text{p}K_a(\text{Substrate}^{\bullet+}) - \text{pH}\} \quad (4)$$

For PT to an associated base:

$$\Delta G_{PT}^{\circ\prime} = 0.059\{\text{p}K_a(\text{Substrate}^{\bullet+}) - \text{p}K_a(\text{HB})\} \quad (5)$$

For PT to "water":

$$\Delta G_{PT}^{\circ\prime} = 0.059\{\text{p}K_a(\text{Substrate}^{\bullet+}) - \text{pH}\} \quad (6)$$

For ET:

$$\Delta G_{ET}^{\circ\prime} = -F\{E^{\circ\prime}(\text{Oxidant}^{\text{III/II}}) - E^{\circ\prime}(\text{Substrate}^{\bullet+/0})\} \quad (7)$$

The importance of water as a proton acceptor has been stressed in biological model reactions involving tyrosine or tryptophan like molecules citing a Grotthaus or Eigen type proton equilibration mechanism.[41,43,47,48] However, this treatment is unsatisfactory on the microscopic level because the proton must first release to a water molecule before equilibrating to bulk solvent. In the case of tyrosine, the driving force for proton release to water is ~ 0 eV given the difference in pK_a values between pK_a(TyrOH$^{\bullet+}$) = -2 and pK_a(H_2O) = -1.74. In the case of tryptophan, the thermodynamics are even more uphill with pK_a(TrpNH$^{\bullet+}$) = 4.3.[49]

An example of the ongoing discussion about water as a proton acceptor is a computational study conducted by Hummer and coworkers, on base assisted (direct) and water mediated PCET between two stacked tyrosine molecules (TyrO$^{\bullet}$ + TyrOH → TyrOH + TyrO$^{\bullet}$) mimicking a key step in the catalytic reaction in class Ia ribonucleotide reductase.[50] Structures with and without a water molecule intervening between the phenol oxygen atoms served as models for water mediated and direct PCET respectively. Results showed an increase in reaction free energy barrier going from $\Delta G^{\ddagger}$ = 6.5 kcal/mol (0.28 eV) for direct PCET, and $\Delta G^{\ddagger}$ = 11.0 kcal/mol (0.47 eV) for water mediated PCET, illustrating the less favored nature of the reaction upon inclusion of water.[50]

Another example of the discussion on proton acceptors in PCET reactions is a set of experiments carried out by Hammarström and coworkers.[43,48,51] In these studies, tyrosine appended metal-tris bipyridine complexes (Figure 9) were synthesized and studied via laser flash-quench. In these studies the excited state of the metal complex is quenched by an external quencher, followed by electron transfer from the tyrosine to a photo-oxidized metal and proposed proton transfer to the bulk solvent or buffer.[51,52]

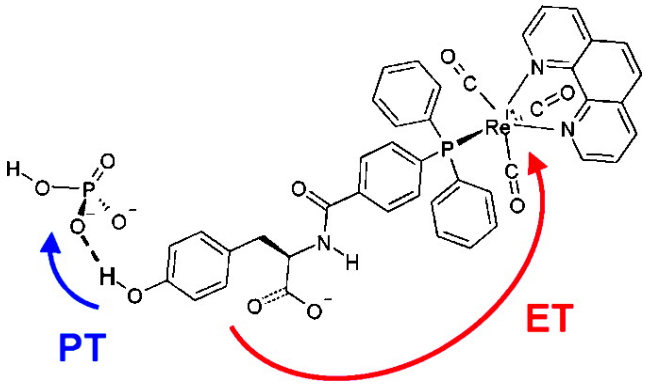

Figure 9. Structure of the rhenium-tyrosine complex that was the subject of reference 51, and 52 with a hydrogen bound phosphate (HPO_4^{2-}) proton acceptor. The MS-EPT reaction occurs via a proton transfer to the phosphate and electron transfer to the Rhenium.

A theoretical study by Hammes-Schiffer and coworkers found that a model, in which the proton acceptor is the phosphate species, HPO_4^{2-}, could successfully reproduce the experimentally observed pH dependence of the overall rate as well as H/D kinetic isotope effects.[52] The model proposed by Hammarström and coworkers with water as a proton acceptor was not physically reasonable for the system. Dibasic phosphate was found to be favored over water as a proton acceptor in part because the proton donor-acceptor distance is ~0.2Å smaller for phosphate because of its negative charge.

Other theoretical treatments have addressed the pH dependence reported by Hammarstöm and coworkers. Savéant and coworkers explored whether or not the driving force and rate constants were pH dependent when H_2O was acting as a proton acceptor.[46] In this study, the pH dependence was attributed to the participation of OH^-, where the concentration of H_2O should not change significantly over the pH range, therefore, failing to explain H_2O as a proton acceptor coupled to pH as a driving force for the reaction.[46] The use of hydroxide as a stoichiometric proton acceptor has been shown in EPT reactions involving tryptophan.[22] There have also been experimental treatments beside the aforementioned that

have experimentally shown increased favorability of PCET reactions in the presence of a base as opposed to just bulk water as a proton acceptor. [19-22]

From Savéant and coworkers' treatment it is plausible that the proton acceptor in aqueous solution must be either hydroxide or a cluster of water. For the former, the OH^- acceptor is at such low concentrations except in very basic solution requiring a wavefunction overlap between donor and acceptor through the solvent matrix. Hydroxide is the only species that changes significantly over the pH range, suggesting its role as a proton acceptor coupled to pH as a driving force. For the latter, however, it is microscopically challenging to calculate a pK_a for a solvent matrix proton acceptor and thus quantitatively assess thermodynamically relevant values such as pK_a. The state of the proton in water is complex with two different water cluster structures proposed. One is the Zundel cation $H_5O_2^+$ (H_2O---H^+---OH_2)[53] and the other the Eigen cation $H_9O_4^+$ ($H_3O^+ \bullet 3H_2O$)[54,55] which undergo rapid dynamical interchange.[56-58] There is also experimental evidence for proton transfer through individual solvent molecules acting as bridges.[59,60] This has also drawn interest in biological studies exploring the role of water molecules as proton relays as reported by Voth and coworkers in Cytochrome *c* proton channels.[61,62]

1.6 The Fundamentals of Proton Coupled Electron Transfer: In summarizing the theory of concerted electron proton transfer, it is useful to first consider simple electron transfer. Below it is assumed that electronic coupling between electron donor and acceptor sites is relatively weak. In this limit, the resonance energy arising from initial and final state wave function mixing, $V_{\mu\nu}$, is small compared to the reorganization energy (λ), $V_{\mu\nu} << \lambda$.

1.6.1 Classical Electron Transfer: In diffusional electron transfer, pre-association between donor D and acceptor A (eqs 8, 9) is followed by electron transfer and separation of products, D^+ and A^-. Pre-association and close contact enhance electronic wave function mixing between the electron donor and acceptor and increase the probability, given a perturbation, in a barrier crossing or tunneling event. Within the classical limit for generic intramolecular electron transfer in a pre-formed structure with electron transfer donor and acceptor spatially arrayed as in a protein. There is no pre-association but changes in local orientation can be influenced k_{ET} by their impact on electronic coupling.

DH-A→D-HA $k_{obs} = k_{ET}$ (8)

DH,A→D, HA $k_{obs} = K_A k_{ET}$ (9)

Transfer of an initial Eigen state (μ) of one energy to a final Eigen state (ν) of another energy, such as the case for election transfer, as well as proton coupled election transfer, is best described using Fermi's Golden Rule as a starting point. This mathematically defines the probability of a transition as the result of a perturbation. The general format for this transition probability is shown in equation 10 below.

$$T_{\mu\nu} = \frac{2\pi}{\hbar}\left|M_{\mu\nu}\right|^2 \rho_{fc} \quad (10)$$

Here the probability of the transition of initial (μ) to a final state (ν) is dictated by the strength of the coupling between these states, represented by the matrix element $M_{\mu\nu}$ as well as the number of ways this transition can occur, which is represented by the Frank-Condon, density of states term, $\rho_{fc.}$

This formalism can be expanded to define rates of election transfer as outlined by the Marcus-Hush theory for election transfer.[63,64] The equation for the Marcus non-adiabatic transition for electron transfer, with weak electronic coupling, is given below in equation 11.

$$k_{ET} = \frac{2\pi}{\hbar}\left|V_{ET}\right|^2 \left(4\pi\lambda_{\mu\nu}k_B T\right)^{-1/2} \exp-\left[\frac{(\Delta G_{ET} + \lambda_{\mu\nu})^2}{4\lambda_{\mu\nu}RT}\right] \qquad (11)$$

V_{ET} is the electron transfer matrix element discussed in detail below. In the Frank-Condon density of states term, $(4\pi\lambda_{\mu\nu}k_BT)^{-1/2}$ is a Boltzmann distribution defining the thermal population of vibrational states. The last exponential term defines the classical thermodynamic barrier crossing. Within these terms $\lambda_{\mu\nu}$ represents intramolecular and solvent reorganizational energies in going from the initial (μ) and final (ν) states in the form of:

$$\lambda_{\mu\nu} = \lambda_i + \lambda_o \qquad (12)$$

The lambda term is a summation of the inner-sphere (λ_i) and outer-sphere (λ_o) reorganizational energies further broken down in equations 13 and 14.

$$\lambda_o = e^2\left(\frac{1}{2a_1} + \frac{1}{2a_2} - \frac{1}{d}\right)\left(\frac{1}{D_{op}} - \frac{1}{D_s}\right) \qquad (13)$$

Here a_1, a_2, d, D_{op} and D_s are the radii of the donor and acceptor, the distance between their centers and the optical frequency and zero frequency dielectric constants of the solvent respectively. The e^2 term represents the amount of charge transferred. This treatment assumes that the geometries of the reactants are simple spherical reactants. The innersphere reorganizational energy is defined by:

$$\lambda_i = \sum_j \frac{1}{2} f_j \left(\Delta Q_{e,j}\right)^2 = \sum_j S_j \qquad (14)$$

Here the summation is over the coupled intramolecular vibrations. The contribution of the j^{th} normal mode to the reorganization energy is given in terms of the force constant f_j and the change in equilibrium position between the reactants and the products, represented by $\Delta Q_{\mu,\nu}$ or the change in equilibrium normal coordinate for the quantum mode between initial

(reactant) and final (product) states. The only contributors to λ_i are those that have $\Delta Q_{\mu,\nu} \neq 0$. S_j is the dimensionless quantity called the Huang-Rhys factor which is the electron-vibrational coupling constant and is given by:

$$S_j = \frac{1}{2}\left(\frac{M_j \omega_j}{\hbar}\right)\left(\Delta Q_{e,j}\right)^2 \qquad (15)$$

Here M_j, is the reduced mass and ω_j the angular frequency. V_{ET} in eq 16 represents the electron transfer matrix element which is the Hamiltonian for the wave function overlap of the initial and final state the form of:

$$V_{ET} = \langle \psi_\mu | H | \psi_\upsilon \rangle \qquad (16)$$

In this case the wave functions ψ_μ and ψ_ν describe the initial and final states of the transition. When the reaction is the sum of all contribution states the wave functions ψ_μ and ψ_ν are the total vibrational wave functions for the initial and final states. They are the products of wave functions for all normal modes including collective solvent vibrations.

1.6.2 Proton Transfer: Proton motion along the proton transfer coordinate is described by a linear combination of the high frequency (2000-4000 cm^{-1}) ν (O-H) vibrational modes before and after proton transfer occurs.[65-67] Because of the high quantum spacings between these vibrational levels, proton transfer occurs by quantum mechanical tunneling not classical barrier crossing.

1.6.3 Proton Coupled Electron Transfer: The coupling of a proton to the above quantum mechanical treatment for pure electron transfer requires the inclusion of terms into equation 16 that take into account the tunneling of a proton in conjunction with the electron. The following will initially define k_{EPT} for a single vibrational transition, between an initial and final state, and then define k_{EPT} as a sum of all states, taking into consideration all possible

modes of transition from any vibrational level of the initial state to any vibrational level of the final state. The complexity of this single state transition treatment in comparison to the summation of states treatment can be illustrated by Figure 10 below.[68]

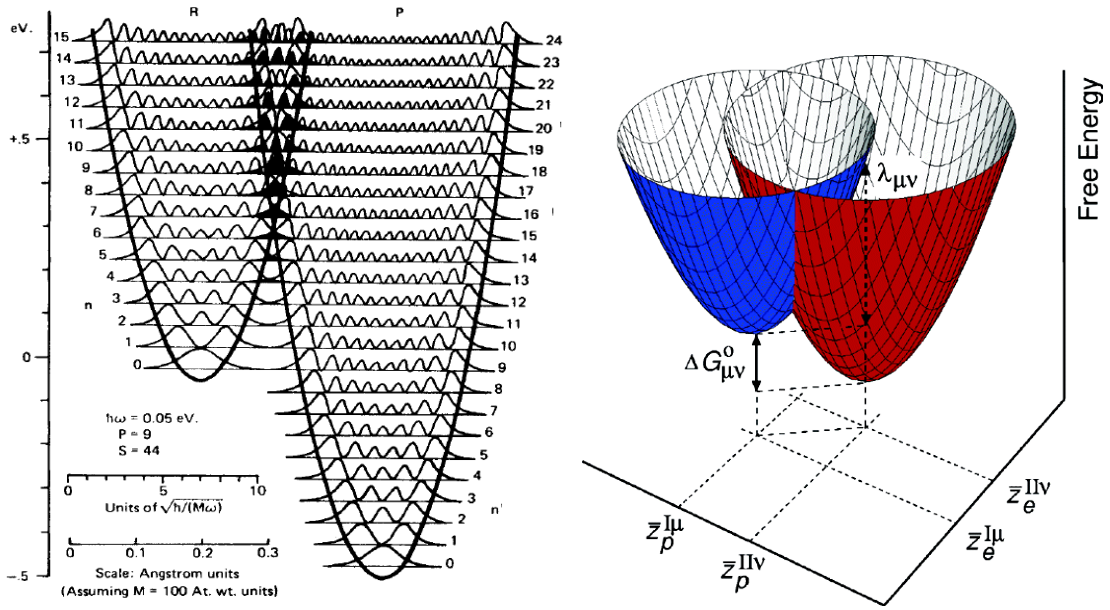

Figure 10. A) Schematic one-dimensional representation of the intersection between reactant and product vibrational levels. The optimal overlap of the ν = 0 initial vibrational level and the ν′ = 9 product level.[68,69] **B**) Two-dimensional vibronic free energy surface as functions of two collective solvent coordinates for a PCET reaction with the lowest energy reactant and product free energy surfaces shown. The notation of $\Delta G°_{\mu\nu}$ represents the free energy difference between initial and final states and $\lambda_{\mu\nu}$ represents the outer-sphere reorganization energy.[4,70] Reproduced with permission from refs. 68 and 70. © 1996 and 2006 American Chemical Society.

In the limit of strong electronic coupling across the hydrogen bond and weak electronic coupling, k_{EPT} is given for a single ν → ν′ transition in eq 17. It describes a single vibronic transition from the initial level $\mu = 0$ in the proton transfer mode to a final level ν in the EPT product state and is analogous to the electron transfer result in eq 11.

$$k_{EPT(\upsilon\rightarrow\upsilon')} = \frac{2\pi}{\hbar}\left|V_{\mu\nu}\right|^2\left(4\pi\lambda_{\mu\nu}k_BT\right)^{-1/2}\exp-\left[\frac{(\Delta G_{\mu\nu}+\lambda_{\mu\nu})^2}{4\lambda_{\mu\nu}k_BT}\right] \quad (17)$$

Initial coupled DH-A vibrational levels (μ), final coupled D-HA vibrational levels (ν) and $\lambda_{\mu\nu}$ is the reorganizational energy from solvent and low frequency (μ→ν) modes. $V_{\mu\nu}$ is the product of the electron transfer matrix element (V_{ET}) and proton vibrational wave functions for initial and final states. Equation 17 above includes a classical barrier crossing term with a Boltzmann distribution of states as well as the exponential term defining the classical thermodynamic barrier crossing as in eq 11.

$$\Delta G_{\mu\nu} = \Delta G_{EPT} + (\mu - \upsilon)\hbar\omega \tag{18}$$

$$V_{\mu\upsilon} = V_{ET}\left\langle \phi_{\mu}^{I} \middle| \phi_{\upsilon}^{II} \right\rangle \tag{19}$$

The EPT matrix element (eq 19) $V_{\mu\nu}$ consists of the ET matrix element V_{ET} (eq 16) and the wave function integral of the proton initial (μ) and final (ν) states. The dynamics of the barrier crossing will depend on the product of the matrix element and the initial and final proton wavefuntion overlap integral. The extent to which the square of this term is large is going to dictate, much like in classical electron transfer, the probability of the initial and final states being along the same spatial coordinate.

Approaching the total equation for k_{EPT} requires the inclusion of all initial and final overlapping states (summation of states) instead of the simplified treatment outlined above which is for a single ν → ν′ transition. Contributions also exist from vibrational levels above μ = 0. Even though populations in these levels fall off rapidly with $\hbar\omega/k_BT$, there can be a considerable compensation due to enhanced vibrational wave function overlap in levels above μ = 0. Inclusion of the fractional population above μ = 0, $P_{I\mu}$, gives the final result in eq 20. In this equation, the first summation is over the vibrational levels in the initial state and the second summation is over all vibrational level in the final state. The summation of states takes into consideration all of the possible interactions that can occur between all

possible initial and final vibrational states over the range of populated and initial and final coupled vibration modes. The terms for $\lambda_{\mu\nu}$, $\Delta G_{\mu\nu}$ and $V_{\mu\nu}$ are the same as defined by eqs 12, 18 and 19 above.

$$k_{EPT} = \frac{2\pi}{\hbar}\sum_{\mu} P_{I\mu}\sum_{\upsilon}\left|V_{\mu\upsilon}\right|^2 (4\pi\lambda_{\mu\nu}k_B T)^{-1/2}\exp-\left[\frac{(\Delta G_{\mu\nu}+\lambda_{\mu\nu})^2}{4\lambda_{\mu\nu}k_B T}\right] \qquad (20)$$

1.6.4 Kinetic Isotope Effects in EPT: The magnitude of the square of the vibrational overlap integral in eq 19 can be very small. Vibrational overlaps for the comproportionation reaction between the species shown in Figure 7, *cis*-$[Ru^{IV}(bpy)_2(py)(O)]^{2+}$ and *cis*-$[Ru^{II}(bpy)_2(py)(OH_2)]^{2+}$ for the $\mu = 0 \rightarrow \nu = 0$ vibronic transition for both the protio and deuterio aqua complex are shown in Figure 11.[40,57,71-73] The decrease in deutero compared to proteo initial and final wavefunction overlap for the $-OD_2$ complex is the origin of the H_2O/D_2O kinetic isotope effect of 16.1.[40] It arises from the effect on vibrational overlap of the decrease in zero point energy between H and D.

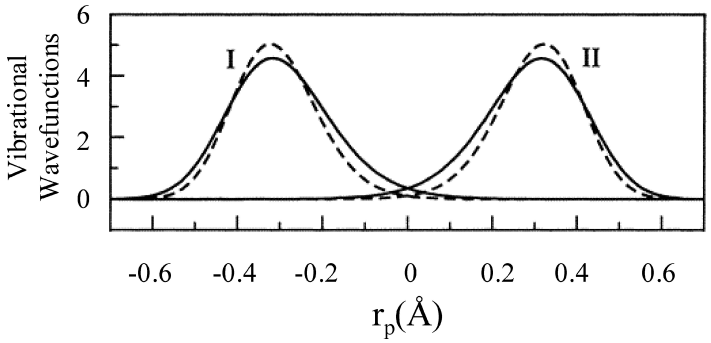

Figure 11. Illustrating reactant (I) and product (II) vibrational wave functions, H (solid curve) and D (dashed curve), for the $\mu = 0 \longrightarrow \nu = 0$ vibronic channel for the *cis*-$[Ru^{IV}(bpy)_2(py)(O)]^{2+}$/ *cis*-$[Ru^{II}(bpy)_2(py)(OH_2)]^{2+}$comproportionation reaction in Figure 7. The plots for *cis*-$[Ru^{IV}(bpy)_2(py)(O)]^{2+}$/ *cis*-$[Ru^{II}(bpy)_2(py)(OD_2)]^{2+}$ illustrate the decrease in vibrational overlap for the $-OD_2$ complex. Reproduced with permission from ref 71. © 2002, American Chemical Society.

1.7 The Role of Tyrosine, Tryptophan and Cysteine in Biological PCET: Much of the work on PCET involving biological redox mediators has revolved around the amino acids, tyrosine, tryptophan and cysteine. Knowledge about how mobile cofactors such as flavin ($FAD/FADH_2$), nicotinamide (NAD, NADP/NADH, NADPH) and quinone (CoQ_{10}, and plastoquinone) participate in biological PCET is still being gathered. The following presents a few examples of biological systems that employ PCET via amino acid redox cofactors.

Photosystem II in green plants is the most widely used example of tyrosine in PCET. PCET involving $Y_Z/Y_Z^{\bullet}$ as an electron transfer relay is outlined above and will not be covered in detail here, however, there are several reviews that cover PCET in PSII in great detail.[1,2,30,31,35,26,75]

1.7.1 Ribonucleotide Reductase (RNR): Class I RNRs are found in *E. coli* and consist of two enzyme subunits, R1 and R2. They catalyze the reduction of nucleosides to deoxynucleosides (Fig. 12). The enzyme initiates the reaction at a diiron tyrosyl radical site (Y122) with radical transfer occurring over 35 Å through a chain of amino acids with termination at cysteine C439 (Fig. 13).[10,76] Radical transfer is thought to occur by a long range EPT "shuttle" mechanism with electron transfer occurring between amino acids coupled with a double concerted electron proton transfer, e.g., $(TyrO^{\bullet}\text{---}^{+}H\text{-}His)\ldots.(TyrOH\text{---}His)' \longrightarrow (TyrO\text{-}H\text{---}His)\ldots.(TyrO^{\bullet}\text{---}^{+}H\text{-}His)'$. Radical transport sites have been isolated at Y122, W48, and Y356 on the R2 unit and Y731, Y730, and C439 at the R1 unit.[76] An impressive number of techniques have been applied to the investigation of radical transport including pulse radiolysis, electron paramagnetic resonance (EPR), and UV/Visible measurements combined with site-directed mutagenesis, X-ray crystallography, magnetic circular dichroism (MCD), density functional theory (DFT), and native protein chemical ligation.[2,10,15,77]

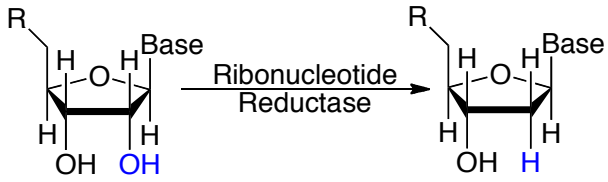

Figure 12. The reaction carried out by class I ribonucleotide reductases.

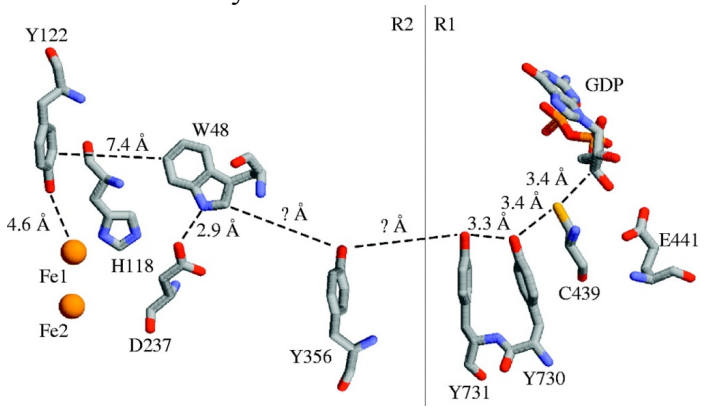

Figure 13. A schematic diagram of amino acid residues along the catalytic chain of class I RNR. The crystal structure suggests that the protein exists as a homodimer with radical transport from subunit R2 to subunit R1. Electron transfers occurs over a 35 Å distance originating at Y122 on the R2 subunit of RNR and terminating at C439 on the R1 subunit. Reproduced with permission from ref. 10, © 2006 American Chemical Society.

The role of Tyr356 is of particular interest due to its position at the interface between the subunits, R1 and R2. Pulse radiolysis has been used to explore radical transport through this interface between peptides modified by site-directed mutagenesis.[77] Chemical ligation has also been used to incorporate fluorinated tyrosine derivatives (F_nY) having potential shifts in the range -50 to 270 mV compared to Y356 and with pK_a values from 5.6 to 9.9. Decreasing the reduction potential has the effect of completely inhibiting RNR activity. Incorporating amino derivatized tyrosines (NH_2Y) at Y730 and Y731 results in radical trapping due to decreases in reduction potential supporting an EPT model.[78,79] The results of these studies were consistent with important roles for EPT and MS-EPT in radical transport in RNR.

1.7.2 DNA Photolyase: is a photoactive protein that selectively binds to and repairs DNA, reversing thymine base dimerization caused by far UV light damage.[80-83] Failure to repair this

dimerization blocks replication and transcription, leading to cytotoxic and mutagenic effects. The repair mechanism is induced by the absorption of the blue light harvesting cofactor 5,10-methylenetetrahydrofolylpolyglutamate (MTHF) which then excites $FADH^{\bullet}$ by energy transfer.[11,12,80,81] The indole group of tryptophan has been demonstrated to be involved in PCET in the mechanism of photo-activation in *Escherichia Coli* DNA photolyase, reported by Aubert and coworkers.[80] In this system the excited state FADH radical ($FADH^{\bullet}$*) undergoes reductive quenching by adjacent tryptophan W382 to give the semi-quinoidal radical anion ($FADH^{\bullet-}$) and $TrpNH^{\bullet+}$.[82] The initial quenching step occurs by rapid (<10 ns) electron transfer to give $FADH^{\bullet-}$, the catalytically active form of the cofactor (Fig. 15).[81,83,84]

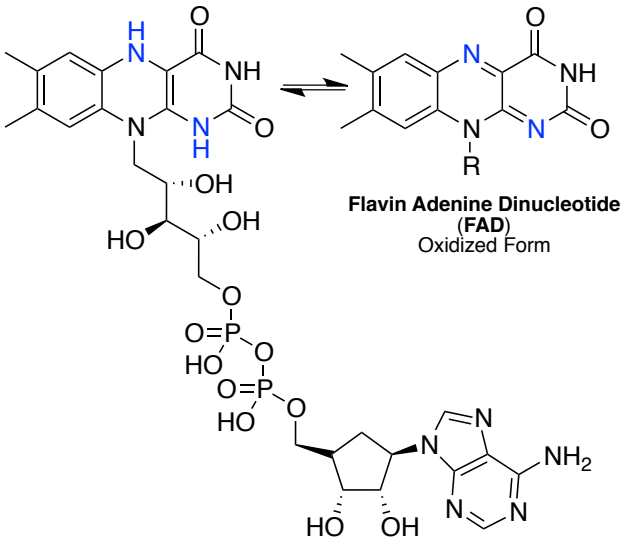

Figure 14. Full structure of the FAD/$FADH_2$ $2e^-/2H^+$ mobile cofactor, the unpared electron on the semi-quinoidal form of the cofactor is distributed into the isoalloxazine ring by resonance.

The triple tryptophan redox relay in DNA photolyase has been explored thoroughly by spectroscopic and mutagenic studies.[12,81-86] Radical formation and charge hopping were found to occur on the picosecond time scale and isolation of intermediates was not possible.

Site-directed mutagenesis studies demonstrated the importance of tryptophan residues located at W306, W359, and W382 (Fig. 15). Subsequent long-range electron transfer occurs by site-to-site electron transfer hopping through tryptophan residue W359 to the terminal tryptophan W306 located 13.4 Å from the flavin. Long range electron transfer is followed by loss of a proton.[11,81,85] Based on XRD, the indolyl N1 atom of $W306^{\bullet+}$ is directly exposed to a shallow pocket open to solvent. Deprotonation is proposed to occur to solvent water within 300 ns after excitation in a net, stepwise ET-PT reaction even though proton transfer from $TrpNH^{\bullet+}$ to water in water is disfavored by > 0.35 eV.[81] In the XRD structure there is no potential proton acceptor within 5 Å of the indolic nitrogen atom. W382 and W559 are surrounded by hydrophobic and polar amino acids but are proposed to be hydrogen bound to a buried water molecule.[86]

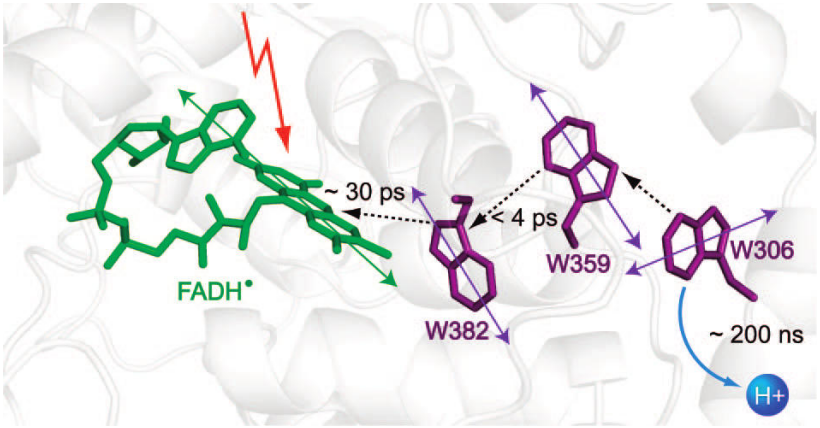

Figure 15. Structural arrangement of the $FADH^{\bullet}$-W382-W359-W306 chain in DNA photolyase following laser flash photolysis at 500 nm with timescales for subsequent electron transfer hopping. The axes in the figure highlight the different orientations of the ring systems. Reproduced with permission from ref. 81, © 2008 American Chemical Society.

1.7.3 Soybean Lipoxygenase: (SLO) is a nonheme iron metalloprotein that catalyzes the oxidation of unsaturated fatty acids.[15-18] A combination of a high-resolution crystal structure by XRD, results from a number of spectroscopic studies, and quantum calculations have given considerable insight into mechanism for this enzyme.[15-18] A key step is thought to

involve net hydrogen atom transfer but by EPT (Fig. 16). In the proposed pathway, the electron is thought to transfer from the π system of the substrate to the iron cofactor while proton transfer occurs from the C11 carbon.[15,16,18]

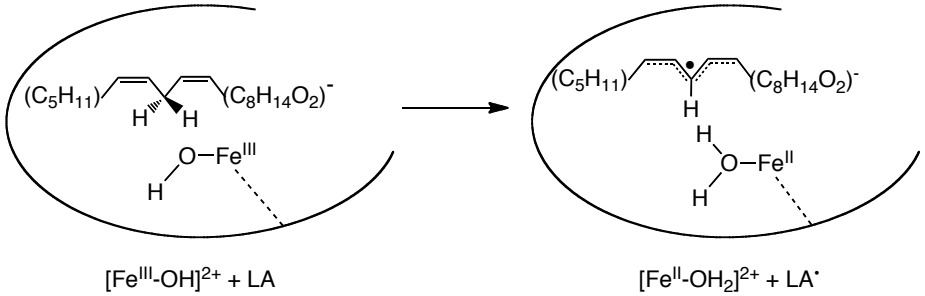

Figure 16. Chemical reaction of soybean lipoxygenase catalyzed oxidation of linoleic acid. Reproduced with permission from ref. 87, © 2002 American Chemical Society.

With linoleic acid as substrate a number of mechanistic conclusions were reached. The concerted process is exothermic by ~ 5 kcal/mol and non-adiabatic toward electron transfer due to weak electronic coupling between the electronic donor and acceptor. Recent advances in dynamic calculations on SLO have shown the importance of protein motion and its effects on substrate position and donor acceptor distance and the role it plays in hydrogen tunneling.[88] Protein motion results in a decrease in proton transfer distance, relative to the equilibrium state, resulting in more efficient proton tunneling due to increased vibrational overlap.[88]

1.8 Experimental Methods: The techniques used to study proton-coupled electron transfer include photophysical methods, such as pump-probe[3,43,48,77,80,83,85] biological spectroscopic analysis of full enzymes[8-12,28,29] electrochemical methods, as well as mixing techniques such as stopped-flow spectroscopy[4,19,20,22,24,25,41,46,47,89,90] just to name a few. The techniques employed to study PECT herein include electrochemical and mixing studies on model systems, which consist of free amino acids in aqueous solution. Model systems are ideal when studying the physical chemistry of PCET because biologically PCET is a part of a

larger cascade of events, as shown above. These systems are remarkably complex, with many things going on at once. Ancillary biological functions like allosteric factors and conformation dynamics potentially make probing chemical phenomena like PCET more difficult.

1.8.1 Electrochemical Methods: Electrochemistry has been a widely used technique to study PCET reactions because most applications of PCET in biology involve the collection and injection of electrons. On a fundamental level, electrochemical studies that change the electrode potential are an easy and continuous method of varying the driving force of a reaction where the current flowing through the electrode is a straightforward measure of rates of reactions. An additional advantage is that the current-potential response is non-destructive and techniques like cyclic voltammetry (CV) can be read as an activation-driving force relationship.[89] Rate constants can be acquired electrochemically by analysis of current-potential responses using numerical simulations, which are discussed below.

1.8.2 Cyclic Voltammetry on Metal Oxide Electrodes: Herein, we use cyclic voltammetry on tin doped In_2O_3 (ITO) and fluorine-doped SnO_2 (FTO) electrodes, where the direct oxidation of small organic molecules, including the redox active amino acid substrates of interest in this work (Tyr, Trp and Cys) do not produce any current within the solvent limit, Figure 17. This is thought to occur as a result of well-ordered water molecules on the surface of the electrode that electrostatically prevent any interaction of the substrate at the electrode. Although this lack of substrate/electrode interaction has not been fully characterized, it can be exploited for a more comprehensive range of driving forces enabling changes in solution conditions to probe the physical chemistry of these molecules. An example of this is the employment of metal mediators in the form of $M(L)_3^{III/II}$ which have a well-defined

reversible electrochemical response at metal-oxide electrodes.[19-22] These metal mediators, and specifically the metal complexes III/II couple can be used to probe the free energy dependent oxidation kinetics of these reactions. The oxidation of the substrate can be probed by the catalytic $M^{III/II}$ electrochemical wave produced by the generation of the M^{3+} species at the electrode. This thereby interacts with the substrate that cannot directly access the electrode, producing current potential responses like those shown in Figure 17 below.

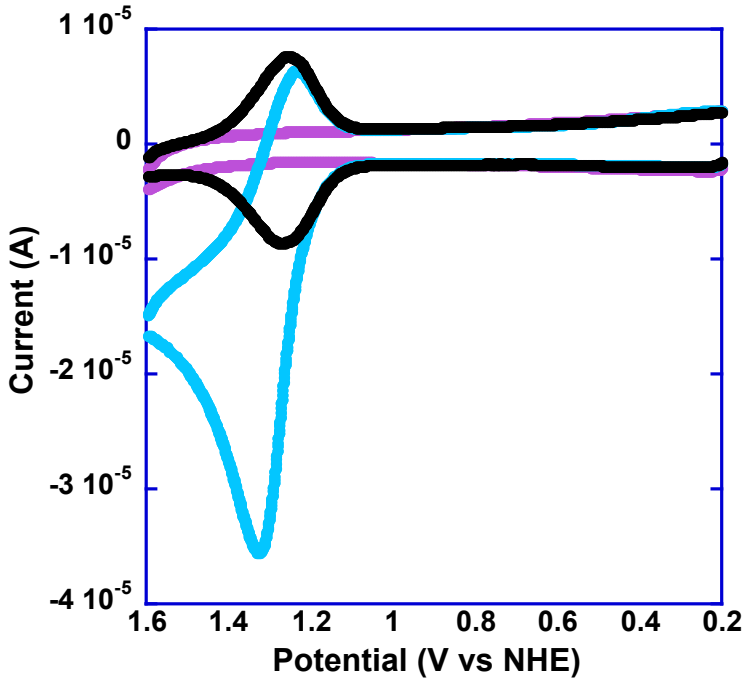

Figure 17. CVs on an ITO working electrode with tyrosine as the substrate (100 μM) without any metal mediator (purple) surface bound metal mediator, without any tyrosine substrate (black) and catalytic $M^{III/II}$ response in the presence of tyrosine (100 mM, blue).

Given the tunable nature of $E°'$ for the $M^{III/II}$ couple, there is a greater range of driving forces that can be explored (eq 3), enabling more information to be gathered from free energy dependence experiments. Also, because the organic substrate does not interact with the electrode, any kind of electrode fouling as a result adsorption of oxidation products or side reactions is mitigated. Additionally, electrochemical techniques have the ability to probe PCET with relatively unstable species. An example of this is the metal mediator $Ru(bpy)_3^{III/II}$,

$E^{\circ\prime}$ = 1.25, which if generated in neutral aqueous solution will convert back to $Ru(bpy)_3^{2+}$ within an hour. Electrochemical techniques are ideal for probing reactions involving species that are difficult to maintain in solution for long periods of time because they are generated directly at the electrode, where they immediately undergo chemistry.

However advantageous electrochemical techniques are, it is still an indirect technique for acquiring information. Complex mechanistic and kinetic schemes require numerical simulation of current potential responses by programs such as DigiSim or DigiElch in order to acquire meaningful kinetic information.[91] While these programs are incredibly valuable, they cannot implicitly identify a mechanism. There are usually many different variables in defining an electrochemical system and thus, a number of different ways to attain a 'good fit' to data. In order to obtain a meaningful simulation it is important to maximize the number of known values and input parameters, and to minimize the number of variables, allowing a *reliable* approximation of the system under study to be made.

1.8.3 Mixing and Spectroscopic Methods: Mixing studies offer a direct way to measure kinetics by spectroscopic monitoring, with single wavelength detection by a PMT or with a diode array, allowing for full, time resolved spectra to be gathered. The mixing studies employed herein include stopped-flow mixing as well as hand mixing with a manually driven syringe-mixing set-up. In both cases two solutions of reagents are mixed and then spectroscopically monitored to probe the kinetics of a [M^{3+} + substrate → M^{2+} + oxidized substrate] type reaction. In these reactions, the kinetics are dominated by the $M^{III/II}$ species MLCT absorption because of high molar absorptivities, making them the only colored species in solution with very few exceptions, unless there is a large excess of the substrate. Most kinetic runs under pseudo-first order conditions produce simple single-exponential fits,

making data easy to acquire directly. However, for more complex kinetic traces, the spectroscopic fitting program SPECFIT/32 can be employed to gather detailed mechanistic information based on simulation of the data. Much like the simulation of electrochemical data, it is important to maximize the number of known parameters while minimizing the number of variables, in order to increase the reliability of a kinetic simulation.

1.9 Concluding Remarks: It has been demonstrated that PCET plays a central role in bio-redox reactions from photosynthesis to respiration as well as chemical reactions required for molecular water splitting and CO_2 reduction. There is ongoing discussion about the roles of proton acceptors in PCET reactions. However, the above analysis clarifies some key points in illustrating why water is a poor proton acceptor and why a base or hydroxide molecule make the best candidates for accepting protons in PCET reactions. The quantum mechanics discussed layout systematically from Fermi's Golden Rule, classical electron transfer, proton transfer and from that, a definition of a PCET involving all initial and final states. The biological prevalence of PCET is also clearly demonstrated in given examples of amino acid cofactors participating in electron proton transfer reactions. The impact of PCET is felt in biological reactions, catalysis, as well as in photochemistry. The full impact of PCET and our understanding of how and when it occurs are still evolving.

1.10 References:

(1) Hyunh, M.-H. V.; Meyer, T. J. **Proton Coupled Electron Transfer**. *Chem. Rev*. **2007**, *107*, 5004- 5064.

(2) Meyer, T. J.; Huynh, M.-H. V.; Thorp, H. H. **The Possible Role of Proton-Coupled Electron Transfer (PCET) in Water Oxidation by Photosystem II**. *Angew. Chem. Int. Ed*. **2007**, *46*, 5284-5304.

(3) Gagliardi, C. J.; Westlake, B. C.; Kent, C. A.; Paul, J. J.; Papanikolas, J. M.; Meyer, T. J. **Integrating Proton Coupled Electron Transfer (PCET) and Excited States**. *Coord. Chem. Rev*. **2010**, *254*, 2459-2471.

(4) Hammes-Schiffer, S.; Soudackov, A. V.; **Proton Coupled Electron Transfer in Solutions, Proteins and Electrochemistry**. *J. Phys. Chem. B* **2008**, *112*, 14108-14123.

(5) Roffey, R. A.; Kramer, D. M.; Govindjee; Sayre, R. T. **Lumenal Side Histidine Mutations in the D1 Protein of Photosystem II Affect Donor Side Electron Transfer in *Chlamydornonas reinhardtii***. *Biochim. Biophys. Acta, Bioenerg*. **1994**, *1185*, 257–270.

(6) Mamedov, F.; Sayre, R. T.; Styring, S. **Involvement of Histidine 190 on the D1 Protein in Electron/Proton Transfer Reactions on the Donor Side of Photosystem II**. *Biochemistry* **1998**, *37*,14245–14256.

(7) Svensson, B.; Etchebest, C.; Tuffery, P.; van Kan, P.; Smith, J.; Styring, S. **A Model for the Photosystem II Reaction Center Core Including the Structure of the Primary Donor P_{680}**. *Biochemistry* **1996**, *35*, 14486–14502.

(8) Mao, S. S.; Holler, T. P.; Yu, G. X.; Bollinger Jr., J. M.; Booker, S.; Johnston, M. I.; Stubbe, J. **A Model for the Role of Multiple Cysteine Residues Involved in Ribonucleotide Reduction: Amazing and Still Confusing**. *Biochemistry* **1992**, *31*, 9733-9743.

(9) Stubbe, J.; Nocera, D. G.; Yee, C. S.; Chang, M. C. Y. **Radical Initiation in the Class I Ribonucleotide Reductase: Long-Range Proton-Coupled Electron Transfer**. *Chem. Rev*. **2003**, *103*, 2167-2201.

(10) Seyedsayamdost, M. R.; Yee, C. S.; Reece, S. Y.; Nocera, D. G.; Stubbe, J. **pH Rate Profiles of F_nY_{356}-R2s (n= 2, 3, 4) in *Escherichia coli* Ribonucleotide Reductase: Evidence that Y356 Is a Redox-Active Amino Acid along the Radical Propagation Pathway**. *J. Am. Chem. Soc.* **2006**, *128*, 1562-1568.

(11) Cheung, M. S.; Daizadeh, I.; Stuchebrukhov, A. A.; Heelis, P. F. **Pathways of Electron Transfer in *Escherichia Coli* DNA Photolyase: Trp^{306} to FADH**. *Biophysical Journal* **1999**, *76*, 1241-1249.

(12) Sancar, A.; **Structure and Function of DNA Photolyase and Cryptochrome Blue-Light Photoreceptors**. *Chem. Rev.* **2003**, *103*, 2203-2237.

(13) Miller, A.; Padmakumar, K.; Sorkin, D. L.; Karapetian, A.; Vance, C. K. **Proton-Coupled Electron Transfer in Fe-superoxide Dismutase and Mn-superoxide Dismutase**. *J. Inorg. Biochem.* **2003**, *93*, 71-83.

(14) Greenleaf, W. B.; Perry, J. P.; Hearn, A. S.; Cabelli, D. E.; Lepcok, J. R.; Stroupe, M. E.; Tainer, J. A.; Nick, H. S.; Silverman, D. N. **Role of Hydrogen Bonding in the Active Site of Human Manganese Superoxide Dismutase**. *Biochemistry* **2004**, *43*, 7038-7045.

(15) Reece, S. Y.; Nocera, D. G. **Proton-Coupled Electron Transfer in Biology: Results from Synergistic Studies in Natural and Model Systems**. *Annu. Rev. Biochem*. **2009**, *78*, 673-699.

(16) Rickert, K. W.; Klinman, J. P. **Nature of Hydrogen Transfer in Soybean Lipoxygenase 1: Seperation of Primary and Secondary Isotope Effects**. *Biochemistry* **1999**, *38*, 12218–12228.

(17) Glickman, M. H.; Klinman, J. P. **Nature of Rate-Limiting Steps in the Soybean Lipoxygenase-1 Reaction**. *Biochemistry* **1995**, *34*, 14077–14092.

(18) Hatcher, E.; Soudackov, A. V.; Hammes-Schiffer S. **Proton-Coupled Electron Transfer in Soybean Lipoxygenase: Dynamical Behavior and Temperature Dependence of Kinetic Isotope Effects**. *J. Am. Chem. Soc.*, **2007**, *129*, 187–196.

(19) Fecenko, C. J.; Meyer, T. J.; Thorp, H. H. **Electrocatalytic Oxidation of Tyrosine by Parallel Rate Limiting Proton Transfer and Multi-Site Electron-Proton Transfer**. *J. Am. Chem. Soc*., **2006**, *128*, 11020-11021.

(20) Fecenko, C. J.; Thorp, H. H.; Meyer, T. J. **The Role of Free Energy Change in Coupled Electron-Proton Transfer**. *J. Am. Chem. Soc*. **2007**, *129*, 15098-15099.

(21) Gagliardi, C. J.; Jurss. J. W.; Thorp, H. H.; Meyer, T. J. **Surface Activation of Electrocatalysis at Oxide Electrodes. Concerted Electron-Proton Transfer**. *Inorg. Chem.* **2011**, *50*, 2076-2078.

(22) Gagliardi, C. J.; Binstead, R. A.; Thorp, H. H.; Meyer, T. J. **Concerted Electron-Proton Transfer (EPT) in the Oxidation of Tryptophan with Hydroxide as a Base**. *J. Am. Chem. Soc*. **2011**, *133*, 19594-19597.

(23) Stewart, D. J.; Napolitano, M. J.; Bakhmutova-Albert, E. V.; Margerum, D. W. **Kinetics and Mechanisms of Chlorine Dioxide Oxidation of Tryptophan**. *Inorg. Chem*. **2008**, *47*, 1639-1647.

(24) Song, N.; Stanbury, D. M.; **Proton-Coupled Electron Transfer Oxidation of Pheonols by Hexachloroiridate(V)**. *Inorg. Chem*. **2008**, *47*, 11458-11469.

(25) Hung, M.; Stanbury, D. M. **Catalytic and Direct Oxidation of Cysteine by Octacyanomolybdate(V)**. *Inorg. Chem.* **2005**, *44*, 3541-3350.

(26) Weinberg D. W.; Gagliardi, C. J.; Hull, J. F.; Murphy, C. F.; Kent, C. A.; Westlake, B.; Paul, A.; Ess, D. H.; McCafferty, D. G.; Meyer, T. J. **Proton-Coupled Electron Transfer**. *Chem. Rev.* **2012**, *112*, 4016-4093.

(27) Mayer, J. M. **Proton-Coupled Electron Transfer: A Reaction Chemist's View**. *Annu. Rev. Phys. Chem.* **2004**, *55*, 363-390.

(28) Loll, B.; Kern, J.; Saenger, W.; Zouni, A.; Biesiadka, J. **Towards Complete Cofactor arrangement in the 3.0 Å Resolution Structure of Photosystem II**. *Nature* **2005**, *438*, 1040-1044.

(29) Barber, J.; Ferreira, K.; Maghlaoui, K.; Iwata, S. **Structural Model of the Oxygen-Evolving Center of Photosystem II with Mechanistic Implications**. *Phys. Chem. Chem. Phys*. **2004**, *6*, 4737-4742.

(30) Tommos, C.; Babcock, G. T. **Oxygen Production in Nature: A Light-Driven Metalloradical Enzyme Process**. *Accts. Chem. Res.* **1998**, *31*, 18-25.

(31) Hoganson, C. W.; Babcock, G. T.; **A Metalloradical Mechanism for the Generation of Oxygen from Water in Photosynthesis**. *Science* **1997**, *277*, 1953-1956.

(32) Krishtalik, L. I. **Activation Energy of Photosynthetic Oxygen Evolution: An Attempt at Theoretical Analysis**. *Bioelectrochem. Bioenerg*. **1990**, *23*, 249-263.

(33) Krishtalik, L. I. **Energetics of Multielectron Reactions. Photosynthetic Oxygen Evolution**. *Biochim. Biophys. Acta* **1986**, *849*, 162-171.

(34) Krishtalik, L. I. **pH-Dependent Redox Potential: How to use it Correctly in the Activation Energy Analysis**. *Biochim. Biophys. Acta*. **2003**, *1604*, 13-21.

(35) Tommos, C.; Hoganson, C. W.; Di Valentin, M.; Lydakis-Simantiris, N.; Dorlet, P.; Westphal, K.; Chu, H.-A.; McCracken, J.; Babcock,G. T. **Manganese and Tyrosyl Radical Function in Photosynthetic Oxygen Evolution**. *Curr. Opin. Chem. Biol.* **1998**, *2*, 244-252.

(36) Rappaport, F.; Guergova-Kuras, M.; Nixon, P. J.; Diner, B. A.; Lavergne, J. **Kinetics and Pathways of Charge Recombination in Photosystem II**. *Biochemistry* **2002**, *41*, 8518-8527.

(37) Westphal, K. L.; Lydakis-Simantiris, N.; Cukier, R. I.; Babcock, G. T. **Effects of Sr^{2+}-Substitution on the Reduction Rates of $Y_z^{\bullet}$ in PSII Membranes-Evidence for Concerted Hydrogen Atom Transfer in Oxygen Evolution**. *Biochemistry* **2000**, *39*, 16220-16229.

(38) Westphal, K. L.; Tommos, C.; Cukier, R. I.; Babcock, G. T. **Concerted Hydrogen-Atom Abstraction in Photosynthetic Water Oxidation**. *Curr. Opin. Plant Biol.* **2000**, *3*, 236-242.

(39) Herrero. C.; Lassalle-Kaiser. B.; Leibl. W.; Rutherford. A. W.; Aukauloo. A. **Artificial Systems Related to Light Driven Electron Transfer Processes in PSII**. *Coord Chem. Rev*. **2008**, *252*, 456-468.

(40) Binstead, R. A.; Moyer, B. A.; Samuels, G. J.; Meyer, T. J. **Proton-Coupled Electron Transfer between $[Ru(bpy)_2(py)OH_2]^{2+}$ and $[Ru(bpy)_2(py)O]^{2+}$. A Solvent Isotope Effect (k_{H_2O}/k_{D_2O}) of 16.1**. *J. Am. Chem. Soc.* **1981**, *103*, 2897-2899.

(41) Costentin, C. **Electrochemical Approach to the Mechanistic Study of Proton-Coupled Electron Transfer**. *Chem. Rev*. **2008**, *108*, 2145-2179.

(42) Cukier, R. I.; Nocera, D. G. **Proton-Coupled Electron Transfer**. *Annu. Rev. Phys. Chem.* **1998**, *49*, 337-369.

(43) Sjödin, M.; Styring, S.; Wolpher, H.; Xu, Y.; Sun, L.; Hammarström, L. **Switching the Redox Mechanism: Models for Proton-Coupled Electron Transfer from Tyrosine and Tryptophan**. *J. Am. Chem. Soc*. **2005**, *127*, 3855-3863.

(44) Hammes-Schiffer, S. **Proton Coupled Electron Transfer: Classification Scheme and Guide to Theoretical Methods**. *Energy and Environ. Sci.* **2012**, *5*, 7696-7703.

(45) Meyer, T. J.; Huynh, M.-H. V. **The Remarkable Reactivity of High Oxidation State Ruthenium and Osmium Polypyridyl Complexes**. *Inorg. Chem.* **2003**, *42*, 8140-8160.

(46) Costentin, C.; Robert, M.; Savéant, J.-M. **Concerted Proton-Electron Transfer Reactions in Water. Are the Driving Force and Rate Constant Depending on pH When Water Acts as Proton Donor or Acceptor?**. *J. Am. Chem. Soc.* **2007**, *129*, 5870-5879.

(47) Bonin, J.; Costentin, C.; Louault, C.; Robert, M.; Savéant, J.-M. **Water (in Water) as an Intrinsically Efficient Proton Acceptor in Concerted Proton Electron Transfer**. *J. Am. Chem. Soc*. **2011**, *133*, 6668-6674.

(48) Zhang, M.-T.; Hammarström, L. **Proton Coupled Electron Transfer from Tryptophan: A Concerted Mechanism with Water as Proton Acceptor**. *J. Am. Chem. Soc*. **2011**, *133*, 8806-8809.

(49) Posener, M. L.; Adams, G. E.; Wardman, P.; Cundall, R. B. **Mechanism of Tryptophan Oxidation by Some Inorganic Radical-Anions: A Pulse Radiolysis Study**. *J. Chem. Soc. Farad. Trans. 1* **1976**, 72, 2231-2239.

(50) Kaila, V. R. I.; Hummer, G. **Energetics of Direct and Water–Mediated Proton-Coupled Electron Transfer**. *J. Am. Chem. Soc*. **2011**, *133*, 19040-19043.

(51) Reece, S. Y.; Nocera, D. G. **Direct Tyrosine Oxidation Using the MLCT Excited States of Rhenium, Polypyridyl Complexes**. *J. Am. Chem. Soc.* **2005**, *127*, 9448-9458.

(52) Ishikita, H.; Soudackov, A. V.; Hammes-Schiffer, S. **Buffer-Assisted Proton-Coupled Electron Transfer in a Model Rhenium-Tyrosine Complex**. *J. Am. Chem. Soc*., **2007**, *129*, 11146-11152.

(53) Prigogine, I.; Rice, S. A. *Adv. Chem. Phys.,* **2000** *Vol 111;* Zundel, G. **Hydrogen Bonds with Large Proton Polarizability and Proton Transfer Processes in Electrochemistry and Biology**. Pp 1-218.

(54) Eigen, M. **Proton Transfer, Acid-Base Catalysis and Enzymatic Hydrolysis**. *Angew. Chem. Int. Ed.* **1964**, *3*, 1-19.

(55) Markovitch, O.; Agmon, N. **Structure and Energetics of the Hydronium Hydration Shells**. *J. Phys. Chem. A* **2007**, *111*, 2253-2256.

(56) Vuilleumier, R.; Borgis, D. **Transport and Spectroscopy of the Hydrated Proton: A Molecular Dynamics Study**. *J. Chem. Phys.,* **1999**, *111*, 4251-4266.

(57) Lapid, H.; Agmon, N.; Petersen, M. K.; Voth, G. A. **A Bond-Order Analysis of the Mechanism for Hydrated Proton Mobility in Liquid Water**. *J. Chem. Phys.* **2005**, *122*, 14506-14511.

(58) Marx, D.; Tuckerman, M. E.; Hutter, J.; Parrinello, M. **The Nature of the Hydrated Proton in Water**. *Nature* **1999**, *397*, 601-604.

(59) Park, S.-Y.; Lee, Y.-S.; Kwon, O.-H.; Jang, D.-J. **Transport of Water in Acid-Base Reactions of 7-hydroxyquinoline**. *Chem. Commun.* **2009**, 926-928.

(60) Mohammed, O. F.; Pines, D.; Dreyer, J.; Pines, E.; Nibbering, E. T. J. **Sequential Proton Transfer Through Water Bridges in Acid-Base Reactions**. *Science* **2005**, *310*, 83-86.

(61) Lee, H. J.; Svahn, E.; Swanson, J. M. J.; Lepp, H.; Voth, G. A.; Brzezinski, P.; Gennis, R. B. **Intricate Role of Water in Proton Transport through Cytochrome *c* Oxidase**. *J. Am. Chem. Soc.* **2010**, *132*, 16225-16239.

(62) Xu, J.; Voth, G. A. **Redox-coupled Proton Pumping in Cytochrome *c* Oxidase: Further Insights from Computer Simulation**. *Biochim. Biophys. Acta Bioenerg.* **2008**, *1777*, 196-201.

63) Marcus, R. A. **Chemical and Electrochemical Electron-Transfer Theory**. *Annu. Rev. Phys. Chem*., **1964**, *15* 155-196.

(64) Hush, N. S. **Adiabatic Theory of Outer Sphere Electron-Transfer Reactions in Solution**. *Trans. Faraday Soc*., **1961**, *57*, 557-580.

(65) Hammes-Schiffer, S.; Hatcher, E.; Ishikita, H.; Skone, J. H.; Soudackov, A. V. **Theoretical Studies of Proton-Coupled Electron Transfer: Models and Concepts Relevant to Bioenergetics**. *Coord. Chem. Rev*. **2008**, *252*, 384-394.

(66) Hammes-Schiffer, S.; Stuchebrukhov, A. A. **Theory of Coupled Electron and Proton Transfer Reactions**. *Chem. Rev.* **2010**, *110*, 6939-6960.

(67) Chakraborty, A.; Pak Michael, V.; Hammes-Schiffer, S. **Development of Electron-Proton Density Functionals for Multicomponent Density Functional Theory**. *Phys. Rev. Lett.* **2008**, *101*, 153001.

(68) Barbara, P. F.; Meyer, T. J.; Ratner, M. A. **Contemporary Issues in Electron Transfer Research**. *J. Phys. Chem.* **1996**, *100*, 13148-13168.

(69) DeVault, D. *Quantum Mechanical Tunneling in Biological Systems*; Cambridge University Press: Cambridge, **1984**. Copyright 1984 Cambridge University Press.

(70) Hames-Schiffer, S. **Hydrogen Tunneling and Protein Motion in Enzyme Reactions**. *Acc. Chem. Res.* **2006**, *39*, 93-100.

(71) Iordanova, N.; Hammes-Schiffer, S. **Theoretical Investigation of Large Kinetic Isotope Effects for Proton-Coupled Electron Transfer in Ruthenium Polypyridyl Complexes**. *J. Am. Chem. Soc.* **2002**, *124*, 4848-4856.

(72) Binstead, R. A.; Meyer, T. J. **Hydrogen-Atom Transfer between Metal Complexes Ions in Solution**. *J. Am. Chem. Soc.* **1987**, *109*, 3287-3297.

(73) Moyer, B. A.; Meyer, T. J. **Oxobis(2,2′-bipyridine)pyridineruthenium(IV) Ion, $[(bpy)_2(py)Ru{=}O]^{2+}$**. *J. Am. Chem. Soc.* **1978**, *100*, 3601-3603.

(74) Georgievskii, Y.; Stuchebrukhov, A. A. **Concerted Electron and Proton Transfer: Transition from Nondiabatic to Adiabatic Proton Tunneling**. *J. Chem. Phys.* **2000**, *113*, 10438-10450.

75) Gagliardi, C. J.; Vannucci, A. K.; Concepcion J. J.; Chen, Z.; Meyer, T. J. **The Role of Proton Coupled Electron Transfer in Water Oxidation**. *Energy and Environ. Sci.* **2012***, 5*, 7704-7717.

(76) Reece, S. Y.; Hodgkiss, J. M.; Stubbe, J.; Nocera, D. G. **Proton-Coupled Electron Transfer: The Mechanistic Underpinning for Radical Transport and Catalysis in Biology**. *Philos. Trans. R. Soc. B* **2006**, *361*, 1351-1364.

(77) Reece, S. Y.; Seyedsayamdost, M. R.; Stubbe, J.; Nocera, D. G. **Direct Observation of a Transient Tyrosine Radical Competent for Initating Turnover in a Photochemical Ribonucleoride Reductase**. *J. Am. Chem. Soc.* **2007**, *129*, 13828-13830.

(78) Minnihan, E. C.; Seyedsayamdost, M. R.; Stubbe, J. **Use of 3-Aminotyrosine To Examine the Pathway Dependence of Radical Propagation in *Escherichia coli* Ribonucleotide Reductase**. *Biochemistry* **2009**, *48*, 12125-12132.

(79) Offenbacher, A. R.; Vassiliev, I. R.; Seyedsayamdost, M. R.; Stubbe, J.; Barry, B. A. **Redox Linked Structural Changes in Ribonucleotide Reductase**. *J. Am. Chem. Soc.* **2009**, *131*, 7496-7497.

(80) Aubert, C.; Vos, M. H.; Mathis, P.; Eker, A. P. M.; Brettel, K. **Intraprotein Radical Transfer During Photoactivation of DNA Photolyase**. *Nature* **2000**, *405*, 586-590.

(81) Lukacs, A.; Eker, A. P. M.; Byrdin, M.; Brettel, K.; Vos, M. H. **Electron Hopping through the 15 Å Triple Tryptophan Molecular Wire in DNA Photolyase Occurs within 30 ps**. *J. Am. Chem. Soc.* **2008,** *130***,** 14394-14395.

(82) Byrdin, M.; Villette, S.; Espagne, A.; Eker, A. P. M.; Brettel, K. **Polarized Transient Absorption To Resolve Electron Transfer between Tryptophans in DNA Photolyase**. *J. Phys. Chem. B* **2008**, *112*, 6866-6871.

(83) Byrdin, M.; Villette, S.; Eker, A. P. M.; Brettel, K. **Observation of an Intermediate Tryphtophanyl Radical in W306F Mutant DNA Photolyase from *Escherichia coli* Supports Electron Hopping along the Triple Tryptophan Chain**. *Biochemistry* **2007**, *46*, 10072-10077.

(84) Byrdin, M.; Lukacs, A.; Thiagarajan, V.; Eker, A. P. M.; Brettel, K.; Vos, M. H. *J.* **Quantum Yield Measurements of Short-Lived Photoactivation Intermediates in DNA Photolyase: Toward a Detailed Understanding of the Triple Tryptophan Electron Transfer Chain**. *J. Phys. Chem. A* **2010**, *114*, 3207-3214.

(85) Langenbacher, T.; Immeln, D.; Dick, B.; Kottke, T. **Microsecond Light-Induced Proton Transfer to Flavin in the Blue Light Sensor Plant Cryptochrome**. *J. Am. Chem. Soc.* **2009**, *131*, 14274-14280.

(86) Lukacs, A.; Eker, A. P. M.; Byrdin, M.; Villette, S.; Pan, J.; Brettel, K.; Vos, M. H. **Role of the Middle Residue in the Triple tryptophan Electron Transfer Chain of DNA Photolyase: Ultra Fast Spectroscopy of a Trp→Phe Mutant**. *J. Phys. Chem. B* **2006**, *110*, 15654-15658.

(87) Knapp, M. J.; Rickert, K.; Klinman, J. P. **Temperature-Dependent Isotope Effects in Soybean Lipoxygenase-1: Correlating Hydrogen Tunneling with Protein Dynamics**. *J. Am. Chem. Soc.* **2002**, *124*, 3865-3874.

(88) Hatcher, E.; Soudackov, A.; Hammes-Schiffer, S. **Proton-Coupled Electron Transfer in Soybean Lipoxygenase**. *J. Am. Chem. Soc.* **2004**, *126*, 5763-5775.

(89) Costentin, C.; Rober, M.; Savéant, J.-M. **Concerted Proton-Electron Transfers: Electrochemical and Related Approaches**. *Accts. Chem. Res*. **2010**, 43, 1019-1029.

(90) Ison, A.; Odeh, I. H.; Margerum, D. W. **Kinetics and Mechanisms of Chlorine Dioxide and Chlorite Oxidations of Cysteine and Glutathione**. *Inorg. Chem.* **2006**, *45*, 8768-8775.

(91) Rudolph, M.; Reddy, D. P.; Feldberg, S. W. **A Simulator for Cyclic Votammetric Responces**. *Anal. Chem*., **1994**, *66*, 598A-600A.

Chapter 2

Surface Activation of Electrocatalysis at Oxide Electrodes. Concerted Electron-Proton Transfer (EPT)[a]

2.1 Abstract: Dramatic rate enhancements are observed for oxidation of phenols, including tyrosine, at ITO electrodes modified by addition of the electron transfer relays $[M^{II}(bpy)_2(4,4'\text{-}(HO)_2P(O)CH_2)_2bpy)]^{2+}$ (M = Ru, Os) with clear evidence for the importance of proton coupled electron transfer (PCET) and concerted electron-proton transfer (EPT). Additional increased rate enhancements are observed in the presence of proton accepting bases increasing with pK_a, a systematic analysis of these effects with ITO electrodes modified with two different surface bound mediators in included.

2.2 Introduction: Conducting oxide electrodes such as ITO, tin-doped In_2O_3 (In_2O_3:Sn), and FTO, fluorine-doped SnO_2, are commonly used in electrochemistry. For reversible couples in nonaqueous solvents, ITO and FTO behave similarly to typical metal or carbon electrodes. However, for small organic molecules in aqueous solution there is often no electrochemical response within the solvent limit. This effect has been exploited, for example, to study amino acid oxidation by diffusional couples such as $Ru(bpy)_3^{III/II}$.[1,2] The absence of facile

[a] Reproduced with permission from the American Chemical Society; Christopher J. Gagliardi, Jonah W. Jurss, H. Holden Thorp and Thomas J. Meyer **Surface Activation of Electrocatalysis at Oxide Electrodes. Concerted Electron-Proton Transfer (EPT)**. *Inorg. Chem.* **2011**, *50*, 2076-2078. © American Chemical Society 2011.

electrochemistry at these electrodes considerably limits their application in analytical and electrocatalytic applications.[1-3]

In an earlier study we reported surface catalysis of water oxidation at ITO derivatized by surface binding of the electron transfer relay $[Ru^{II}(bpy)(4,4'\text{-}(HO)_2P(O)CH_2)_2bpy)_2]^{2+}$ (bpy = 2,2′-bipyridine; 4,4′-$(HO)_2P(O)CH_2)_2$bpy = 4,4′-bis-methylenephosphonato-2,2′-bipyridine).[4] Here we report dramatic rate enhancements for oxidation of the phenols - tyrosine (TyrOH), tyrosine methyl ester (MeC(O)O-TyrOH, TyrOMe), *N*-acetyl-tyrosine (NAceTyr) and 4-methylphenol(4-MeArOH) (Figure 1) at ITO electrodes modified by surface attached $[Ru^{II}(bpy)_2(4,4'\text{-}(HO)_2P(O)CH_2)_2bpy)]^{2+}$ (**ITO-Ru^{II}**) and ITO bound $[Os^{II}(bpy)_2(4,4'\text{-}(HO)_2P(O)CH_2)_2bpy)]^{2+}$ (**ITO-Os^{II}**) with important implications for electrocatalysis and analysis at these surfaces. We also provide clear evidence for an important role for proton coupled electron transfer (PCET) and concerted electron-proton transfer (EPT) pathways in surface electrochemical reactivity.

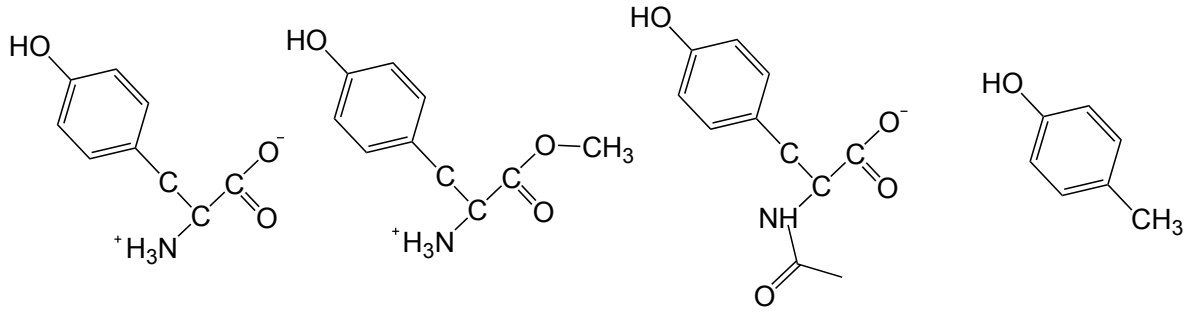

tyrosine **tyrosine-methyl-ester** ***N*-acetyl-tyrosine** **4-methylphenol**

Figure 1. The phenols - tyrosine (TyrOH), tyrosine methyl ester (MeC(O)O-TyrOH), *N*-acetyl-tyrosine (NAceTyr) and 4-methylphenol (4-MeArOH).

Surface phosphonate binding to oxide electrodes including ITO, FTO, and nanostructured TiO_2 is well documented.[5-10] We prepared **ITO-Ru^{II}** and **ITO-Os^{II}** by soaking slides in solutions containing $1x10^{-4}$ M complex in 0.1M HNO_3 or $HClO_4$ for 4h followed by rinsing with methanol.[4] Different surface loadings were studied by soaking slides in solutions

containing lower concentrations of complex. The surface coverage was determined by cyclic voltammetry (CV) by peak current measurements as described below.[11]

The electrochemistry of phenols, including the role of PCET, has been studied in detail by Savéant and coworkers at glassy carbon electrodes.[3] As shown in Figure 2 at ITO there is no electrochemical response with the added amino acid tyrosine to the background limit at ~1.6 V vs NHE from pH = 1 to 8. A similar lack of electrochemical signal is also observed for tyrosine methyl ester, *N*-acetyl-tryrosine and 4-methylphenol (Figure 3).

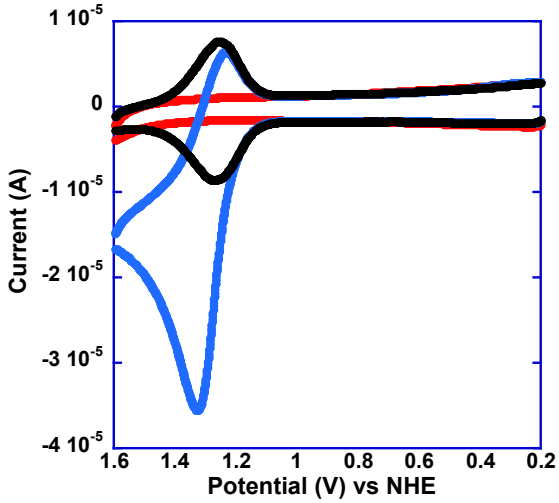

Figure 2. Cyclic voltammograms (CV) of TyrOH (0.1 mM) in 0.1 M $HClO_4$/0.8M in $LiClO_4$ at 300 mV/s, at ITO (red), at **ITO-Ru^{II}** (Γ = 1.2x10^{-10} mol/cm^2, black, see text) and at **ITO-Ru^{II}** + TyrOH at 25±2 °C (blue).

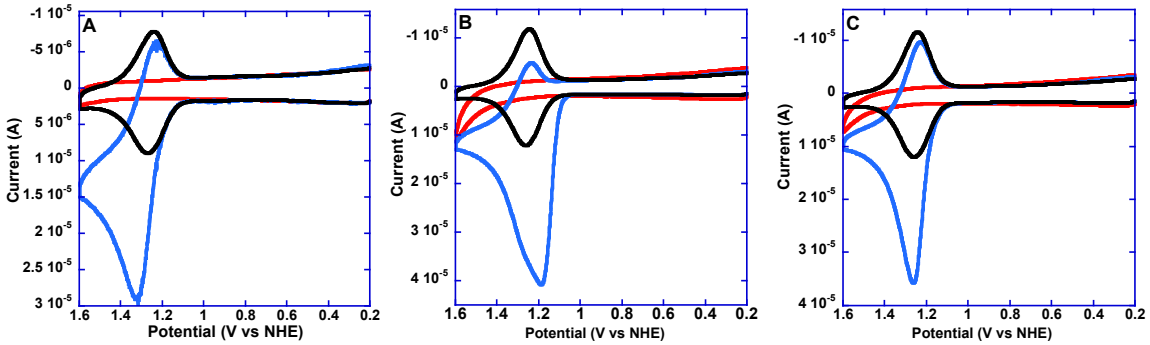

Figure 3. (**A**) Cyclic voltammogram (CV) at plain ITO (red), at **ITO-Ru^{II}** (black), and at **ITO-Ru^{II}** with 0.1 mM TyrOMe (blue) in 0.1 M $HClO_4$, and 0.8M $LiClO_4$, at 25 ± 2 °C and υ = 300 mV/s. (**B**) CV of 4-MeArOH under identical conditions as in A (**C**) CV of NAceTyr under identical conditions as A.

Surface modification results in dramatic changes in electrochemical response for the four phenols. At **ITO-Ru^{II}** in aqueous solution, a reversible surface wave appears for the **ITO-Ru$^{III/II}$** couple at 1.25 V vs NHE. With added TyrOH in 0.1 M $HClO_4$/0.8 M $LiClO_4$, an additional, irreversible wave appears for the pH dependent TyrO$^{\bullet}$/TyrOH couple at E_p = 1.33V vs NHE.[3] As shown in Fig. 4, the peak current (i_p) varies with scan rate (ν) for the **ITO-Ru$^{III/II}$** surface couple and with $\nu^{1/2}$ for the TyrO$^{\bullet}$/TyrOH couple as predicted for surface and diffusional couples, respectively.[12] Similar results were obtained for both the ester and phenol.

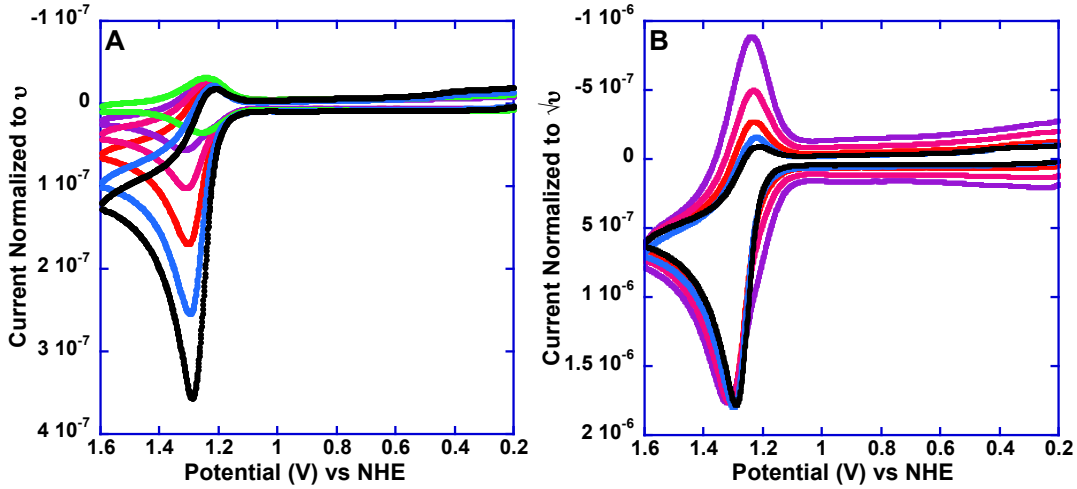

Figure 4. Scan rate dependent CVs of 0.1 mM TyrOMe at **ITO-Ru^{II}** normalized to either (**A**) scan rate (υ) or (**B**) square root of scan rate ($\upsilon^{1/2}$). Solution conditions were 0.1 M $HClO_4$, I = 0.8M $LiClO_4$, at 25 ± 2 °C. CVs were collected with a scan rate of 25 mV/s (black), 50 mV/s (blue), 100 mV/s (red) 300 mV/s (pink), 1000 mV/s (purple), No TyrOMe, 300 mV/s (green).

2.3 Methods and Materials

2.3.1 General: Deionized water was purified by passing in-house distilled water through a MilliQ deionizing system (18Ω) and was used to prepare all aqueous solutions. All buffers were purchased from Sigma Aldrich (St. Louis, MO) and used as received.

2.3.2 Reaction Solutions: Buffered aqueous solutions were prepared with H_2O purified with a MilliQ purification system (Model: Synthesis A10) with $LiClO_4$ at 0.8 M to maintain

constant ionic strength. The total buffer concentration was kept at 0.05 M unless otherwise mentioned. All buffers (acetate, citrate, phosphate, and Tris), perchloric acid ($HClO_4$), tyrosine (TyrOH) *N*-methyl-tyrosine (tyrosine-methyl-ester, TyrOMe), *p*-methylphenol (4-MeArOH), and *N*-acetyl-tyrosine (NAceTyr) were purchased from Sigma Aldrich (St. Louis, MO) and used as received. Buffered solutions were brought to the correct pH using $HClO_4$ or LiOH using a Fisher Scientific Accumet Basic model AB15 pH meter. Buffer concentrations were kept at a 10:1 acid to base ratio to favor the concerted PCET pathway shown in the derived rate law (Appendix 1) for competing EPT and PT-ET pathways, which is further discussed below and illustrated in scheme 1.[1]

2.3.3 Deuterated Reaction Solutions and Kinetic Isotope Experiments: All deuterated solutions were prepared from deuterium oxide (99%) purchased from Cambridge isotope labs (Andover, MA) and brought to the desired pD using an H_2O calibrated a Fisher Scientific Accumet Basic model AB15 pH meter (in D_2O, pD = pH meter reading + 0.4). All solutions were adjusted with $DClO_4$, DCl or NaOD purchased from Cambridge isotope labs (Andover, MA). H/D exchange in all phenol substrates was assumed to be instantaneous.

Scheme 1.

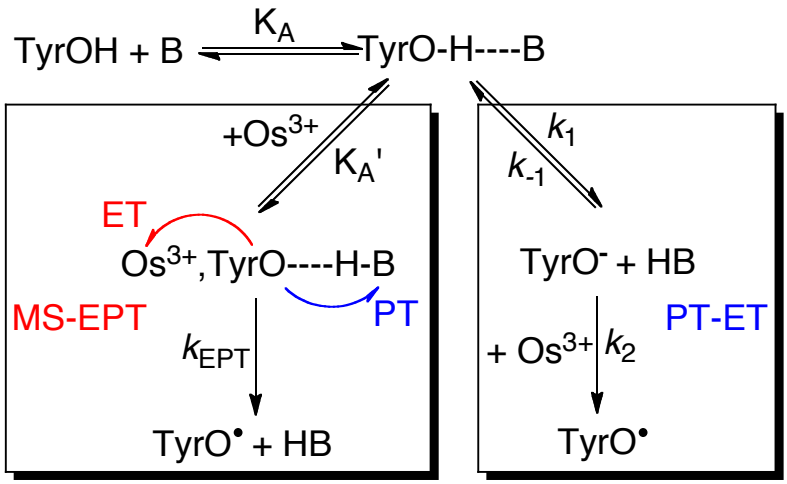

2.3.4 Sample and Electrode Preparation: $M(bpy)_2(4,4'\text{-}(HO)_2P(O)CH_2)_2bpy)$, M = Os, Ru complexes were prepared according to literature procedures.[5] Phosphonated bipyridine ligand ($(4,4'\text{-}(HO)_2P(O)CH_2)_2bpy$), bpy = 2,2′-bipyridine) was prepared according to a literature procedure.[5,11] $M(bpy)_2(4,4'\text{-}(HO)_2P(O)CH_2)_2bpy)$ modified electrodes were prepared by soaking an ITO electrode in $1x10^{-4}$ M complex in either 0.1 M nitric acid or perchloric acid for 4h. Samples prepared in perchloric acid were soaked for an additional 4h in clean 0.1 M perchloric acid in order to remove additional complex from the surface.[4] All slides were rinsed with methanol and allowed to dry in air. Full 100% surface coverage was calculated to be $1.2x10^{-10}$ mol/cm^2.[4,5,11,13] Surface coverage was quantified electrochemically using the equation $\Gamma = Q/nFA$ where Γ is the surface coverage in mol/cm^2, Q is the integrated area of the oxidative peak in coulombs, n (=1)[1] is the number of electrons transferred in the reaction, F is 96,485 C/mol and A is the area of the electrode in cm^2 (A = 0.32 cm^2).[4,11] Binding constants for surface attachment were measured in 0.1 M $HClO_4$ at 298 K, which gave K = $2x10^7$ M^{-1} and $2x10^6$ M^{-1} for M = Ru and Os, respectively.

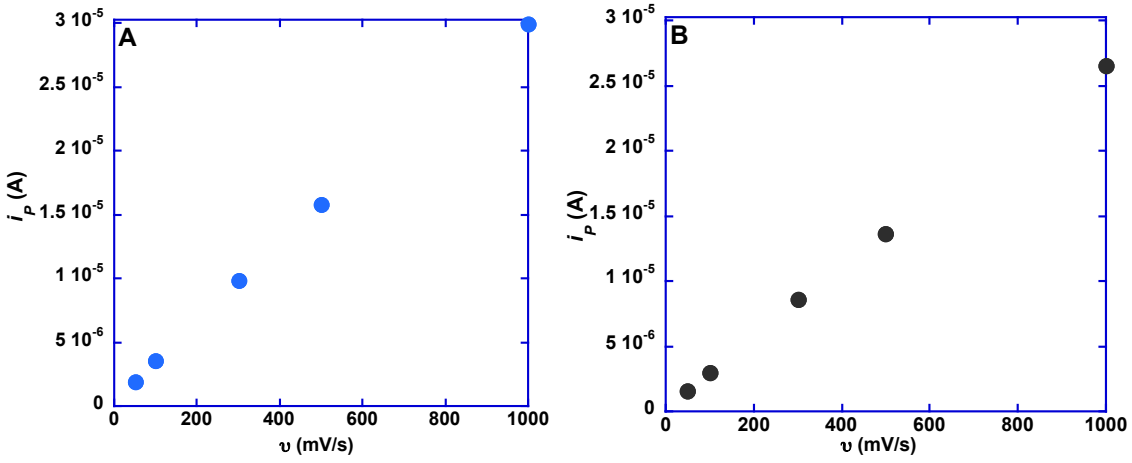

Figure 5. Scan Rate Dependence for $M(bpy)_2(4,4'\text{-}(HO)_2P(O)CH_2)_2bpy)$, M = (**A**) Ru, (**B**) Os. Solution conditions were 0.1 M $HClO_4$, I = 0.8M $LiClO_4$, at 25 ± 2 °C, Γ = 1.

2.3.5 Electrochemistry: All electrochemical experiments were performed with a CH Instruments (CHI) model 601D potentiostat. Electrochemical measurements were performed in a previously described cell.[14] Sample volumes for each experiment were typically 100 μL. Tin-doped indium oxide coated glass (ITO) was used as a working electrode (area 0.32 cm^2), purchased from Delta Technologies (Stillwater, MN). ITO was cleaned by sonicating in water, 2-propanol, and then water (2x) for 15 minutes each. The Ag/AgCl reference electrode (+0.197 V vs NHE) was purchased from Cyprus Systems Inc. (Lawrence, KS) and a platinum wire was used as the auxiliary electrode. Before acquiring cyclic voltammetry traces, at least 6 background scans of both surface modified and plain electrodes were taken of buffer or acid alone through the potential range of the experiment.

2.3.6 Thermodynamics: Values for $E_{1/2}$ were calculated using equation 1. Free energy calculations (in eV) were made according to the equation 2. The pK_a for $TyrOH^{\bullet+}$ used was -2[15,16], pK_a values for all bases (HB) used are also reported in the manuscript. The potential used for the $TyrOH^{\bullet+/0}$ couple in both following equations is 1.46 V vs NHE.[2,17] Formal potentials, E°′, for the $[M(bpy)_2(4,4'\text{-}(HO)_2P(O)CH_2)_2bpy)]^{III/II}$ couples, M = Os, Ru are 0.80 V and 1.25 V vs NHE respectively.

$$E^{\circ\prime} \sim E_{1/2}(TyrOH^{\bullet+/0}) + 0.059\{pK_a(TyrOH^{\bullet+}) - pK_a(HB)\} \quad (1)$$

$$\Delta G^{\circ\prime} = -F\{E^{\circ\prime}(M(bpy)_2(CH_2pbpy)^{III/II}) - (E^{\circ\prime}(TyrOH^{\bullet+/0})\} + 0.059\{pK_a(TyrOH^{\bullet+}) - pKa(HB)\} \quad (2)$$

2.4 Results and Discussion

2.4.1 Measurement of Rate Constants: Peak currents for the TyrOH oxidation wave, i_p, vary linearly with [TyrOH] (50 -150 μM) and linearly with Ru^{II} surface coverage from $\Gamma/\Gamma_o = 1$ (monolayer surface coverage: $\Gamma_o = 1.2x10^{-10}$ mol/cm^2) to $4.2x10^{-11}$ mol/cm^2 ($\Gamma/\Gamma_o = 0.35$),

Figure 6. The peak potential at pH = 1 (1.33V), is consistent with E°′ ≈ 1.5 V for the $TyrOH^{\bullet+}$/TyrOH couple and pK_a = -2 for $TyrOH^{\bullet+}$.[15,16,18,19]

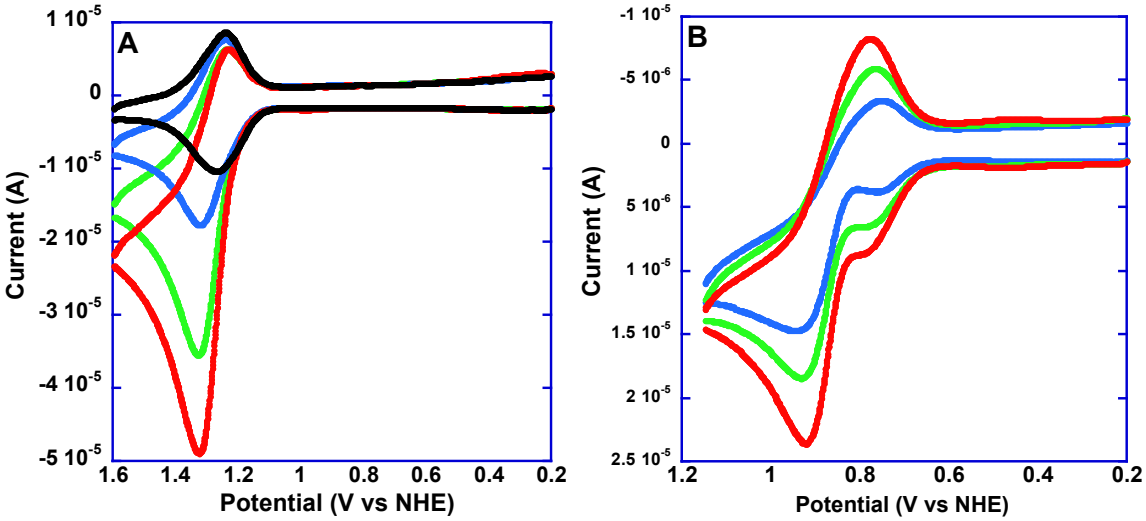

Figure 6. (**A**) Tyrosine concentration dependence CVs at **ITO-Ru^{II}**, I = 0.8M $LiClO_4$,0.1M $HClO_4$ and υ = 300 mV/s; 0.15 mM TyrOH (red) 0.1M TyrOH (green), 0.05mM TyrOH (blue) and **ITO-Ru^{II}** (black) (**B**) **ITO-Os^{II}** surface loading (Γ/Γ_o) dependence with 50 mM tris buffer, pH 7.1, 10:1 acid:base, 0.1mM TyrOH and I = 0.8M $LiClO_4$; Γ/Γ_o = 1 (red), 0.72 (green), and 0.35 (blue).

The experimental observations are consistent with surface activation of electron transfer by the mechanism shown in Scheme 2. In this mechanism, rapid surface oxidation of **ITO-Ru^{II}** to **ITO-Ru^{III}** is followed by rate limiting interfacial oxidation of TyrOH to $TyrOH^{\bullet+}$ by electron transfer.[20-22] The surface **ITO-Ru$^{III/II}$** couple is electrochemically reversible over a wide range of scan rates; the rate constant for $Ru(bpy)_3^{III/II}$ self exchange in solution is ~10^9 $M^{-1}s^{-1}$.[23]

Scheme 2.

$$ITO\text{-}Ru^{2+} \overset{e^-}{\rightleftharpoons} ITO\text{-}Ru^{3+}$$

$$ITO\text{-}Ru^{3+} + TyrOH \rightleftharpoons ITO\text{-}Ru^{3+},TyrOH: K_A$$

$$ITO\text{-}Ru^{3+},TyrOH \longrightarrow ITO\text{-}Ru^{2+} + TyrOH^{\bullet+}: k_{ET}$$

$$2TyrOH^{\bullet+} \longrightarrow (TyrO)_2 + 2H^+$$

A rate constant for surface oxidation of TyrOH was obtained by peak current measurements and the expression, $i_{cat} = nFAk_{cat}\Gamma[TyrOH]$, with i_{cat} the catalytic current, n the number of electrons transferred assumed to be 1, A the surface area, Γ the surface coverage of **ITO-Ru^{II}** in mol/cm^2, and k_{cat} the surface catalytic rate constant.[24] As shown by the plot of $i_{cat}/nFA\Gamma$ vs. [TyrOH] in Figure 7, k_{cat} varies with [TyrOH] and from the slope, k = 8.0x10^4 M^{-1}s^{-1} at 25±2 °C in 0.1M $HClO_4$, 0.8M $LiClO_4$. For the solution oxidation of TyrOH by $Ru(bpy)_3^{3+}$ under comparable conditions, $k = K_A k_{ET}$ = 3.0x10^5 M^{-1}s^{-1}.[1,2]

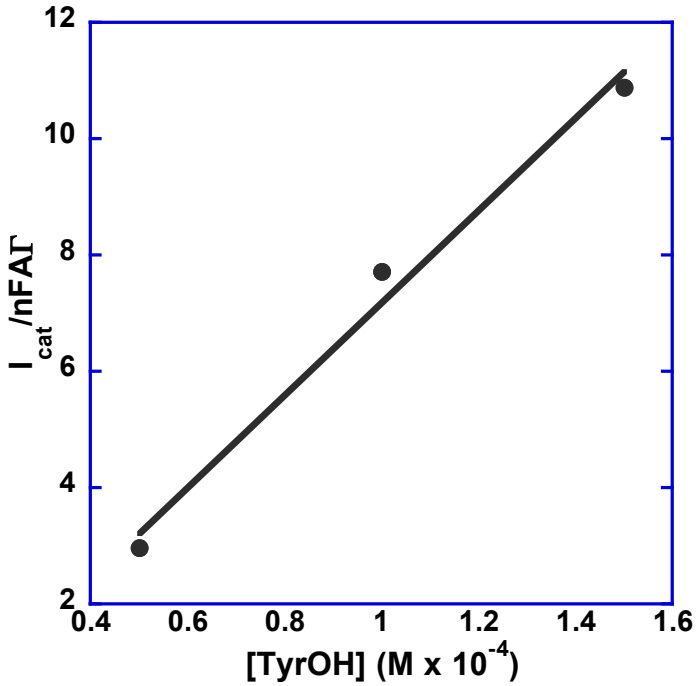

Figure 7. $i_{cat}/nFA\Gamma$ vs [TyrOH] (M) for tyrosine concentration dependence at **ITO-Ru^{II}**, I = 0.8M $LiClO_4$, 0.1M $HClO_4$, υ = 300 mV/s, Γ/Γ_o = 1, slope = $k_{obs,ET}$ = 8.0x10^4 M^{-1}s^{-1}.

In contrast to phenol oxidation at glassy carbon,[3] the H_2O/D_2O kinetic isotope (KIE) is small with k_{H_2O}/k_{D_2O} ~ 1.2, consistent with electron transfer as the dominant redox step at the electrode rather than concerted electron-proton transfer with proton transfer to the solvent.

2.4.2 Catalytic Buffer Effects: As shown in Figure 8, there is evidence for an additional catalytic effect with added acetate (10:1 HOAc/OAc^- at pH = 3.7), citrate (10:1 $H_3C_6H_5O_7/H_2C_6H_5O_7^-$ at pH 5.4) or phosphate (10:1 $H_2PO_4^-/HPO_4^{2-}$ at pH = 6.2) buffers. At high, limiting buffer base concentrations, 4.5 mM, and a scan rate of 300 mV/sec, E_p shifts to 1.24, 1.20, and 1.18 V, respectively. This is a buffer base effect and not a pH effect. As noted in Figure 9 for the HOAc/OAc^- buffer, E_p is virtually unaffected by pH changes from 3.8 to 5.8 at [OAc^-] = 4.5 mM. In solutions dilute in citrate buffer (pH 5.4, 0.01mM), there is no buffer effect with E_p = 1.24 V, the same value as in 10^{-3} M $HClO_4$ (Fig 9). The shift in E_p to 1.24 V in 10^{-3} M $HClO_4$ and dilute $1x10^{-5}$ M HOAc/OAc^- buffer from 1.31 V in 0.1M $HClO_4$, shown in Figure 10 provides evidence for the participation of surface phosphonate groups with pK_a ~ 1.5 acting as an EPT acceptor base (Figure 11).[25] There is precedent for this in the literature where surface phosphonates have been suggested to act as a proton accepting in the oxidation of surface bound Ruthenium polypyridyl complex: $[Ru^{II}$(Mebimpy)(4,4′-bis-methlylenephosphonato-2,2′-bipyridine)$(OH_2)]^{2+}$, where Mebimpy = 2,6-bis(1-mehtylbenzimidazol-2-yl)pyridine.[25]

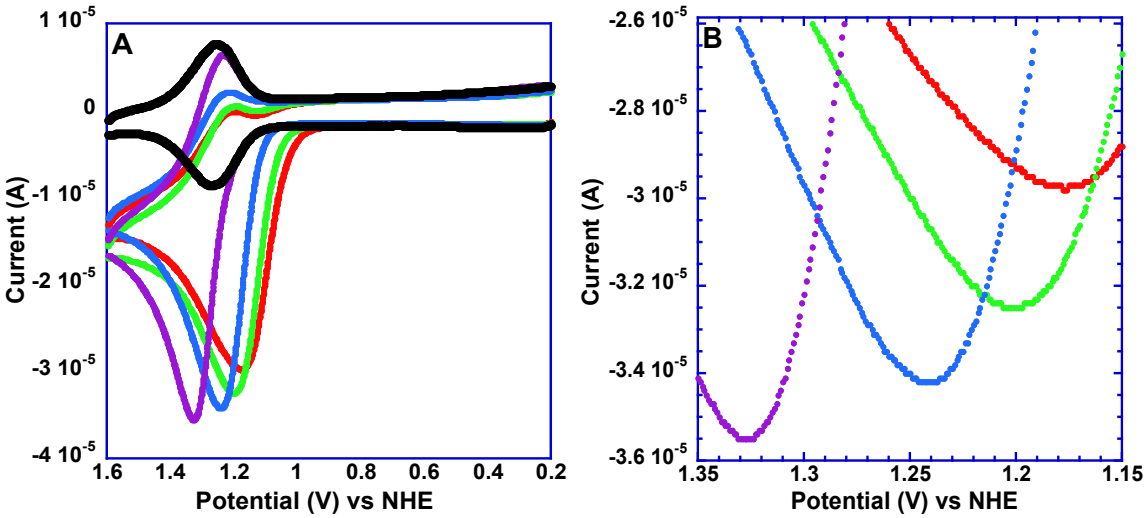

Figure 8. Cyclic voltammograms (CV) of TyrOH (0.1 mM) in 0.1 M $HClO_4$/0.8M in $LiClO_4$ at 300 mV/s, at ITO (**A**) in 0.1M $HClO_4$/0.8 M $LiClO_4$ (blue) and in 50 mM buffers, 4.55 mM in buffer base at a 10:1 acid:base buffer ratio of: acetate (purple- HOAc/OAc^-, pK_a 4.7 at pH 3.7); citrate (green- $H_3C_6H_5O_7/H_2C_6H_5O_7^-$, p$K_a$ 6.4 at pH 5.4); phosphate (red- $H_2PO_4^-/HPO_4^{2-}$, pK_a 7.2 at pH 6.2); **ITO-Ru^{II}** (black). (**B**) as in A, Close up of E_p shifts.

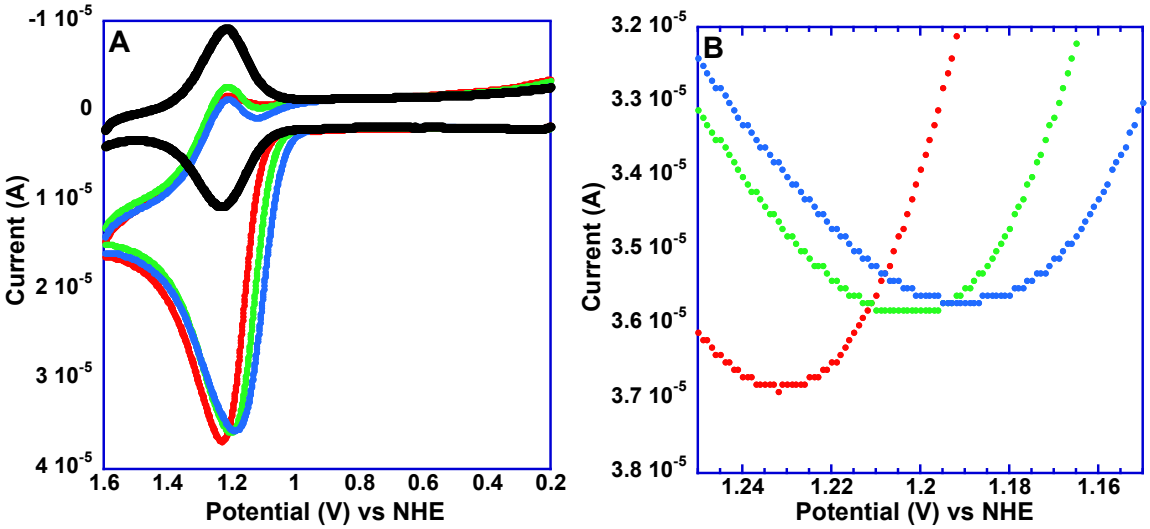

Figure 9. (**A**) CVs of 0.1 mM TyrOMe at **ITO-Ru^{II}**, I = 0.8M $LiClO_4$ and υ = 300 mV/s in 50 mM acetate buffer with constant [AcO^-] = 4.54 mM, pH 3.76 (red), [AcO^-/AcOH] = 9.09 mM, pH 4.76 (green) and [AcO^-/AcOH] = 4.99 mM, pH 5.76 (blue). (**B**) as in A, Close up of E_p shifts.

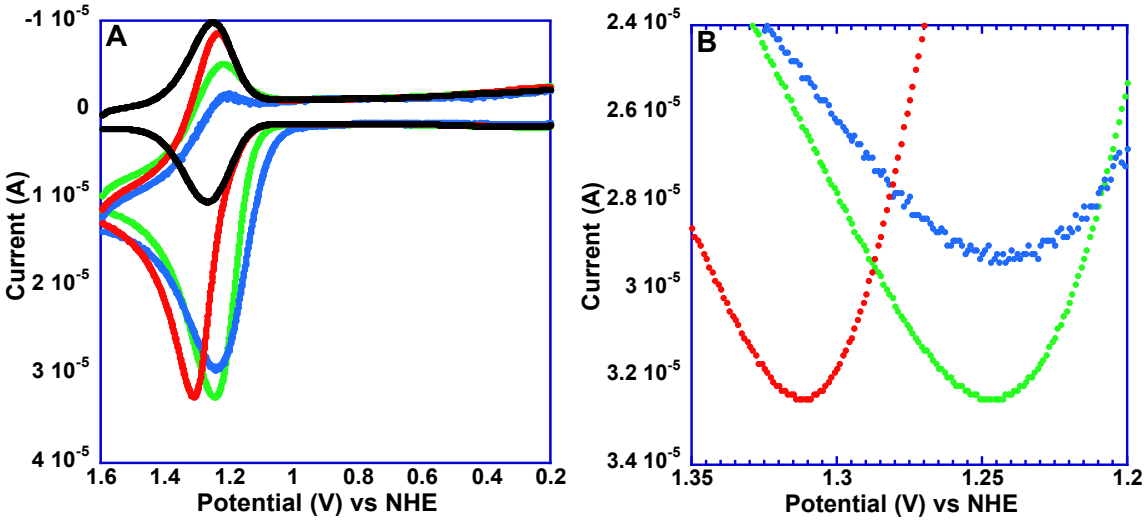

Figure 10. (**A**) CVs of 0.1 mM TyrOMe at **ITO-Ru^{II}**, I = 0.8M $LiClO_4$ and υ = 300 mV/s in 0.1 and 1x10^{-3} M $HClO_4$ and 1x10^{-5} M citrate buffer, ($H_3C_6H_5O_7/H_2C_6H_5O_7^-$). **ITO-Ru^{II}** (black); 10 μM citrate, pH 5.4 (blue), 1 mM $HClO_4$. (green), 0.1 M in $HClO_4$ (red). (**B**) as in A, Close up of E_p shifts.

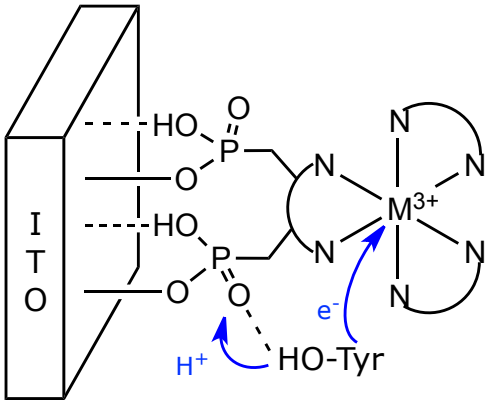

Figure 11. Illustrating surface MS-EPT with electron transfer to ITO-Ru^{3+} to Surface bound phosphonates (pK_a ~ 1.5) acting as a proton accepting base.

The trend in E_p values in Figure 8 follows the base strengths of the buffer bases with pK_a(HB) = 4.8, 6.4 and 7.2 for acetate, citrate, and HPO_4^{2-}, respectively. They are more positive than $E°'$ values for the pH dependent TyrO$^{\bullet}$/TyrOH couple with $E°'$ = 1.06 (pH 3.8), 0.96 (pH 5.4), and 0.92 (pH 6.2) V. These values were calculated from E°′(TyrOH$^{\bullet+}$/TyrOH) = 1.46 V and pK_a(TyrOH$^{\bullet+}$) = -2 (eq 1).[15,16,18,19]

Quantitative simulations of the CVs are not yet available, but the base effect is qualitatively consistent with the mechanism in Scheme 3. In this scheme, pre-association occurs with the buffer base to give the H-bonded adduct, TyrOH---B, followed by concerted, multi-site electron-proton transfer (MS-EPT) at the electrode with electron transfer to **ITO-Ru^{III}** and proton transfer to B, Figure 12. A related pathway has been identified in the oxidation of TyrOH by $M(bpy)_3^{3+}$ (M = Fe, Ru, Os) in solution.[1,2]

Scheme 3.

$$TyrOH + B \rightleftharpoons TyrOH\text{--}B: K_A$$

$$ITO\text{-}Ru^{2+} \overset{e^-}{\rightleftharpoons} ITO\text{-}Ru^{3+}$$

$$ITO\text{-}Ru^{3+} + TyrOH\text{--}B \rightleftharpoons ITO\text{-}Ru^{3+},TyrOH\text{--}B: K_A'$$

$$ITO\text{-}Ru^{3+},TyrOH\text{--}B \longrightarrow ITO\text{-}Ru^{2+} + TyrO^{\bullet} + {}^{+}HB: k_{EPT}$$

$$2TyrO^{\bullet} \longrightarrow (TyrO)_2$$

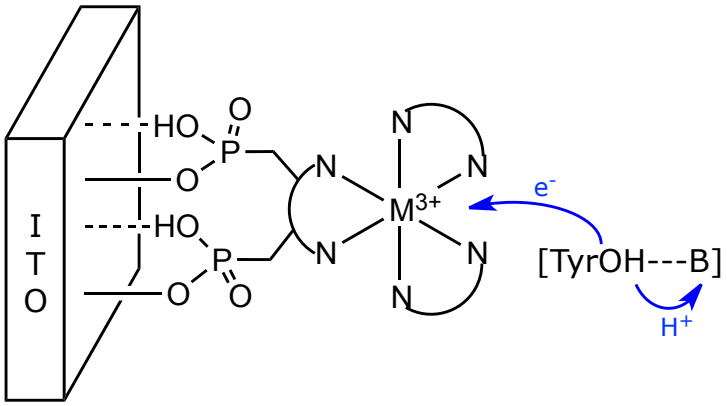

Figure 12. Illustrating surface MS-EPT with electron transfer to **ITO-Ru^{3+}** and proton transfer to an added buffer base, B, as proton acceptor.

As calculated from the expression, $E_{1/2}$(calc) ~ $E_{1/2}(TyrOH^{\bullet+/0})$ + $0.059\{pK_a(TyrOH^{\bullet+}) - pK_a(HB)\}$, E°′ values for the adduct couples in Scheme 3, TyrOH--B/$TyrO^{\bullet}$--$^{+}$H-B, are more positive than expected. For example, E_p = 1.24 V for OAc^- while $E_{1/2}$(calc) = 1.06V.[17] The waves are also scan rate dependent with E_p shifting to more negative potentials as the scan rate is decreased and i_p decreasing as E_p decreases, Figure 13.

These observations are qualitatively consistent with surface EPT rate limited by the low surface concentration of **ITO-Ru^{III}** at the potentials at which oxidation occurs. For the surface couple, $E_{1/2}$(**ITO-Ru$^{III/II}$**) = 1.25 V.

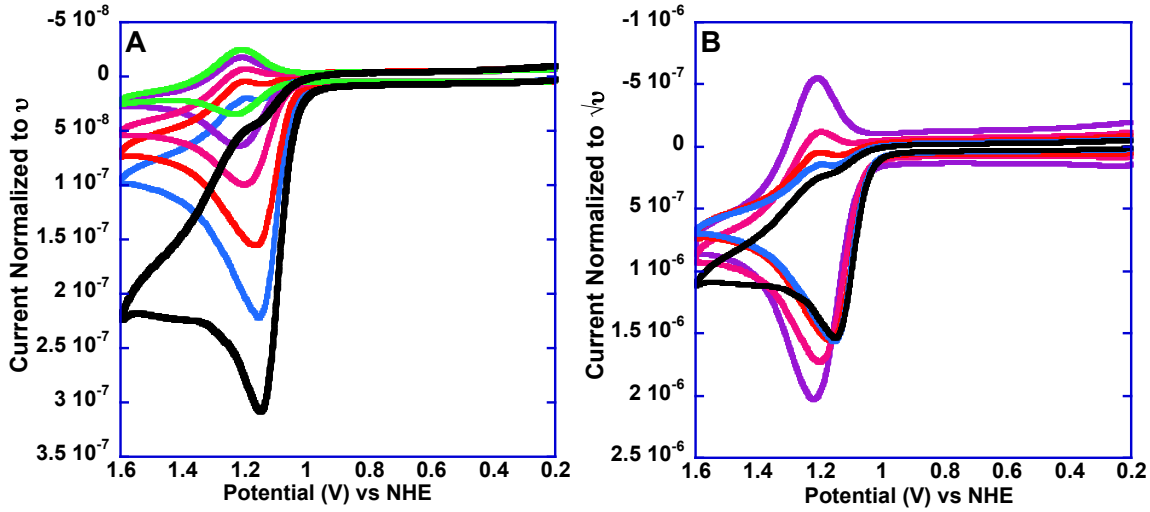

Figure 13. Scan rate dependent CVs of 0.1 mM TyrOMe at **ITO-Ru^{II}** normalized to either **A**) scan rate (υ) or **B**) square root of san rate ($\upsilon^{1/2}$). Solution conditions were 50 mM citrate buffer, pH 5.4, 10:1 acid to base buffer, I = 0.8M $LiClO_4$, at 25 ± 2 °C. CVs were collected with a scan rate of 25 mV/s (black), 50 mV/s (blue), 100 mV/s (red) 300 mV/s (pink), 1000 mV/s (purple), No TyrOMe, 300 mV/s (green), 80 mV E_p shift observed.

We have also observed electrocatalysis of phenol oxidation at **ITO-Os^{II}** based on the less strongly oxidizing **ITO-Os$^{III/II}$** couple with E°′ = 0.80 V. Oxidation of TyrOH by $Os(bpy)_3^{3+}$ in solution (pH = 7) is relatively slow with k_o (25±2 °C, I = 0.8 M) = 1.7x10^2 $M^{-1}s^{-1}$.[1] Significant rate enhancements are observed with added buffer bases. They arise from initial TyrOH--B adduct formation followed by MS-EPT oxidation with k values ranging from 2.0x10^5 (acetate pK_a($^+$HB) = 4.7) to 3.7x10^6 $M^{-2}s^{-1}$ (Tris, pK_a = 8.1). MS-EPT is in competition with proton transfer followed by electron transfer (PT-ET), Scheme 3.[2]

In Figure 13 are shown CVs of **ITO-Os^{II}** with added citrate (pK_a=6.4) and Tris (pK_a = 8.1) with and without added TyrOH at a scan rate of 300 mV/s. With added Tris (4.5 mM) significant electrocatalysis is observed. As shown in Figures 15 and 16, i_p for the surface

wave varies with ν and the TyrOH oxidation wave with $\nu^{1/2}$ as found for **ITO-Ru^{II}**. At constant [Tris], E_p for TyrOH oxidation varies with pH from 0.97 V at pH = 6.6 ($^+$HB/B = 31.6) to 0.91 V at pH = 7.6 ($^+$HB/B = 3.1). The pH dependence is consistent with the predicted pH dependence of the TyrO$^\bullet$/TyrOH couple, TyrOH $\xrightarrow{-e^-}$ TyrO$^\bullet$ + H$^+$.[3]

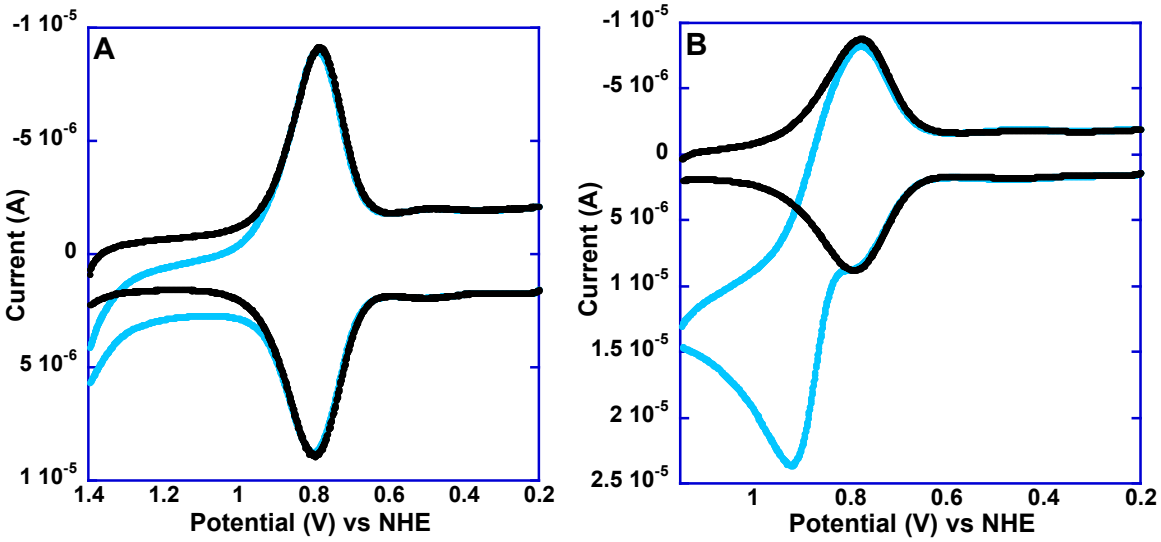

Figure 14. Oxidation of 0.1 mM tyrosine (blue) at **ITO-Os^{II}** ($E_{1/2}$ = 0.8V vs NHE; Γ/Γ_o = 1 (Γ_o = 1.2x10^{-10}; black) in 0.8M $LiClO_4$ at 300 mV/s with 50 mM added buffer (10:1 acid:base): (**A**) citrate ($H_3C_6H_5O_7/H_2C_6H_5O_7^-$), pH 5.4, (**B**) Tris ($(HOCH_2)_3CNH_3^+/(HOCH_2)_3CNH_2$), pH 7.1.

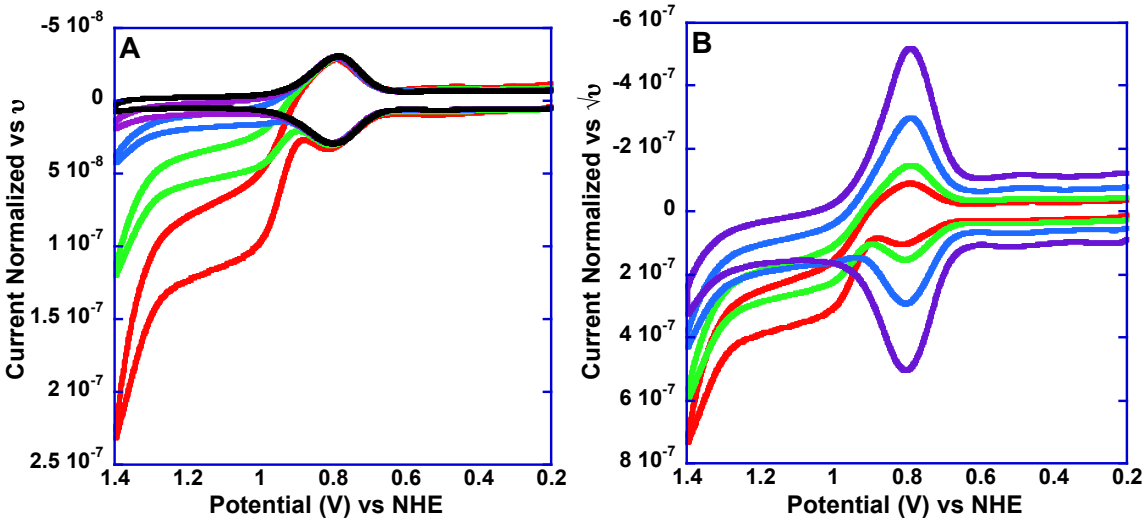

Figure 15. Scan rate dependent CVs of 0.1 mM TyrOH at **ITO-Os^{II}** normalized to either (**A**) scan rate (υ) or (**B**) square root of san rate ($\upsilon^{1/2}$). Solution conditions were 50 mM citrate buffer, pH 5.4, 10:1 acid to base buffer, I = 0.8M $LiClO_4$, at 25 ± 2 °C. CVs were collected with a scan rate of 10 mV/s (red), 25 mV/s (green), 100 mV/s (blue) 300 mV/s (purple), No TyrOH, 300 mV/s (black).

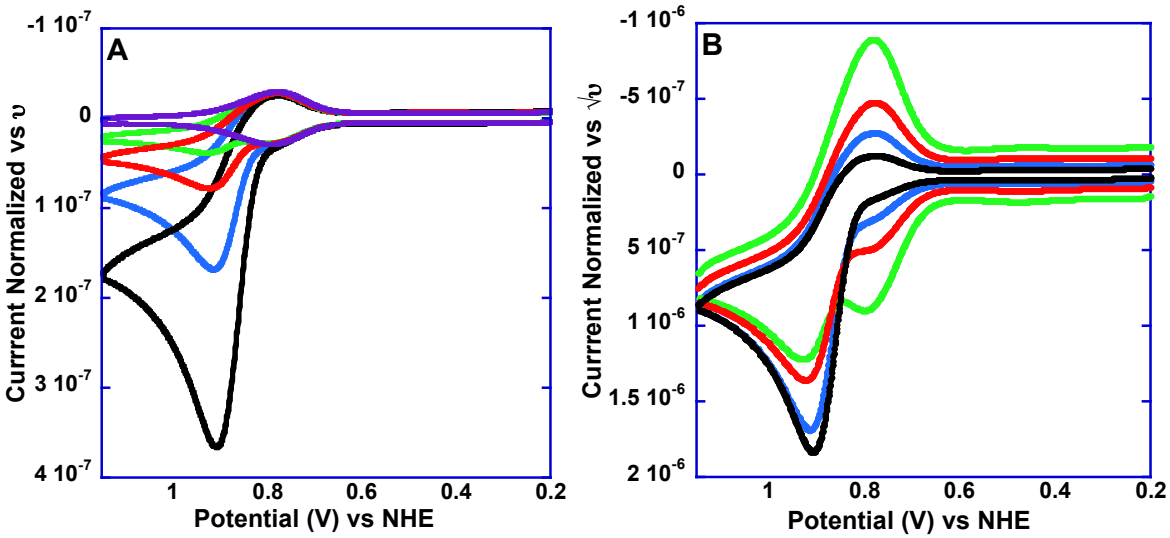

Figure 16. Scan rate dependent CVs of 0.1 mM TyrOH at **ITO-Os^{II}** normalized to either (**A**) scan rate (υ) or (**B**) square root of san rate ($\upsilon^{1/2}$). Solution conditions were 50 mM Tris buffer, pH 7.1, 10:1 acid to base buffer, I = 0.8M $LiClO_4$, at 25 ± 2 °C. CVs were collected with a scan rate of 25 mV/s (black); 100 mV/s (blue); 300 mV/s (red); 1000 mV/s (green); No TyrOH (purple).

Surface electrocatalysis under these conditions presumably occurs by a mechanism analogous to Scheme 3 with prior adduct formation followed by a combination of interfacial MS-EPT and initial proton loss followed by oxidation of $TyrO^-$, PT-ET, Scheme 4. Consistent with this conclusion, at fixed pH, i_p for TyrOH oxidation increases linearly with [Tris], Figure 17. The first order dependence is consistent with adduct formation followed by oxidation at the electrode as illustrated in Scheme 1.

Scheme 4.

$$TyrOH + B \rightleftharpoons TyrOH\text{---}B: K_A$$

$$TyrOH\text{---}B \longrightarrow TyrO^- + {}^+H\text{-}B$$

$$ITO\text{-}Os^{2+} \overset{e^-}{\rightleftharpoons} ITO\text{-}Os^{3+}$$

$$ITO\text{-}Os^{3+} + TyrO^- \longrightarrow ITO\text{-}Os^{2+} + TyrO^{\bullet}: k_{TyrO^-}$$

$$ITO\text{-}Os^{3+} + TyrOH\text{--}B \rightleftharpoons ITO\text{-}Os^{3+},TyrOH\text{--}B: K_A'$$

$$ITO\text{-}Os^{3+},TyrOH\text{--}B \longrightarrow ITO\text{-}Os^{2+} + TyrO^{\bullet} + {}^+HB: k_{EPT}$$

$$2TyrO^{\bullet} \longrightarrow (TyrO)_2$$

Peak current measurements with added buffer in a 10:1 acid:base ratio with pH = pD = 7.1 with added Tris in H_2O and D_2O reveal a H_2O/D_2O KIE of 2.1. For the oxidation of TyrOH by $Os(bpy)_3^{3+}$ in solution with added Tris by the mechanism in Scheme 3, $k_{EPT}K_{A(H_2O)}/k_{EPT}K_{A(D_2O)}$ = 2.3 and $k_{TyrO^-}K_{A(H_2O)}/k_{TyrO^-}K_{A(D_2O)}$ = 1.3. This comparison suggests involvement of MS-EPT in the surface reaction. [1,2]

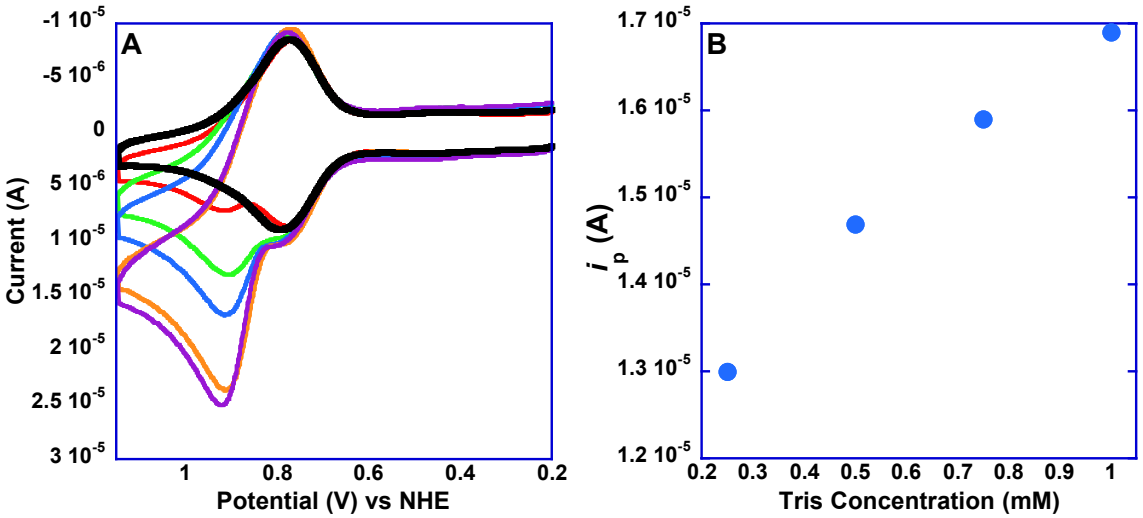

Figure 17. (**A**) Tris buffer dependence, of 0.1 mM TyrOMe at **ITO-Os^{II}**, I = 0.8M $LiClO_4$, and υ = 300 mV/s with 50 mM Tris buffer, pH 7.1, 10:1 acid to base; **ITO-Os^{II}** (black) no Tris (red); 0.25 mM Tris (green); 1 mM Tris (blue); 5 mM Tris (orange); 50 mM Tris (purple). **B**) i_p vs concentration of Tris buffer (mM) showing the first order dependence of peak current on base between 250 uM to 1 mM buffer concentration.

2.5 Concluding Remarks: The modification of conducting metal oxide electrodes with the electron transfer mediators **ITO-Os^{II}** and **ITO-Ru^{II}** allow for in-depth analysis of tyrosine and a class of structurally analogous phenols which demonstrate a kinetically slow electrochemical response when analyzed in the absence of any electron transfer mediator. The role of PCET in the manipulation of the electrochemical responses has been clearly demonstrated by varying the driving force of the reaction varying the strength (pK_a) of the proton accepting base, the potential of the surface bound species mediating the reaction and pH. Several observations worthy of note are the reproducibility of the rate of tyrosine oxidation by **ITO-Os^{II}** compared to solution studies, the increase in catalytic current with [Tris] indicating the formation of an adduct species that undergoes subsequent MS-EPT or base assisted PT-ET and finally, the observation by surface titration that the phosphonates which anchor the **ITO-M^{II}** mediator to the surface can also act as a proton accepting base under some conditions. Overall this work has provided insight into how surface mediated

electron transfer reactions are similar, and different from there solution based counterparts and provided a solid frame work for future work on surface mediated solution based chemistry.

2.6 References:

(1) Fecenko, C. J.; Meyer, T. J.; Thorp, H. H. **Electrocatalytic Oxidation of Tyrosine by Parallel Rate-Limiting Proton Transfer and Multisite Electron-Proton Transfer**. *J. Am. Chem. Soc.* **2006**, *128*, 11020-11021.

(2) Fecenko, C. J.; Thorp, H. H.; Meyer, T. J. **The Role of Free Energy Change in Coupled Electron-Proton Transfer**. *J. Am. Chem. Soc.* **2007**, *129*, 15098-15099.

(3) Costentin, C.; Louault, C.; Robert, M.; Savéant, J.-M. **The Electrochemical Approach to Concerted Proton-Electron Transfers in the Oxidation of Phenols in Water**. *Proc. Natl. Acad. Sci. USA*. **2009**, *106*, 18143-18148.

(4) Jurss, J. W.; Concepcion, J. J.; Norris, M. R.; Templeton, J. L.; Meyer, T. J. **Surface Catalysis of Water Oxidation by the Blue Ruthenium Dimer**. *Inorg. Chem.* **2010**, *49*, 3980-3982.

(5) Gillaizeau-Gauthier, I.; Odobel, F.; Alebbi, M.; Argazzi, R.; Costa, E.; Bignozzi, C. A.; Qu, P.; Meyer, G. J. **Phosphonate-Based Bipyridine Dyes for Stable Photovoltaic Devices**. *Inorg. Chem.* **2001**, *40*, 6073-6079.

(6) Hornstein, B. J.; Dattelbaum, D. M.; Schoonover, J. R.; Meyer, T. J. **Reactivity of an Adsorbed Ru(VI)-Oxo Complex: Oxidation of Benzyl Alcohol**. *Inorg. Chem.* **2007**, *46*, 8139-8145.

(7) Chen, Z.; Concepcion, J. J.; Hull, J. F.; Hoertz, P. G.; Meyer, T. J. **Catalytic Water Oxidation on Derivatized *nano*ITO**. *Dalton Trans.* **2010**, *30*, 6950-6952.

(8) Concepcion, J. J.; Jurss, J. W.; Hoertz, P. G.; Meyer, T. J. **Catalytic and Surface-Electrocatalytic Water Oxidation by Redox Mediator–Catalyst Assemblies**. *Angew. Chem. Int. Ed.* **2009**, *48*, 9473–9476.

(9) Chen, Z.; Concepcion, J. J.; Jurss, J. W.; Meyer, T. J. **Single-Site, Catalytic Water Oxidation on Oxide Surfaces**. *J. Am. Chem. Soc.* **2009**, 131, 15580–15581.

(10) Concepcion, J. J.; Jurss, J. W.; Templeton, J. L.; Meyer, T. J. **Mediator-Assisted Water Oxidation by the Ruthenium ''Blue Dimer'' *cis,cis*-$[(bpy)_2(H_2O)RuORu(OH_2)(bpy)_2]^{4+}$.** *Proc. Natl. Acad. Sci. USA*. **2008**, *105*, 17632-17635.

(11) Meyer, T. J.; Meyer, G. J.; Pfennig, B. W.; Schoonover, J. R.; Timpson, C. J.; Wall, J. F.; Kobusch, C.; Chen, X. H.; Peek, B. M.; Wall, C. G.; Ou, W.; Erickson, B. W.; Bignozzi, C. A. **Molecular-Level Electron Transfer and Excited State Assemblies on Surfaces of Metal Oxides and Glass**. *Inorg. Chem*. **1994**, *33*, 3952-3964.

(12) Bard A. J.; Faulkner, L. R. *Electrochemical Methods; Fundamentals and Applications*; Wiley: New York, **2001**; 14, 591.

(13) Trammell, S. A.; Meyer, T. J. **Diffusional Mediation of Surface Electron Transfer on TiO_2**. *J. Phys. Chem. B* **1999**, *103*, 104-107.

(14) Willit, J. L.; Bowden, E. F. **Adsorption and Redox Thermodynamics of Strongly Adsorbed Cytochrome *c* on Oxide Electrodes**. *J. Phys. Chem.* **1990**, *94*, 8241-8245.

(15) Dixon, W. T.; Murphy, D. **Determination of the Acidity Constants of some Phenol Radical Cations by Means of Electron Spin Resonance**. *J. Chem. Soc., Faraday. Trans. 2* **1976**, 72, 1221-1230.

(16) Sjödin, M.; Stenbjörn, S.; Åkermark, B.; Sun, L.; Hamarström, L. **Proton-Coupled Electron Transfer from Tyrosine in a Tyrosine−Ruthenium−tris-Bipyridine Complex: Comparison with $Tyrosine_z$ Oxidation in Photosystem II**. *J. Am. Chem. Soc.* **2000**, *122*, 3932-3936.

(17) Huynh, M.-H. V.; Meyer, T. J. **Proton-Coupled Electron Transfer**. *Chem. Rev*. **2007**, *107*, 5004-5064.

(18) Sjödin, M.; Irebo, T.; Utas, J. E.; Lind, J.; Merényi, G.; Åkermark, B.; Hammarström, L. **Kinetic Effects of Hydrogen Bonds on Proton-Coupled Electron Transfer from Phenols**. *J. Am. Chem. Soc.* **2006**, *128*, 13076-13083.

(19) Carra, C.; Iordanova, N.; Hammes-Schiffer, S. **Proton-Coupled Electron Transfer in a Model for Tyrosine Oxidation in Photosystem II**. *J. Am. Chem. Soc.* **2003**, *125*, 10429-10436.

(20) Alleman, K. S.; Weber, K.; Creager, S. E. **Electrochemical Rectification at a Monolayer-Modified Electrode**. *J. Phys. Chem.* **1996**, *100*, 17050-17058.

(21) Albery, W. J.; Hillman, A. R. **Transport Kinetics on Modified Electrodes**. *J. Electroanal. Chem.* **1984**, *170*, 27-49.

(22) Andrieux, C. P.; Saveant, J.-M. In *Techniques of Chemistry: Molecular Design of Electrode Surfaces*; Murray, R. W., Wiley: New York, **1992**; Vol. 22 pp 207-270.

(23) Young, R. C.; Keene, F. R.; Meyer, T. J. **Measurement of Rates of Electron Transfer between $Ru(bpy)_3^{3+}$ and $Fe(phen)_3^{2+}$ and between $Ru(phen)_3^{3+}$ and $Ru(bpy)_3^{2+}$ by Differential Excitation Flash Photolysis**. *J. Am. Chem. Soc.* **1977**, *99*, 2468-2473.

(24) Nakagawa, T.; Beasley, C. A.; Murray, R. W. **Efficient, Electro-Oxidation of Water near Its Reversible Potential by a Mesoporous IrO_x Nanoparticle Film**. *J. Phys. Chem. C* **2009**, *113*, 12958-12961.

(25) Chen, Z.; Vannucci, A. K.; Concepcion, J. J.; Jurss, J. W.; Meyer, T. J. **Proton-Coupled Electron Transfer at Modified Electrodes by Multiple Pathways**. *Proc. Natl Acad. Sci. USA*. **2011**, *108*, E1461-E1469.

Chapter 3

Concerted Electron-Proton Transfer (EPT) in the Oxidation of Tryptophan with Hydroxide as a Base[a]

3.1 Abstract: Tryptophan is unique among the redox-active amino acids owing to its weakly acidic indolic proton (p$K_a \approx 16$) compared to the -O-H proton of tyrosine (p$K_a = 10.1$) or the -S-H proton of cysteine (p$K_a = 8.2$). Stopped-flow and electrochemical measurements have been used to explore the roles of proton-coupled electron transfer and concerted electron-proton transfer (EPT) in tryptophan oxidation. The results of these studies have revealed a role for OH^- as a proton acceptor base in EPT oxidation of *N*-acetyl-tryptophan but not for other common bases. The reorganizational barrier for (*N*-acetyl-tryptophan)$^{+/\bullet}$ self-exchange is also estimated.

3.2 Introduction: The amino acids tyrosine, cysteine, and tryptophan play important roles as electron transfer carriers and mediators in biology with important examples appearing in photosystem II, class I ribonucleotide reductase, and DNA photolyase.[1-8] In tyrosine and cysteine oxidation, proton coupled electron transfer (PCET) is important in avoiding charge build up. Concerted electron-proton transfer (EPT) pathways are used to avoid high-energy protonated intermediates that arise from electron transfer (ET).[9] As an example, $E^{\circ\prime} \sim 1.5$ V

[a] Reproduced with permission from the American Chemical Society; Christopher J. Gagliardi, Robert A. Binstead, H. Holden Thorp and Thomas J. Meyer **Concerted Electron-Proton Transfer (EPT) in the Oxidation of Tryptophan with Hydroxide as a Base**. *J. Am. Chem. Soc.* **2011**, *49*, 19594-19597. © American Chemical Society, 2011.

vs. NHE for tyrosine oxidation to $TyrOH^{\bullet+}$ while $E°' \sim 1.0$ V for TyrOH-histidine oxidation to $TyrO^{\bullet}$-$^{+}$H-histidine, which is important in photosystem II.[3,4] In proteins, pendent bases or solvent molecules have been suggested to act as EPT proton acceptors as a way of avoiding high energy intermediates such as $TyrOH^{\bullet+}$. Protein structures with redox active tyrosine residues typically include an associated histidine base, and for cysteine oxidation, a carboxylate base such as aspartate.[3,4,10,11]

EPT is utilized in tyrosine oxidation by $M(bpy)_3^{3+}$ (M = Fe, Ru, Os) with added bases by the Multiple Site-Electron Proton Transfer (MS-EPT) pathway.[12-14] In this pathway concerted electron-proton transfer occurs, but to different e^- and H^+ acceptors. Related observations have been made at ITO electrodes (Sn(IV) doped In_2O_3) derivatized by surface binding of the electron transfer mediator $[Ru^{II}(bpy)(4,4'\text{-}(HO)_2P(O)CH_2)_2bpy)_2]^{2+}$ (bpy = 2,2′-bipyridine; 4,4′-$(HO)_2P(O)CH_2)_2$bpy = 4,4′-bis-methylenephosphonato-2,2′-bipyridine)[11,12] and in oxidation of the related solution complex *cis*-$Os^{III}(bpy)_2(py)(OH)^{2+}$ to $Os^{IV}(bpy)_2(py)(O)^{2+}$.[15]

In contrast to tyrosine ($pK_a = 10.1$) and cysteine ($pK_a = 8.2$), with readily dissociable protons, tryptophan is a secondary amine ($pK_a \sim 16$-17) with $E°'(TrpNH^{+\bullet}/TrpNH) = 1.21$ V (vs. NHE)[16] and $pK_a(TrpNH^{\bullet+}) = 4.3$.[17] The increase in pK_a compared to tyrosine with $pK_a(TryOH^{\bullet+}) = -2$ decreases the driving force for $TrpNH^{\bullet+}$ EPT compared to $TryOH^{\bullet+}$ EPT by ~0.059 (ΔpK_a) = 0.37 eV. Also mitigating against EPT oxidation of tryptophan by EPT is the fact that EPT pathways are microscopically more complex than electron transfer (ET) with higher barriers due to the transferring proton. All things being equal, ET is expected to be favored over EPT.[18]

The lack of an easily dissociable proton for tryptophan has important consequences in biological electron transfer. In peptides, tryptophan is often found in solvent exposed sites without an associated base, suggesting that EPT may not play a role. Tryptophan has been shown to act as an electron transfer carrier in DNA photolyase, class I ribonucloeotide reductase, and in azurin proteins.[1,2,5,7,19]

The role of EPT in tryptophan oxidation remains an open question. Evidence for buffer base and pH effects in oxidation of a tryptophan derivative in a $Ru(bpy)_3^{3+}$-based molecular assembly have been observed under certain conditions by Hammarström and coworkers by use of laser flash photolysis.[20,21]

Reported here is the oxidation of *N*-acetyl-tryptophan (NAceTrpNH, Figure 1), as a model for tryptophan in peptides, by the homologous series of polypyridyl metal complex oxidants $M(bpy)_3^{3+}$ (M = Fe, Ru, Os) by a combination of stopped-flow spectrophotometry and catalytic cyclic voltammetry. An important finding, consistent with tryptophan as an electron transfer mediator, is a failure to observe EPT pathways with a variety of acceptor bases. The only exception is OH^- which facilitates tryptophan oxidation by MS-EPT and not by prior deprotonation of NAceTrpNH and oxidation of the anion. We also report a detailed kinetic analysis that provides an independent estimate of $E°'$ for the ($TrpNH^{\bullet+}$/TrpNH) couple and an estimate of the reorganization barrier to electron transfer.

Stopped-flow mixing with diode array optical monitoring (375-775 nm) was applied to the oxidation of *N*-acetyl-tryptophan by $Os(bpy)_3^{3+}$, $E°'(Os^{III/II})$ = 0.80 V vs. NHE. The oxidant was generated *in situ* by Cl_2 oxidation followed by an argon purge. The kinetics were monitored by the appearance of the $Os(bpy)_3^{2+}$ MLCT absorption band at λ_{max} = 480 nm

following rapid mixing with solutions containing *N*-acetyl-tryptophan under various conditions.

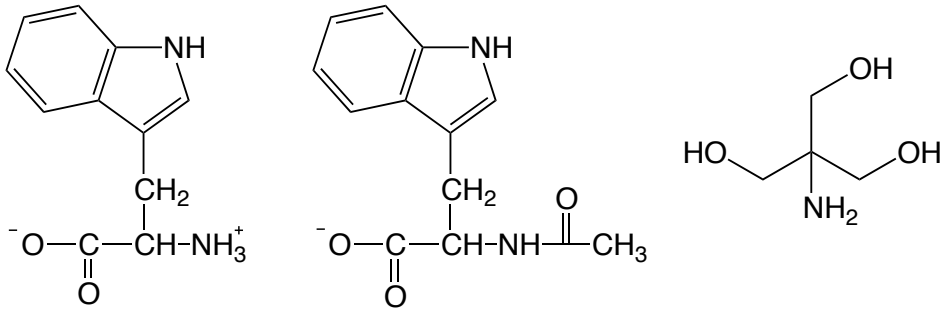

tryptophan **_N_-acetyl-tryptophan** **Tris**

Figure 1. Structures of tryptophan and *N*-acetyl-tryptophan at neutral pH as well as the structure of the Tris base, 2-Amino-2-hydroxymethyl-propane-1,3-diol.

3.3 Methods and Materials

3.3.1 Reaction Solutions: For electrochemical measurements buffered aqueous solutions were prepared from water purified with a MilliQ purification system (Synthesis A10) with added NaCl at 0.8 M to maintain constant ionic strength. The buffers (phosphate, Tris), perchloric acid ($HClO_4$) and hydrochloric acid (HCl) were purchased from Sigma Aldrich (St. Louis, MO) and were used as received. *N*-acetyl-tryptophan was purchased from Bachem and was used as received. Buffered solutions were adjusted to the correct pH using HCl or NaOH with use of a Fisher Scientific Accumet AB15 pH meter. Buffer concentrations were kept at a 10:1 acid to base ratio for Tris (pH 7.1) and phosphate (pH 6.2) in order to favor the concerted PCET pathway previously shown in the derived rate law for competing EPT and PT-ET pathways for tyrosine (Appendix 1).[13]

For kinetics experiments, buffered and unbuffered aqueous reaction solutions were prepared with water purified with a MilliQ purification system (Synthesis A10) with added 0.8 M NaCl to maintain constant ionic strength. $Os(bpy)_3^{3+}$ was generated from solutions of $Os(bpy)_3^{2+}$ by bubbling with Cl_2 gas, followed by purging with Argon. The concentrations of

$Os(bpy)_3^{3+}$ were determined in CH_3CN, where the UV-Visible absorbance properties of $Os(bpy)_3^{3+}$ in this solvent are well documented (ε = 39,300 cm^{-1} M^{-1} at 306 nm).[22]

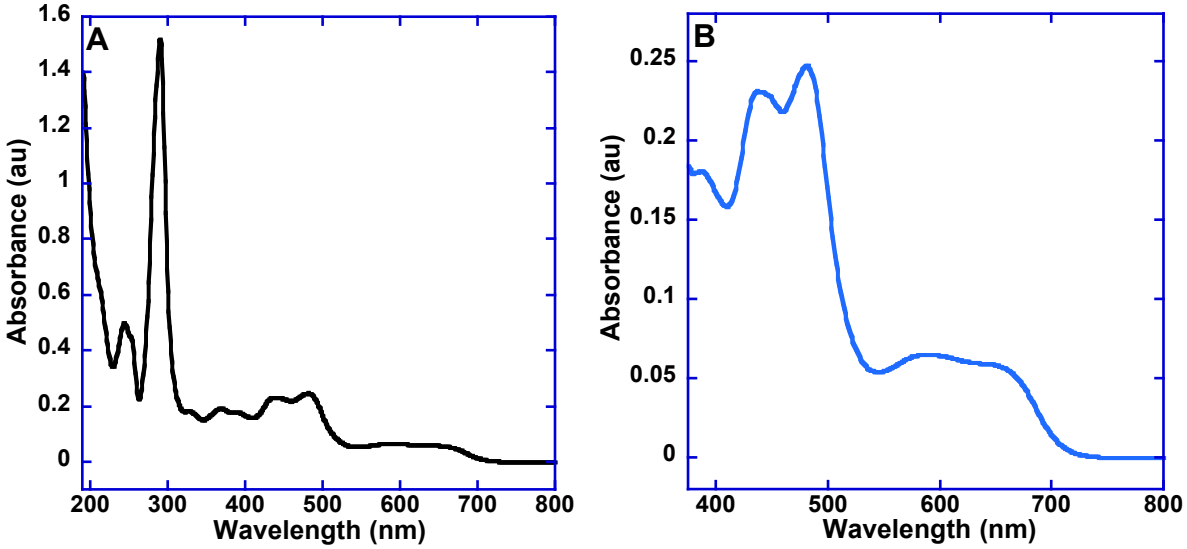

Figure 2. UV-vis spectra of $Os(bpy)_3^{2+}$ in H_2O, (**A**) Wavelength range 190-800 nm (**B**) Wavelength range employed in stopped-flow experiments, 375-775 nm. US-Vis spectra of $Os(bpy)_3^{3+}$ as well as a comprehensive characterization of its vibronic structure are available in reference 22.

3.3.2 Stopped-Flow Kinetics: Kinetics experiments were performed on a HI-TECH SF-61DX2 double mixing stopped-flow spectrophotometer fitted with either a single-beam photodiode array detector and Xenon light source for multi-wavelength analysis, or dual-beam photomultiplier tubes (Hamamatsu R928) and a Tungsten light source for single wavelength observations. Initial studies were performed with a MG-6050 diode array (1.5 ms integration time) with the KinetAsyst software, while later work utilized a MG-6560S diode array detector (3 ms integration time) operated by the Kinetic Studio software (TgK Scientific Ltd.). In most cases, measurements were obtained with a 1 cm optical path. Sample temperatures were controlled by either a Neslab RTE-110 or a Thermo Haake A28 water bath and monitored via the internal sensor of the mixing unit.

For pH < 9.2 the time scales (5-100 s) were suitable for diode array detection. The

latter mode was used with an automatic shutter system (Uniblitz LS3) for time scales longer than 3 s as a precaution against photolysis of $Os(bpy)_3^{3+}$ by the intense Xenon light source. Kinetic analysis of the diode array scans (375-775 nm) vs. time was performed with the SPECFIT/32 software (Spectrum Software Associates). Typically, the kinetics were monitored with a pseudo-first order excess of *N*-acetyl-tryptophan (200 μM) over $Os(bpy)_3^{3+}$ (20 μM), though additional studies were also performed at 1:1 and 200:1 ratios of the reagents. Even with a large excess of *N*-acetyl-tryptophan, the kinetic traces were complex, requiring treatment of both the redox and acid-base properties of the reagents and intermediates.

For pH > 10 the kinetics were often too rapid (<0.1 s) for use of the diode array detector. Higher quality kinetic traces were obtained instead with use of the photomultiplier detectors, which provided better time resolution and lower noise. In this pH region the observed kinetics were uncomplicated, allowing simplified kinetic analyses to be performed with the HI-TECH KinetAsyst or Kinetic Studio software (See section 3.4.5 below). Typically, the kinetics were found to follow exponential decays with a pseudo-first order excess of *N*-acetyl-tryptophan, and second order, equal concentration decays with a 1:1 ratio of initial reagents. Reported hydroxide concentrations were based upon pH meter readings taken after the mixing of solutions. To correct for the effect of sodium ions on pH readings, a calibration curve was used, based upon serial dilutions of NaOH in degassed 0.8M NaCl (Fig. 3).

Kinetic experiments were also performed at pH 4.0 with use of an Agilent 8453 diode array spectrophotometer and a manual mixing apparatus comprising two 1 ml gastight syringes and valves (Hamilton), connected via a T-mixer (3-way valve) to a compact flow

cell (Agilent, 1 cm path) with FEP tubing. Sample temperature was controlled by a Thermo Haake A28 water bath and thermostated cell holder.

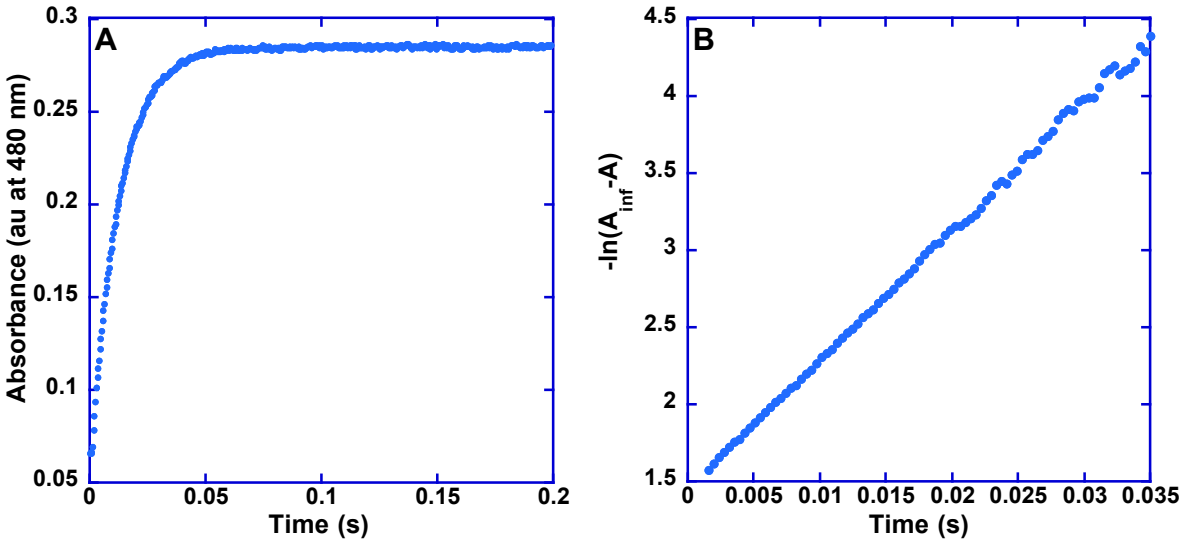

Figure 3. Oxidation of *N*-acetyl-tryptophan (300 μM) by $Os(bpy)_3^{3+}$ (20 μM) at pH 10.7, (I = 0.8 M NaCl, T = 20 °C) OH^- (500 μM). (**A**) Stopped-flow kinetic trace for $Os^{3+} \rightarrow Os^{2+}$ monitored at 480 nm. (**B**) Plot of $\ln(A_\infty - A)$ vs. Time (k_{obs} = 83.3 s^{-1}).

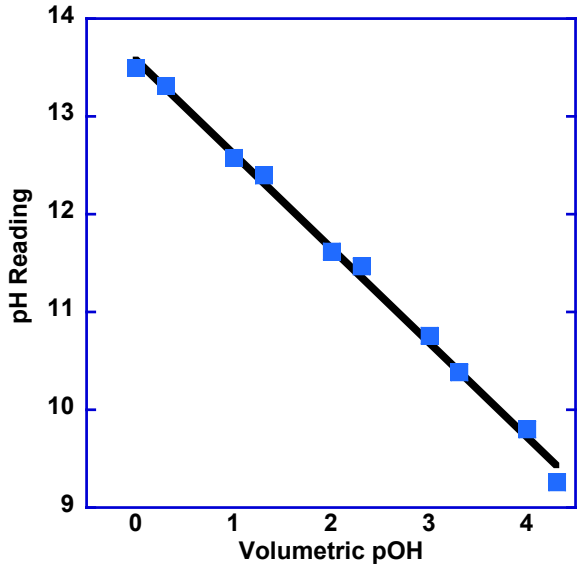

Figure 4. Calibration curve generated using volumetric dilution of NaOH in 0.8 M NaCl, for the correction of sodium ion effects on the measured pH.

3.3.3 Electrochemistry: Electrochemical experiments were performed with a CH Instruments model 601D potentiostat, using a cell design that has been described previously.[13,23,24] Sample volumes for each experiment were typically 100 μL. Tin-doped indium oxide coated glass (ITO) was used as a working electrode (area = 0.32 cm^2), as purchased from Delta Technologies (Stillwater, MN). ITO slides were cleaned by sonicating in water, 2-propanol, and then water (2×) for 15 minutes each. The Ag/AgCl reference electrode (+0.197 V vs. NHE) was purchased from Cypress Systems Inc. (Lawrence, KS) and a platinum wire was used as the auxiliary electrode. Before acquiring cyclic voltammetry traces, at least 6 backgrounds scans of the plain electrode were taken in buffer or acid alone throughout the potential range of the experiment.

3.4 Results and Discussion

3.4.1 Analysis of Stopped-Flow data using SPECFIT/32: SPECFIT/32 was used to analyze and model the kinetics of *N*-acetyl-tryptophan oxidation by $Os(bpy)_3^{3+}$ in Tris and phosphate buffer (0.5 mM - 400 mM) at pH 7.1 while maintaining a constant ionic strength (I = 0.8M) with NaCl. A typical data set is shown below in Figure 5. Factor analysis of the diode array spectra revealed only two dominant factors. As shown in Figure 6, there was no evidence for colorimetric contributions from intermediates in the concentration eigenvectors (**U×S**). The third spectroscopic eigenvector (**V**) mirrors the first principal factor, and its vector product, $\mathbf{U \times S \times V'}$, just represents experimental noise arising from the Xenon lamp fluctuations with time. Calculated concentration profiles for a sample reaction are shown in Figure 7.

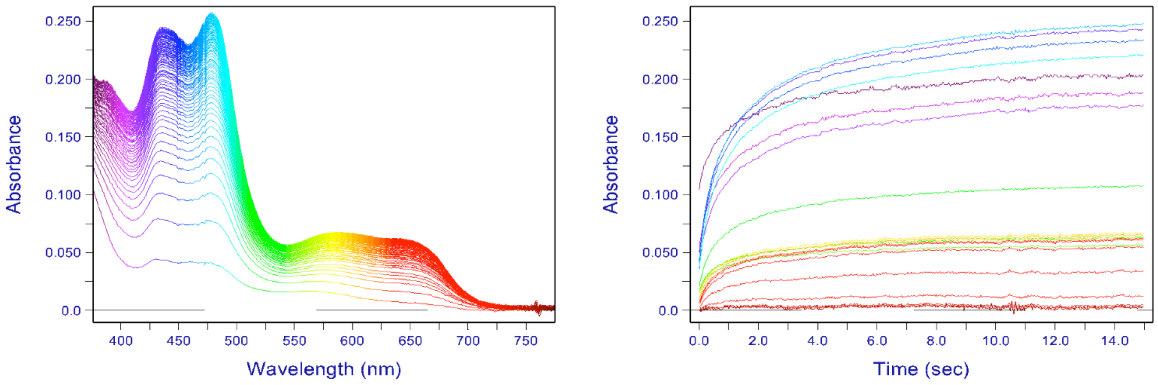

Figure 5. Diode array kinetic scans and representative kinetic traces for the reaction between $Os(bpy)_3^{3+}$ (20 μM) and *N*-acetyl-tryptophan (200 μM) in 40 mM Tris buffer (10:1 acid:base) at pH 7.1 (I = 0.8 M, NaCl; T = 20 °C).

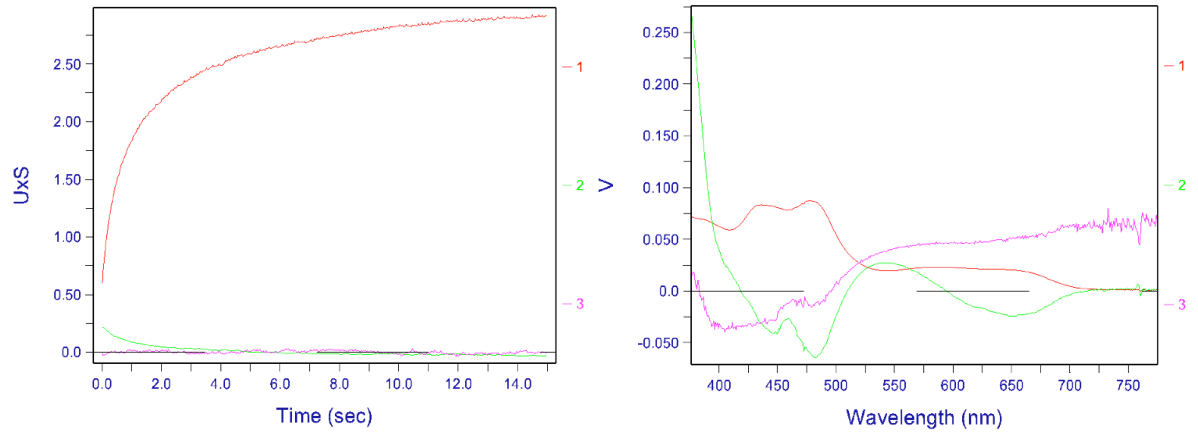

Figure 6. Principal factors (1-3) obtained by singular value decomposition (SVD) analysis of the diode array scans in Fig. 5. Only the first two sets of eigenvectors (**U×S** and **V**) contain colorimetric data related to the reaction. The third set (shown) and remaining eigenvectors (not shown for clarity) represents lamp fluctuations that could be factored from the experimental data.

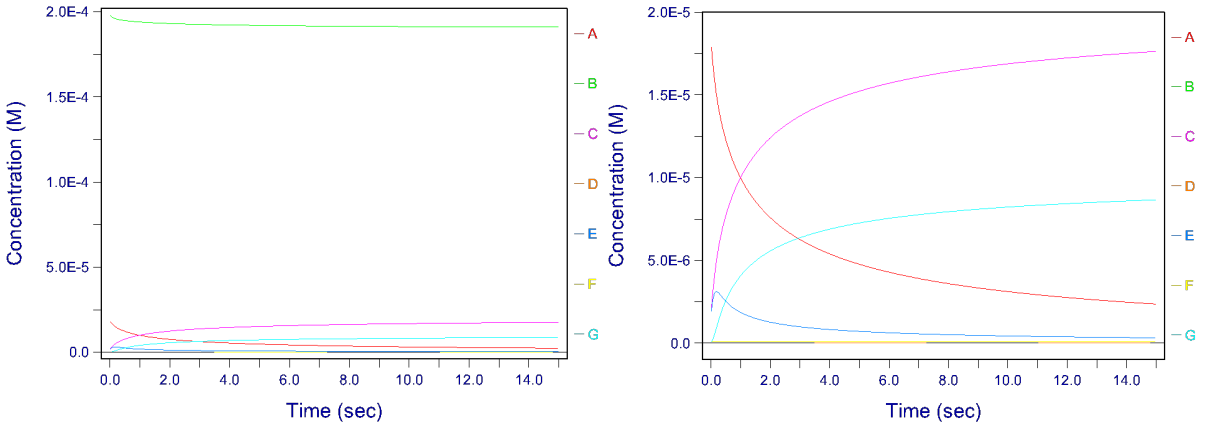

Figure 7. Calculated concentration profiles for the reaction between $Os(bpy)_3^{3+}$ (20 μM) and *N*-acetyl-tryptophan (200 μM) in 40 mM Tris buffer (10:1 acid:base) at pH 7.1 (I = 0.8 M, NaCl; T = 20 °C). Trace: A (Os^{3+}), B (NAceTrpNH), C (Os^{II}), D ($NAceTrpH^{\bullet+}$), E ($NAceTrpH^{\bullet}$), F (H^+), G (NAceTrp oxidation product).

The appearance of complex kinetics even with a 200× excess of *N*-acetyl-tryptophan suggested that the reaction must occur in a regime where initial outer-sphere electron transfer (ET) is coupled to a rate determining second-order reaction like that shown in Scheme 1. In the proposed mechanism, the initial product is the protonated radical cation of *N*-acetyl-tryptophan ($TrpNH^{\bullet+}$), which undergoes rapid H^+ equilibration with the buffer medium, followed by a special type of disproportionation that produces equal amounts of the starting reagent and an oxidized form that undergoes irreversible reactions to form one or more oxidation products. The proposed model avoids the formation of deprotonated *N*-acetyl-tryptophan anion ($TrpN^-$), which would be a high energy intermediate based on the estimated pK_a ~ 16-17 for TrpNH. The hydroxide pathway that dominates at pH >10 is included for completeness, such that the role of k_{OH^-}, although minimal, can be modeled at intermediate pH values.

Scheme 1. (*TrpNH* = *N*-acetyl-tryptophan)

$$M^{3+} + TrpNH \underset{k_{-1}}{\overset{k_1}{\rightleftharpoons}} M^{2+} + TrpNH^{\bullet +} \quad \textbf{(1)}$$

$$TrpNH^{\bullet +} \underset{k_{-2}}{\overset{k_2}{\rightleftharpoons}} TrpN^{\bullet} + H^{+} \quad \textbf{(2)}$$

$$TrpNH^{\bullet +} + TrpN^{\bullet} \xrightarrow{k_3} TrpNH + TrpN^{+} \quad \textbf{(3)}$$

$$TrpN^{+} \xrightarrow{H_2O/O_2} oxidation\ products \quad \textbf{(4)}$$

$$M^{3+} + TrpNH + OH^{-} \xrightarrow{k_{OH^-}} M^{2+} + TrpN^{\bullet} + H_2O \quad \textbf{(5)}$$

Stopped-flow kinetic absorbance-time traces (Fig. 8) were well modeled in SPECFIT/32 by the mechanism in Scheme 1. The key features in the mechanism are: (a) a reversible $1e^-$ redox pre-equilibrium with the protonated radical cation[23] where $E°'(TrpNH^{\bullet +}/TrpNH)$ = 1.21 V vs. NHE for tryptophan[16] and ~1.1 V for *N*-acetyl-tryptophan;[25] (b) proton transfer equilibration of the radical cation with the buffer medium to give the neutral radical at pH 7.1; and (c) reaction of the neutral radical with the protonated radical cation (pK_a = 4.3)[16,17] to form *N*-acetyl-tryptophan and the cationic form as initial products. The assumed stoichiometry of 2:1 Os^{3+}:*N*-acetyl-tryptophan is in good agreement with previous reports at neutral pH.[16,20,26] The ultimate product(s) were not investigated but oxidation products reported earlier for tryptophan include *N*-formylkynurenine, oxindolylalanine and dioxindolylalanine, whose structures are shown in Figure 10.[16,27-30]

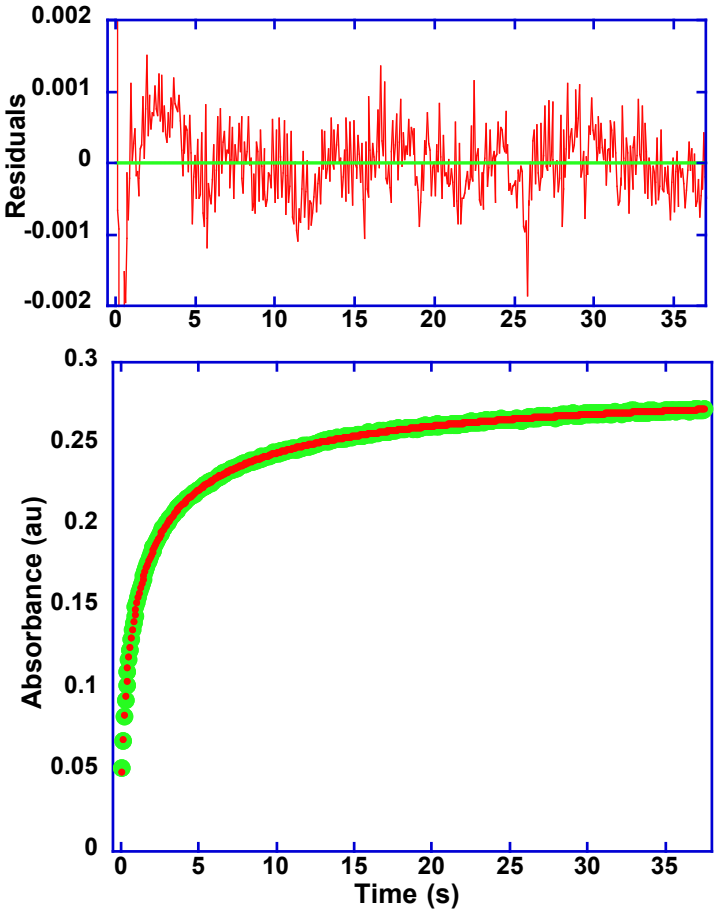

Figure 8. Typical kinetic trace at 480 nm (green) and fit (red) for the reaction of $Os(bpy)_3^{3+}$ (20 μM) with *N*-acetyl-tryptophan (200 μM) at T = 20 °C, pH 7.1 40 mM Tris buffer (10:1 acid:base), I = 0.8 M NaCl).

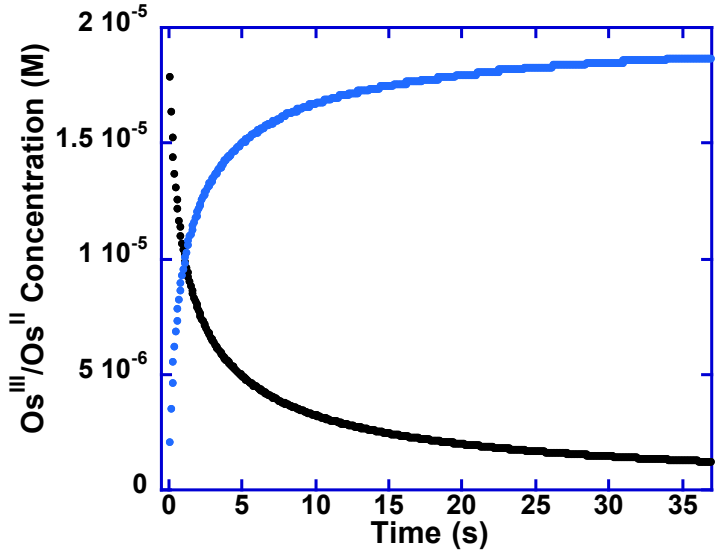

Figure 9. The inset shows the calculated concentration profiles for Os^{3+} (black) and Os^{2+} (blue) only. The top trace shows the residuals of the fit. The relative error of individual fits averaged 0.55% (< .001 a.u.).

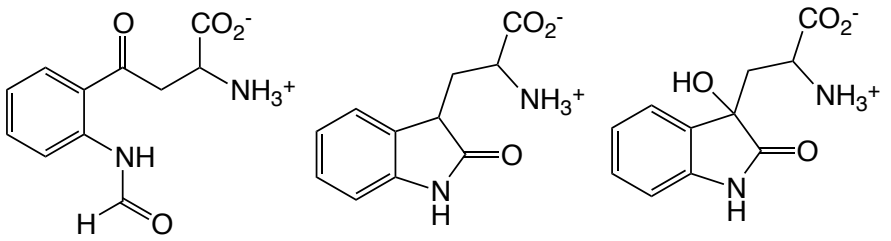

***N*-formylkynurenine** **oxindolylalanine** **dioxindolylalanine**

Figure 10. Previously reported oxidation products of native, free tryptophan.[27-30]

The data were fit with variable rate constants for k_1 and k_{-1}, while holding fixed the values of $k_2 = 5.0\times10^5$ s^{-1}, $k_{-2} = 1\times10^{10}$ M^{-1} s^{-1} based on pulse radiolysis studies for native tryptophan, where $pK_a = 4.3$ for the radical cation ($TrpNH^{\bullet+}$) and $k_3 = 3.2\times10^8$ M^{-1} s^{-1} for the pH independent disproportionation observed in pulse radiolysis experiments.[17] Diffusion controlled protonation was assumed to occur for protonation of the neutral radical. The value of the ratio (k_2/k_{-2}) is important in the fitting procedure, as is the value of k_3 as these provide a pathway that competes with the back electron transfer step (k_{-1}). Tris buffer equations were included in the numerical model only for the lowest ratio of Tris/TrpNH. Otherwise, the fitting procedure in SPECFIT/32 utilized a fixed $[H^+]$ for numerically simulated buffering (i.e., $d[H^+]/dt = 0$). Based on these values and the kinetic model in Scheme 1, fits to the stopped-flow kinetic data were made with two adjustable parameters, the rate constants for the reversible pre-equilibrium, k_1 and k_{-1}. The resulting fits at pH 7.1 (40 mM Tris) gave $k_1 = (5.1\pm0.2)\times10^3$ M^{-1} s^{-1}, $k_{-1} = (2.3\pm0.2)\times10^8$ M^{-1} s^{-1}, and $K_{eq} = k_1/k_{-1} = 2.2 \times 10^{-5}$. Similar results were obtained over the pH range 6.10-9.16.

The resulting rate constants (k_1 and k_{-1}) from the fits are summarized below in Table 1. Each buffer concentration represents 10-26 replicates spanning time scales of 15-150 s. The standard deviations reported are those of the replicates and represent the variability from run-to-run. The standard deviations for individual fits were typically one third of the reported

values, and the relative error of individual fits averaged ±0.55% (<0.001 a.u.). The ratio (k_1/k_{-1}) was used to calculate the redox pre-equilibrium constant, and therefore the Nernstian redox potential difference between the $Os(bpy)_3^{III/II}$ and $TrpNH^{\bullet+}$/TrpNH couples (eq 1). The estimated errors in the ΔE values were obtained by propagation of errors for the ratio (k_1/k_{-1}) with their standard deviations. While the estimated errors are relatively large, it was gratifying to find that there was little variability in the mean value, ΔE_{avg} = (0.28±0.01 V). Assuming that the potential of $Os(bpy)_3^{III/II}$ is +0.80 V vs. NHE, the fits to the kinetic model provide an estimate of $E°'(TrpNH^{\bullet+}/TrpNH)$ = +1.08 V. This agrees well with the electrochemically measured value of $E°'$ = 1.06 V.[25]

$$\Delta E°' = E_{ox}(NAceTrp^{\bullet+/0}) - E_{ox}(M^{III/II}) = 0.059\ pK_{eq} \quad (1)$$

Table 1. Rate constants obtained from SPECFIT/32 for the redox pre-equilibrium in Scheme 1 while maintaining experimental values of the pH independent decay rate for the radical cation (3.2×10^8 M^{-1} s^{-1}), and its experimental pK_a = 4.3.[16,17]

pH 7.1 Buffer (mM)	N^a	k_1 ($M^{-1}s^{-1}$)	σ (k_1)	k_{-1} ($M^{-1}s^{-1}$)	σ (k_{-1})	K_{eq} (k_1/k_{-1})	log (K_{eq})	ΔE (V)	σ (ΔE)	$E°'$(NAceTrp) (V vs NHE)
Tris (0.5 mM)	16	5.55E+03	1.05E+03	6.29E+08	1.78E+08	8.82E-06	5.055	0.299	0.100	1.099
Tris (5 mM)	11	6.36E+03	4.37E+02	3.24E+08	4.93E+07	1.97E-05	4.706	0.278	0.047	1.078
Tris (10 mM)	17	6.18E+03	4.97E+02	2.84E+08	3.61E+07	2.18E-05	4.662	0.276	0.041	1.076
Tris (20 mM)	16	5.70E+03	5.33E+02	2.33E+08	2.99E+07	2.44E-05	4.612	0.273	0.043	1.073
Tris (30 mM)	14	5.33E+03	2.31E+02	2.29E+08	1.93E+07	2.33E-05	4.633	0.274	0.026	1.074
Tris (40 mM)	19	5.14E+03	2.29E+02	2.33E+08	1.85E+07	2.20E-05	4.657	0.276	0.025	1.076
Tris (50 mM)	26	5.60E+03	5.85E+02	2.82E+08	4.54E+07	1.98E-05	4.703	0.278	0.053	1.078
Tris (400 mM)	15	7.96E+03	1.15E+03	2.40E+08	5.52E+07	3.32E-05	4.478	0.265	0.072	1.065
Phosphate (0.5 mM)	13	5.48E+03	5.14E+02	4.56E+08	6.69E+07	1.20E-05	4.920	0.291	0.051	1.091
Phosphate (5 mM)	14	5.39E+03	4.20E+02	3.85E+08	4.76E+07	1.40E-05	4.854	0.287	0.042	1.087
Phosphate (50 mM)	10	7.60E+03	2.59E+02	6.38E+08	3.62E+07	1.19E-05	4.924	0.291	0.019	1.091

[a] number of replicates

An alternative mechanism (Scheme 2) involving disproportionation solely of the neutral tryptophan radical provided equally good fits to the experimental data and cannot be excluded on the basis of least squares fit residual errors alone. However, this scheme requires initial formation of deprotonated *N*-acetyl-tryptophan anion ($TrpN^-$), a high energy intermediate, followed by its rapid proton equilibration with the medium. In addition, this

model requires diffusion controlled back electron transfer (k_{-1}) in order to fit the experimental data. While not impossible, that rate constant seems implausible. Furthermore, the predicted ΔE from the fitting procedure leads to an estimated value of $E°'(\mathrm{TrpNH}^{\bullet+}/\mathrm{TrpNH})$ = +1.17 V vs. NHE, which is higher than the measured peak potential in cyclic voltammograms.

Scheme 2 (*TrpNH* = *N*-acetyl-tryptophan)

$$M^{3+} + TrpNH \underset{k_{-1}}{\overset{k_1}{\rightleftharpoons}} M^{2+} + TrpNH^{\bullet+} \qquad \textbf{(1)}$$

$$TrpNH^{\bullet+} \underset{k_{-2}}{\overset{k_2}{\rightleftharpoons}} TrpN^{\bullet} + H^{+} \qquad \textbf{(2)}$$

$$2TrpN^{\bullet} \xrightarrow{k_3} TrpN^{-} + TrpN^{+} \qquad \textbf{(3)}$$

$$TrpN^{-} + H^{+} \underset{k_{-4}}{\overset{k_4}{\rightleftharpoons}} TrpNH \qquad \textbf{(4)}$$

$$TrpN^{+} \xrightarrow{H_2O/O_2} oxidation\ products \qquad \textbf{(5)}$$

$$M^{3+} + TrpNH + OH^{-} \xrightarrow{k_{OH^-}} M^{2+} + TrpN^{\bullet} + H_2O \qquad \textbf{(6)}$$

Table 2. Rate constants obtained from SPECFIT/32 for the redox pre-equilibrium in Scheme 2 while maintaining experimental values of the pH independent decay rate for the radical cation (3.2×10^8 M^{-1} s^{-1}), and its experimental pK_a = 4.3.[16,17]

pH 7.1 Buffer (mM)	N^a	k_1 ($M^{-1}s$-1)	σ (k_1)	k_{-1} ($M^{-1}s^{-1}$)	σ (k_{-1})	K_{eq} (k_1/k_{-1})	log (K_{eq})	ΔE (V)	σ (ΔE)	$E°'$(NAceTrp) (V vs NHE)
Tris (0.5 mM)	16	7.59E+03	2.32E+03	2.48E+10	1.13E+10	3.06E-07	6.514	0.385	0.212	1.185
Tris (5 mM)	11	7.22E+03	6.33E+02	1.04E+10	1.56E+09	6.98E-07	6.156	0.364	0.630	1.164
Tris (10 mM)	17	6.88E+03	7.12E+02	8.83E+09	1.35E+09	7.80E-07	6.108	0.361	0.067	1.161
Tris (20 mM)	16	6.27E+03	6.51E+02	7.19E+09	1.01E+09	8.72E-07	6.060	0.358	0.062	1.158
Tris (30 mM)	14	5.85E+03	2.94E+02	7.03E+09	5.84E+08	8.32E-07	6.080	0.360	0.035	1.160
Tris (40 mM)	19	5.61E+03	3.16E+02	7.12E+09	6.43E+08	7.88E-07	6.103	0.361	0.038	1.161
Tris (50 mM)	26	6.28E+03	8.95E+02	9.02E+09	1.86E+09	6.96E-07	6.157	0.364	0.091	1.164
Tris (400 mM)	15	8.92E+03	1.51E+03	7.60E+09	2.06E+09	1.17E-06	5.931	0.351	0.112	1.151
Phosphate (0.5 mM)	13	6.19E+03	1.00E+03	1.55E+10	3.51E+09	4.01E-07	6.397	0.378	0.095	1.178
Phosphate (5 mM)	14	6.11E+03	7.19E+02	1.17E+10	2.08E+09	5.21E-07	6.284	0.372	0.079	1.172
Phosphate (50 mM)	10	9.65E+03	9.42E+02	2.21E+10	3.00E+09	4.37E-07	6.359	0.376	0.063	1.176

[a] number of replicates

Another plausible mechanism (Scheme 3) involves direct oxidation of $TrpN^{\bullet}$ by $Os(bpy)_3^{3+}$. While this model produced equally good fits to the experimental data, it required three adjustable parameters (k_1, k_{-1} and k_3) which exhibited a high degree of cross-correlation.

This resulted in much larger standard deviations in the rate constants, and the ratios (k_1/k_{-1}) had estimated errors approaching 100% when based on the propagation of errors in the rate constants.

Scheme 3 (*TrpNH* = *N*-acetyl-tryptophan)

$$M^{3+} + TrpNH \underset{k_{-1}}{\overset{k_1}{\rightleftharpoons}} M^{2+} + TrpNH^{\bullet +} \qquad \textbf{(1)}$$

$$TrpNH^{\bullet +} \underset{k_{-2}}{\overset{k_2}{\rightleftharpoons}} TrpN^{\bullet} + H^{+} \qquad \textbf{(2)}$$

$$M^{3+} + TrpN^{\bullet} \xrightarrow{k_3} TrpN^{+} + M^{2+} \qquad \textbf{(3)}$$

$$TrpN^{+} \xrightarrow{H_2O/O_2} oxidation\ products \qquad \textbf{(4)}$$

While quite unsatisfactory from a statistical viewpoint, we report the following values at 40 mM Tris buffer are reported for completeness. The average rate constants were: k_1 = (3.7±0.4)×10^3 M^{-1} s^{-1}; k_{-1} = (2.1±2.8)×10^8 M^{-1} s^{-1}; and k_3 = (1.5±2.0)×10^5 M^{-1} s^{-1} for the direct oxidation of the TrpN$^{\bullet}$ by Os(bpy)$_3^{3+}$. These give an estimated value of $E°'$(TrpNH$^{+\bullet}$/TrpNH) = +1.08 V vs. NHE. However, with an estimated uncertainty of ±0.38 V, caused by the highly correlated rate constants, the result is not statistically significant. The model simply has too many variable parameters to be used to estimate the pre-equilibrium constant reliably.

3.4.2 Modeling pH Dependence in SPECFIT/32: SPECFIT/32 was also used to analyze and model the kinetics of *N*-acetyl-tryptophan oxidation by Os(bpy)$_3^{3+}$ in Tris and phosphate buffers (50 mM) between pH 6.1 and 9.16 while maintaining a constant ionic strength (I = 0.8 M) with NaCl. For pH < 7, the time scales of these experiments were kept between 5-20 seconds by increasing the ratio of NAceTrp to Os(bpy)$_3^{3+}$ to 500:1. The hydroxide pathway (discussed in sect 3.4.5) k_{OH^-} = (7.5±0.9)×10^8 M^{-1} s^{-1}, was included in the fits at all pH values. However, this contribution was minimal for pH < 8. Under these conditions, fits to

the model in Scheme 1 were excellent. The standard deviations reported are those of the replicates and represent the variability from run-to-run. The standard deviations for individual fits were typically less than one third of the reported values, and the relative error of individual fits averaged ±0.53% (<0.001 a.u.). The resulting rate constants (k_1 and k_{-1}) from the fits are summarized below in Table 3.

Table 3. Rate constants obtained from SPECFIT/32 for the redox pre-equilibrium in Scheme 1 while maintaining experimental values of the pH independent decay rate for the radical cation (3.2×10^8 M^{-1} s^{-1}), and its experimental pK_a = 4.3. [16,17]

Buffer (50 mM)	pH	N^a	k_1 ($M^{-1}s^{-1}$)	σ (k_1)	k_{-1} ($M^{-1}s^{-1}$)	σ (k_{-1})	K_{eq} (k_1/k_{-1})	log (K_{eq})	ΔE (V)	σ (ΔE)	$E°'$(Trp) (V vs NHE)
Tris	9.16	10	8.96E+03	1.49E+03	4.06E+08	1.01E+08	2.21E-05	4.656	0.275	0.069	1.075
Tris	8.48	13	8.73E+03	2.14E+02	8.56E+07	3.29E+07	1.02E-04	3.991	0.236	0.091	1.036
Tris	8.07	13	6.35E+03	9.56E+01	9.78E+07	1.07E+07	6.50E-05	4.187	0.248	0.027	1.048
Tris	7.49	8	6.03E+03	1.25E+02	1.75E+08	1.11E+07	3.44E-05	4.464	0.264	0.018	1.064
Tris	7.10	26	5.60E+03	5.85E+02	2.82E+08	4.54E+07	1.98E-05	4.703	0.278	0.053	1.078
Phosphate	7.13	10	7.60E+03	2.59E+02	6.38E+08	3.62E+07	1.19E-05	4.924	0.291	0.019	1.091
Phosphate[b]	6.60	10	4.97E+03	4.26E+02	3.29E+08	4.74E+07	1.51E-05	4.821	0.285	0.048	1.085
Phosphate[b]	6.12	8	2.24E+03	4.25E+02	2.75E+08	6.86E+07	8.15E-06	5.089	0.301	0.094	1.101

[a] number of replicates [b]At lower pH values larger ratios of *N*-acetyl-tryptophan:$Os(bpy)_3^{3+}$, (500:1) were used to keep the time scale of the kinetics below 60 seconds.

For pH < 7 the kinetics were complicated by biphasic kinetic behavior which consisted of a faster initial step followed by a slower secondary reaction. By increasing the ratio of *N*-acetyl-tryptophan to $Os(bpy)_3^{3+}$ from 20:1 to 100:1 (or 500:1) the time scale for completion of the initial reaction was reduced, and the effects of the following reaction were minimized. This resulted in data sets at pH 6.1 and 6.6 that were well modeled by Scheme 1, albeit with some apparent pH dependence in the fitted values of k_1 and k_{-1}.

3.4.3 Validating Kinetic Model at Low pH: The kinetics of *N*-acetyl-tryptophan oxidation by $Os(bpy)_3^{3+}$ were monitored at pH 4.0 without buffer (I = 0.8 M NaCl, T = 22 °C) for a 500:1 ratio of *N*-acetyl-tryptophan (0.01M) to $Os(bpy)_3^{3+}$ (20 μM). Under these conditions, factor analysis (Fig. 11) revealed five colorimetric states evolving with time. It was apparent that

additional, uncharacterized kinetic processes overlapped and followed the redox reactions of interest in Scheme 1. This precluded the possibility of an accurate fit to the model at pH 4.0, though the initial formation of $Os(bpy)_3^{2+}$ did occur on the correct time scale predicted by Scheme 1.

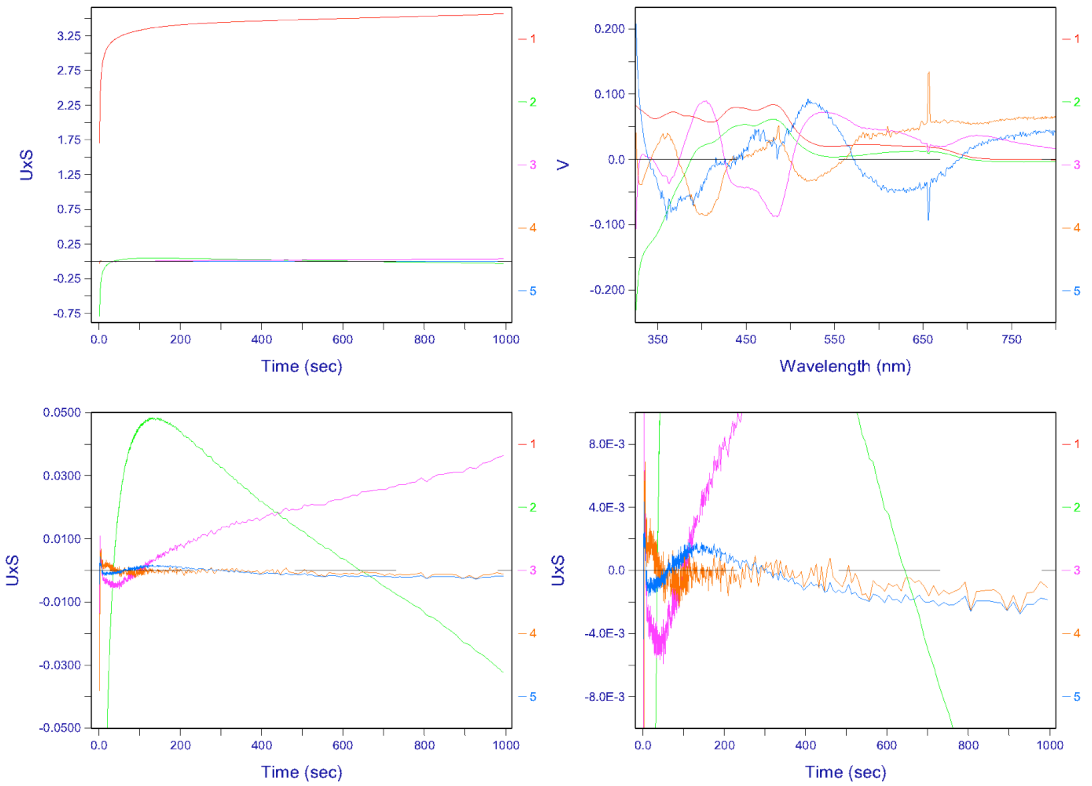

Figure 11. Principal factors **U×S** and **V** (1-5) obtained by singular value decomposition (SVD) analysis of the diode array scans at pH 4.0. The concentration eigenvectors (**U×S**) are also plotted on expanded scales to allow the minor eigenvectors (3-5) to be illustrated.

3.4.4 Testing Kinetic Model For Effects of Oxygen SPECFIT/32 was also used to model the stopped-flow kinetics of *N*-acetyl-tryptophan oxidation by $Os(bpy)_3^{3+}$ in 50 mM Tris buffer at pH 7.1 (I = 0.8 M, NaCl) with and without the presence of oxygen in the system. Identical solutions were either purged with argon for 30 minutes or were used as prepared. The mechanism shown in Scheme 1 was used to model the kinetics and gave excellent fits. The

similarity of the derived rate constants (Table 4) indicates that oxygen does not affect the kinetics at neutral pH.

Table 4. Rate constants obtained from SPECTFIT/32 for the redox pre-equilibrium in Scheme 1 while maintaining experimental values of the pH independent decay rate for the radical cation (3.2×10^8 M^{-1} s^{-1}), and its experimental pK_a = 4.3. [16,17]

Tris (50 mM)	pH	N^a	k_1 (M^{-1} s^{-1})	σ (k_1)	k_{-1} (M^{-1} s^{-1})	σ (k^{-1})	K_{eq} (k_1/k_{-1})	Log (K_{eq})	ΔE (V)	σ (ΔE)	$E°'$(NAceTrp) (V vs NHE)
With O_2	7.1	26	5.60E+03	5.85E+02	2.82E+08	4.54E+07	1.98E-05	4.703	0.278	0.053	1.078
O_2 Free[b]	7.1	8	5.50E+03	2.70E+02	3.29E+08	1.38E+07	1.67E-05	4.777	0.283	0.018	1.083

[a] number of replicates [b] oxygen free solutions were prepared by a 30 minute argon purge prior to mixing while maintaining an argon head space purge throughout the experiment.

3.4.5 Hydroxide Dependence: A hydroxide dependence study was performed on the stopped-flow instrument by combining equal volumes (A+B, 120 μL) of the following solutions: A = *N*-acetyl-tryptophan in 0.80 M NaCl (with added OH^-); and B = $Os(bpy)_3^{3+}$ in 0.80 M NaCl only. This scheme prevented degradation of the metal oxidant at high pH, where $Os(bpy)_3^{3+}$ → Os^{2+} products conversion occurs, probably via OH^- attack on the ligand. Upon mixing, the kinetics were monitored at 480 nm, which is a maximum of the MLCT absorption band of $Os(bpy)_3^{2+}$ in the visible region. The pH was measured after combining the reagents. Table 5 below includes the values for k_{OH^-}.

The role of OH^- as base was investigated over the pH range 10.00-11.94, [OH^-] = 0.10-8.9 mM without added buffer (I = 0.8 M, NaCl, T = 20 °C). Under pseudo-first order conditions the rate law was first order in both *N*-acetyl-tryptophan and OH^-. Plots of k_{obs}/[NAceTrp] vs. [OH^-] and k_{obs}/[OH^-] vs. [NAceTrp] were linear (Fig. 12), consistent with the rate law in eq 2. From the slopes of these plots, k_{OH^-} = $(7.5\pm0.9)\times10^8$ M^{-2} s^{-1} (Table 5).

Rate = $k_{obs}[Os(bpy)_3^{3+}]$ (2a)

$k_{obs} = k_{OH^-}[TrpN\text{-}H][OH^-]$ (2b)

Table 5. Rate constants obtained for the hydroxide dependent oxidation of NAceTrp by $Os(bpy)_3^{3+}$. Reported rate constants are from single exponential fits of stopped-flow data unless otherwise stated.

Buffer (Ionic Strength)	N[a]	pH	[OH⁻] (M)	k_{obs} (s^{-1})	σ k_{obs}	k_{OH^-} ($M^{-2}s^{-1}$)	σ k_{OH^-}
None (I =0.8M NaCl)	5	11.94	8.90E-03	1280	22.5	7.192E+08	1.264E+07
None (I = 0.8M NaCl)	10	11.74	5.53E-03	737	13.4	6.671E+08	1.215E+07
None (I = 0.8M NaCl)	10	11.60	3.95E-03	649	13.8	8.212E+08	1.746E+07
None (I = 0.8M aCl)	15	11.31	2.03E-03	237	4.65	5.852E+08	1.147E+07
None (I = 0.8M NaCl)	15	11.25	1.76E-03	230	2.81	6.549E+08	7.983E+06
None (I = 0.8M NaCl)	15	11.01	1.02E-03	136	2.74	6.712E+08	1.349E+07
None (I = 0.8M NaCl)	15	10.66	4.56E-04	67	1.31	7.395E+08	1.438E+07
None (I = 0.8M NaCl)	12	10.61	4.09E-04	89	1.49	1.093E+09	1.821E+07
None (I = 0.8M NaCl)	13	10.00	1.00E-04	28.6	0.61	1.422E+09	3.056E+07
50 mM Tris (I = 0.8M NaCl)	10	9.16[b]	1.45E-05	3.91	0.075	1.354E+09	2.591E+07
50 mM Tris (I = 0.8M NaCl)	10	9.16[c]	1.45E-05	2.66	0.014	9.197E+08	4.867E+06

[a] Number of replicates. [b] Analysis of these data was carried out by fitting to a single exponential, ignoring contributions to k_{obs} from k_1 and k_{-1} in Scheme 1. [c] Analysis of these data was carried out using SPECFIT/32 for the mechanism in Scheme 1, where contributions to k_{obs} arising both from k_{OH^-} and k_1, k_{-1} are considered. The rate constants for the redox equilibrium, k_1 and k_{-1} were kept constant at 6.90×10^3 $M^{-1}s^{-1}$ and 2.80×10^8 $M^{-1}s^{-1}$, respectively.

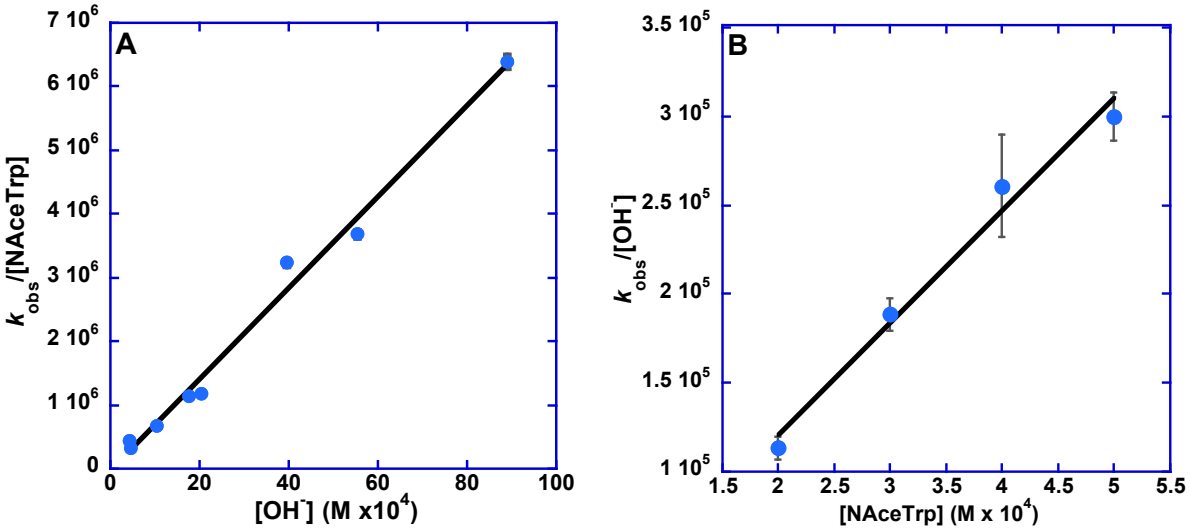

Figure 12. Rates of oxidation of *N*-acetyl-tryptophan by $Os(bpy)_3^{3+}$ as a function of reagent concentrations (I = 0.8 M, NaCl; T = 20 °C). (**A**) Plot of k_{obs}/[NaceTrp] vs. [OH^-] (0.10 – 8.9 mM) for $Os(bpy)_3^{3+}$ (20 μM), *N*-acetyl-tryptophan (200 μM). Error bars are included, however they are smaller than the data point symbols. (**B**) Variation of k_{obs}/[OH^-] vs. [NAceTrp] (200-500 μM) for $Os(bpy)_3^{3+}$ (20 μM), OH^- (500 μM). The linear fits yielded the third order rate constant, $k_{OH^-} = (7.5\pm0.9)\times10^8$ M^{-2} s^{-1}.

Stoichiometric oxidation of *N*-acetyl-tryptophan (TrpNH) by $Os(bpy)_3^{3+}$ under 1:1 conditions at pH 10.7 gave excellent fits to second order, equal concentration kinetics (Fig.13). This is consistent with a mechanism in which $Os(bpy)_3^{3+}$ reacts only with *N*-acetyl-tryptophan without complications from further oxidation of $TrpN^{\bullet}$ or $TrpNH^{+\bullet}$. Under identical conditions with a 2:1 ratio of Os^{3+}:TrpNH only 1 equivalent of $Os(bpy)_3^{3+}$ was reduced on the stopped-flow time scale, in agreement with the known 1-electron stoichiometry for oxidation of tryptophan at high pH.[16,20]

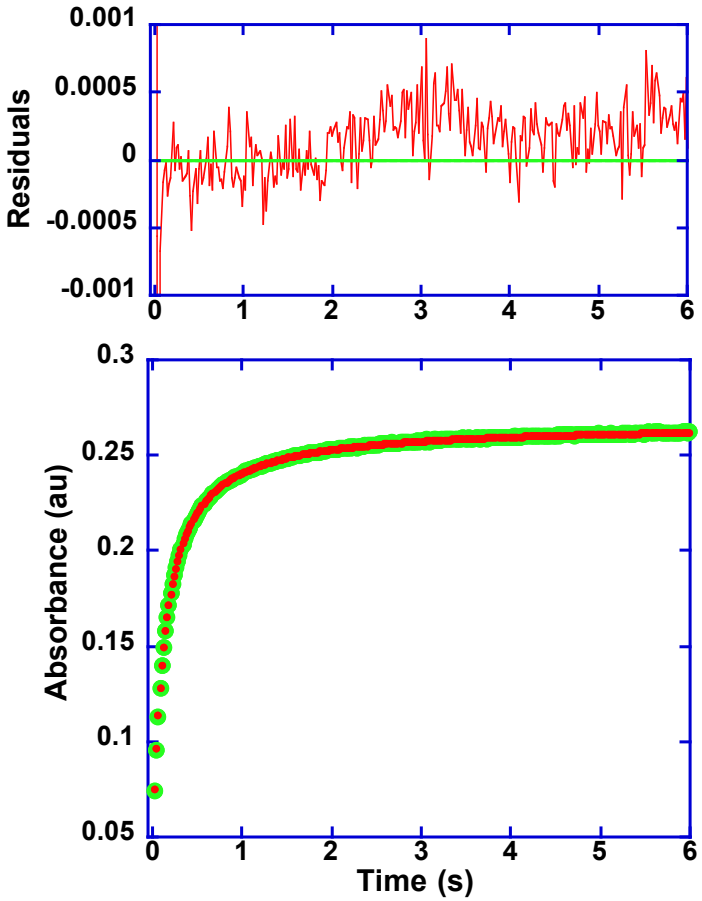

Figure 13. Stoichiometric (1:1) reaction of $Os(bpy)_3^{3+}$ (20 μM) with *N*-acetyl-tryptophan (20 μM) at pH 10.7 (I = 0.8 M NaCl, T = 20 °C) demonstrating second-order, equal concentration kinetics. The fit (red) to the kinetic trace data (green) was excellent, with very small residuals (top trace). The relative fit errors of individual traces averaged ±0.14% (< 0.0005 a.u.). The series of replicates yielded a second order rate constant of k' = $(3.8\pm0.1)\times10^5$ M^{-1} s^{-1} where $k_{ET} = k'/[OH^-]$, giving $k_{ET} = (7.6\pm0.3)\times10^8$ M^{-2} s^{-1}.

A mechanism involving initial deprotonation of *N*-acetyl-tryptophan (pK_a ~ 16) followed by oxidation of the anion by $Os(bpy)_3^{3+}$ (Scheme 4) can be ruled out on kinetic grounds. In this case, $k_{obs} = (K_a/K_w)k_{2(OH^-)}[TrpNH][OH^-]$, with $K_a/K_w \sim 10^{-2}$, from which $k_{2(OH^-)} = 8\times10^{10}$ M^{-1} s^{-1}. This value exceeds the diffusion controlled limit under these conditions by a factor of ~ 5.[31,32]

Scheme 4. (*TrpNH* = *N*-acetyl-tryptophan)

$$TrpNH + OH^- \rightleftharpoons TrpN^- + H_2O: \quad \boldsymbol{K_A/K_W} \qquad \textbf{(1)}$$

$$TrpN^- + Os(bpy)_3^{3+} \xrightarrow{k_{2(OH^-)}} TrpN^{\bullet} + Os(bpy)_3^{2+} \qquad \textbf{(2)}$$

$$TrpN^{\bullet} \longrightarrow oxidation\ products \qquad \textbf{(3)}$$

Oxidation of *N*-acetyl-tryptophan by $Os(bpy)_3^{3+}$ was also investigated by stopped-flow kinetic measurements in OD^-/D_2O with *N*-acetyl-tryptophan varied from 200 to 500 μM at pH = pD = 11 (in D_2O, pD = pH meter reading + 0.4), as shown in Figure 14. Analysis of these data gave $k_{OD^-} = (5.4\pm0.5)\times10^7$ M^{-2} s^{-1} and a solvent kinetic isotope effect (KIE) of $k_{H_2O}/k_{D_2O} = 13.8\pm0.9$. This value is considerably in excess of typical solvent kinetic isotope effects for outer-sphere electron transfer reactions which fall in the range 1.0 – 2.8.[33] There is precedence for large kinetic isotope effects in biological oxidations with $k_{C\text{-}H}/k_{C\text{-}D}$ values in excess of 80 reported for the oxidation of linoleic acid by soybean lipoxygenase by Klinman and coworkers.[34,35]

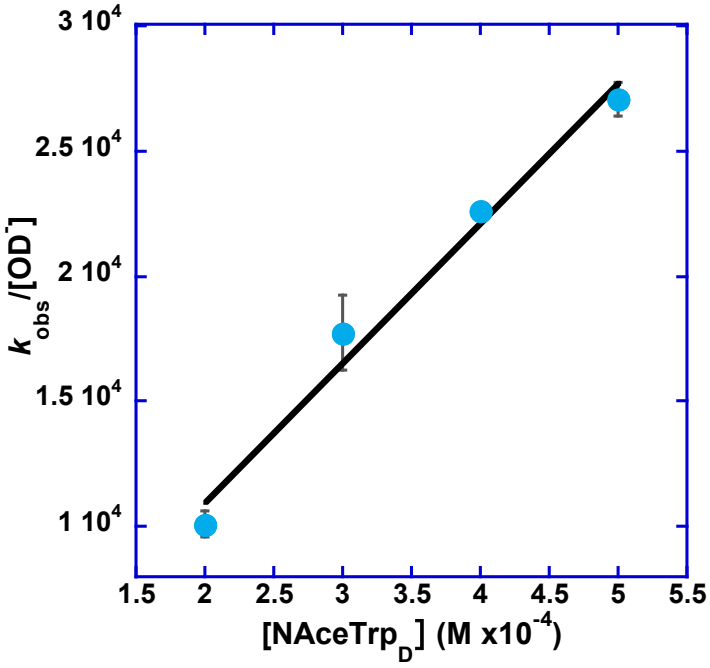

Figure 14. Plot of $k_{obs}/[OD^-]$ vs. [*N*-acetyl-tryptophan] (200-500 μM) in D_2O (I = 0.8 M, NaCl; T = 20 °C) for $Os(bpy)_3^{3+}$ (20 μM), OD^- (500 μM). The linear fit yielded the third order rate constant, $k_{OD^-} = (5.4\pm0.5)\times10^7$ M^{-2} s^{-1}.

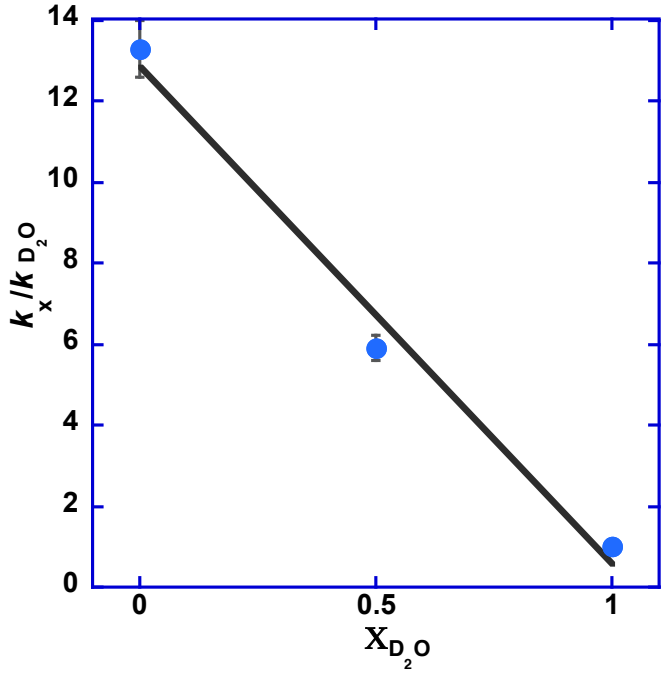

Figure 15. Mole fraction dependence (k_X/k_{D_2O}) for oxidation of *N*-acetyl-tryptophan (200 μM) by $Os(bpy)_3^{3+}$ (20 μM) at pH 10.7, $[OH^-]$ = 500 μM (I = 0.8 M, NaCl; T = 20 °C). The experimental kinetic traces from the stopped-flow instrument were fit to a single exponential decay.

As shown in Scheme 5, an alternate mechanism, consistent with the observed rate law and isotope effect, is prior H-bond association between OH^- and TrpNH, followed by MS-EPT. In the MS-EPT step, ET occurs to $Os(bpy)_3^{3+}$ in concert with indolic N-H proton transfer to OH^-. The magnitude of this KIE is considerably greater than the value of k_{H_2O}/k_{D_2O} = 2.8 observed for oxidation of tyrosine by $Os(bpy)_3^{3+}$ with acetate ($CH_3CO_2^-$) as the acceptor base.[36] A larger KIE for secondary amine oxidation is expected qualitatively owing to a less symmetric H-bond in the ion-pair adduct between the base and NAceTrpNH, resulting in a longer proton tunneling distance.[37] As noted by Savéant and coworkers, a concerted reaction is most competitive with stepwise pathways at the midpoint between pK_a values for the oxidized ($TrpNH^{\bullet+/0}$) and reduced (TrpNH) forms of the couple.[15] This is the case for MS-EPT oxidation with OH^- as base under our conditions, with $\Delta pK_a/2 \approx$ 9-10.

Scheme 5. (*TrpNH* = *N*-acetyl-tryptophan)

$$TrpN\text{-}H + OH^- \overset{K_A}{\rightleftharpoons} TrpN\text{-}H\text{--}OH^- \quad \textbf{(1)}$$

$$Os(bpy)_3^{3+} + TrpN\text{-}H\text{--}OH^- \overset{K_A'}{\rightleftharpoons} \{Os(bpy)_3^{3+}, TrpN\text{-}H\text{--}OH^-\} \quad \textbf{(2)}$$

$$\{Os(bpy)_3^{3+}, TrpN\text{-}H\text{--}OH^-\} \xrightarrow{k_{EPT}} Os(bpy)_3^{2+} + TrpN^{\bullet} + H_2O \quad \textbf{(3)}$$

$$TrpN^{\bullet} \longrightarrow oxidation\ products \quad \textbf{(4)}$$

3.5 Electrochemistry: We also investigated electrochemical oxidation of *N*-acetyl-tryptophan in 50 mM Tris buffer (pH = 7.1, I = 0.8M NaCl) by cyclic voltammetry measurements. As for other small organic molecules, *N*-acetyl-tryptophan has a kinetically slow response at ITO electrodes, with only small currents in excess of the background observed near the solvent oxidation limit. In the presence of a suitable redox mediator much larger catalytic currents were observed (Fig. 16) with rate information available by simulation of cyclic voltammetry waveforms.[14] We investigated the influence of *N*-acetyl-tryptophan on catalysis

of the $M(bpy)_3^{2+} \xrightarrow{e^-} M(bpy)_3^{3+}$ wave for the redox couples: $M(bpy)_3^{III/II}$ (M = Fe, Os); $M(dmb)_3^{III/II}$ (M = Fe, Ru); and $Ru(dmb)_2(bpy)^{III/II}$ (dmb = 4,4′-dimethyl-2,2′-bipyridine; bpy = 2,2′-bipyridine) with $E°'$ values ranging from 0.8 to 1.13 V vs. NHE, Table 6. All of these couples are electrochemically reversible.[14]

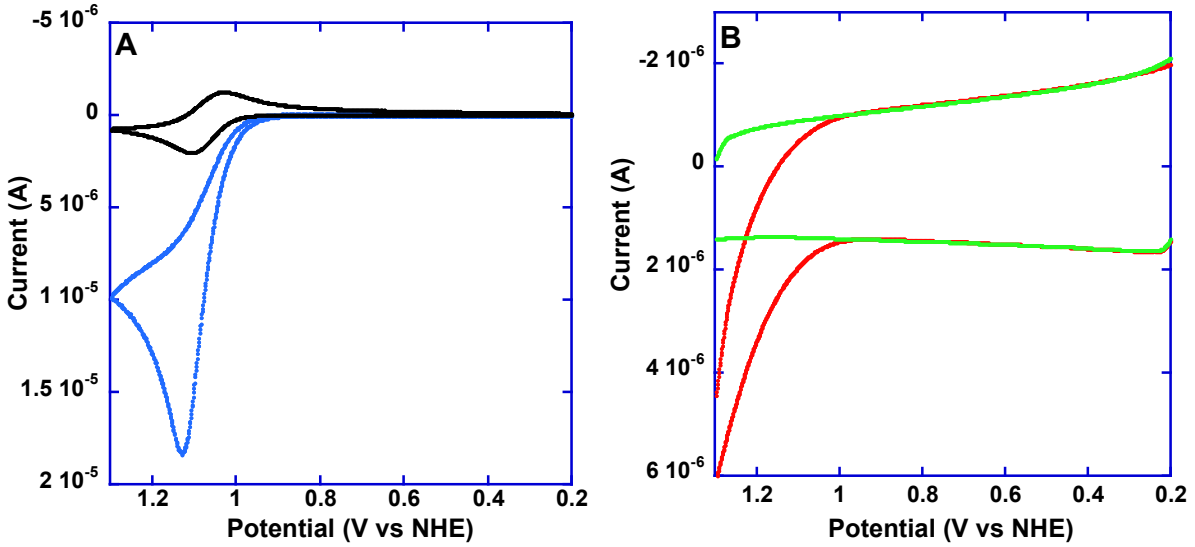

Figure 16. Cyclic voltammograms (ν = 300 mV/s; I = 0.8 M, NaCl; T = 25±2 °C) in 50 mM $H_2PO_4^-/HPO_4^{2-}$ (10:1 acid/base) at pH 6.2 (**A**) ITO + $Ru(dmb)_3^{2+}$ (20 μM, dmb = 4,4′-dimethyl-2,2′-bipyridine, black); ITO + NAceTrp (100 μM) + $Ru(dmb)_3^{2+}$ (20 μM, blue). (**B**) ITO only (green); (b) ITO + NAceTrp (100 μM, red).

Table 6: Experimental electrochemical parameters for each metal mediator used in the investigation.

Metal Mediator	Potential Range (V vs NHE)	Scan Rate (V/s)	Metal Concentration (μM)
$Ru(bpy)_2(dmb)^{III/II}$	0-1.45	0.300	20
$Ru(dmb)_2(bpy)^{III/II}$	0-1.4	0.300	20
$Ru(dmb)_3^{III/II}$	0-1.3	0.300	20
$Fe(bpy)_3^{III/II}$	0-1.25	0.300	20
$Fe(dmb)_3^{III/II}$	0-1.05	0.300	20
$Os(bpy)_3^{III/II}$	0-1.0	0.300	20

With the $M^{III/II}$ couples above as the redox mediators, there was no appreciable change in electrochemical behavior (Fig. 17) between different buffers and pH, {i.e., phosphate, ($H_2PO_4^-/HPO_4^{2-}$, pK_a 7.2, pH 6.2) and Tris (pK_a 8.1, pH 7.1)}, indicating that the solution kinetics at neutral pH were dominated by an outer-sphere electron transfer mechanism.

Furthermore, k_{H_2O}/k_{D_2O} = 1.3 with NAceTrp (100 μM) + $Ru(dmb)_3^{2+}$ (20 μM) in 50 mM Tris (10:1 acid/base) at pH 7.1 (I = 0.8 M, NaCl, T = 25 ± 2 °C) with a scan rate of 300 mV/s. This behavior is in dramatic contrast to tyrosine oxidation with significant rate enhancements observed under the same conditions.[14] The absence of significant base or isotope effects is consistent with oxidation by rate-limiting outer-sphere electron transfer, Scheme 6. A free-energy dependence was conducted over a range of $M^{III/II}$ oxidants in order to examine the effect of mediator redox potential on the electrochemical kinetics (Section 3.6). Where current enhancements were observed, the cyclic voltammetry responses were analyzed using numerical simulations.

Scheme 6. (*TrpNH* = *N*-acetyl-tryptophan)

$$M(bpy)_3^{3+} + TrpNH \underset{}{\overset{K_A}{\rightleftharpoons}} \{M(bpy)_3^{3+}, TrpNH\} \quad \textbf{(1)}$$

$$\{M(bpy)_3^{3+}, TrpNH\} \xrightarrow{k_{ET}} \{M(bpy)_3^{2+}, TrpNH^{\bullet+}\} \quad \textbf{(2)}$$

$$\{M(bpy)_3^{2+}, TrpNH^{\bullet+}\} \underset{}{\overset{K_A'}{\rightleftharpoons}} M(bpy)_3^{2+} + TrpNH^{\bullet+} \quad \textbf{(3)}$$

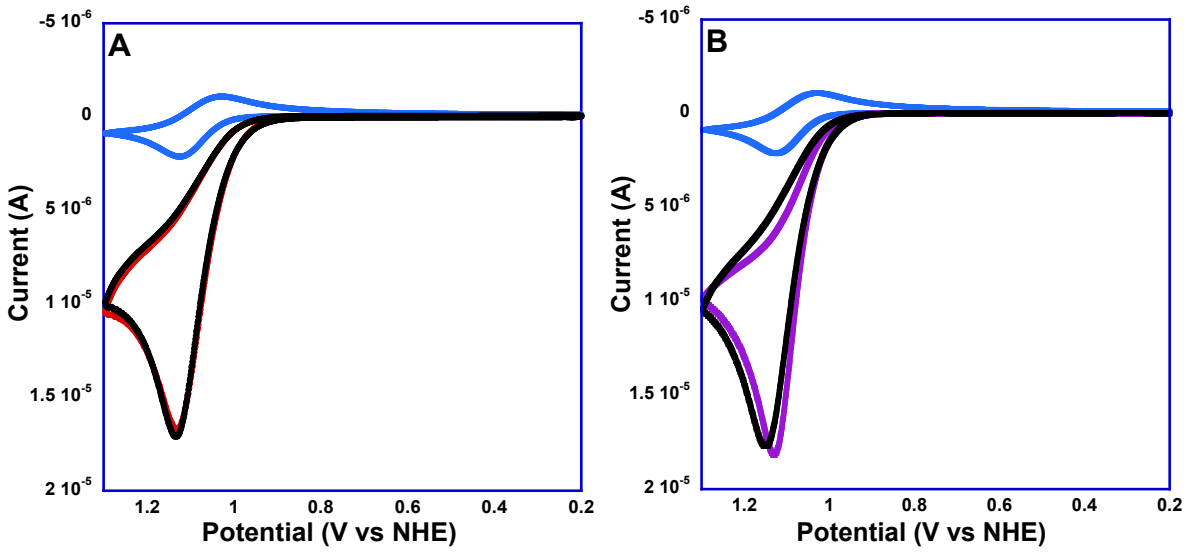

Figure 17. Cyclic voltammograms at an ITO working electrode (ν = 300 mV/s; I = 0.8 M, NaCl; T = 25±2 °C) for: (**A**) $Ru(dmb)_3^{2+}$ (20 μM, blue); $Ru(dmb)_3^{2+}$ (20 μM) + *N*-acetyl-tryptophan (100 μM) in 50 mM, Tris, 4.54 mM in buffer base, pH 7.1 (black); $Ru(dmb)_3^{2+}$ (20 μM) + *N*-acetyl-tryptophan (100 μM) in 5 mM Tris, 0.454 mM in buffer base, pH 7.1 (red); (**B**) $Ru(dmb)_3^{2+}$ (20 μM, blue); $Ru(dmb)_3^{2+}$ (20 μM) + *N*-acetyl-tryptophan (100 μM) in 50 mM Tris, 4.54 mM in buffer base, pH 7.1 (black); $Ru(dmb)_3^{2+}$ (20 μM) + *N*-acetyl-tryptophan (100 μM) in 50 mM $H_2PO_4^-/HPO_4^{2-}$, 4.54 mM in HPO_4^{2-}, pH 6.2. (purple).

The electrochemistry of $Fe(dmb)_3^{III/II}$ + *N*-acetyl-tryptophan was unique in that the mediator has a lower potential ($E^{\circ\prime}$ = 0.86V vs. NHE) than *N*-acetyl-tryptophan and the other complexes studied. Cyclic voltammograms of $Fe(dmb)_3^{III/II}$ + *N*-acetyl-tryptophan in 50 mM Tris buffer, pH 7.1 are shown below in Figure 18. As expected, the voltammograms show a much smaller catalytic current in the presence of *N*-acetyl-tryptophan than the other complexes. The onset of another peak appears at the vertex potential in Figure 18A. When the scan is widened (Fig. 18B) a poorly defined oxidation peak appears, which is attributed to the direct oxidation of *N*-acetyl-tryptophan at the electrode. This can also be seen at high potentials without the presence of a metal mediator (Fig. 19).

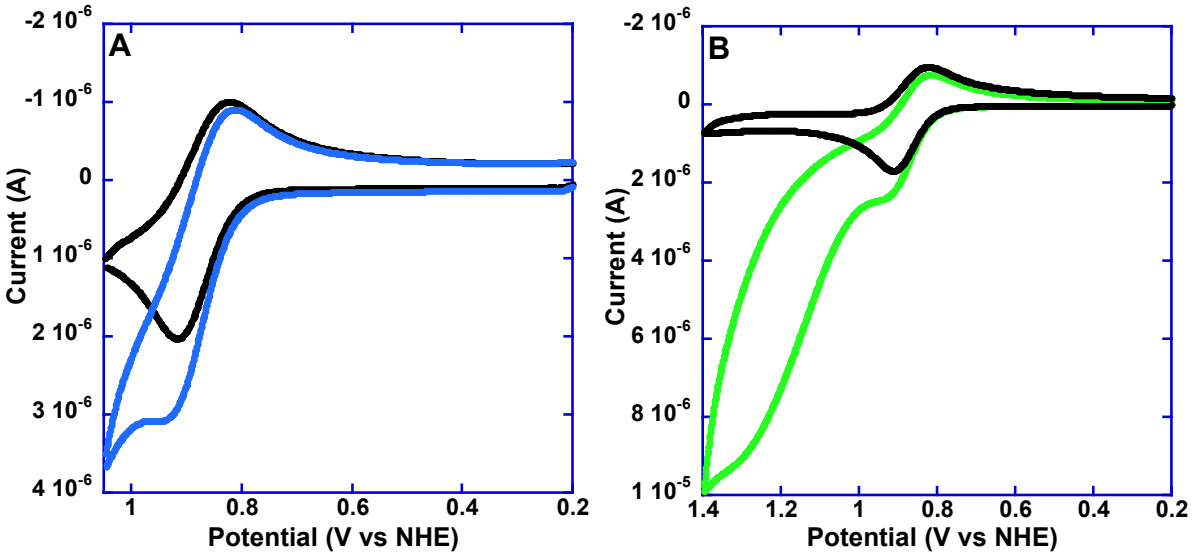

Figure 18. Cyclic voltammograms at an ITO working electrode (ν = 300 mV/s; I = 0.8 M, NaCl, T = 25±2 °C) for: (**A**) $Fe(dmb)_3^{2+}$ (20 μM) in 50 mM Tris, pH 7.1, (black); $Fe(dmb)_3^{2+}$ (20 μM) + *N*-acetyl-tryptophan (100 μM, blue); (**B**) $Fe(dmb)_3^{2+}$ (20 μM) in 50 mM Tris, pH 7.1, (black); $Fe(dmb)_3^{2+}$ (20 μM) + *N*-acetyl-tryptophan (100 μM, green)**.**

The waveforms in Figure 18 are expected when a metal mediator couple, with facile heterogeneous kinetics, has a lower potential than the organic substrate. In this case the slow heterogeneous kinetics between the electrode and the substrate alone can be seen in the cyclic voltammograms (Fig. 19). This contribution was included in the simulations discussed below by adding the direct oxidation of the substrate at the electrode ($k_D = 5\times10^{-4}$ cm s^{-1}).

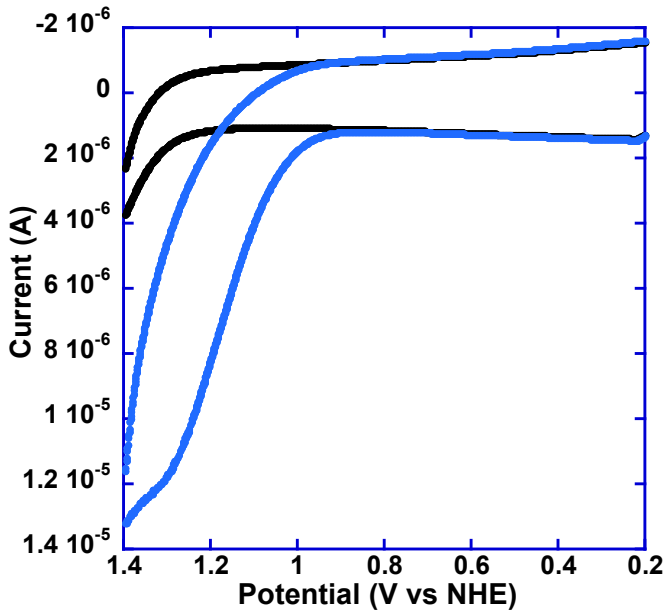

Figure 19. Background cyclic voltammograms (ν = 300 mV/s; I = 0.8 M, $LiClO_4$; T = 25±2 °C) at a plain ITO working electrode (A = 0.32 cm^2) for: 50 mM, pH 7.1 Tris buffer (black); buffer + *N*-acetyl-tryptophan (100 μM, blue).

3.5.1 Fitting Electrochemical Data Using Digital Simulations: Numerical simulations were performed with the DigiSim software package (Bioanalytical Systems, Inc., West Lafayette, IN).[38] The mechanisms shown in Schemes 1, 2, and 3 were used to fit representative electrochemical data. The models employed fixed [H^+] buffering in the numerical simulations. For each scheme, protonation of the *N*-acetyl-tryptophan radical was assumed to occur at diffusion control (k_{-2} = 1×10^{10} M^{-1} s^{-1}), and the deprotonation rate constant, k_2 = 5×10^5 s^{-1}, was set by ratio, based on the experimental pK_a($TrpNH^{\bullet+}$) = 4.3.[17] The rate constant for the disproportionation of $TrpN^{\bullet}$ was set to the value of 3.2×10^8 $M^{-1}s^{-1}$ reported for the pH independent, second order decay of tryptophan radical.[17,39] In Scheme 2, the protonation of the tryptophan anion (k_4 = 1×10^{10} M^{-1} s^{-1}) was also assumed to be near diffusion controlled. All parameters other than the forward rate constant (k_1) for the initial redox pre-equilibrium, $K_{eq} = k_1/k_{-1}$, (and k_3 in Scheme 3) were either calculated or set to literature values.

Table 7: Simulation parameters imported into DigiSim. Scan rates and potential ranges reported above for experimental parameters were also imported into the program. Electron transfer rate constants between the metal mediator and the electrode (k_s) were typically 0.01 cm s^{-1}, and were determined from cyclic voltammograms of the metal mediator alone.

Metal Mediator	$E°'$ (V vs NHE)	D_{metal} (10^{-6} cm^2/s)	$D_{NAceTrp}$ (10^{-6} cm^2/s)	[Metal] (μM)	[NAceTrp] (μM)
$Ru(bpy)_2(dmb)^{III/II}$	1.18	6.0	4.5	20	100
$Ru(dmb)_2(bpy)^{III/II}$	1.13	6.0	4.5	20	100
$Ru(dmb)_3^{III/II}$	1.06	6.0	4.5	20	100
$Fe(bpy)_3^{III/II}$	1.03	6.0	4.5	20	100
$Fe(dmb)_3^{III/II}$	0.86	6.0	4.5	20	100
$Os(bpy)_3^{III/II}$	0.80	6.0	4.5	20	100

In the simulations there were two adjustable parameters, k_s, the rate of heterogeneous electron transfer at the electrode for oxidation of $M(bpy)_3^{2+}$, and k_1, the rate constant for oxidation of *N*-acetyl-tryptophan by $M(bpy)_3^{3+}$. The value of k_1 was varied to obtain the best fit to the waveforms with k_{-1} determined by the equilibrium ratio, $k_1/k_{-1} = K_{eq} = \exp\{(E°'(M^{III/II}) - (E°'(TrpNH^{\bullet+/0})/0.026\}$, and $E°'(TrpNH^{\bullet+/0}) = 1.06$ V. Diffusion coefficients used in the simulations were either measured or reported previously.[14] The electrochemical model produced satisfactory fits to the cyclic voltammograms providing rate constants for outer-sphere electron transfer, k_1, (Fig. 20) and $k_1 = k_{ET}K_A$, Scheme 7. The results are summarized in Table 8 together with $E°'$ values for the $M(bpy)_3^{III/II}$ couples, and $\Delta G°'$ values for oxidation of *N*-acetyl-tryptophan. For $Os(bpy)_3^{3+}$ as oxidant, there was no significant catalytic current and the rate constant obtained by stopped-flow measurements is reported in Table 1.

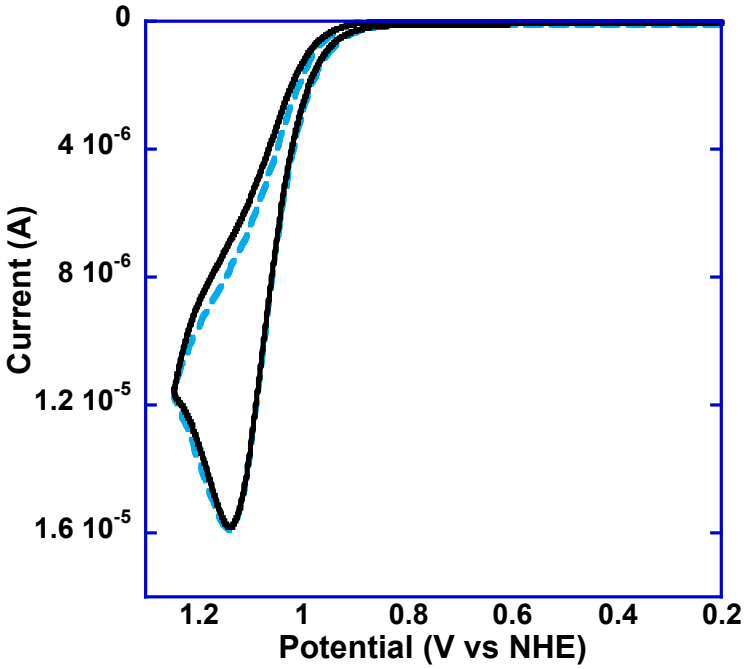

Figure 20. Cyclic voltammogram (ν = 300 mV/s; I = 0.8 M, NaCl) of $Fe(bpy)_3^{2+}$ (20 μM) + *N*-acetyl-tryptophan (100 μM) in 50 mM Tris at pH 7.1 at an ITO electrode (black, solid); and the simulation result (blue, dotted) from DigiSim for the mechanism in Scheme 7.

Scheme 7 (*TrpNH* = *N*-acetyl-tryptophan)

$$M^{2+} \underset{}{\overset{k_s}{\rightleftharpoons}} M^{3+} \qquad \textbf{(1)}$$

$$TrpNH \overset{k_D}{\rightleftharpoons} TrpNH^{\bullet +} \qquad \textbf{(2)}$$

$$M^{3+} + TrpNH \underset{k_{-1}}{\overset{k_1}{\rightleftharpoons}} M^{2+} + TrpNH^{\bullet +} \qquad \textbf{(3)}$$

$$TrpNH^{\bullet +} \underset{k_{-2}}{\overset{k_2}{\rightleftharpoons}} TrpN^{\bullet} + H^{+} \qquad \textbf{(4)}$$

$$TrpNH^{\bullet +} + TrpN^{\bullet} \xrightarrow{k_3} TrpNH + TrpN^{+} \qquad \textbf{(5)}$$

The mechanism shown in Scheme 7 gave the best fits to the electrochemical data. The rate constants (k_1) in Table 8 are based on Scheme 7, which is equivalent to Scheme 1, but includes additional terms required for heterogeneous electrochemical modeling purposes. These include the rate constant ($k_D \sim 5\times10^{-4}$ cm s^{-1}) for direct electron transfer between *N*-acetyl-tryptophan and the electrode, reflecting the slow kinetics for oxidation of *N*-acetyl-

tryptophan at ITO. The mechanism outlined in Scheme 7 was preferred over the mechanism in Scheme 2 because simple disproportionation would require initial formation of the energetically unfavorable product, *N*-acetyl-tryptophan anion. Scheme 3 was disfavored because of the larger number of adjustable parameters.

K_{eq} for the initial redox equilibrium was calculated from equation 3 below with $E°'(\text{TrpNH}^{\bullet+}/\text{TrpNH})$ = +1.06V vs. NHE and the $E°'$ for the respective $M^{III/II}$ couple (Table 7). The diffusion coefficient for *N*-acetyl-tryptophan was measured at neutral pH (I = 0.8 M, NaCl) by rotating disk voltammetry and the Levich equation, where n = 2 was assumed for the number of electrons transferred at the electrode.[29]

$$K_{eq} = e^{\frac{E_{Ox}(M^{III/II})-E_{Ox}(Trp)}{-0.0255}} \qquad (3)$$

The values $\Delta G° = -nF\Delta E°$ in Table 8 were calculated from $E°'$(*N*-acetyl-tryptophan) - $E°'(M^{III/II})$, where $E°'$(*N*-acetyl-tryptophan) = 1.06 V vs. NHE. Over the range of metal mediators studied there was a Marcus type dependence of $RT\ln(k_{ET})$ vs. $\Delta G°$, (Figure 21).

Table 8. Rate constants (k_1) obtained by numerical simulation of oxidative sweep cyclic voltammograms with NAceTrpNH (100 μM) + oxidant (20 μM) in 50 mM Tris (10:1 acid/base) at pH 7.1 (I = 0.8 M, NaCl), T = 25 ± 2 °C with a scan rate of 300 mV/s.

Metal Mediator	$E°'$ **(V vs.NHE)**	$\Delta G°$ **(eV)**	k_1 (k_{ET}) ($M^{-1}s^{-1}$)	RT ln(k_{ET}) **(eV)**
$Ru(dmb)_2(bpy)^{III/II}$	1.13	-0.07	2.3 E+07	0.430
$Ru(dmb)_3^{III/II}$	1.06	0	1.7 E+07	0.423
$Fe(bpy)_3^{III/II}$	1.03	0.03	1.1 E+07	0.410
$Fe(dmb)_3^{III/II}$	0.86	0.2	4.4 E+04	0.269
$Os(bpy)_3^{III/II}$	0.80	0.26	5.6 E+04[a]	0.221

[a] Rate constants for $Os(bpy)_3^{III/II}$ were taken from stopped-flow experiments from kinetic analysis with SPECFIT/32.

3.6 Marcus Treatment for Lambda: In the classical limit, the rate constant for electron transfer, $k_{obs} = k_{ET}K_A$ (= k_1 in Scheme 1) is given by eqs 4,5.

$$RT\ln k_{ET} = RT\ln k_0 + \frac{\Delta G_{ET}}{2} + \left(1 + \frac{\Delta G_{ET}}{2\lambda}\right) \quad (4)$$

$$k_0 = \nu_{ET} K_A (4\pi RT\lambda)^{-1/2} \exp -\left[\frac{\lambda}{4RT}\right] \quad (5)$$

In these equations, ν_{ET} is the electron transfer barrier crossing frequency, and ΔG_{ET} is the free energy change for the electron transfer step. It is given by: ΔG_{ET}(eV) = -{$E°'(M^{III/II})$ - $E°'(TrpNH^{+\bullet}/TrpNH)$} - 0.059(p$K_a$' – p$K_a$), with K_A and K_A' the association constants for the electron transfer reactants (1) and products (3) in Scheme 6 respectively. In eq 4, k_0 is the rate constant at ΔG_{ET} = 0 and λ is the sum of intramolecular (λ_i) and medium (λ_o) reorganization energies.[3,40]

Figure 21 shows a plot of $RT\ln(k_{ET})$ vs. $-\Delta G°'$(eV), with $\Delta G°'$(eV) = -{$E°'(M^{III/II})$ - $E°'(TrpNH^{+\bullet}/TrpNH)$} which neglects K_A and K_A'. In the figure a plot of a fit to eq 5 (red) is shown through the data (blue circles) with the parameters $k_0 = 1.7\times10^7$ M^{-1} s^{-1} and λ = 0.6. The value of k_0 was taken for the $Ru(dmb)_3^{III/II}$ couple with $E°'$ = 1.06 V vs. NHE, where $\Delta G°'$ = 0. Based on λ = 0.39 eV for $M(bpy)_3^{III/II}$ self-exchange and the relationship, λ = (λ_{TrpNH} + $\lambda_{[M(bpy)_3]^{3+}}$)/2, assuming the pre-exponential factor in eq 7 is ν_{ET} K_A ~10^{11} gives λ_{TrpNH} ~ 0.8 eV.[41, 42]

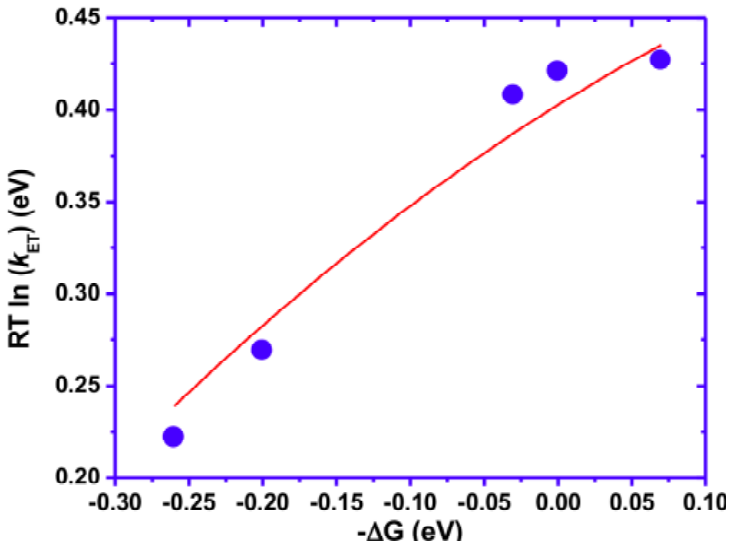

Figure 21. Variation of $RT\ln(k_{ET})$ vs. $-\Delta G°'$(eV) for outer-sphere electron transfer between *N*-acetyl-tryptophan and the oxidants $M(bpy)_3^{3+}$, from Table 8.

3.7 Concluding Remarks: A number of meaningful conclusions appear from this study focused on tryptophan oxidation and by implication, tryptophan charge transfer reactions in biological systems.

- There is no pH, buffer concentration, or base p*K*a dependence on rates of N-acetyl-tryptophan oxidation over a large potential range of $M^{III/II}$ oxidants, all indicating an outer-sphere electron transfer mechanism.
- There was observed 2:1 $[M^{3+}]$:[NAceTrp] stoichiometry at intermediate pH, with a special disproportionation mechanism, used to fit both spectroscopic and electrochemical data.
- At pHs > 9, hydroxide becomes a stoichiometric reagent, as a base that associates with tryptophan before concerted electron proton transfer, a mechanism also suggested by the measured $k_{H_2O}/k_{D_2O} \sim 14$ at basic pH.

- A Marcus treatment of *N*-acetyl-tryptophan oxidation by a series of metal oxidants, taken electrochemically and simulated in DigiSim, gave $\lambda_{TrpNH} \sim 0.8$ eV, in good agreement with previously reported values.
- There are important implications in these results for tryptophan oxidation in biology. Because of the high pK_a of the indolic nitrogen of tryptophan (p$K_a \approx 16$) a mechanism involving the formation of a hydrogen bound base adduct prior to electron transfer, as seen between His190 and Tyr161 in photosystem II, is absent. As for W306, W359 and W382 tryptophan residues in DNA photolyase, intervention of an acceptor base to facilitate an EPT mechanism is absent, where these residues are found to be in solvent exposed pockets of the enzyme, and not within hydrogen bonding distance of a H^+ accepting base.

3.8 References:

(1) Aubert, C.; Vos, M. H.; Mathis, P.; Eker, A. P. M.; Brettel, K. **Intraprotein Radical Transfer During Photoactivation of DNA Photolyase**. *Nature* **2000**, *405*, 586-590.

(2) Lukacs, A.; Eker, A. P. M.; Byrdin, M.; Brettel, K.; Vos, M. H. **Electron Hopping through the 15 Å Triple Tryptophan Molecular Wire in DNA Photolyase Occurs within 30 ps**. *J. Am. Chem. Soc.* **2008**, *130*, 14394-14395.

(3) Huynh, M.-V. H.; Meyer, T. J. **Proton Coupled Electron Transfer**. *Chem. Rev.* **2007**, *107*, 5004-5064.

(4) Meyer, T. J.; Huynh, M.-V. H.; Thorp, H. H. **The Possible Role of Proton-Coupled Electron Transfer (PCET) in Water Oxidation by Photosystem II**. *Angew. Chem. Int. Ed*. **2007**, *46*, 5284-5304.

(5) Stubbe, J.; van der Donk, W. A. **Protein Radicals in Enzyme Catalysis**. *Chem. Rev*. **1998**, *98*, 705-762.

(6) Reece, S.; Hodgkiss, J. M.; Stubbe, J.; Nocera, D. G. **Proton-Coupled Electron Transfer: The Mechanistic Underpinning for Radical Transport and Catalysis in Biology**. *Philos. Trans. R. Soc. B* **2006**, *361*, 1351-1364.

(7) Seyedsayamdost, M. R.; Yee, C. S.; Reece, S. Y.; Nocera, D. G.; Stubbe, J. **pH Rate Profiles of F_nY_{356}-R2s (n= 2, 3, 4) in *Escherichia coli* Ribonucleotide Reductase: Evidence that Y356 Is a Redox-Active Amino Acid along the Radical Propagation Pathway**. *J. Am. Chem. Soc.* **2006**, *128*, 1562-1568.

(8) Zouni, A. Z.; Witt, H.; Kern, J.; Fromme, P.; Krauss, N.; Saenger, W.; Orth, P. **Crystal structure of photosystem II from *Synechococcus elongatus* at 3.8 Å resolution**. *Nature* **2001**, *409*, 739-743.

(9) Persson, A. L.; Erikson, M.; Katterle, B.; Pötsch, S.; Sahlin, M.; Sjöberg, B. **A New Mechanism-based Radical Intermediate in a Mutant R1 Protein Affecting the Catalytically Essential Glu^{441} in *Escherichia coli* Ribonucleotide Reductase**. *J. Biol. Chem*. **1997**, *272*, 31533-31541.

(10) Ekberg, M.; Pötsch, S.; Sandin, E.; Thunnissen M.; Nordlund, P.; Sahlin, M.; Sjöberg, B. **Preserved Catalytic Activity in an Engineered Ribonucleotide Reductase R2 Protein with a Nonphysiological Radical Transfer Pathway**. *J. Biol. Chem*. **1998**, *273*, 21003-21008.

(11) Gagliardi, C. J.; Jurss. J. W.; Thorp, H. H.; Meyer, T. J. **Surface Activation of Electrocatalysis at Oxide Electrodes. Concerted Electron-Proton Transfer**. *Inorg. Chem.* **2011**, *50*, 2076-2078.

(12) Jurss, J. W.; Concepcion, J. C.; Norris, M, R.; Templeton, J. L.; Meyer, T. J. **Surface Catalysis of Water Oxidation by the Blue Ruthenium Dimer**. *Inorg. Chem.* **2010**, *49*, 3980-3982.

(13) Fecenko, C. J.; Meyer, T. J.; Thorp, H. H. **Electrocatalytic Oxidation of Tyrosine by Parallel Rate Limiting Proton Transfer and Multi-Site Electron-Proton Transfer**. *J. Am. Chem. Soc*. **2006**, *128*, 11020-11021.

(14) Fecenko, C. J.; Thorp, H. H.; Meyer, T. J. **The Role of Free Energy Change in Coupled Electron-Proton Transfer**. *J. Am. Chem. Soc*. **2007**, *129*, 15098-15099.

(15) Costentin, C.; Robert, M.; Savéant, J.-M. **Concerted Proton-coupled Electron Transfers in aquo/hydroxo/oxo Metal Complexes: Electrochemistry of $[Os^{II}(bpy)_2py(OH_2)]^{2+}$ in Water**. *Proc. Natl. Acad. Sci. USA*. **2009**, *106*, 11829-11836.

(16) Stewart, D. J.; Napolitano, M. J.; Bakhmutova-Albert, E. V.; Margerum, D. W. **Kinetics and Mechanisms of Chlorine Dioxide Oxidation of Tryptophan**. *Inorg. Chem*. **2008**, *47*, 1639-1647.

(17) Posener, M. L.; Adams, G. E.; Wardman, P.; Cundall, R. B. **Mechanism of Tryptophan Oxidation by Some Inorganic Radical-Anions: A Pulse Radiolysis Study**. *J. Chem. Soc. Farad. Trans. 1* **1976**, 72, 2231-2239.

(18) Weinberg, D. R.; Gagliardi, C. J.; Hull, J. F.; Murphy, C. F.; Kent, C. A.; Westlake, B.; Paul, A.; Ess, D. H.; McCafferty, D. G.; Meyer, T. J. **Proton-Coupled Electron Transfer**. *Chem. Rev.* **2012**, 112, 4016-4093.

(19) Shih, C.; Museth, A. K.; Abrahamsson, M.; Blnco-Rodriguez, A. M.; Di, Bilio, A. J.; Sudhamsu, J.; Crane, B. R.; Ronayne, K. L.; Towrie, M.; Vlček Jr. A.; Richards, J. H.; Winkler, J. R.; Gray, H. B. **Tryptophan-Accelerated Electron Flow Through Proteins**. *Science* **2008**, *320*, 1760-1762.

(20) Sjödin, M.; Stenbjörn, S.; Åkermark, B.; Sun, L.; Hamarström, L. **Proton-Coupled Electron Transfer from Tyrosine in a Tyrosine−Ruthenium−tris-Bipyridine Complex: Comparison with $Tyrosine_z$ Oxidation in Photosystem II**. *J. Am. Chem. Soc.* **2000**, *122*, 3932-3936.

(21) Zhang, M.-T; Hammarström, L. **Proton-Coupled Electron Transfer from Tryptophan: A Concerted Mechanism with Water as Proton Acceptor**. *J. Am. Chem. Soc.* **2011**, *133*, 8806-8809.

(22) Demadis, K. D.; Dattelbaum, D. M.; Kober, E. M.; Concepcion, J. J.; Paul, J. J. Meyer, T. J.; White, P. S. **Vibrational and Structural Mapping of $[Os(bpy)_3]^{3+/2+}$ and $[Os(phen)_3]^{3+/2+}$**. *Inorg. Chim. Acta* **2007**, *360*, 1143-1153.

(23) Jovanovic, S. V.; Harriman, A.; Simic, M. **Electron-Transfer Reactions of Tryptophan and Tyrosine Derivatives**. *J. Phys. Chem.* **1986**, *90*, 1935-1939.

(24) Willit, J. L.; Bowden, E. F. **Adsorption and Redox Thermodynamics of Strongly Adsorbed Cytochrome *c* on Tin Oxide Electrodes**. *J. Phys. Chem*. **1990**, *94*, 8241-8245.

(25) Malfoy, B.; Reynaud, J. A. **Electrochemical Investigations of Amino Acids at Solid Electrodes: Part II. Amino Acids Containing no Sulfur atoms: Tryptophan, Tyrosine, Histidine and Derivatives**. *J. Electroanal. Chem.* **1980**, *114*, 213-223.

(26) Merényi, G.; Lind, J.; Shen, X. **Electron Transfer from Indoles, Phenols and Sulfite (SO_3^{2-}) to Chlorine Dioxide ($ClO_2^{\bullet}$)**. *J. Phys. Chem.* **1988**, *92*, 134–137.

(27) Ogata, N. **Denaturation of Protein by Chlorine Dioxide: Oxidative Modification of Tryptophan and Tyrosine Residues**. *Biochemistry* **2007**, *46*, 4898-4911.

(28) Savige, W. E. **Isolation and Identification of Some Photo-oxidation Products of Tryptophan**. *Aust. J. Chem.* **1971**, *24*, 1285–1293.

(29) Nguyen, N. T.; Wrona, M. Z.; Dryhurst, G. **Electrochemical Oxidation of Tryptophan**. *J. Electroanal. Chem.* **1986**, *199*, 101-126.

(30) Savige, W. E. **New Oxidation Products of Tryptophan**. *Aust. J. Chem.* **1975**, *28*, 2275-2287.

(31) Alberty R. A., Hammes G. G. **Application of the Theory of Diffusion-controlled Reactions to Enzyme Kinetics**. *J. Phys. Chem.* **1958**, *62*, 154-159.

(32) Hammes, G. G. *Principles of Chemical Kinetics*; Academic Press: New York, 1978; p 203.

(33) Weaver, M. J.; Tyma, P. D.; Nettles, S. M. **Solvent Isotope Effects upon the Kinetics of some Simple Electrode Reactions**. *J. Electroanal. Chem*. **1980**, *114*, 53-72.

(34) Rickert, K. W.; Klinman, J. P. **Nature of Hydrogen Transfer in Soybean Lipoxygenase 1: Seperation of Primary and Secondary Isotope Effects**. *Biochemistry* **1999**, *38*, 12218–12228.

(35) Glickman, M. H.; Klinman, J. P. **Nature of Rate-Limiting Steps in the Soybean Lipoxygenase-1 Reaction**. *Biochemistry* **1995**, *34*, 14077–14092.

(36) C. F. Murphy. Ph.D dissertation, University of North Carolina, Chapel Hill, N.C., **2009**.

(37) Iordanova, N.; Hammes-Schiffer, S. **Theoretical Investigation of Large Kinetic Isotope Effects for Proton-Coupled Electron Transfer in Ruthenium Polypyridyl Complexes**. *J. Am. Chem. Soc.* **2002**, *124*, 4848-4856.

(38) Rudolph, M.; Reddy, D. P.; Feldberg, S. W. **A Simulator for Cyclic Votammetric Responces**. *Anal. Chem*. **1994**, *66*, 598A-600A.

(39) Solar, S.; Getoff, N.; Surdhar, P. S.; Armstrong, D. A.; Singh, A. **Oxidation of Tryptophan and N-Methylindole by $N_3^{\bullet}$, $Br_2^{\bullet-}$ and $(SCN)_2^{\bullet-}$ Radicals in Light- and Heavy- Water Solutions: A Pulse Radiolysis Study**. *J. Phys. Chem*. **1991**, *95*, 3639-3643.

(40) Chen, P.; Meyer, T. J. **Medium Effects on Charge Transfer in Metal Complexes**. *Chem. Rev.* **1998**, *98*, 1439-1477.

(41) Young, R. C.; Keene, F. R.; Meyer, T. J. **Measurement of Rates of Electron Transfer Between $Ru(bpy)_3^{3+}$ and $Fe(phen)_3^{2+}$ and Between $Ru(phen)_3^{3+}$ and $Ru(bpy)_3^{2+}$ by Differential Excitation Flash Photolysis**. *J. Am. Chem. Soc.* **1977**, *99*, 2468-2473.

(42) Marcus, R. A. **On the Theory of Oxidation-Reduction Reactions Involving Electron Transfer. V. Comparison and Properties of Electrochemical and Chemical Rate Constants**. *J. Phys. Chem*. **1963**, *67*, 853-857.

Chapter 4

Concerted Electron-Proton Transfer (EPT) in the Oxidation of Cysteine[a]

4.1 Abstract: Cysteine is distinct among the redox active amino acids owing to its acidic thiol (–S-H) proton (pK_a = 8.2) compared to the –O-H proton of tyrosine (pK_a = 10.1) or the very weakly acidic indolic –N-H proton of tryptophan (pK_a ~16). Stopped-flow and electrochemical measurements have been used to explore the role of proton coupled electron transfer (PCET) and concerted electron-proton transfer (EPT) in *L*-cysteine and *N*-acetyl-cysteine oxidation. The results of these studies have revealed a role for acetate (AcO^-) and phosphate (HPO_4^{2-}) as a proton acceptor base in concerted electron-proton transfer (EPT) oxidation of *L*-cysteine and *N*-acetyl-cysteine, with good agreement between rate constants measured by electrochemical and spectroscopic techniques.

4.2 Introduction: The amino acids tyrosine, cysteine, and tryptophan play important roles as electron transfer carriers and mediators in biology with important examples appearing in photosystem II, class I ribonucleotide reductase, and DNA photolyase.[1-8] In tyrosine and cysteine oxidation, proton coupled electron transfer (PCET), half reactions in which protons and electrons are gained or lost, is important in avoiding charge build up. Concerted electron-

[a] Reproduced in parts with permission from the American Chemical Society; Christopher J. Gagliardi, Christine F. Murphy, H. Holden Thorp and Thomas J. Meyer **Concerted Electron-Proton Transfer (EPT) in the Oxidation of Cysteine**. *J. Am. Chem. Soc.* **2012**, *In Preparation*.

proton transfer (EPT) pathways are used to avoid high-energy protonated intermediates that arise from initial electron transfer (ET) or proton transfer (PT). As an example, $E°' \sim 1.5$ V vs. NHE for tyrosine oxidation to $TyrOH^{\bullet+}$ while $E°' \sim 1.0$ V for oxidation of the TyrOH-histidine base adduct to $TyrO^{\bullet}$-$^{+}$H-histidine, which is a key reaction in photosystem II.[3,4] In proteins, pendent bases or solvent molecules have been suggested to act as EPT proton acceptors as a way of avoiding high energy intermediates such as $TyrOH^{\bullet+}$.[9]

Protein structures with redox active cysteine residues typically include an associated carboxylate base such as aspartate and, for tyrosine, a histidine which provide the base for EPT pathways to occur.[3,4,10,11] Tryptophan lacks a readily dissociable proton and, in peptides, is often found in solvent exposed sites without an associated base. Its dominant mode of oxidation in these sites appears to be stepwise ET-PT with electron transfer followed by proton transfer. In a recent study on *N*-acetyl-tryptophan oxidation by $Os(bpy)_3^{3+}$ there was no evidence for EPT pathways with added phosphate or Tris buffers over extended concentration ranges[12] although evidence for buffer base and pH effects have been reported for tryptophan oxidation in a recent photochemical study by Hammarström and coworkers.[13,14]

Utilization of EPT has been demonstrated in tyrosine oxidation by $M(bpy)_3^{3+}$ (M = Fe, Ru, Os) with added bases by Multiple Site-Electron Proton Transfer (MS-EPT), Scheme 2.[15-18] In this pathway concerted electron-proton transfer occurs, but to different e^- and H^+ acceptors. Related observations have been made at ITO electrodes (Sn(IV) doped In_2O_3) derivatized by surface binding of the electron transfer mediator $[Ru^{II}(bpy)(4,4'\text{-}(HO)_2P(O)CH_2)_2bpy)_2]^{2+}$ (bpy = 2,2′-bipyridine; 4,4′-$(HO)_2P(O)CH_2)_2$bpy = 4,4′-bis-methylenephosphonato-2,2′-bipyridine)[15,16] and in the solution oxidation of *cis*-

$Os^{III}(bpy)_2(py)(OH)^{2+}$ to $Os^{IV}(bpy)_2(py)(O)^{2+}$.[19] Proton Coupled Electron Transfer (PCET) and the role of EPT have also been discussed in recent reviews.[3-6,20]

Cysteine is a thiol with pK_a = 8.2 in contrast to the weaker acids tyrosine (pK_a = 10.1) and tryptophan (pK_a ~ 16) with a reduction potential for the cysteine radical cation $E°'(CysSH^{\bullet+}/CysSH)$ > 1.5 V (vs. NHE) and p$K_a(CysSH^{\bullet+})$ < -2.0. The decrease in pK_a compared to tyrosine with p$K_a(TyrOH^{\bullet+})$ = -2 increases the driving force for $CysSH^{\bullet+}$ EPT compared to $TyrOH^{\bullet+}$ EPT by ~0.059 (ΔpK_a). All things being equal, ET is expected to be favored over EPT.[3,20] The role of EPT in cysteine oxidation has not been systematically addressed although Stanbury and coworkers have reported on the results of a detailed study on electron transfer oxidation of cysteine by $Mo(CN)_8^{-3}$ with $E°'(Mo^{3-/4-})$ = 0.77 V vs. NHE.[21] Cysteine oxidation by chlorine dioxide has also been investigated by Margerum and coworkers.[22]

The goal of this study was to investigate a possible role for EPT pathways in cysteine oxidation especially in the context of its reactivity as a biological electron transfer mediator.

4.3 Methods and Materials

4.3.1 Reaction Solutions: Buffered aqueous solutions were prepared from water purified with a MilliQ purification system (Synthesis A10) with added NaCl at 0.8 M to maintain constant ionic strength. The buffers (acetate, histidine, phosphate and Tris), hydrochloric acid (HCl) and sodium hydroxide (NaOH) were purchased from Sigma Aldrich (St. Louis, MO) and were used as received. The concentration of buffer components was calculated based on the Henderson-Hasselbalch equation. The pK_a values used in the calculations are standard values for each buffer in aqueous solution. *N*-acetyl-*L*-cysteine, and dipicolinic acid (DPA, pyridine-2,6-dicarboxylic acid) were purchased from Alfa Aesar and the *L*-cysteine from Sigma

Aldrich and were used as received. Buffered solutions were adjusted to the correct pH using HCl or NaOH with use of a Fisher Scientific Accumet AB15 pH meter. Buffer and solution conditions used to establish the rate law for cysteine oxidation are discussed below. *N*-acetyl-cysteine was used in place of *L*-cysteine in mixing studies in order to mitigate the effect of trace copper catalysis (see below)

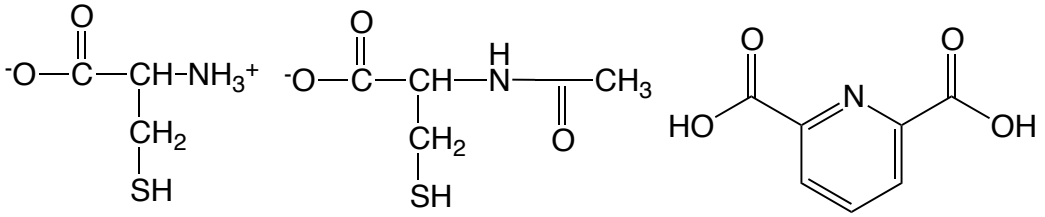

Figure 1. Structures of the dominant forms of cysteine and *N*-acetyl-cysteine at neutral pH and of dipicolinic acid, pyridine-2,6-dicarboxylic acid.

For stopped-flow mixing experiments, buffered aqueous solutions were prepared in 0.8 M NaCl to maintain constant ionic strength. For mixing studies $Os(bpy)_3^{3+}$ or $Ru(dmb)_3^{3+}$ were generated from solutions of $M(L)_3^{2+}$ by bubbling with Cl_2 gas, followed by purging with argon. The concentration of $Os(bpy)_3^{3+}$ was determined spectrophotometrically in CH_3CN, $\varepsilon = 39{,}300\ cm^{-1}\ M^{-1}$ at 306 nm.[23] The concentrations of $Ru(dmb)_3^{3+}$ was determined in CH_3CN, prior to Cl_2 bubbling.

4.3.2 Deuterated Solutions: For electrochemical experiments, deuterated cysteine was prepared by dissolving protonated cysteine in D_2O and deprotonating by adding NaOD. The d-cysteine was isolated by a distillation method that left the d-cysteine in the bottom of the reaction flask. Proton content was monitored by ^{1}H-NMR. Deuterated buffers were prepared similarly and isolated through distillation. The deuterated components were subsequently re-dissolved in D_2O, and pD measured by the pH meter.

In mixing experiments, deuterated *N*-acetyl-cysteine was prepared by dissolving *N*-acetyl-cysteine in D_2O, where the H/D exchange rate is instantaneous. Buffers were prepared by dissolving either acetate and deuterated acetic acid or sodium phosphate and deuterated phosphoric acid to the appropriate concentration and pH/pD with pD = pH + 0.4 on an H_2O calibrated pH meter. Solution pH values were adjusted by adding DCl or NaOD to the solutions and measuring the pH/pD.

4.3.3 Stopped-Flow Kinetics*:* Kinetics experiments were performed on a HI-TECH SF-61DX2 double mixing stopped-flow spectrophotometer fitted with either a single-beam photodiode array detector and Xenon light source for multi-wavelength analysis, or dual-beam photomultiplier tubes (Hamamatsu R928) and a Tungsten light source for single wavelength observations. Initial studies were performed with a MG-6050 diode array (1.5 ms integration time) with the KinetAsyst software, while later work utilized an MG-6560S diode array detector (3 ms integration time) operated by the Kinetic Studio software (TgK Scientific Ltd.). In most cases, measurements were obtained with a 1 cm optical path. Sample temperatures were controlled by a Thermo Haake A28 water bath and monitored via the internal sensor of the mixing unit.

Solutions containing buffer, *N*-acetyl-cysteine, and dipicolinic acid at known pH values and, of the same composition with added $Os(bpy)_3^{3+}$ in a separate solution, were deaerated with argon 30 minutes prior to kinetic measurements. Because of its long term instability toward reduction in buffered solutions, solutions containing $Ru(dmb)_3^{3+}$ were bubble deaerated for 30 minutes separately from the buffer before mixing. pH measurements at the end of each kinetic run were used to ensure that pH was constant over the course of the experiment.

Time scales from 1-100 s were suitable for diode array detection. The latter mode was used with an automatic shutter system (Uniblitz LS3) for time scales longer than 3 s as a precaution against photolysis of $Os(bpy)_3^{3+}$ or $Ru(dmb)_3^{3+}$ by the intense Xenon light source. Higher quality kinetic traces were obtained instead with photomultiplier detection with a Tungsten lamp which provided better time resolution and lower noise. Typically, the kinetics were monitored with a pseudo-first order excess of *N*-acetyl-cysteine (100 μM) over $Os(bpy)_3^{3+}$ (20 μM) with 500-5000 μM added dipicolinic acid (Fig. 2). In this region the observed kinetics were uncomplicated, allowing simplified kinetic analysis to be preformed with the HI-TECH KinetAsyst or Kinetic Studio software (Fig. 3).

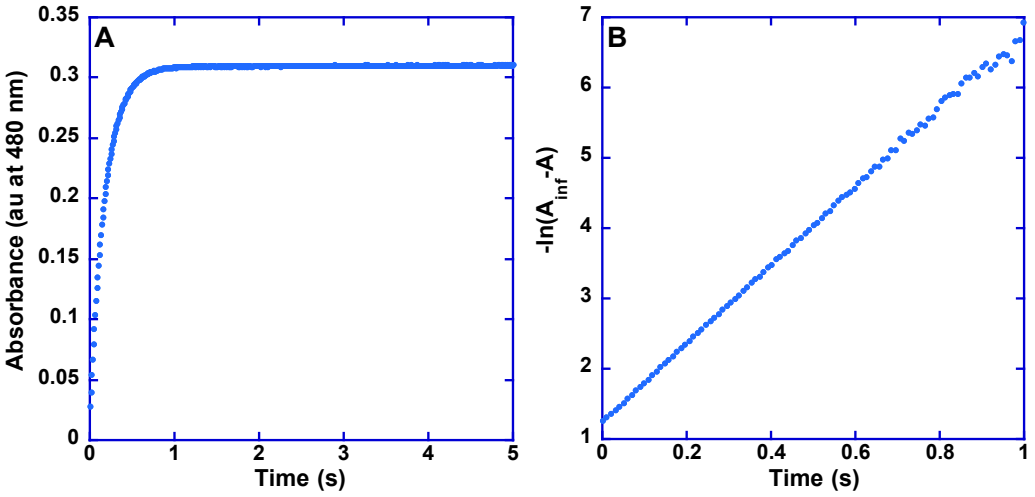

Figure 2. Oxidation of *N*-acetyl-cysteine (200 μM) by $Os(bpy)_3^{3+}$ (20 μM) at pH 5.76, (I = 0.8 M NaCl, T = 20 °C) acetate buffer, $AcOH/AcO^-$ (500 mM). (**A**) Stopped-flow kinetic trace for $Os^{3+} \rightarrow Os^{2+}$ monitored at 480 nm. (**B**) Plot of $\ln(A_\infty - A)$ vs. time (k_{obs} = 5.56 s^{-1}).

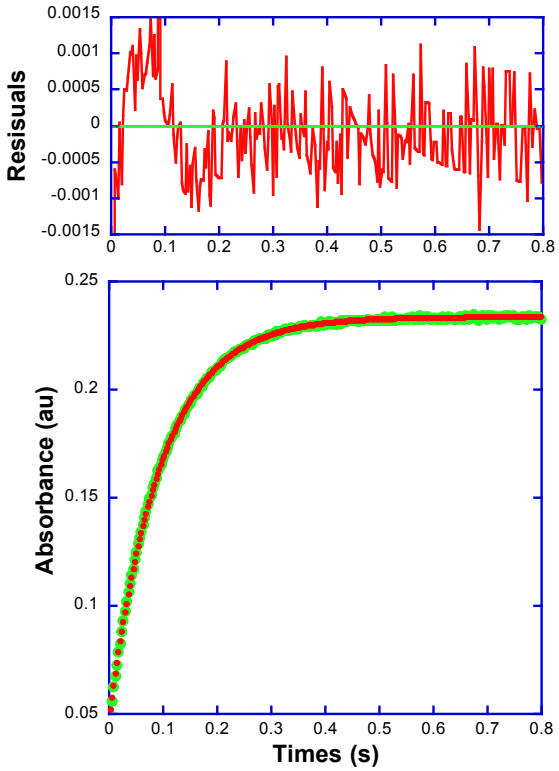

Figure 3. Stoichiometric (2:1, [CysSH]:[Ru^{3+}]) reaction of *N*-acetyl-cysteine (40 μM) with $Ru(dmb)_3^{3+}$ (20 μM), at pH 5.76, 50 mM acetate buffer, DPA (100 μM) (I = 0.8 M NaCl, T = 20 °C) with a single exponential fit. The fit (red) to the kinetic trace is shown with residuals in the top trace. The relative fit errors for individual traces were < 0.0008 a.u. A series of 10 replicates yielded k_{obs} = 10.3±0.2 s^{-1}.

4.3.4 Electrochemistry: Cyclic voltammetry experiments were performed by using a BAS100B/W or a CH Instruments (CHI) 601D series potentiostat in conjunction with a three electrode cell described previously.[25] For experiments testing the effect of dipicolinic acid on rates, a two compartment cell was used with separate solution volumes of 3 ml. Solutions were deaerated for 15 minutes with argon prior to measurement with headspace deaeration maintained throughout the experiment. The working electrode was tin doped indium oxide coated glass (ITO) purchased from Delta Technologies (Stillwater, MN). In kinetic experiments, working electrode areas of 0.32 cm^2 or 1 cm^2 were used with the area defined by Kapton tape or an O-ring. The reference electrode was a teflon coated Ag/AgCl micro-electrode purchased from Cypress Systems, Inc (Lawrence, KS) or a saturated calomel

reference electrode (SCE) purchased from BioAnalytical Systems (BASi, Lafayette, IN). The auxiliary electrode was a platinum wire purchased from Sigma Aldrich (St. Louis, MO). ITO electrodes were treated before use by sonication in MilliQ water for 15 minutes, isopropanol for 15 minutes, and two washes with MilliQ water for 15 minutes each. ITO electrodes were laid flat and allowed to dry overnight. Experimental volumes for most kinetic experiments were typically 50-100 μL.

In voltammetric measurements the potential was scanned in a positive potential sweep for 6 consecutive scans in the buffer solution before a final background scan was taken. In sequence, a scan of buffer plus metal complex was recorded and then a scan of buffer with metal complex and *L*-cysteine. After the scan was completed, the ITO electrode was discarded and a new electrode used for the next set of experiments. Cyclic voltammograms (CV) were background corrected by subtracting scans of solutions containing only buffer from those with complex and cysteine added.

4.4 Results and Discussion

4.4.1 Stopped-Flow Evaluation of Electron Transfer: Stopped-flow measurements at a variety of pHs and thiol concentrations were used to establish the rate law for *N*-acetyl-cysteine oxidation with $Os(bpy)_3^{3+}$ as the oxidant. Typically, the kinetics were found to follow exponential absorbance-time behavior with a pseudo-first order excess of *N*-acetyl-cysteine added, note Figure 4.

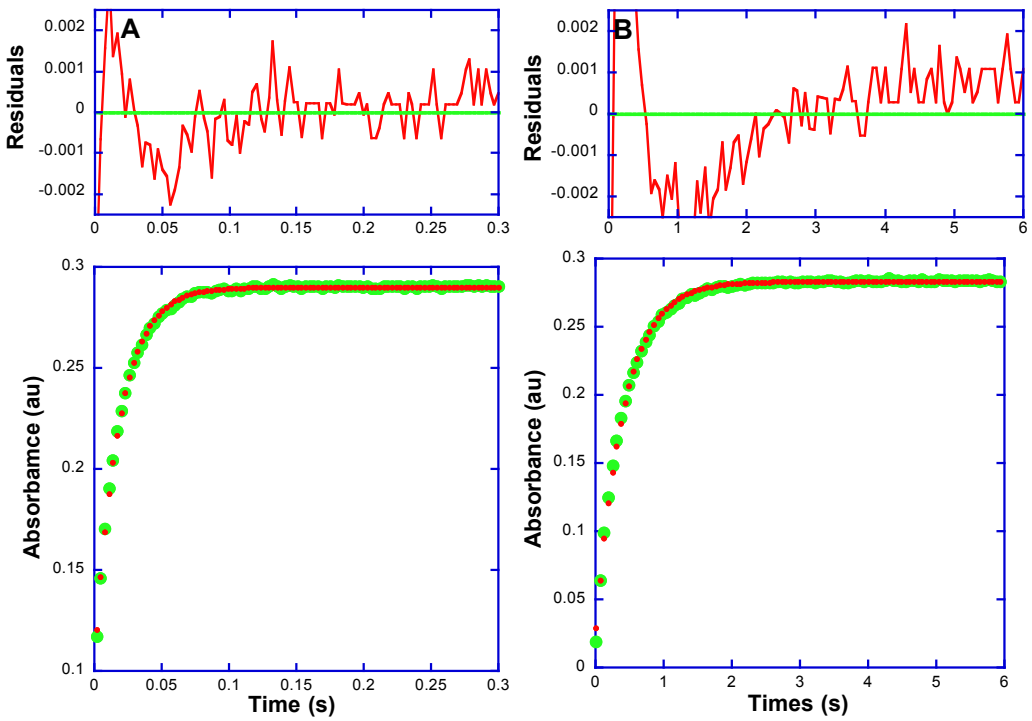

Figure 4. (**A**) Reaction of $Os(bpy)_3^{3+}$ (20 μM) with *N*-acetyl-cysteine (1500 μM) and DPA (1000 μM) at pH 6.0 (I = 0.8 M NaCl, T = 20.0±0.1 °C) (**B**) Reaction of $Os(bpy)_3^{3+}$ (20 μM) with *N*-acetyl-cysteine (1500 μM) and DPA (100 μM) at pH 4.5 (I = 0.8 M NaCl, T = 20.0±0.1 °C) All fits to single exponential kinetics. If added to control pH, buffer concentrations were sufficiently low, <1 mM, that base-assisted pathways were unimportant, see text. In a series of 10 replicates gave k_{obs} = (55.0 ±0.1 s^{-1} for (**A**) and 2.54±0.07 s^{-1} for (**B**).

The experiments were conducted with high, pseudo-first order concentrations of *N*-acetyl-cysteine. 500-3000 μM with 20-100 μM $Os(bpy)_3^{3+}$ over the pH range 4.0 to 6.0, with low concentrations or no buffer in order to avoid participation by base-assisted pathways, see below. At each pH the kinetics were clearly first order in $[Os^{3+}]$ and first order in *N*-acetyl-cysteine as shown by the kinetic plots in Figure 4 and 5. These observations are consistent with the rate law in eq 1 with $[CysSH]_T$ the total concentration of *N*-acetyl-cysteine.

$$-d[Os^{3+}]/dt = k_{obs}[Os^{3+}][CysSH] \quad (1)$$

From the data in Figure 5, k_{obs} is pH dependent. Over the pH range investigated the pH was significantly below pK_a = 8.2 for cysteine with $[CysSH] \sim [CysSH]_T$ with $[CysSH]_T$

the total concentration of added *N*-acetyl-cysteine. From the data in Figure 5, k_{obs} varies with $[H^+]$ according to eq 2.

$$k_{obs} = k_o + k'/[H^+] \quad (2)$$

The appearance of the two rate constant expression is consistent with oxidation of the cysteine derivative by two electron transfer pathways; electron transfer followed by proton transfer (ET-PT), eqs 3,4 and initial deprotonation of Cys-SH followed by oxidation of the *N*-acetyl-cysteine anion, $CysS^-$, PT-ET, eqs. 5,6. with $k' = k_{Cys^-} K_{a,Cys\text{-}SH}$ (Scheme 1).

$$Os(bpy)_3^{3+} + CysSH \rightarrow Os(bpy)_3^{2+} + CysSH^{\bullet+} : k_o \quad (3)$$

$$CysSH^{\bullet+} \rightarrow CysSSCys \quad \text{(rapid)} \quad (4)$$

The products of cysteine oxidation have been characterized by Stanbury and coworkers in the oxidation of cysteine by the 1 electron oxidant octacyanomolybdate(V). The predominant oxidation products are cystine (RSSR) and cysteinesulfinateare (RSO_2^-) as determined by ^1H NMR measurements on the reaction mixture.[21] The formation of the cysteine dimer (eq 7) from the deprotonated cysteine radical ($2RS^{\bullet} \rightarrow RSSR$) occurs rapidly with a reported rate constant of $\sim 10^{10}$ M^{-1} s^{-1}, making it the dominant oxidation product under these conditions.[21,24] The thiyl radical can also react with thiolate anion to give the cystine radical anion (eq 8), with $k \sim 10^9$ M^{-1} s^{-1}, followed by further oxidation to RSSR. [21,26]

$$CysSH \rightleftharpoons CysS^- + H^+ : K_{a,Cys\text{-}SH} \quad (5)$$

$$Os(bpy)_3^{3+} + CysS^- \rightarrow Os(bpy)_3^{2+} + CysS^{\bullet} : k_{Cys^-} \quad (6)$$

$$2\ CysS^{\bullet} \rightarrow CysSSCys \quad \text{(rapid)} \quad (7)$$

$$CysS^{\bullet} + CysS^- \rightarrow CysSSCys^{\bullet-} \quad \text{(rapid)} \quad (8)$$

From eq 2 and the slopes and intercepts of $k_{obs}/[CysSH]$ vs $[H^+]^{-1}$ in Figure 3A-F, k_o = $(4.8\pm1.6) \times 10^2$ M^{-1} s^{-1} and $k' = k_{Cys^-}K_{a,Cys\text{-}SH} = (3.49\pm0.03) \times 10^{-2}$ s^{-1}. Similar values for k_o

and k' were reported by digital simulations of cyclic voltammograms under comparable conditions with *L*-cysteine which gave $k_0 = (3.5 \pm 1.2) \times 10^2\ M^{-1}\ s^{-1}$ and k_{Cys^-} (k_2) = $2.5 \times 10^5\ M^{-1}\ s^{-1}$ with the stopped flow data assumed to be more accurate. Based on $K_{a,Cys\text{-}SH} = 6.30 \times 10^{-9}$, the outer-sphere rate constant for oxidation of cysteine anion is, $k_{Cys^-} = (5.5 \pm 0.5) \times 10^6\ M^{-1}\ s^{-1}$, Scheme 1. Outer-sphere electron transfer (k_o) and non-base assisted PT-ET pathways (k') for NAceCys oxidation are illustrated in Scheme 1.

Scheme 1. Outer-sphere electron transfer (k_o) and non-base assisted PT-ET (k') pathways for NAceCys oxidation.

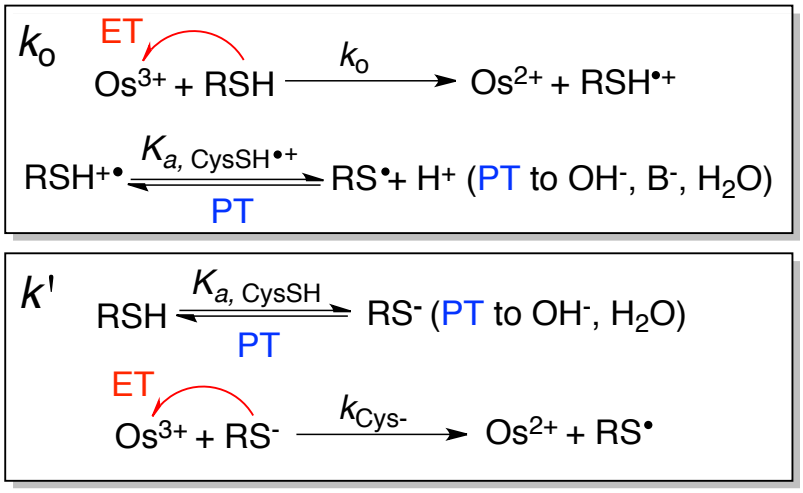

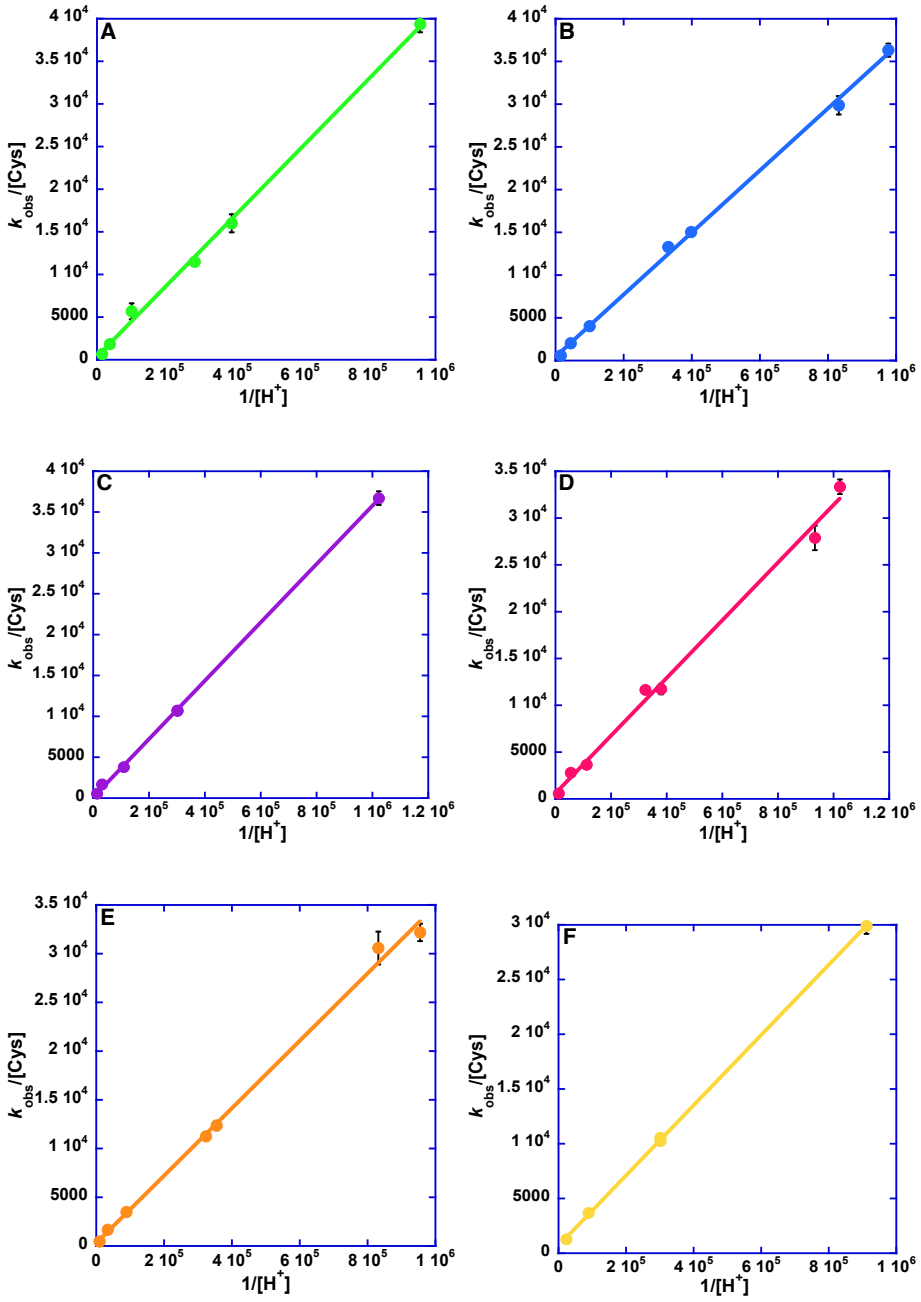

Figure 5. Plots of k_{obs}/[NAceCys] vs. 1/[H$^+$] for oxidation of *N*-acetyl-cysteine by $Os(bpy)_3^{3+}$(20 μM), pH 4-6 (I = 0.8 M, NaCl; T = 20 °C) consistent with eq. 2 with 5000 μM added DPA. Each data point is the average of 10 replicates with most error bars smaller than the data point symbols. (**A**) *N*-acetyl-cysteine (500 μM) (**B**) 1000 μM (**C**) 1500 μM (**D**) 2000 μM (**E**) 2500 μM (**F**) 3000 μM. The linear fits to eq 2 yielded $k_o = (4.8 \pm 1.6) \times 10^2$ M^{-1} s^{-1} and $k' = (3.49 \pm 0.03) \times 10^{-2}$ s^{-1}.

4.4.2 Stopped-Flow Evaluation of PCET with Added Bases: The mechanism in Scheme 2, for oxidation of cysteine with added bases, has been established for oxidation of tyrosine by $M(bpy)_3^{3+}$ and was assumed for cysteine oxidation. The general form of the rate law consistent with this mechanism is given in equations 9 and 10. As shown by the labels in Scheme 2, following H-bond pre-association of an added base, competing pathways exist for cysteine oxidation by MS-EPT and proton transfer (to B^-) followed by oxidation of $CysS^-$. Equation 9 is a limiting form of eq. 10 in the limit that prior adduct formation is negligible and $K_A[B^-] << 1$.

Scheme 2. Base-assisted pathways for cysteine oxidation by $M(bpy)_3^{3+}$.

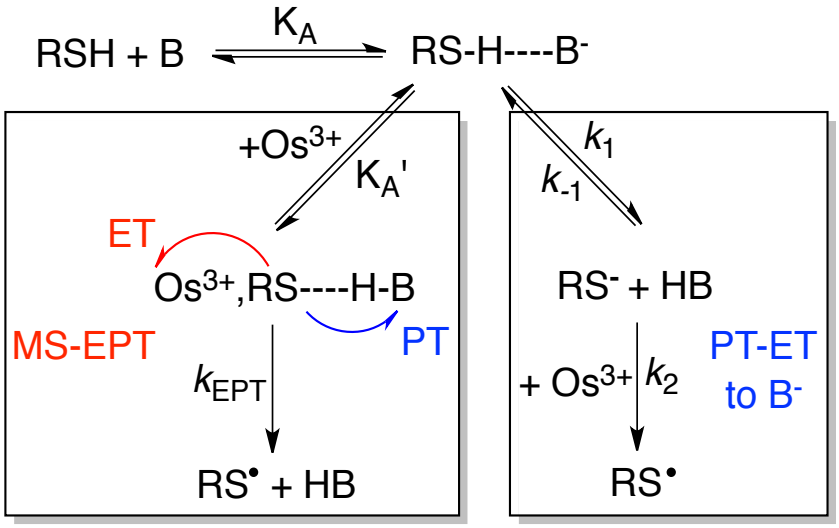

$$\frac{-d[Os^{III}]}{dt} = K_A[CysSH][B^-][Os^{III}]\left(k_{EPT}K_{A'} + \frac{k_1k_2}{k_2[Os^{III}] + k_{-1}[HB]}\right) \qquad (9)$$

$$\frac{-d[Os^{III}]}{dt} = \left(\frac{K_A[CysSH]_T[B^-]}{1 + K_A[B^-]}\right)[Os^{III}]\left(k_{EPT}K_{A'} + \frac{k_1k_2}{k_2[Os^{III}] + k_{-1}[HB]}\right) \qquad (10)$$

Stopped-flow mixing was used to investigate oxidation of *N*-acetyl-cysteine by $Os(bpy)_3^{3+}$ and $Ru(dmb)_3^{3+}$ with both acetate (AcO^-/AcOH) and phosphate buffers ($H_2PO_4^-$ /HPO_4^{-2}) at pH 5.76 and 6.2, respectively. Over the range of acetate concentrations, (0-0.7 M

total buffer) at fixed pH (5.76) and ionic strength (I = 0.8), the observed rate constant nearly doubled, with a slope of 5.04×10^4 and a y-intercept equal to 2.05×10^4, in good agreement with $k_o + k'/[H^+]$ at pH 5.76 ($k_o + k'/[H^+] = 2.55\times10^4$). Over a much smaller range of dibasic phosphate (0-0.6M total buffer) at fixed pH (6.2) observed rate constants increased by more than a factor of two with a y-intercept equal to 8.60×10^4, in agreement with $k_o + k'/[H^+]$ at pH 6.2 ($k_o + k'/[H^+] = 5.58\times10^4$). However unlike electrochemical experiments there is no saturation in $[B^-]$ was observed, making the determination of K_A and separation of the rate constants $K_AK_A'k_{EPT}$ under EPT favoring conditions or k_1, k_{-1} and k_2 under PT-ET favoring conditions not feasible.

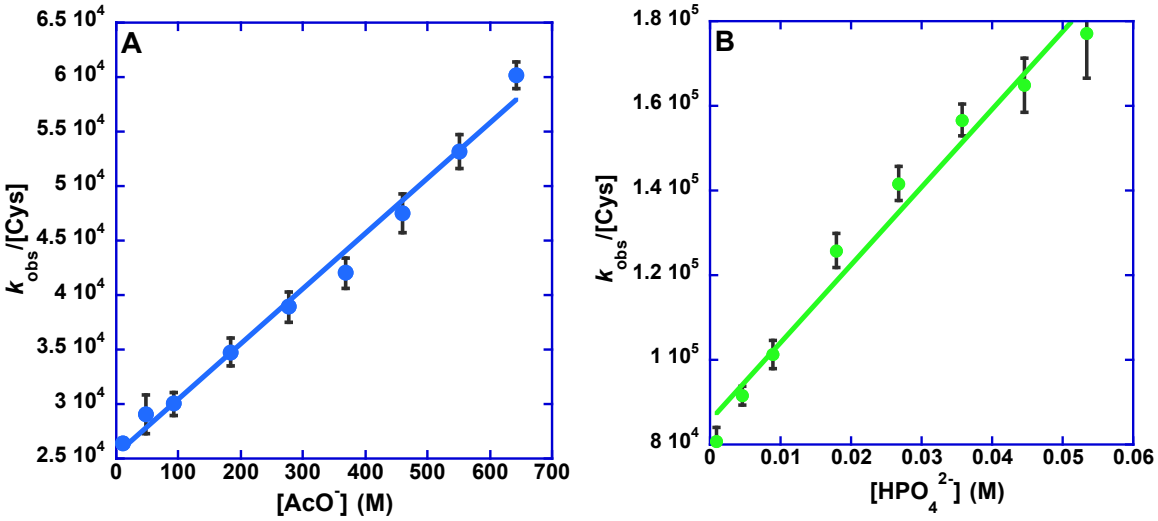

Figure 6. Rates of oxidation of *N*-acetyl-cysteine by $Os(bpy)_3^{3+}$ as a function of base concentrations (I = 0.8 M, NaCl; T = 20 °C). (**A**) Plot of k_{obs}/[NAceCys] vs. [AcO$^-$] (0 – 0.7 M, pH = 5.76) for $Os(bpy)_3^{3+}$ (20 μM), *N*-acetyl-cysteine (100 μM), y-int = 2.05×10^4. (**B**) Variation of k_{obs}/[NAceCys] vs. [HPO^{2-}] (0-0.1 M) for $Os(bpy)_3^{3+}$ (20 μM), *N*-acetyl-cysteine (100 μM). pH = 6.2, y-int = 8.60×10^4.

There was no evidence for limiting conditions, EPT or PT-ET in the stopped-flow base dependence studies, however, the k_{H_2O}/k_{D_2O} suggest the participation of EPT at pH 6.2 (10:1, $[H_2PO_4^-]$:$[HPO_4^{2-}]$). In this limit of $[HB]/[B^-] > 10$, and $K_A[B^-] \sim 1$ the MS-EPT pathway dominates and, $k_{obs} \sim K_A'k_{EPT}$ (section 4.6.2) In this limit the slope of Figure 6B (=

1.83×10^6) should give the product of K_A' and k_{EPT} (Scheme 2). This value compares well to the product of the individual electrochemically simulated values ($K_A'k_{EPT} = 7.2\times10^5$) for *L*-Cys (see 4.6.1).

4.4.3 Kinetic Isotope Effects Measured by Stopped-Flow: Oxidation of *N*-acetyl-cysteine by $Os(bpy)_3^{3+}$ was also investigated by stopped-flow kinetic measurements in D_2O with [AcO^-/AcOD] varied from 10 to 300 mM at pH = pD = 5.76. Analysis of these data gave a solvent kinetic isotope effect (KIE) of k_{H_2O}/k_{D_2O} = 2.2±0.5 at all buffer concentrations. This value is typical for solvent kinetic isotope effects for outer-sphere electron transfer reactions which fall in the range 1.0 – 2.8.[27] Kinetic measurements in D_2O were also conducted with [$D_2PO_4^-$/DPO_4^{2-}] at 10, 200, and 600 mM at pH = pD = 6.2. Analysis of these data gave a solvent kinetic isotope effect (KIE) of k_{H_2O}/k_{D_2O} = 3.76±0.4 at 10 mM total phosphate, 3.2±0.1 at 200 mM and 2.9±0.1 at 600 mM, indicating the participation of additional pathways and that the MS-EPT pathway may not be completely isolated. However, the magnitude of the KIE is still in excess of those measured for analogous outersphere electron transfer reactions of this kind, suggesting an MS-EPT mechanism as the dominant pathway. This is expected according to the limiting conditions of the derived rate law for base assisted PCET pathways outlined below. The rate law can be simplified to favor PT-ET or EPT through limiting conditions. In the case with [AcO^-/AcOD] at pH 5.76 the buffer acid to base ratio is 1:10 and PT-ET is favored. In the case with [$DPO_4^{2-}/D_2PO_4^-$], at pH 6.2 the buffer acid to base ratio is 10:1 and favors EPT.

4.4.4 Stopped-Flow Stoichiometry Measurements: Stoichiometric studies of *N*-acetyl-cysteine oxidation by $Ru(dmb)_3^{3+}$ or $Os(bpy)_3^{3+}$ (20 μM) at 5:1, 2:1 and 1:1 [CysSH]:[Ru^{3+}] with 0.7 and 0.05M [AcO^-/AcOH] at various pHs 3.76, 4.76 and 5.76 were carried out. All

measurements taken with $Ru(dmb)_3^{3+}$ gave good single exponential fits, suggesting that rate limiting proton transfer is playing a dominant role in these reactions suggesting a PT-ET mechanism. The measurements taken with $Os(bpy)_3^{3+}$ at pH 3.76 did not give good single exponential fits likely because of the lower cysteine concentrations permitted other side-reactions to compete. For example, the pK_a of DPA is ~ 4, protonation may allow the Cu^{2+} catalyzed pathway (section 4.5) to play a role in the observed kinetics.[21] Stanbury and coworkers have reported "intractable kinetics" for cysteine at pHs lower than the pK_a of DPA.[21] These results are reported in Table 1 below.

Table 1. *N*-acetyl-cysteine oxidation by $Ru(dmb)_3^{3+}$ and $Os(bpy)_3^{3+}$ (20 μM) at 5:1, 2:1 and 1:1 [NAceCys]:[M^{3+}], [AcO^-/AcOH] = 0.05 and 0.7 M at pH = 3.76, 4.76 and 5.76, Ionic strength was maintained at I = 0.8M with NaCl, T = 22.0±0.1 °C.

Oxidant	[M^{3+}] (μM)	[Cys] (μM)	[Cys]: [M^{3+}]	Desired pH	Measured pH	[AcO^-]/ [AcOH]	Single Exponential	k_{obs} (s^{-1})	σ
$[Ru(dmb)_3]^{3+}$	20	20	1:1	3.76	3.76	0.7M	Yes	0.359	0.003
$[Ru(dmb)_3]^{3+}$	20	40	2:1	3.76	3.79	0.7M	Yes	0.670	0.006
$[Ru(dmb)_3]^{3+}$	20	100	5:1	3.76	3.79	0.7M	Yes	1.680	0.034
$[Ru(dmb)_3]^{3+}$	20	20	1:1	4.76	4.73	0.7M	Yes	1.725	0.027
$[Ru(dmb)_3]^{3+}$	20	40	2:1	4.76	4.74	0.7M	Yes	3.144	0.043
$[Ru(dmb)_3]^{3+}$	20	100	5:1	4.76	4.73	0.7M	Yes	7.174	0.138
$[Ru(dmb)_3]^{3+}$	20	20	1:1	5.76	5.73	0.7M	Yes	9.882	0.223
$[Ru(dmb)_3]^{3+}$	20	40	2:1	5.76	5.73	0.7M	Yes	19.006	0.318
$[Ru(dmb)_3]^{3+}$	20	100	5:1	5.76	5.75	0.7M	Yes	44.957	0.545
$[Ru(dmb)_3]^{3+}$	20	20	1:1	3.76	3.73	0.05M	Yes	0.267	0.004
$[Ru(dmb)_3]^{3+}$	20	40	2:1	3.76	3.70	0.05M	Yes	0.489	0.007
$[Ru(dmb)_3]^{3+}$	20	100	5:1	3.76	3.74	0.05M	Yes	1.364	0.020
$[Ru(dmb)_3]^{3+}$	20	20	1:1	5.76	5.72	0.05M	Yes	6.419	0.132
$[Ru(dmb)_3]^{3+}$	20	40	2:1	5.76	5.71	0.05M	Yes	10.705	0.237
$[Ru(dmb)_3]^{3+}$	20	100	5:1	5.76	5.72	0.05M	Yes	25.614	0.545
$[Os(bpy)_3]^{3+}$	20	20	1:1	5.76	5.75	0.7M	Yes	1.272	0.024
$[Os(bpy)_3]^{3+}$	20	40	2:1	5.76	5.75	0.7M	Yes	2.531	0.052
$[Os(bpy)_3]^{3+}$	20	100	5:1	5.76	5.74	0.7M	Yes	6.379	0.175
$[Os(bpy)_3]^{3+}$	20	20	1:1	3.76	3.78	0.7M	No	*a*	-
$[Os(bpy)_3]^{3+}$	20	40	2:1	3.76	3.80	0.7M	No	*a*	-
$[Os(bpy)_3]^{3+}$	20	100	5:1	3.76	3.75	0.7M	No	*a*	-

a Fits under these conditions did not fit to a single exponential, and no rate constants were reported.

Additional stoichiometric studies were also performed with $Os(bpy)_3^{3+}$ in excess at 1:1 - 16:1 [Os^{3+}]:[CysSH], [AcO^-/AcOH] = 0.7 M at pH 5.76, I = 0.8 with NaCl, T = 22.0±0.1 °C. Experiments at 1:1 gave good single exponential fits, however at 2:1 – 16:1 [Os^{3+}]:[CysSH] ratios produced complex kinetic traces that could not be fit to a single exponential. After mixing, the initial traces produced a rapid initial growth corresponding to Os^{3+} + CysSH → Os^{2+} + [$CysS^{\bullet}$] at 480nm from the oxidation of *N*-acetyl-cysteine, followed by a slow growth of absorbance, suggesting the interaction of the excess $Os(bpy)_3^{3+}$ with cystine (RSSR) and cysteinesulfinateare (RSO_2^-). Although the kinetics of M^{3+} interacting with these oxidation products are slow as documented by Stanbury and coworkers, they can still contribute to the observation of non-first order kinetics.[20]

4.5 Dipicolinic Acid Inhibition of Cu^{2+} Catalysis: It has been reported that trace amounts of Cu^{2+} dominate the reaction kinetics involving the oxidation of cysteine and other thiols such as glutathione.[21,24,28] Specifically, mixing studies analogous to the ones reported herein have reported the significant change in reaction kinetics in the presence of only trace Cu^{2+}. The mechanism by which this catalysis occurs is beyond the scope of this work. It is however, reported that the formation of the cuprous bis-cysteine complex (RS-Cu^+-SR) is the catalytic species involved in the oxidation of cysteine, this species is characterized more in-depth in reference 24. Stanbury and coworkers reported that this catalytic effect can be mitigated in mixing studies by the redox innocuous chelating agent, dipiolinic acid, pyridine-2,6-dicarboxylic acid, which has a pK_{a1}=2.07 and pK_{a2}=4.66, making it a less effective copper chelate below pH ~3-4.[29] In the presence of DPA, observed rate constants were more reproducible, we have also confirmed this trace metal catalysis in our mixing experiments as well as its mitigation by using DPA.[21] The effectiveness of this chelating agent is confirmed

and reproduced here in this work for mixing studies involving $Os(bpy)_3^{3+}$ as an oxidant over a pH range of 3.76-6.65. Additionally, the importance of trace Cu^{2+} on electrochemical experiments was tested, and was not found to pose the same problem that it does in mixing experiments.

4.5.1 Stopped-Flow Evaluation of DPA Effects: Experiments conducted at pH 4.0 and 5.0 in 50 and 500 mM acetate buffer in the presence of 20 μM $Os(bpy)_3^{3+}$ and 1-2 mM DPA without any *N*-acetyl-cysteine substrate showed less than a 20% $Os^{3+} \rightarrow Os^{2+}$ conversion over >1000s, suggesting that any direct reaction between the chelating agent will not effect the observation of the intended $M(L)_3^{3+}$ + cysteine reaction kinetics

The effect of dipicolinic acid on the rate of *N*-acetyl-cysteine oxidation by $Os(bpy)_3^{3+}$ was measured in solutions of pH 4.0 and 5.0 and 50 and 500 mM acetate buffer, the results from this experiment are summarized below in Table 2. The absence of DPA makes error values high due to poor reproducibility; k_{obs} values for these reactions are also 2-10 times larger compared to the values taken under the same conditions in the presence of DPA.

Table 2. Oxidation of *N*-acetyl-cysteine (2000 μM) by $Os(bpy)_3^{3+}$ (20 μM) at variable pHs and acetate buffer concentrations, with and without 1000 μM DPA.

Desired pH	$[B^-/HB]$ (mM)	[DPA] (μM)	[NAceCys] (μM)	pH[a]	k_{obs} (s^{-1})	σ
4.0	50	0	2000	4.03	*b*	*b*
4.0	50	1000	2000	3.96	1.26	0.05
4.0	500	0	2000	4.01	3.5	1.1
4.0	500	1000	2000	3.99	1.70	0.07
5.0	50	0	2000	5.05	*b*	*b*
5.0	50	1000	2000	4.99	9.6	0.3
5.0	500	0	2000	4.99	99	4
5.0	500	1000	2000	4.97	14.5	0.3

a pHs measured after the reaction by mixing 4 ml of each reaction mixture and than taking the pH, representing the final pH measurement for the reaction. *b* these values were either too fast (k_{obs} > 1000 s^{-1}) to be measured or had kinetic traces that could not be fit to a single exponential.

The dependence of k_{obs} in the oxidation of *N*-acetyl-cysteine by $Os(bpy)_3^{3+}$ on the concentration of DPA was tested by stopped-flow at pH 4.0 in 50 mM acetate buffer. These results are summarized in Table 3 below. The concentration of NAceCys was 2000 μM and DPA was varied between 500 and 2000 μM. The observed rate constant did not change by more than 20%. Indicating that even at lower concentrations of DPA compared to NAceCys, the effects of the trace metal catalyzed reaction is mitigated.

Table 3. Oxidation of *N*-acetyl-cysteine (2000 μM) by $Os(bpy)_3^{3+}$ (20 μM) at pH 4.0 and 50 mM acetate buffer, with varied concentrations of DPA.

Desired pH	**[B^-/HB] (mM)**	**[DPA] (μM)**	**[NAceCys] (μM)**	**pH[a]**	**k_{obs} (s^{-1})**	**σ**
4.0	50	500	2000	4.03	1.65	0.02
4.0	50	1000	2000	4.05	1.36	0.03
4.0	50	1500	2000	4.04	1.34	0.04
4.0	50	2000	2000	3.96	1.20	0.03

a pHs measured after the reaction by mixing 4 ml of each reaction mixture and than taking the pH, representing the final pH measurement for the reaction.

4.5.2 Electrochemical Evaluation of DPA Effects: The role of dipicolinic acid in *L*-cysteine oxidation was tested using cyclic voltammetry, where CVs were taken on ITO glass working electrodes to measure the current in the oxidation of *N*-acetyl-cysteine by the $Os(bpy)_3^{III/II}$ couple with and without DPA in solution (Figure 7). Cyclic voltammograms taken with DPA displayed no catalytic current resulting from the Os^{3+} oxidation of cysteine at the electrode, suggesting an electrode interaction with DPA that inhibits the thiol from entering the diffusion layer of the electrode. Fast solution kinetics were observed for the analogous reaction measured in mixing studies. This suggests that the inclusion of DPA would make acquiring any kinetic information impossible because of this interaction. Without DPA a typical current potential response is observed.

The absence of DPA in electrochemical experiments does not permit copper catalysis to dominate the kinetics. *L*-Cys on a plain ITO electrode shows no significant current in addition to the background out to 1.2 V vs NHE (Fig. 8). If trace copper were catalyzing the oxidation of *L*-cysteine, significant current in the absence of $Os(bpy)_3^{2+}$ would be observed.

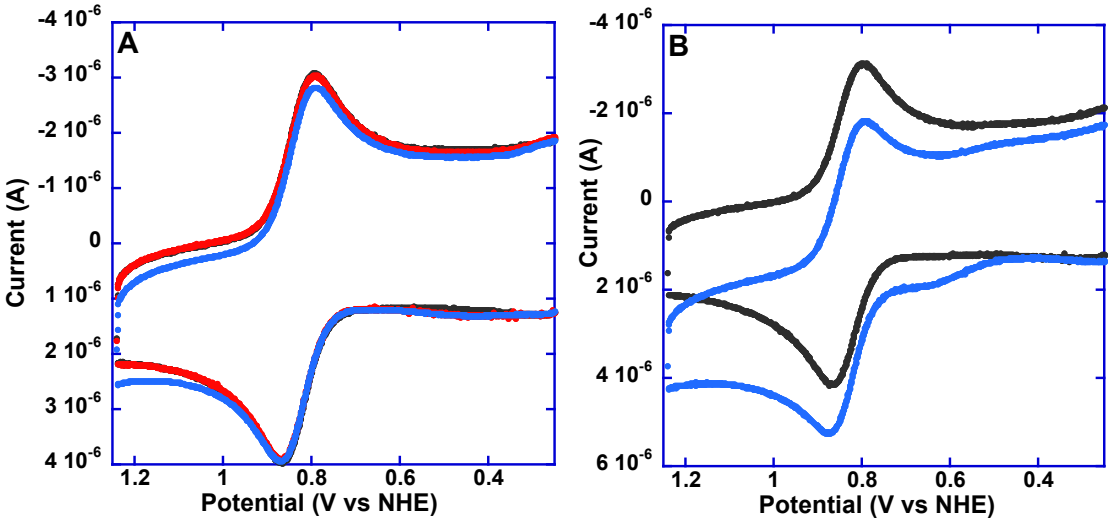

Figure 7: (**A**) Cyclic voltammograms at ITO in 0.7M [AcO^-/AcOH], I = 0.8M with NaCl at υ = 100 mV/s $Os(bpy)_3^{2+}$ (20 μM, black); $Os(bpy)_3^{2+}$ (20 μM) + DPA (1 mM, red); $Os(bpy)_3^{2+}$ (20 μM) + DPA (1 mM) + NAceCys (0.1 mM ,blue) (**B**) as in (**A**) except no DPA, $Os(bpy)_3^{2+}$ (20 μM, black); $Os(bpy)_3^{2+}$ (20 μM) + NAceCys (0.1 mM, blue).

4.6 Electrochemical Evaluation of Cysteine Oxidation Kinetic Pathways: We investigated the electrochemical oxidation of cysteine in phosphate buffer [$H_2PO_4^-$/HPO_4^{2-}] under different pH's, acid base ratios and total buffer concentrations in order to isolate the individual base assisted kinetic pathways shown in Scheme 2, EPT and PT-ET. Experiments under limiting conditions of the derived rate law (eq. 10) for the mechanism outlined in Scheme 2 allowed isolation of individual EPT and PT-ET pathways, see below.

Like tyrosine and tryptophan, cysteine has a kinetically slow response at ITO electrodes, with only small currents in excess of the background observed near the solvent oxidation limit, Figure 8. In the CV experiments, the effect of added *L*-cysteine and buffer on the $M(bpy)_3^{2+} \xrightarrow{e^-} M(bpy)_3^{3+}$ waveform was recorded for the couples $M(bpy)_3^{III/II}$ (M = Fe,

Ru, Os); $M(dmb)_3^{III/II}$ (M = Fe, Ru, Os); and $Ru(dmb)_2(bpy)^{III/II}$ (dmb = 4,4′-dimethyl-2,2′-bipyridine; bpy = 2,2′-bipyridine). All of the $M^{III/II}$ couples are electrochemically reversible with $E°'$ values ranging from 0.8 to 1.25 V vs. NHE, Table 4. Kinetics experiments were run with $[Os(bpy)_3^{2+}]$ = 20 μM and [CysSH] = 100 μM to test the limiting forms of the derived rate law.

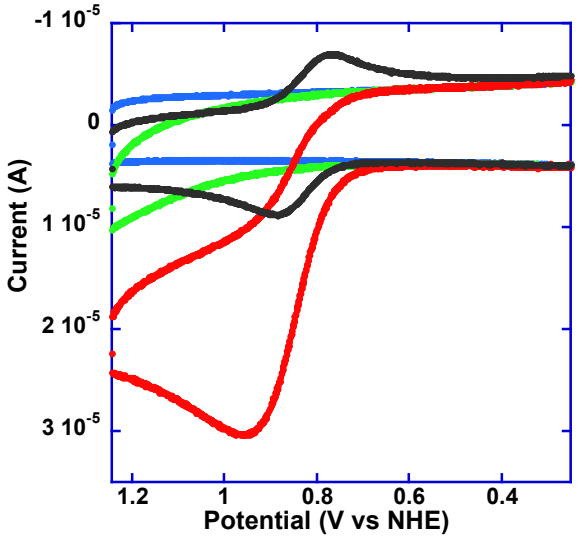

Figure 8. Cyclic voltammograms (300 mV/s) in 50 mM $[H_2PO_4^-/ HPO_4^{2-}]$ (1:1 acid/base) at pH 7.2 (I = 0.8 M NaCl), T = 23 ± 2 °C. Plain ITO background (blue); *L*-Cys (100 μM green); $Os(bpy)_3^{2+}$ (20 μM, black); *L*-Cys (100 μM) + $Os(bpy)_3^{2+}$ (20 μM, Red). Note: CVs are not background subtracted, to better illustrate ITO and ITO + Cys CVs.

Table 4. Experimental electrochemical parameters for each metal mediator used in the investigation. Experiments with M = Ru, Fe were conducted for a driving force dependence study, however are not included herein because the calculation of free energies requires $E°'(CysSH^{\bullet+/0})$ and $pK_a(CysSH^{\bullet+})$, both of which are unreported. These values are included for purposes of completeness.

Metal Mediator	Potential Range (V) vs NHE	Scan Rate (V/s)	Metal Concentration (μM)
$Ru(bpy)_3^{III/II}$	0-1.6	0.300	20
$Ru(dmb)_3^{III/II}$	0-1.3	0.300	20
$Fe(bpy)_3^{III/II}$	0-1.25	0.300	20
$Os(bpy)_3^{III/II}$	0-1.0	0.300	20

With the $M^{III/II}$ couples above as the redox mediators, there was appreciable change in electrochemical behavior (Fig. 9, 10) between different concentrations of buffer and pH, (i.e.,

phosphate, $H_2PO_4^-/HPO_4^{2-}$, pK_a 7.2, pH 6.2) indicating that the solution kinetics at neutral pH were dominated by competing base assisted pathways with outer-sphere electron transfer mechanism (k_o) and a pH dependent pathway (k_2) also playing a role in the observed kinetics. This behavior is qualitatively similar to tyrosine oxidation with significant rate enhancements observed under the same conditions.[17.18] The presence of significant base and isotope effects is consistent with competing EPT and PT-ET pathways, each which were isolated through conducting experiments under rate-limiting conditions as defined by the rate law in equation 14-16 below. Where current enhancements were observed, the cyclic voltammetry responses were analyzed using numerical simulations. Limiting conditions were used in the electrocatalytic experiments to simplify the mechanism in Scheme 2 by kinetically isolating either the MS-EPT pathway or the PT-ET pathway.

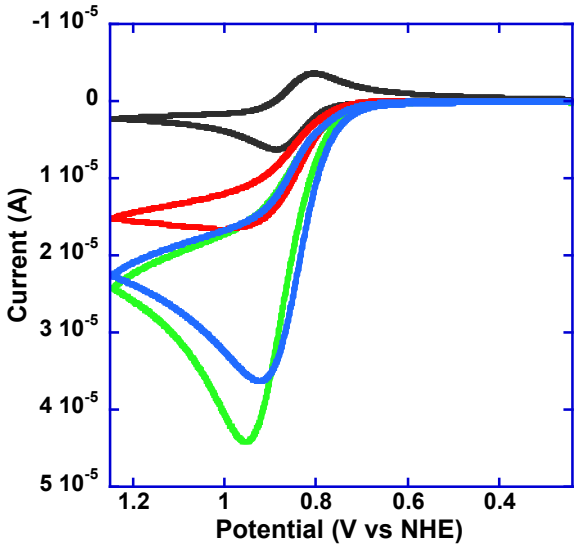

Figure 9. Cyclic voltammograms (300 mV/s) in 300 mM [$H_2PO_4^-/HPO_4^{2-}$], (I = 0.8 M NaCl), T = 23 ± 2 °C. $Os(bpy)_3^{2+}$ (20 μM) on plain ITO (black), $Os(bpy)_3^{2+}$ (20 μM) + *L*-Cys (100 μM), 10:1 acid/base, pH 6.2 (red), 1:1 acid/base, pH 7.2 (blue), 10:1 acid/base, pH 8.2 (green).

4.6.1 Digital Simulation of Electrochemical Data: Numerical simulations of electrochemical data were performed by using the DigiSim software package, purchased from BioAnalytical

Systems (West Layfayette, IN). The DigiSim software uses the Butler-Volmer equation to relate current-time data as a function of applied potential to evaluate homogeneous rate constants for oxidation of tyrosine by $M(bpy)_3^{3+}$. In eq 12 i_o is the exchange current, η the overvoltage, and α the transfer coefficient.[18,30,31]

$$i = i_o\left(\exp\left(\frac{(1-\alpha)F\eta}{RT}\right) - \exp\left(\frac{-\alpha F\eta}{RT}\right)\right) \qquad (12)$$

In the simulation of current-potential profiles, heterogeneous electron transfer rate constants (k_s = 0.01 cm/s) were obtained by fitting cyclic voltammograms of the metal complex alone for the oxidant $M(bpy)_3^{III/II}$ and the reductant (CysSH).[30,31] The diffusion coefficients used were $6.0x10^{-6}$ cm^2/s for $Os(bpy)_3$ and $3.0x10^{-6}$ cm^2/s^2 for cysteine.[32-34] The reduction potential of the metal, complex ($E°'$ = 0.80 V-1.25 vs NHE in 0.05M phosphate and 0.8M NaCl at 23±2°C) and the heterogeneous electron transfer rate constant (k_s = 0.01cm/s) were obtained by fitting cyclic voltammograms of the metal complex alone in solution. These parameters are outlined in Table 5 below.

Table 5. Simulation parameters imported into DigiSim. Scan rates and potential ranges reported above for experimental parameters were also imported into the program.

Metal Mediator	E^o **(V vs NHE)**	D_{metal} **(10^{-6} cm^2/s)**	D_{Cys} **(10^{-6} cm^2/s)**	**[Metal] (μM)**	**[CysSH] (μM)**
$Ru(bpy)_3^{3+/2+}$	1.25	6.0	3.0	20	100
$Ru(dmb)_3^{3+/2+}$	1.06	6.0	3.0	20	100
$Fe(bpy)_3^{3+/2+}$	1.03	6.0	3.0	20	100
$Os(bpy)_3^{3+/2+}$	0.80	6.0	3.0	20	100

The cyclic voltammetric data for *L*-cysteine oxidation were fit in DigiSim by assuming the electrochemical mechanism in eq 13. The simulated waveforms were satisfactorily fit to the mechanisms in Scheme 3-5, consistent with eqs 14 and 15, involving initial $1e^-$ oxidation to the intermediate radical with n = 1 followed by disulfide formation

without complication from further oxidation of the disulfide.[22,28] The full fitting parameters included limiting conditions isolating the different parts of the pathways in Scheme 2. Systematic treatment of these conditions through derivation of the rate law shown in eq. 10 into limiting forms is reported in the next section with simulations shown in Figure 10. Dipicolinic acid was not used in electrochemical experiments due to the above electrochemical DPA analysis that showed no catalytic current in the presence of *L*-Cys as reported above.

$$Os^{2+} \rightarrow Os^{3+} + e^- \qquad (13a)$$

$$Os^{3+} + CysSH \xrightarrow{k_{obs}} Os^{2+} + CysSH'_{ox} \qquad (13b)$$

$$2CysSH'_{ox} \rightarrow CysSSCys \qquad \text{(rapid)} \qquad (13c)$$

The simulations were used to obtain k_{obs} under a variety of buffer concentrations and buffer ratios. In the absence of added buffer (pH = 5.76, T = 23±2 °C in I = 0.8M NaCl) a simulated CV with $[Os(bpy)_3^{3+}]$ = 20 μM, [CysSH] = 100 μM, and $D_{Os(bpy)_3^{3+}} = 6.0\text{x}10^{-6}$m/s, $k_{obs} = 2.5\text{x}10^5$ $M^{-1}s^{-1}$, in agreement with the value $k_{obs} = k_o + k_2$.

With added buffers, a mechanism analogous to that found for $M(bpy)_3^{3+}$ oxidation of tyrosine in Scheme 2, was initially assumed. In this mechanism initial pre-association with H-bonding occurs between the added buffer base B^- and cysteine. Formation of the association complex is followed by competing pathways for CysSH oxidation; initial proton loss to B^- followed by oxidation of $CysS^-$ (PT-ET) and MS-EPT with concerted electron transfer to $M(bpy)_3^{3+}$ and proton transfer to B^-. Given the quantum nature and distance dependences of proton transfer and EPT, initial H-bonding with the proton acceptor is key.[3,4,20]

4.6.2 Limiting Conditions of the Rate Law: Numerical simulations of the mechanism in Scheme 2 in DigiSim have been described in previous papers.[3,11,17,18] Limiting conditions used to isolate either the MS-EPT or PT-ET pathways kinetically are also discussed there. For the MS-EPT pathway $H_2PO_4^-/HPO_4^{2-}$ buffers with the buffer acid to base ratio > 10:1 were used. Under these conditions, $k_{obs} = K_A K_A' k_{EPT}$ [CysSH].

Cyclic voltammograms consistent with the mechanism in Scheme 2 were simulated using the general electrochemical mechanism in Scheme 3. A rate law for the mechanism shown in Scheme 2, is shown below in eq 14 where $[CysSH]_T$ is the total concentration of CysSH distributed between CysSH and its adduct with the buffer base. With high, pseudo-first order concentrations of CysSH and buffer, the rate law becomes eq 15 with k_{obs} given by eq 16.

$$\frac{-d[Os^{III}]}{dt} = \left(\frac{K_A[CysSH]_T[B^-]}{1+K_A[B^-]}\right)[Os^{III}]\left(k_{EPT}K_{A'} + \frac{k_1k_2}{k_2[Os^{III}]+k_{-1}[HB]}\right) \quad (14)$$

$$\frac{-d[Os^{III}]}{dt} = kobs\left[CysSH\right]_T\left[Os^{3+}\right] \quad (15)$$

$$\frac{k_{obs}}{[CysSH]_T} = \left[\frac{K_A[B^-]}{1+K_A[B^-]}\right]\left(k_{EPT}K_AK_A' + \frac{k_1k_2}{k_2[Os^{III}]+k_{-1}[HB]}\right) \quad (16)$$

Scheme 3:

$$Os^{II} \underset{}{\overset{k_s}{\rightleftharpoons}} Os^{III} + e^- \quad \textbf{(1)}$$

$$HB \underset{}{\overset{K_a}{\rightleftharpoons}} H^+ + B^- \quad \textbf{(2)}$$

$$CysSH + B^- \underset{}{\overset{K_A}{\rightleftharpoons}} CysS\text{-}H\text{--}B^- \quad \textbf{(3)}$$

$$CysS\text{-}H\text{--}B^- + Os^{III} \overset{K_A' k_{EPT}}{\longrightarrow} CysS^{\bullet}\text{-}H\text{-}B + Os^{II} \quad \textbf{(4)}$$

$$CysS^{\bullet}\text{-}H\text{-}B^- \underset{}{\overset{K_A''}{\rightleftharpoons}} CysS^{\bullet} + HB \quad \textbf{(5)}$$

$$CysS\text{-}H\text{--}B^- \underset{}{\overset{k_1/k_{-1}}{\rightleftharpoons}} CysS^- + HB \quad \textbf{(6)}$$

$$CysS^- + Os^{III} \overset{k_2}{\longrightarrow} CysS^{\bullet} + Os^{II} \quad \textbf{(7)}$$

$$2CysS^{\bullet} \longrightarrow (CysS)_2 \quad \textbf{(8)}$$

Limiting conditions were used to simplify the mechanism in Scheme 2 by kinetically isolating either the MS-EPT or PT-ET pathways. At high buffer ratios, $[HB]/[B^-] > 10$, the

MS-EPT pathway dominates and eq 16 becomes 17 or, if $K_A[B^-] << 1$, eq 18.

$$\frac{k_{obs}}{[CysSH]_T} = \left(k_{EPT}K_A'\right)\left[\frac{K_A[B^-]}{1+K_A[B^-]}\right] \quad (17)$$

$$\frac{k_{obs}}{[CysSH]_T} = k_{EPT}K_AK_A'\left[B^-\right] \quad (18)$$

Under these conditions the electrochemical mechanism simplifies to Scheme 4.

Scheme 4:

$$Os^{II} \underset{}{\overset{k_s}{\rightleftharpoons}} Os^{III} + e^- \quad \textbf{(1)}$$

$$HB \underset{}{\overset{K_a}{\rightleftharpoons}} H^+ + B^- \quad \textbf{(2)}$$

$$CysSH + B^- \underset{}{\overset{K_A}{\rightleftharpoons}} CysS\text{-}H\text{--}B^- \quad \textbf{(3)}$$

$$CysS\text{-}H\text{--}B^- + Os^{III} \xrightarrow[K_A''}{K_A'\,k_{EPT}} CysS^{\bullet}\text{-}H\text{-}B + Os^{II} \quad \textbf{(4)}$$

$$CysS^{\bullet}\text{-}H\text{-}B^- \rightleftharpoons CysS^{\bullet} + HB \quad \textbf{(5)}$$

$$2CysS^{\bullet} \longrightarrow (CysS)_2 \quad \textbf{(6)}$$

At relatively high concentrations of [CysSH] and [B^-] the CysSH---B adduct, CysSH---OPO_2OH^{2-} for $B^- = HPO_4^{2-}$, (Scheme 2) dominates with $[CysSH]_T \sim [CysSH\text{---}B]$. Under these conditions the rate law in eq 15 becomes eq 19. As noted below, at high concentrations of complex, CysSH, and buffer base (B^-) there is evidence for additional saturation kinetics arising from association complex formation between CysSH---B and $M(bpy)_3^{3+}$ (Figure 13) with EPT occurring within the complex, $\{M(bpy)_3^{3+}, CysSH\text{---}B\} \xrightarrow{k_{EPT}} \{M(bpy)_3^{2+}, CysS^{\bullet}\text{---}^{+}H\text{-}B\}$. Under these conditions with CysSH---B in high, pseudo first order excess, the rate law becomes eq 20 with k_{obs} given by 21.

$$-\frac{d[Os^{III}]}{dt} = k_{obs}[CysSH]_T[Os^{III}] = k_{obs}[CysSH-B][Os^{III}] \quad (19)$$

$$-\frac{d[Os^{III}]}{dt} = k_{obs}[CysSH-B, Os^{III}] = \left(\frac{k_{EPT}K_A'[CysSH-B][Os^{III}]}{1+K_A'[CysSH-B]}\right) = \frac{k_{EPT}K_A'[CysSH]_T[Os^{III}]}{1+K_A'[CysSH]_T} = k_{obs}[Os^{III}] \quad (20)$$

$$k_{obs} = \frac{k_{EPT} K_A'[CysSH]_T}{1 + K_A'[CysSH]_T} \tag{21}$$

At low buffer ratios, $[HB]/[B^-] < 0.1$, the PT-ET pathway dominates and the rate law in eq. 14 and 15 becomes eq. 22 or, in solutions dilute in B^- with $K_A[B^-] << 1$ and $[CysSH]_T \sim [CysSH]$ and cysteine in pseudo first order excess, eq 23.

$$-\frac{d[Os^{III}]}{dt} = \left(\frac{K_A[CysSH]_T[B^-]}{1 + K_A[B^-]}\right)[Os^{III}]\left(\frac{k_1 k_2}{k_2[Os^{III}] + k_{-1}[HB]}\right) \tag{22}$$

$$-\frac{d[Os^{III}]}{dt} = [Os^{III}][B^-][CysSH]\left(\frac{k_1 k_2}{k_2[Os^{III}] + k_{-1}[HB]}\right) \tag{23}$$

At high buffer concentrations with $k_2[Os^{3+}] << k_{-1}[HB]$, the rate law further simplifies to eq 24 and with $K_A[B^-] << 1$ and $[CysSH]_T \sim [CysSH]$, to eq 25 with k_{obs} given in eq 26 and with $K_A[B^-] << 1$, to eq 27.

$$-\frac{d[Os^{III}]}{dt} = \left(\frac{K_A[CysSH]_T[B^-]}{1 + K_A[B^-]}\right)[Os^{III}]\left(\frac{k_1 k_2}{k_{-1}[HB]}\right) = k_{obs}[Os^{III}][CysSH]_T \tag{24}$$

$$-\frac{d[Os^{III}]}{dt} = k_{obs}\left[Os^{III}\right]\left[CysSH\right] \tag{25}$$

$$\frac{k_{obs}}{[CysSH]_T} = \left[\frac{K_A[B^-]}{1 + K_A[B^-]}\right]\left(\frac{k_1 k_2}{k_{-1}[HB]}\right) \tag{26}$$

$$\frac{k_{obs}}{[CysSH]} = \left(\frac{k_1 k_2}{k_{-1}[HB]}\right) K_A[B^-] \tag{27}$$

The electrochemical mechanism in this limit is shown in Scheme 5.

Scheme 5.

$$Os^{II} \underset{}{\overset{k_s}{\rightleftharpoons}} Os^{III} + e^- \quad \textbf{(1)}$$

$$HB \overset{K_a}{\rightleftharpoons} H^+ + B^- \quad \textbf{(2)}$$

$$CysSH + B^- \overset{K_A}{\rightleftharpoons} CysS\text{-}H\text{--}B^- \quad \textbf{(3)}$$

$$CysS\text{-}H\text{--}B^- \overset{k_1/k_{-1}}{\rightleftharpoons} CysS^- + HB \quad \textbf{(4)}$$

$$CysS^- + Os^{III} \xrightarrow{k_2} CysS^{\bullet} + Os^{II} \quad \textbf{(5)}$$

$$2CysS^{\bullet} \longrightarrow (CysS)_2 \quad \textbf{(6)}$$

At low buffer concentrations in the limit $k_2[Os^{3+}] >> k_{-1}[HB]$, the rate law in eq 22 becomes independent of $[Os^{3+}]$ giving eq 28 or with $K_A[B^-] << 1$ and $[CysSH]_T \sim [CysSH]$, eq 29 with the corresponding expressions for k_{obs} in eqs 30 and 31.

$$-\frac{d[Os^{III}]}{dt} = \left[\frac{K_A[CysSH]_T[B^-]}{1+K_A[B^-]}\right]\left(\frac{k_1k_2}{k_2}\right) = k_{obs}[CysSH]_T \quad (28)$$

$$-\frac{d[Os^{III}]}{dt} = \left(\frac{k_1k_2K_A}{k_2}\right)[CysSH][B^-] = k_{obs}[CysSH][B^-] \quad (29)$$

$$\frac{k_{obs}}{[CysSH]_T} = k_1\left[\frac{K_A[B^-]}{1+K_A[B^-]}\right] \quad (30)$$

$$\frac{k_{obs}}{[CysSH]} = k_1K_A[B^-] \quad (31)$$

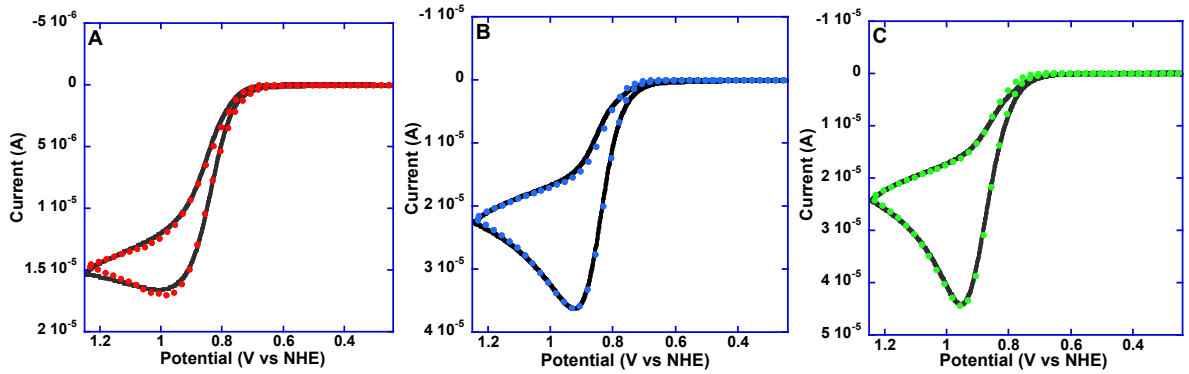

Figure 10. Typical simulations of cyclic voltammograms (300 mV/s) in 300 mM [$H_2PO_4^-$/HPO_4^{2-}], (I = 0.8 M NaCl), T = 23 ± 2 °C, under limiting conditions of the rate law. Dotted line (simulation) solid black line (experimental data); $Os(bpy)_3^{2+}$ (20 μM) + *L*-Cys (100 μM), 10:1 acid/base, pH 6.2, using the mechanism in Scheme 4 (**A**), 1:1 acid/base, pH 7.2, using the mechanism in Scheme 3 (**B**), 10:1 acid/base, pH 8.2, using the mechanism in Scheme 5 (**C**).

For completeness, the comprehensive rate law for cysteine oxidation, including anion and outer-sphere oxidation pathways (k_o, k') is shown in equation 23 below.

$$\frac{-d[Os^{III}]}{dt}\frac{1}{[CysSH]_T} = \left\{k_o + \frac{k'}{[H^+]} + k_{EPT}K_A'K_A[B^-] + \frac{k_1k_2K_A[B^-]}{k_2[Os^{III}] + k_{-1}[HB]}\right\}[Os^{III}] \qquad (32)$$

In the limit, $k_2[Os^{3+}] << k_{-1}[HB]$, k_a (k_o + $k'/[H^+]$), k_b ($K_AK_A'k_{EPT}$), and k_1/k_{-1} can be estimated from the difference in pK_a values for cysteine and the added base (eq 33). k_2 for CysSH is also independently known. Based on this analysis, a plot of k_{obs} vs (a + b[B] + c[B^-]/[HB] gives K_A and $k_{EPT}K_A'$ (eq 34).

$$\frac{-d[Os^{III}]}{dt}\frac{1}{[CysSH]_T} = \left\{k_o + \frac{k'}{[H^+]} + k_{EPT}K_A'K_A[B^-] + \frac{k_1k_2K_A[B^-]}{k_{-1}[HB]}\right\}[Os^{III}] \qquad (33)$$

$$k_{obs} = k_a + k_b[B^-] + \frac{k_1k_2K_A[B^-]}{k_{-1}[HB]} \qquad (34)$$

With $k_2[Os^{3+}] >> k_{-1}[HB]$, the differential equation is of the form $-dx/dt$ = ax + b with a varying with [B^-]. This analysis gives k_1 (Eq. 35).

$$-\frac{d[Os^{III}]}{dt}\frac{1}{[CysSH]_T}=\left\{k_o+\frac{k'}{[H^+]}+K_AK_A'k_{EPT}[B^-]\right\}[Os^{III}]+k_1K_A[B^-] \quad (35)$$

4.7 Isolating EPT and PT-ET using Limiting Conditions of the Rate Law

4.7.1 Pre-association between [CysSH] and [B^-]; Determination of K_A and $k_{EPT}K_A'$: The absolute concentration, base to acid ratio, was held constant in all pH studies, while the actual concentration of total buffer in solution was varied from 10-500 mM. Figure 11 below illustrates the increase in catalytic current in the presence of increasing total concentration of phosphate buffer at neutral pH.

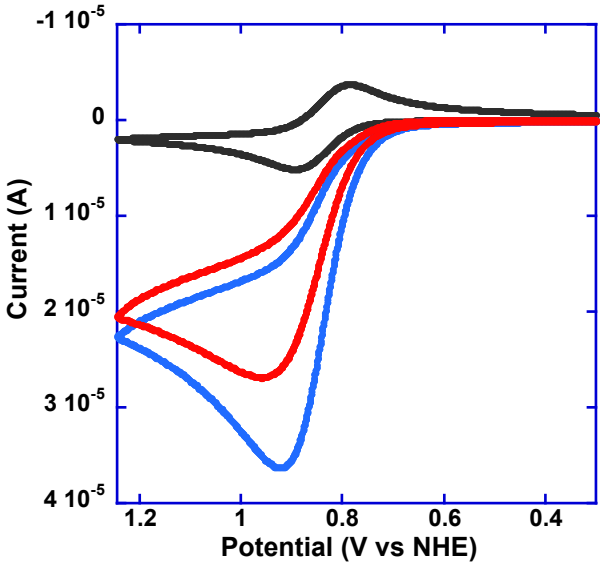

Figure 11. Cyclic voltammograms on an ITO working electrode (300 mV/s) illustrating the dependence of catalytic current on [$H_2PO_4^-$/HPO_4^{2-}] (pH 7.2, I = 0.8 M NaCl) T = 23 ± 2 °C. $Os(bpy)_3^{2+}$ (20 μM, Black), $Os(bpy)_3^{2+}$ (20 μM) + *L*-Cys (100 μM) in 300 (blue) and 50 mM (red) [$H_2PO_4^-$/HPO_4^{2-}].

The oxidation mechanism of cysteine occurs through the formation of the hydrogen bonded association complex in Scheme 2 (K_A). Cysteine demonstrates an increase in the oxidative current as a function of [$H_2PO_4^-$/HPO_4^{2-}] at neutral pH. Limiting currents are observed at concentrations of [HPO_4^{2-}] exceeding 80 mM (Figure 12). Saturation kinetics are consistent with the formation of a hydrogen bonded adduct between cysteine and [HPO_4^{2-}] in

solution followed by rate determining MS-EPT or PT-ET. The association constant for complex formation between cysteine and HPO_4^{2-} can be isolated through double reciprocal plots of k_{obs}^{-1} vs $[HPO_4^{2-}]^{-1}$ (Fig. 12B). The association constant for HPO_4^{2-} is 50.0±10 M^{-1} and can be obtained directly from the slope of the line, where slope = $(K_AK_A'k_{EPT})^{-1}$ = 2.37×10^{-9} and $K_AK_A'k_{EPT}$ = 4.21×10^{8}; y-intercept = $(K_A'k_{EPT})^{-1}$ = 1.005×10^{-7}, $K_A'k_{EPT}$ = 1.0×10^{7} y-intercept/slope = $K_A \sim 50$ M^{-1}. This non-zero intercept and slope are consistent with Scheme 2 and the rate law in eq. 17-18.

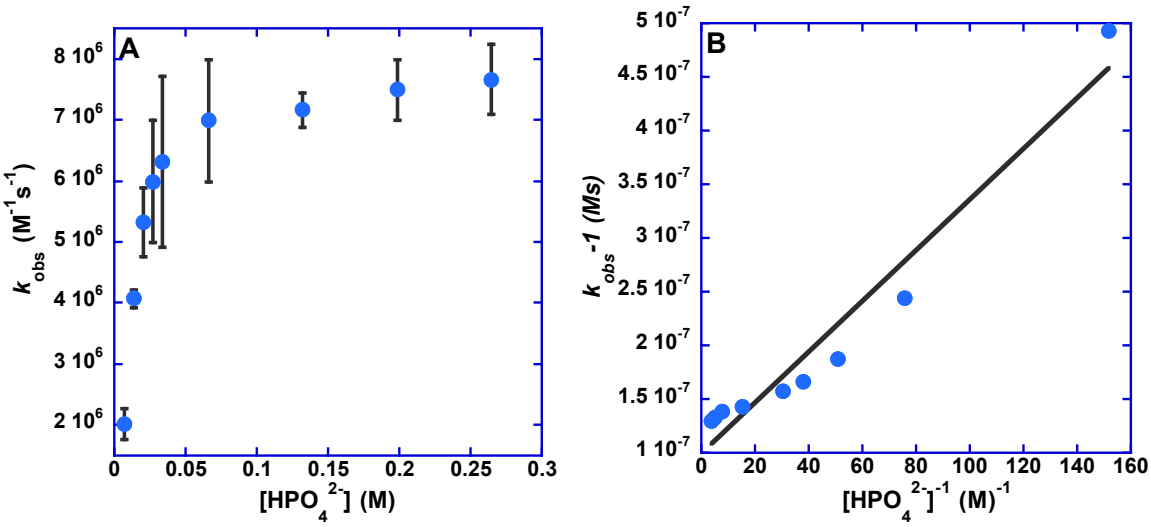

Figure 12: (**A**) Plot of k_{obs} ($M^{-1}s^{-1}$) vs $[HPO_4^{2-}]$ in a $[H_2PO_4^{-}/HPO_4^{2-}]$ buffer at pH 7.0 in 0.8M NaCl at 23±2°C, for the oxidation of *L*-Cys (100 μM) by $Os(bpy)_3^{3+}$ (20 μM). **B**) As in (**A**) except, plot of k_{obs}^{-1} vs $[HPO_4^{2-}]^{-1}$. Slope = $(K_AK_A'k_{EPT})^{-1}$ = 2.37×10^{-9} intercept = $(K_A'k_{EPT})^{-1}$ = 1.01×10^{-7}, K_A = 50±10 M^{-1}.

4.7.2 Pre-Association between [CysSH---HPO^{2-}] and [$M(bpy)_3^{3+}$]; Determination of K_A' The MS-EPT pathway can be isolated independently by increasing the concentration of acid and decreasing the concentration of base in the limit of k_{-1}>>k_2. In this limit, the equilibrium of PT-ET is unfavorable and the anion formation does not occur; reactivity is forced down the MS-EPT pathway. In the MS-EPT pathway in Scheme 2, the cysteine complex undergoes association with the $Os(bpy)_3^{3+}$ (K_A') and then rapidly reacts to transfer a proton to HPO_4^{2-} and an electron to the $Os(bpy)_3^{3+}$ (k_{EPT}). The independent rate constants can be resolved from

one another under saturation conditions with respect to phosphate and an increase in cysteine concentration. Under conditions where the $Os(bpy)_3^{3+}$ is saturated with complex ([CysSH---B^-]=$[CysSH]_T$), K_A' and k_{EPT} are isolated from double reciprocal plots of k_{obs}^{-1} vs $[complex]^{-1}$, Figure 13 and the y-intercept from the linearization study (Figure 14). The values isolated were K_A'=29.9 M^{-1} and k_{EPT}=2.4x10^4 s^{-1}. The value for k_{EPT} is determined directly from the intercept in Figure 12, and K_A' is determined from the intercept in Figure 14.

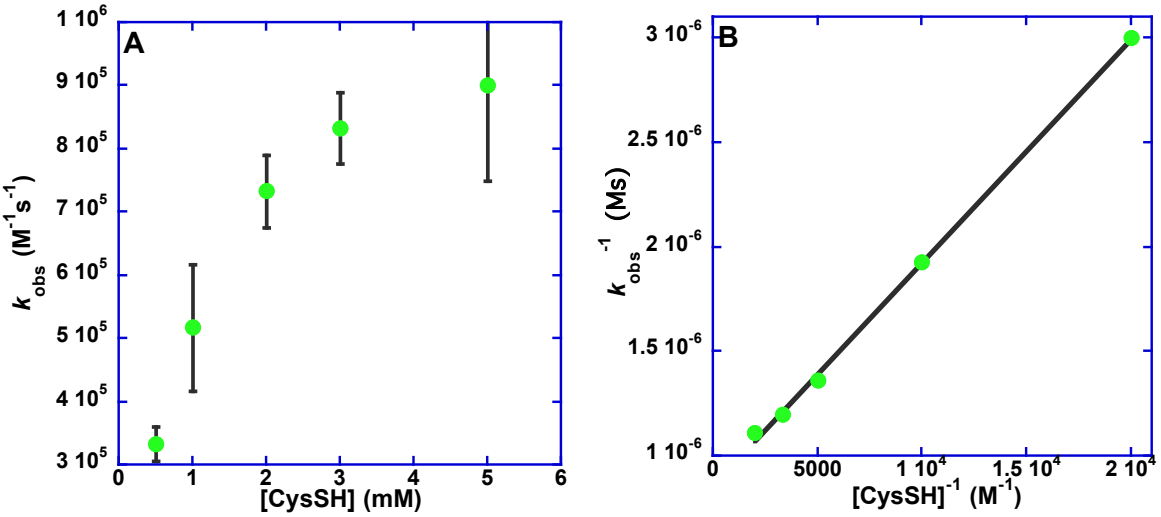

Figure 13. Oxidation of *L*-Cys (100 μM) by $Os(bpy)_3^{3+}$ (20 μM) at pH 6.2, exhibiting saturation kinetics at $[CysSH]_T > 4\times10^{-3}$ M; 10:1, Acid:Base, $[HPO_4^{2-}/H_2PO_4^-]$ = 0.5M I = 0.8M NaCl at 23±2°C. (**A**) Plot of k_{obs} vs $[CysSH]_T$ (**B**) k_{obs}^{-1} vs $[CysSH]^{-1}$. Complex is [CysSH--B^-], where under conditions saturated in [B^-], $[CysSH]_T$ = [CysSH--B^-].

4.7.3 Rapid Pre-equilibrium Formation of $CysS^-$ Followed by Rate Limiting Oxidation or Rate Limiting Proton Transfer; Determination of k_1, k_{-1} and k_2: According to Scheme 2, there are two base assisted pathways of reactivity available for cysteine, the concerted MS-EPT pathway and the stepwise PT-ET pathway. In the stepwise PT-ET pathway, cysteine undergoes a rate limiting deprotonation to yield a deprotonated anion. The anion reacts quickly with the oxidant once deprotonation has occurred. This pathway can be isolated independently at high concentrations of base and low concentrations of acid. In this limit, k_2

>> k_{-1} due to the low concentration of acid in solution. In this limit, the value for k_1 is $1.7x10^3 s^{-1}$ for proton transfer from cysteine to HPO_4^{2-} in a saturated system.

With $H_2PO_4^-/HPO_4^{2-}$ as the buffer, the PT-ET pathway becomes dominant at a buffer ratio of 10:1 [$H_2PO_4^-$:HPO_4^{2-}]. Under the electrochemical conditions, we did not detect a pH dependent pathway. Under these conditions, it follows from eq 31 that $k_{obs} = K_A k_1$. $k_{obs}=K_A k_1 = 8.5\times10^4\ M^{-1}s^{-1}$. This value is in good agreement with the product of K from the known pK_a values for *N*-acetyl-cysteine and phosphate ($K = 10^{-pK_a(CysSH)/}10^{-pK_a(H_2PO_4^-)} = 0.1$) and $k_2 = k_{CysS^-} = 2.0x10^5 M^{-1}s^{-1}$, determined independently in the stopped flow study.

The rate law was investigated further through plots of k_{obs} vs $[H_2PO_4^-]^{-1}$ where the concentration of $[H_2PO_4^-]$ was varied, while the concentration of $[HPO_4^{2-}]$ was held constant (Figure 14). From the slope we are able to isolate the rate constant for k_{-1} where $k_{-1} = 1.3x10^7\ M^{-1}s^{-1}$. The intercept of Figure 14 (y-intercept = 5.26×10^5) reflects the acid independent MS-EPT pathway, $K_A' k_{EPT}$. These values are identical within experimental error to the product of the rate constants isolated from the double reciprocal plots in Figure 12 and 13 above ($K_A' k_{EPT} = 7.2\times10^5$).

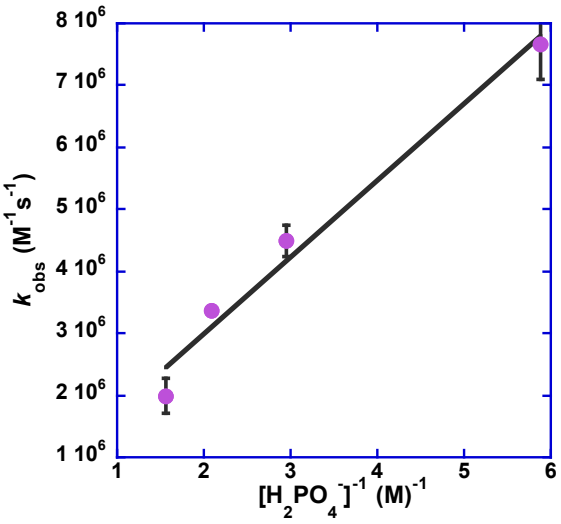

Figure 14. The plot of k_{obs} vs $[H_2PO_4^-]^{-1}$ in 0.8M NaCl at 23±2°C. The slope of the line results in the acid dependent deprotonation pathway and the intercept relates to the MS-EPT pathway, which is independent of the acid form of the buffer.

At higher concentrations of CysSH, > 0.001M, saturation kinetics are observed allowing separation of $k_{EPT}K_A'$ and K_A. At high concentrations of both cysteine and $Os(bpy)_3^{2+}$, onset of a second region of saturation kinetics allows for the separation of k_{EPT} and K_A'. These rate constants are outlined in Table 6 below.

Table 6. Rate and equilibrium constants from DigiSim for cysteine in (100 μM) phosphate ($H_2PO_4^-/HPO_4^{2-}$) buffer with $Os(bpy)_3^{3+}$ (20 μM) as the oxidant with 0.8M NaCl at 23±2°C.

Base	**pK_a**	**K_A (M^{-1})**	**$K_{A'}$ (M^{-1})**	**k_{EPT} ($M^{-1}s^{-1}$)**	**k_1 (s^{-1})**	**k_{-1} (s^{-1})**	**k_2($M^{-1}s^{-1}$)**
HPO_4^{2-}	7.2	50	29.9	$2.4x10^4$	$1.7x10^3$	$1.3x10^7$	$2.0x10^5$

4.7.4 Electrochemical Kinetic Isotope Effects: The k_{H_2O}/k_{D_2O} kinetic isotope effect for k_{EPT} in Table 6 is 3.5 which is comparatively higher than deuterium kinetic isotope effects reported for simple electron transfer reactions illustrating the quantum nature of the concerted reaction. This value matches well with the k_{H_2O}/k_{D_2O} kinetic isotope effect measured in stopped-flow experiments, ~ 3.7. As discussed above, this is in excess of typical for solvent kinetic isotope effects for outer-sphere electron transfer reactions which fall in the range 1.0 - 2.8.[27] For the above the deuterium kinetic isotope effects values for K_A, and k_1 were

determined through the comparison of reaction rates of the deuterated and protonated solutions and are 1.3 and 1.2 respectively.

The mole fraction data below indicate a linear dependence on the mole fraction of D_2O, but also indicate a lower KIE for experiments at higher pHs where the oxidation of $CysS^-$ is expected to dominate, where at pH 5.5, 15:1, $[H_2PO_4^-:HPO_4^{2-}]$ acid to base, MS-EPT will dominate the observed kinetics.

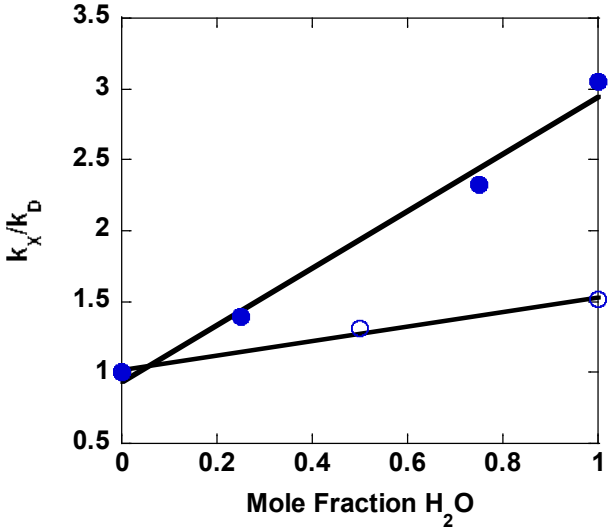

Figure 15: Mole fraction study at pH 5.5 (closed circles) and 8.0 (open circles). Under limiting conditions, EPT and PT-ET can be isolated independently. Under these solution conditions, examination of the mole fraction results in a linear dependence on the isotope effect vs the mole fraction of deuterium in solution. The isotope effects at pH 5.5 are higher than those at pH 8.0.

4.8 Concluding Remarks: Rate constants that were derived from numerical simulations of electrochemical data and measured directly from spectroscopic stopped-flow experiments were in good agreement over a range of pHs, and solution conditions, indicating both techniques are complementary in probing PCET. There are multiple competing pathways for cysteine oxidation: i) outer-sphere electron transfer followed by the rapid loss of a proton (ET-PT), ii) proton transfer followed by electron transfer (PT-ET) In this case, PT can either be to [B-] or simply H_2O via the pH, pK_a equilibrium of the thiol, iii) coupled electron-proton

transfer (EPT) with an added base as a proton acceptor. Depending on the conditions of these experiments all of these pathways may be competitive. Rate limiting conditions can also be used to isolate, or favor EPT or PT-ET pathways. There are important implications for these results in biological cysteine oxidation. As a result of the estimated high oxidation potential for $E°'(\mathrm{CysSH}^{\bullet+/0}) > 1.5$ V; mechanisms involving initial oxidation in the absence of a base is inhibited, where in the presence of a proton accepting base, such as HPO_4^{2-}, EPT is facilitated.

4.9 References:

(1) Aubert, C.; Vos, M. H.; Mathis, P.; Eker, A. P. M.; Brettel, B. **Intraprotein Radical Transfer During Photoactivation of DNA Photolyase**. *Nature* **2000**, *405*, 586-590.

(2) Lukacs, A.; Eker, A. P. M.; Byrdin, M.; Brettel, K.; Vos, M. H. **Electron Hopping through the 15 Å Triple Tryptophan Molecular Wire in DNA Photolyase Occurs within 30 ps**. *J. Am. Chem. Soc.* **2008**, *130***,** 14394-14395.

(3) Huynh, M.-H. V.; Meyer, T. J. **Proton Coupled Electron Transfer**. *Chem. Rev.* **2007**, *107*, 5004-5064.

(4) Meyer, T. J.; Huynh, M.-H. V.; Thorp, H. H. **The Possible Role of Proton-Coupled Electron Transfer (PCET) in Water Oxidation by Photosystem II**. *Angew. Chem. Int. Ed*. **2007**, *46*, 5284-5304.

(5) Stubbe, J.; van der Donk, W. A. **Protein Radicals in Enzyme Catalysis**. *Chem. Rev*. **1998**, *98*, 705-762.

(6) Reece, S.; Hodgkiss, J. M.; Stubbe, J.; Nocera, D. G. **Proton-Coupled Electron Transfer: The Mechanistic Underpinning for Radical Transport and Catalysis in Biology**. *Philos. Trans. R. Soc. B* **2006**, *361*, 1351-1364.

(7) Seyedsayamdost, M. R.; Yee, C. S.; Reece, S. Y.; Nocera, D. G.; Stubbe, J. **pH Rate Profiles of F_nY_{356}-R2s (n= 2, 3, 4) in *Escherichia coli* Ribonucleotide Reductase: Evidence that Y356 Is a Redox-Active Amino Acid along the Radical Propagation Pathway**. *J. Am. Chem. Soc.* **2006**, *128*, 1562-1568.

(8) Zouni, A. Z.; Witt, H.; Kern, J.; Fromme, P.; Krauss, N.; Saenger, W.; Orth, P. **Crystal Structure of Photosystem II from *Synechococcus elongatus* at 3.8 Å Resolution**. *Nature* **2001**, *409*, 739-743.

(9) Reece, S. Y.; Seyedsayamdost, M. R.; Stubbe, J.; Nocera, D. G. **Electron Transfer Reactions of Fluorotyrosyl Radicals.** *J. Am. Chem. Soc.* **2006**, *128*, 13654-13655.

(10) Persson, A. L.; Erikson, M.; Katterle, B.; Pötsch, S.; Sahlin, M.; Sjöberg, B. **A New Mechanism-based Radical Intermediate in a Mutant R1 Protein Affecting the Catalytically Essential Glu^{441} in Escherichia coli Ribonucleotide Reductase**. *J. Biol. Chem*. **1997**, *272*, 31533-31541.

(11) Ekberg, M.; Pötsch, S.; Sandin, E.; Thunnissen M.; Nordlund, P.; Sahlin, M.; Sjöberg, B. **Preserved Catalytic Activity in an Engineered Ribonucleotide Reductase R2 Protein with a Nonphysiological Radical Transfer Pathway**. *J. Biol. Chem*. **1998**, *273*, 21003-21008.

(12) Gagliardi, C. J.; Binstead, R. A.; Thorp, H. H.; Meyer, T. J. **Concerted Electron-Proton Transfer in the Oxidation of Tryptophan with Hydroxide as a Base**. *J. Am. Chem. Soc.* **2011**, *133*, 19594-19597.

(13) Sjödin, M.; Stenbjörn, S.; Åkermark, B.; Sun, L.; Hamarström, L. **Proton-Coupled Electron Transfer from Tyrosine-Ruthenium-tris-Bipyridine Complex: Comparison with Tyrosine$_Z$ Oxidation in Phtotsystem II**. *J. Am. Chem. Soc.* **2000**, *122*, 3932-3936.

(14) Zhang, M.-T.; Hammarström, L. **Proton-Coupled Electron Transfer from Tryptophan: A Concerted Mechanism with Water as a Proton Acceptor**. *J. Am. Chem. Soc.* **2011**, *133*, 8806-8809.

(15) Gagliardi, C. J.; Jurss, J. W.; Thorp, H. H.; Meyer, T. J. **Surface Activation of Electrocatalysis at Oxide Electrodes. Concerted Electron-Proton Transfer**. *Inorg. Chem.* **2011**, *50*, 2076–2078.

(16) Jurss, J. W.; Concepcion, J. C.; Norris, M, R.; Templeton, J. L.; Meyer, T. J. **Surface Catalysis of Water Oxidation by the Blue Ruthenium Dimer**. *Inorg. Chem.* **2010**, *49*, 3980-3982.

(17) Fecenko, C. J.; Meyer, T. J.; Thorp, H. H. **Tyrosine Oxidation through Parallel Rate-Limiting Proton Transfer and Multi-Site Electron-Proton Transfer**. *J. Am. Chem. Soc.* **2006**, *128*, 11020-1102116.

(18) Fecenko, C. J.; Thorp, H. H.; Meyer, T. J. **The Role of Free Energy Change in Coupled Electron Proton Transfer**. *J. Am. Chem. Soc.* **2007**, *129*, 15098-15099.

(19) Costentin, C.; Robert, M.; Savéant, J.-M. **Concerted Proton-coupled Electron Transfers in aquo/hydroxo/oxo Metal Complexes: Electrochemistry of $[Os^{II}(bpy)_2py(OH_2)]^{2+}$ in Water**. *Proc. Natl. Acad. Sci. USA*. **2009**, *106*, 11829-11836.

(20) Weinberg, D. R.; Gagliardi, C. J.; Hull, J. F.; Murphy, C. F.; Kent, C. A.; Westlake, B.; Paul, A.; Ess, D. H.; McCafferty, D. G.; Meyer, T. J. **Proton Coupled Electron Transfer**. *Chem. Rev.* **2012**, 112, 4016-4093.

(21) Hung, M.; Stanbury, D. M. **Catalytic and Direct Oxidation of Cysteine by Octacyanomolybdate(V)**. *Inorg. Chem.* **2005**, *44*, 3541-3550.

(22) Ison, A.; Odeh, I. N.; Margerum, D. W. **Kinetics and Mechanisms of Chlorine Dioxide and Chlorite Oxidations of Cysteine and Glutathione**. *Inorg. Chem*. **2006**, *45*, 8768-8775.

(23) Demadis, K. D.; Dattelbaum, D. M.; Kober, E. M.; Concepcion, J. J.; Paul, J. J. Meyer, T. J.; White, P. S. **Vibrational and Structural Mapping of $[Os(bpy)_3]^{3+/2+}$ and $[Os(phen)_3]^{3+/2+}$**. *Inorg. Chim. Acta* **2007**, *360*, 1143-1153.

(24) Pecci, L.; Montefoshi, G.; Musci, G.; Cavallini, D. **Novel Findings on the Copper Catalyzed Oxidation of Cysteine**. *Amino Acids* **1997**, *13*, 355-367.

(25) Willit, J. L.; Bowden, E. F. **Adsorption and Redox Thermodynamics of Strongly Adsorbed Cytochrome *c* on Oxide Electrodes**. *J. Phys. Chem.* **1990**, *94*, 8241-8245.

(26) Hoffman, M. Z.; Hayon, E. **One-Electron Reduction of the Disulfide Linkage in Aquious Solution. Formation, Protonation and Decay Kinetics of the RSSR Radical**. *J. Am. Chem. Soc*. **1972**, *94*, 7950-7957.

(27) Weaver, M. J.; Tyma, P. D.; Nettles, S. M. **Solvent Isotope Effects upon the Kinetics of some Simple Electrode Reactions**. *J. Electroanal. Chem*. **1980**, *114*, 53-72.

(28) Bridgart, G. J.; Fuller, M. W.; Wilson, I. R. **Metal-Ion Catalysis in Some Reactions of Hexacyanoferrate(III) Ions. Part I. Copper Catalysis in the Oxidation of Cysteine and Related Thiols.** *J. Chem. Soc. Dalton Trans.* **1973,** 1274-1280.

(29) Zhou, Y.; Yu, B.; Levon, K. **Potentiometric Sensor for Dipicolinic Acid**. *Biosensors and Bioelectronics* **2005**, *20*, 1851-1855.

(30) Rudolph, M.; Reddy, D. P.; Feldberg, S. W. **A Simulator for Cyclic Voltammetric Responses**. *Anal. Chem.* **1994**, *66*, 589A-600A.

(31) Bard, A. J.; Faulkner, L. R. **Electrochemical Methods: Fundamentals and Applications**; John Wiley and Sons, Inc., Hoboken, NJ **2004**.

(32) Kober, E. M.; Casper, J. V.; Sullivan, B. P.; Meyer, T. J. **Highly Luminescent Polypyridyl Complexes of Osmium(II)**. *J. Am. Chem. Soc.* **1980**, *102*, 7383-7385.

(33) Nekrassova, O.; Allen, G. D.; Lawrence, N. S.; Jiang, L.; Jones, G. I.; Compton, R. G. **The Oxidation of Cysteine by Aqueous Ferricyanide: A Kinetic Study.** *Chem. Phys. Phys. Chem.* **2004**, *6*, 1316-1320.

(34) Nekrassova, O.; Allen, G. D.; Lawrence, N. S.; Jiang, L.; Jones, T. G. J.; Compton, R. G. **The Oxidation of Cysteine by Aqueous Ferricyanide: A Kinetic Study using a Boron Doped Diamond Electrode Voltammetry**. *Electroanalysis* **2002**, *14,* 1464-1469.

Appendix 1:

Derivation of Full and Limiting Forms of the Rate Law for Base Assisted Proton Coupled Electron Transfer pathways.

Single electron-proton ($1H^+/1e^-$) transfer reactions can occur through several different mechanistic pathways with differences that can be kinetically observed through variation of reaction conditions, including acid and base ratios of a proton accepting base as well as variation in the driving force for the overall reaction, which in the case of proton transfer followed by electron transfer is dictated solely by the ΔpK_a between the initial and final protonation states, in the case with concerted electron proton transfer (EPT) the overall driving force of the reaction ($\Delta G°'$) is dictated by both the driving force for pure outer-sphere electron transfer (ΔG_{ET}) and the ΔpK_a between the initial and final protonation states, a quantum mechanical treatment of the differences between concerted electron proton transfer and pure outer-sphere electron transfer can be found in Chapter 1 of this work.

The derivation of the rate law for the base assisted PCET pathways is based upon the mechanistic scheme shown in Scheme 1. For the sake of clarity, the derivation is done using tyrosine (TyrOH) as a substrate but is also generally applicable to any analogous single electron-proton ($1H^+/1e^-$) transfer reaction, the same applies to the metal in the derivation, Os^{3+} acts as the oxidant, but any $1e^-$ oxidant can be used in its place, $[B^-]$ is used for a generic base.

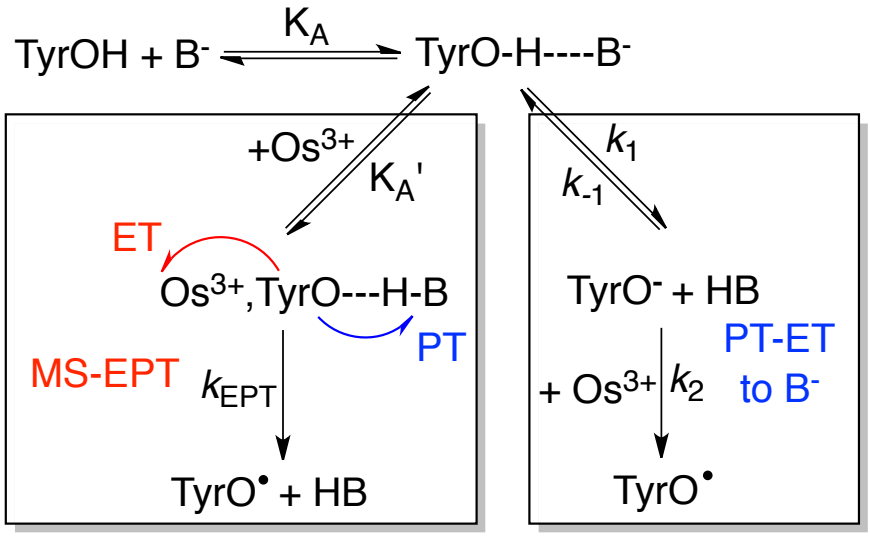

Scheme 1. Kinetic pathways that arise from base dependent kinetics, Multi-site electron proton transfer (MS-EPT) and sequential Proton transfer (to the base) followed by electron transfer.

Derivation of EPT, PT-ET Rate Law:

For The Concerted EPT Pathway:

$$\frac{-d[Os^{III}]}{dt} = k_{EPT}[Os^{III},TyrO\cdots HB] \quad (1)$$

$$[Os^{III},TyrO\cdots HB] = K_{A'}[TyrO\cdot H\cdots B^-][Os^{III}] \quad (2)$$

$$[TyrO\cdot H\cdots B^-] = K_A[TyrOH][B^-] \quad (3)$$

$$\frac{-d[Os^{III}]}{dt} = k_{EPT}K_A{}'K_A[TyrOH][B^-][Os^{III}] \quad (4)$$

For The Stepwise PT-ET Pathway:

$$\frac{-d[Os^{III}]}{dt} = k_2[Os^{III}][TyrO^-] \quad (5)$$

$$[TyrO^-]_{SS} = \frac{\dfrac{k_1[TyrO\cdot H\cdots B^-]}{k_2[Os^{III}][TyrO^-]+k_{-1}[TyrO^-][HB]}}{[TyrO^-]} = \frac{k_1[TyrO\cdot H\cdots B^-]}{k_2[Os^{III}]+k_{-1}[HB]} \quad (6)$$

Insertion of eq 6 into eq 5 gives eq 7

$$\frac{-d[Os^{III}]}{dt} = \frac{k_1 k_2 [Os^{III}][TyrO \cdot H \cdots B^-]}{k_2[Os^{III}] + k_{-1}[HB]} \tag{7}$$

$$K_A = \frac{[TyrO \cdot H \cdots B^-]}{[TyrOH][B^-]} \text{ where } [TyrO \cdot H \cdots B^-] = K_A[TyrOH][B^-] \text{ as in eq 3} \tag{8}$$

Insertion of eq 3 into eq 7 gives eq 9

$$\frac{-d[Os^{III}]}{dt} = \frac{k_1 k_2 K_A [Os^{III}][TyrOH][B^-]}{k_2[Os^{III}] + k_{-1}[HB]} \tag{9}$$

Combination of pathways and separation of terms:

$$\frac{-d[Os^{III}]}{dt} = k_{EPT} K_A' K_A [TyrOH][B^-][Os^{III}] + \frac{k_1 k_2 K_A [Os^{III}][TyrOH][B^-]}{k_2[Os^{III}] + k_{-1}[HB]} \tag{10}$$

$$\frac{-d[Os^{III}]}{dt} = K_A[TyrOH][B^-][Os^{III}]\left(k_{EPT} K_A' + \frac{k_1 k_2}{k_2[Os^{III}] + k_{-1}[HB]}\right) \tag{11}$$

The total concentration of tyrosine needs to be taken into consideration:

$$[TyrOH]_T = [TyrOH] + [TyrO \cdot H \cdots B^-] \tag{12}$$

$$K_A = \frac{[TyrO \cdot H \cdots B^-]}{[TyrOH][B^-]} \text{ such that } [TyrO \cdot H \cdots B^-] = K_A[TyrOH][B^-] \text{ as in 3 and 8} \tag{13}$$

Insert into eq 12 to get:

$$[TyrOH]_T = [TyrOH] + K_A[TyrOH][B^-] \tag{14}$$

$$[TyrOH]_T = [TyrOH] + (1 + K_A[B^-]) \tag{15}$$

Rearrangement gives:

$$[TyrOH] = \frac{[TyrOH]_T}{1 + K_A[B^-]} \tag{16}$$

Insert into eq 11 to get:

$$\frac{-d[Os^{III}]}{dt} = \left(\frac{K_A[TyrOH]_T[B^-]}{1 + K_A[B^-]}\right)[Os^{III}]\left(k_{EPT} K_A' + \frac{k_1 k_2}{k_2[Os^{III}] + k_{-1}[HB]}\right) \tag{17}$$

Non-Base Assisted Pathways: Additional kinetic pathways may contribute to the observed kinetics of a single electron-proton ($1H^+/1e^-$) transfer reaction: 1) ET-PT, pure outer-sphere electron transfer followed by deprotonation or 2) PT-ET, oxidation of the anion form of the substrate as a result of its acid base equilibrium (pK_a). The latter is a pH dependent portion of and therefore inversely proportional to $[H^+]$.

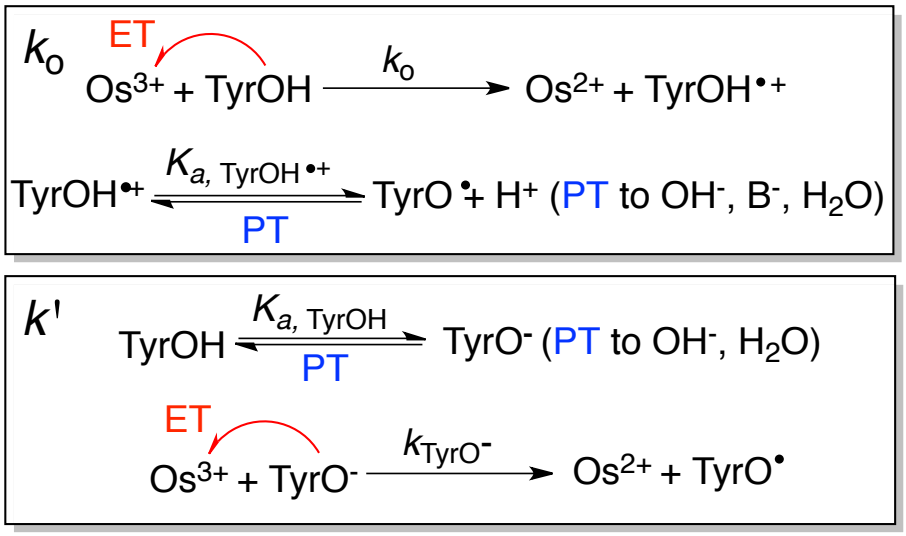

Scheme 2. Kinetic pathways that arise from non-base dependent kinetics, ET-PT, and sequential proton transfer (to solvent) followed by electron transfer $k_{TyrO^-} = k_2$ in Scheme 1, $k' = k_{TyrO^-}K_{a,TyrOH}$.

Inclusion of k_o (rate constant for outer-sphere electron transfer) and k' (rate constant for pH dependent, PT-ET) into the rate law gives eq 18. Although k' is essentially the rate constant for the anionic form of the substrate, it is given in terms of the added substrate and not concentration of the anion because [SubH] and not $[Sub^-]$ is the measured value when conducting the experiment:

$$\frac{-d[Os^{III}]}{dt} = k_o + \frac{k'}{[H^+]} + \left\{\left(\frac{K_A[Tyr]_T[B^-]}{1+K_A[B^-]}\right)\left(k_{EPT}K_A' + \frac{k_1k_2}{k_2[Os^{III}]+k_{-1}[HB]}\right)\right\}[Os^{III}] \qquad (18)$$

Removal of the tyrosine term gives:

$$\frac{-d[Os^{III}]}{dt} = k_o + \frac{k'}{[H^+]} + \left\{\left(\frac{K_A[B^-]}{1+K_A[B^-]}\right)\left(k_{EPT}K_A' + \frac{k_1k_2}{k_2[Os^{III}]+k_{-1}[HB]}\right)\right\}[Os^{III}][TyrOH]_T \quad (19)$$

Limiting forms of the Rate Law: The Following are the limiting forms of the reaction that can be isolated by tailoring solution conditions to favor one over the other, the following is a derivation based upon the above rate law of each of the rate limiting forms of this rate law to favor either the PT-ET or MS-EPT pathway.

$$\frac{-d[Os^{III}]}{dt}\frac{1}{[TyrOH]_T} = k_o + \frac{k'}{[H^+]} + \left\{\left(\frac{K_A[B^-]}{1+K_A[B^-]}\right)\left(k_{EPT}K_A' + \frac{k_1k_2}{k_2[Os^{III}]+k_{-1}[HB]}\right)\right\}[Os^{III}] \quad (20)$$

$$\frac{-d[Os^{III}]}{dt}\frac{1}{[TyrOH]_T} = \left\{k_o + \frac{k'}{[H^+]} + \left\{\left(\frac{K_A[B^-]}{1+K_A[B^-]}\right)(k_{EPT}K_A')\right\} + \left\{\left(\frac{K_A[B^-]}{1+K_A[B^-]}\right)\frac{k_1k_2}{k_2[Os^{III}]+k_{-1}[HB]}\right\}\right\}[Os^{III}] \quad (21)$$

Distribution of terms gives:

$$\frac{-d[Os^{III}]}{dt}\frac{1}{[TyrOH]_T} = k_o + \frac{k'}{[H^+]} + \left\{k_{EPT}K_A'K_A[B^-] + \frac{k_1k_2K_A[B^-]}{k_2[Os^{III}]+k_{-1}[HB]}\right\}[Os^{III}] \quad (22)$$

In the limit that $k_2[Os^{3+}] << k_{-1}[HB]$, which would be close to a 10:1 acid:base buffer ratio, where it is postulated that the MS-EPT pathways dominates

$$\frac{-d[Os^{III}]}{dt}\frac{1}{[TyrOH]_T} = \left\{k_o + \frac{k'}{[H^+]} + k_{EPT}K_A'K_A[B^-] + \frac{k_1k_2K_A[B^-]}{k_{-1}[HB]}\right\}[Os^{III}] \quad (23)$$

In this case the observed rate constant, k_{obs} would be given by

$$k_{obs} = k_a + k_b[B^-] + \frac{k_1k_2K_A[B^-]}{k_{-1}[HB]} \quad (24)$$

In the limit $k_2[Os^{3+}] >> k_{-1}[HB]$: Under these conditions, -dx/dt = ax +b with varying with $[B^-]$ from this plot we would get k_1K_A:

$$\frac{-d[Os^{III}]}{dt}\frac{1}{[TyrOH]_T} = \left\{k_o + \frac{k'}{[H^+]} + k_{EPT}K_A'K_A[B^-]\right\}[Os^{III}] + k_1K_A[B^-] \quad (25)$$

Derivation of Double Reciprocal Plot Function: In some instances, under high concentration base conditions, a saturation in observed rate constant occurs, this is either demonstrated in a plateau in k_{obs} values for mixing experiments or in the case with electrochemical experiments, is observed through the saturation in catalytic current, where with additional base, the rate of the reaction no longer increase. This is indicative of the formation and saturation of the substrate base adduct, which is postulated to be the kinetically active species in all base assisted PCET pathways, the formation constant is K_A in Scheme 1. The value of K_A can be found through a double reciprocal plot. The derivation for the double reciprocal plot from the full-derived rate law (eq 17) is shown below.

Beginning from eq 17 above, the derived rate law for Scheme 1:

$$\frac{-d[Os^{III}]}{dt} = \left(\frac{K_A[Tyr]_T[B^-]}{1+K_A[B^-]}\right)[Os^{III}]\left(k_{EPT}K_A' + \frac{k_1k_2}{k_2[Os^{III}]+k_{-1}[HB]}\right) \quad (26)$$

Negate the PT-ET portion of the above rate law and redistribute terms:

$$k_{obs} = \frac{-d[Os^{III}]}{dt} = \frac{k_{EPT}K_AK_A'[TyrOH]_T[B^-]}{1+K_A[B^-]} \quad (27)$$

$$\frac{1}{k_{obs}} = \frac{1+K_A[B^-]}{k_{EPT}K_AK_A'[TyrOH]_T[B^-]} \quad (28)$$

$$\frac{1}{k_{obs}} = \frac{1}{k_{EPT}K_AK_A'[TyrOH]_T}\frac{1}{[B^-]} + \frac{K_A[B^-]}{k_{EPT}K_AK_A'[TyrOH]_T[B^-]} \quad (29)$$

$$\frac{1}{k_{obs}} = \frac{1}{k_{EPT}K_AK_A'[TyrOH]_T}\frac{1}{[B^-]} + \frac{1}{k_{EPT}K_A'[TyrOH]_T} \quad (30)$$

Such that y=mx+b and slope^{-1} is equal to:

$$\frac{1}{m} = k_{EPT} K_A K_A' [TyrOH]_T \quad (31)$$

and int^{-1} is equal to:

$$\frac{1}{b} = k_{EPT} K_{A'} [TyrOH]_T \quad (32)$$

Simple algebra cancels terms to give K_A.

Overall these treatments are useful in approaching the kinetics of proton coupled electron transfer reactions, and their inclusion as an appendix into this work serves to act as a reference.

References:

Alberty R. A.; Hammes G. G. **Application of the Theory of Diffusion-controlled Reactions to Enzyme Kinetics**. *J. Phys. Chem.* **1958**, *62*, 154-159.

Albery, W. J.; Hillman, A. R. **Transport Kinetics on Modified Electrodes**. *J. Electroanal. Chem.* **1984**, *170*, 27-49.

Alleman, K. S.; Weber, K.; Creager, S. E. **Electrochemical Rectification at a Monolayer-Modified Electrode**. *J. Phys. Chem.* **1996**, *100*, 17050-17058.

Andrieux, C. P.; Saveant, J. M. In *Techniques of Chemistry: Molecular Design of Electrode Surfaces*; Murray, R. W., Wiley: New York, **1992**; Vol. 22 pp 207-270

Aubert, C.; Vos, M. H.; Mathis, P.; Eker, A. P. M.; Brettel, K. **Intraprotein Radical Transfer During Photoactivation of DNA Photolyase**. *Nature* **2000**, *405*, 586-590.

Barbara, P. F.; Meyer, T. J.; Ratner, M. A. **Contemporary Issues in Electron Transfer Research**. *J. Phys. Chem.* **1996**, *100*, 13148-13168.

Barber, J.; Ferreira, K.; Maghlaoui, K.; Iwata, S. **Structural Model of the Oxygen-Evolving Center of Photosystem II with Mechanistic Implications**. *Phys. Chem. Chem. Phys*. **2004**, *6*, 4737-4742.

Bard, A. J.; Faulkner, L. R. *Electrochemical Methods: Fundamentals and Applications*; John Wiley and Sons, Inc., Hoboken, NJ **2004.**

Binstead, R. A.; Meyer, T. J. **Hydrogen-Atom Transfer between Metal Complexes Ions in Solution**. *J. Am. Chem. Soc.* **1987**, *109*, 3287-3297.

Binstead, R. A.; Moyer, B. A.; Samuels, G. J.; Meyer, T. J. **Proton-Coupled Electron Transfer between $[Ru(bpy)_2(py)OH_2]^{2+}$ and $[Ru(bpy)_2(py)O]^{2+}$. A Solvent Isotope Effect (k_{H_2O}/k_{D_2O}) of 16.1**. *J. Am. Chem. Soc.* **1981**, *103*, 2897-2899.

Bonin, J.; Costentin, C.; Louault, C.; Robert, M.; Savéant, J.-M. **Water (in Water) as an Intrinsically Efficient Proton Acceptor in Concerted Proton Electron Transfer**. *J. Am. Chem. Soc*. **2011**, *133*, 6668-6674.

Bridgart, G. J.; Fuller, M. W.; Wilson, I. R. **Metal-Ion Catalysis in Some Reactions of Hexacyanoferrate(III) Ions. Part I. Copper Catalysis in the Oxidation of Cysteine and Related Thiols**. *J. Chem. Soc. Dalton Trans.* **1973**, 1274-1280.

Butler, J.; Koppenol, W. H. **Kinetics and Mechanism of the Reduction of Ferricytochrome *c* by the Superoxide Anion**. *J. Biol Chem.* **1982**, *257*, 10747-10750.

Byrdin, M.; Lukacs, A.; Thiagarajan, V.; Eker, A. P. M.; Brettel, K.; Vos, M. H. *J.* **Quantum Yield Measurements of Short-Lived Photoactivation Intermediates in DNA Photolyase: Toward a Detailed Understanding of the Triple Tryptophan Electron Transfer Chain**. *J. Phys. Chem. A* **2010**, *114*, 3207-3214.

Byrdin, M.; Villette, S.; Eker, A. P. M.; Brettel, K. **Observation of an Intermediate Tryphtophanyl Radical in W306F Mutant DNA Photolyase from *Escherichia coli* Supports Electron Hopping along the Triple Tryptophan Chain**. *Biochemistry* **2007**, *46*, 10072-10077.

Byrdin, M.; Villette, S.; Espagne, A.; Eker, A. P. M.; Brettel, K. **Polarized Transient Absorption To Resolve Electron Transfer between Tryptophans in DNA Photolyase**. *J. Phys. Chem. B* **2008**, *112*, 6866-6871.

Carra, C.; Iordanova, N.; Hammes-Schiffer, S. **Proton-Coupled Electron Transfer in a Model for Tyrosine Oxidation in Photosystem II**. *J. Am. Chem. Soc.* **2003**, *125*, 10429-10436.

C. F. Murphy. Ph.D dissertation, University of North Carolina, Chapel Hill, N.C., **2009**.

Chakraborty, A.; Pak Michael, V.; Hammes-Schiffer, S. **Development of Electron-Proton Density Functionals for Multicomponent Density Functional Theory**. *Phys. Rev. Lett.* **2008**, *101*, 153001.

Chen, P.; Meyer, T. J. **Medium Effects on Charge Transfer in Metal Complexes**. *Chem. Rev.* **1998**, *98*, 1439-1477.

Chen, Z.; Concepcion, J. J.; Jurss, J. W.; Meyer, T. J. **Single-Site, Catalytic Water Oxidation on Oxide Surfaces**. *J. Am. Chem. Soc.* **2009**, 131, 15580–15581.

Chen, Z.; Concepcion, J. J.; Hull, J. F.; Hoertz, P. G.; Meyer, T. J. **Catalytic Water Oxidation on Derivatized *nano*ITO**. *Dalton Trans.* **2010**, *30*, 6950-6952 .

Chen, Z.; Vannucci, A. K.; Concepcion, J. J.; Jurss, J. W.; Meyer, T. J. **Proton-Coupled Electron Transfer at Modified Electrodes by Multiple Pathways**. *Proc. Natl. Acad. Sci. USA.* **2011**, *108*, E1461-E1469.

Cheung, M. S.; Daizadeh, I.; Stuchebrukhov, A. A.; Heelis, P. F. **Pathways of Electron Transfer in *Escherichia Coli* DNA Photolyase: Trp^{306} to FADH**. *Biophysical Journal* **1999**, *76*, 1241-1249.

Concepcion, J. J.; Jurss, J. W.; Templeton, J. L.; Meyer, T. J. **Mediator-Assisted Water Oxidation by the Ruthenium ''Blue Dimer'' *cis,cis*-$[(bpy)_2(H_2O)RuORu(OH_2)(bpy)_2]^{4+}$**. *Proc. Natl. Acad. Sci. USA.* **2008**, *105*, 17632-17635.

Concepcion, J. J.; Jurss, J. W.; Hoertz, P. G.; Meyer, T. J. **Catalytic and Surface-Electrocatalytic Water Oxidation by Redox Mediator–Catalyst Assemblies**. *Angew. Chem. Int. Ed.* **2009**, *48*, 9473 –9476.

Costentin, C. **Electrochemical Approach to the Mechanistic Study of Proton-Coupled Electron Transfer**. *Chem. Rev*. **2008**, *108*, 2145-2179.

Costentin, C.; Louault, C.; Robert, M.; Savéant, J-M. **The Electrochemical Approach to Concerted Proton-Electron Transfers in the Oxidation of Phenols in Water**. *Proc. Natl. Acad. Sci. USA*. **2009**, *106*, 18143-18148.

Costentin, C.; Robert, M.; Savéant, J.-M. **Concerted Proton-Electron Transfer Reactions in Water. Are the Driving Force and Rate Constant Depending on pH When Water Acts as Proton Donor or Acceptor?**. *J. Am. Chem. Soc.* **2007**, *129*, 5870-5879.

Costentin, C.; Robert, M.; Savéant, J.-M. **Concerted Proton-Coupled Electron Transfers in aquo/hydroxo/oxo Metal Complexes: Electrochemistry of $[Os^{II}(bpy)_2py(OH_2)]^{2+}$ in Water**. *Proc. Natl. Acad. Sci. USA*. **2009**, *106*, 11829-11836.

Costentin, C.; Robert, M.; Savéant, J.-M. **Concerted Proton-Electron Transfers: Electrochemical and Related Approaches**. *Accts. Chem. Res*. **2010**, *43*, 1019-1029.

Cukier, R. I.; Nocera, D. G. **Proton-Coupled Electron Transfer**. *Annu. Rev. Phys. Chem.* **1998**, *49*, 337-369.

Demadis, K. D.; Dattelbaum, D. M.; Kober, E. M.; Concepcion, J. J.; Paul, J. J.; Meyer, T. J.; White, P. S. **Vibrational and Structural Mapping of $[Os(bpy)_3]^{3+/2+}$ and $[Os(phen)_3]^{3+/2+}$**. *Inorg. Chim. Acta* **2007**, *360*, 1143-1153.

DeVault, D. *Quantum Mechanical Tunneling in Biological Systems*; Cambridge University Press: Cambridge, **1984**. Copyright 1984 Cambridge University Press.

Dixon, W. T.; Murphy, D. **Determination of the Acidity Constants of some Phenol Radical Cations by Means of Electron Spin Resonance**. *J. Chem. Soc., Faraday. Trans. 2* **1976**, *72*, 1221-1230.

Ekberg, M.; Pötsch, S.; Sandin, E.; Thunnissen M.; Nordlund, P.; Sahlin, M.; Sjöberg, B. **Preserved Catalytic Activity in an Engineered Ribonucleotide Reductase R2 Protein with a Nonphysiological Radical Transfer Pathway**. *J. Biol. Chem*. **1998**, *273*, 21003-21008.

Eigen, M. **Proton Transfer, Acid-Base Catalysis and Enzymatic Hydrolysis**. *Angew. Chem. Int. Ed.* **1964**, *3*, 1-19.

Fecenko, C. J.; Meyer, T. J.; Thorp, H. H. **Electrocatalytic Oxidation of Tyrosine by Parallel Rate Limiting Proton Transfer and Multi-Site Electron-Proton Transfer**. *J. Am. Chem. Soc*. **2006**, *128*, 11020-11021.

Fecenko, C. J.; Thorp, H. H.; Meyer, T. J. **The Role of Free Energy Change in Coupled Electron-Proton Transfer**. *J. Am. Chem. Soc*. **2007**, *129*, 15098-15099.

Gagliardi, C. J.; Binstead, R. A.; Thorp, H. H.; Meyer, T. J. **Concerted Electron-Proton Transfer (EPT) in the Oxidation of Tryptophan with Hydroxide as a Base**. *J. Am. Chem. Soc*. **2011**, *133*, 19594-19597.

Gagliardi, C. J.; Jurss. J. W.; Thorp, H. H.; Meyer, T. J. **Surface Activation of Electrocatalysis at Oxide Electrodes. Concerted Electron-Proton Transfer**. *Inorg. Chem.* **2011**, *50*, 2076-2078.

Gagliardi, C. J.; Vannucci, A. K.; Concepcion J. J.; Chen, Z.; Meyer, T. J. **The Role of Proton Coupled Electron Transfer in Water Oxidation**. *Energy and Environ. Sci.* **2012***, 5*, 7704-7717.

Gagliardi, C. J.; Westlake, B. C.; Kent, C. A.; Paul, J. J.; Papanikolas, J. M.; Meyer, T. J. **Integrating Proton Coupled Electron Transfer (PCET) and Excited States**. *Coord. Chem. Rev*. **2010**, *254*, 2459-2471.

Georgievskii, Y.; Stuchebrukhov, A. A. **Concerted Electron and Proton Transfer: Transition from Nonadiabatic to Adiabatic Proton Tunneling**. *J. Chem. Phys.* **2000**, *113*, 10438-10450.

Gillaizeau-Gauthier, I.; Odobel, F.; Alebbi, M.; Argazzi, R.; Costa, E.; Bignozzi, C. A.; Qu, P.; Meyer, G. J. **Phosphonate-Based Bipyridine Dyes for Stable Photovoltaic Devices**. *Inorg. Chem.* **2001**, *40*, 6073-6079.

Glickman, M. H.; Klinman, J. P. **Nature of Rate-Limiting Steps in the Soybean Lipoxygenase-1 Reaction**. *Biochemistry* **1995**, *34*, 14077–14092.

Greenleaf, W. B.; Perry, J. P.; Hearn, A. S.; Cabelli, D. E.; Lepcok, J. R.; Stroupe, M. E.; Tainer, J. A.; Nick, H. S.; Silverman, D. N. **Role of Hydrogen Bonding in the Active Site of Human Manganese Superoxide Dismutase**. *Biochemistry* **2004**, *43*, 7038-7045.

Hammes, G. G. *Principles of Chemical Kinetics*; Academic Press: New York, **1978**; p 203.

Hames-Schiffer, S. **Hydrogen Tunneling and Protein Motion in Enzyme Reactions**. *Acc. Chem. Res.* **2006**, *39*, 93-100.

Hammes-Schiffer, S. **Proton Coupled Electron Transfer: Classification Scheme and Guide to Theoretical Methods**. *Energy and Environ. Sci.* **2012**, *5*, 7696-7703.

Hammes-Schiffer, S.; Hatcher, E.; Ishikita, H.; Skone, J. H.; Soudackov, A. V. **Theoretical Studies of Proton-Coupled Electron Transfer: Models and Concepts Relevant to Bioenergetics**. *Coord. Chem. Rev*. **2008**, *252*, 384-394.

Hammes-Schiffer, S.; Soudackov, A. V. **Proton Coupled Electron Transfer in Solutions, Proteins and Electrochemistry**. *J. Phys. Chem. B* **2008**, *112*, 14108-14123.

Hammes-Schiffer, S.; Stuchebrukhov, A. A. **Theory of Coupled Electron and Proton Transfer Reactions**. *Chem. Rev.* **2010**, *110*, 6939-6960.

Hatcher, E.; Soudackov, A. V.; Hammes-Schiffer S. **Proton-Coupled Electron Transfer in Soybean Lipoxygenase: Dynamical Behavior and Temperature Dependence of Kinetic Isotope Effects**. *J. Am. Chem. Soc.* **2007**, *129*, 187–196.

Hatcher, E.; Soudackov, A.; Hammes-Schiffer, S. **Proton-Coupled Electron Transfer in Soybean Lipoxygenase**. *J. Am. Chem. Soc.* **2004**, *126*, 5763-5775.

Herrero. C.; Lassalle-Kaiser. B.; Leibl. W.; Rutherford. A. W.; Aukauloo. A. **Artificial Systems Related to Light Driven Electron Transfer Processes in PSII**. *Coord Chem. Rev*. **2008**, *252*, 456-468.

Hoffman, M. Z.; Hayon, E. **One-Electron Reduction of the Disulfide Linkage in Aquious Solution. Formation, Protonation and Decay Kinetics of the RSSR Radical**. *J. Am. Chem. Soc*. **1972**, *94*, 7950-7957.

Hoganson, C. W.; Babcock, G. T.; **A Metalloradical Mechanism for the Generation of Oxygen from Water in Photosynthesis**. *Science* **1997**, *277*, 1953-1956.

Hornstein, B. J.; Dattelbaum, D. M.; Schoonover, J. R.; Meyer, T. J. **Reactivity of an Adsorbed Ru(VI)-Oxo Complex: Oxidation of Benzyl Alcohol.** *Inorg. Chem.* **2007**, *46*, 8139-8145.

Hung, M.; Stanbury, D. M. **Catalytic and Direct Oxidation of Cysteine by Octacyanomolybdate(V)**. *Inorg. Chem.* **2005**, *44*, 3541-3350.

Hush, N. S. **Adiabatic Theory of Outer Sphere Electron-Transfer Reactions in Solution**. *Trans. Faraday Soc*. **1961**, *57*, 557-580.

Hyunh, M.-V.; Meyer, T. J. **Proton Coupled Electron Transfer**. *Chem. Rev*. **2007**, *107*, 5004- 5064.

Iordanova, N.; Hammes-Schiffer, S. **Theoretical Investigation of Large Kinetic Isotope Effects for Proton-Coupled Electron Transfer in Ruthenium Polypyridyl Complexes**. *J. Am. Chem. Soc.* **2002**, *124*, 4848-4856.

Ishikita, H.; Soudackov, A. V.; Hammes-Schiffer, S. **Buffer-Assisted Proton-Coupled Electron Transfer in a Model Rhenium-Tyrosine Complex**. *J. Am. Chem. Soc*. **2007**, *129*, 11146-11152.

Ison, A.; Odeh, I. H.; Margerum, D. W. **Kinetics and Mechanisms of Chlorine Dioxide and Chlorite Oxidations of Cysteine and Glutathione**. *Inorg. Chem.* **2006**, *45*, 8768-8775.

Jovanovic, S. V.; Harriman, A.; Simic, M. **Electron-Transfer Reactions of Tryptophan and Tyrosine Derivatives**. *J. Phys. Chem.* **1986**, *90*, 1935-1939.

Jurss, J. W.; Concepcion, J. J.; Norris, M. R.; Templeton, J. L.; Meyer, T. J. **Surface Catalysis of Water Oxidation by the Blue Ruthenium Dimer**. *Inorg. Chem.* **2010**, *49*, 3980-3982.

Kaila, V. R. I.; Hummer, G. **Energetics of Direct and Water–Mediated Proton-Coupled Electron Transfer**. *J. Am. Chem. Soc*. **2011**, *133*, 19040-19043.

Knapp, M. J.; Rickert, K.; Klinman, J. P. **Temperature-Dependent Isotope Effects in Soybean Lipoxygenase-1: Correlating Hydrogen Tunneling with Protein Dynamics**. *J. Am. Chem. Soc.* **2002**, *124*, 3865-3874.

Kober, E. M.; Casper, J. V.; Sullivan, B. P.; Meyer, T. J. **Highly Luminescent Polypyridyl Complexes of Osmium(II).** *J. Am. Chem. Soc.* **1980,** *102*, 7383-7385.

Krishtalik, L. I. **Activation Energy of Photosynthetic Oxygen Evolution: An Attempt at Theoretical Analysis**. *Bioelectrochem. Bioenerg*. **1990**, *23*, 249-263.

Krishtalik, L. I. **Energetics of Multielectron Reactions. Photosynthetic Oxygen Evolution**. *Biochim. Biophys. Acta* **1986**, *849*, 162-171.

Krishtalik, L. I. **pH-Dependent Redox Potential: How to use it Correctly in the Activation Energy Analysis**. *Biochim. Biophys. Acta* **2003**, *1604*, 13-21.

Langenbacher, T.; Immeln, D.; Dick, B.; Kottke, T. **Microsecond Light-Induced Proton Transfer to Flavin in the Blue Light Sensor Plant Cryptochrome**. *J. Am. Chem. Soc.* **2009**, *131*, 14274-14280.

Lapid, H.; Agmon, N.; Petersen, M. K.; Voth, G. A. **A Bond-Order Analysis of the Mechanism for Hydrated Proton Mobility in Liquid Water**. *J. Chem. Phys.* **2005**, *122*, 14506-14511.

Lee, H. J.; Svahn, E.; Swanson, J. M. J.; Lepp, H.; Voth, G. A.; Brzezinski, P.; Gennis, R. B. **Intricate Role of Water in Proton Transport through Cytochrome *c* Oxidase.** *J. Am. Chem. Soc.* **2010**, *132*, 16225-16239.

Loll, B.; Kern, J.; Saenger, W.; Zouni, A.; Biesiadka, J. **Towards Complete Cofactor Arrangement in the 3.0 Å Resolution Structure of Photosystem II**. *Nature* **2005**, *438*, 1040-1044.

Lukacs, A.; Eker, A. P. M.; Byrdin, M.; Brettel, K.; Vos, M. H. **Electron Hopping through the 15 Å Triple Tryptophan Molecular Wire in DNA Photolyase Occurs within 30 ps.** *J. Am. Chem. Soc.* **2008**, *130*, 14394-14395.

Lukacs, A.; Eker, A. P. M.; Byrdin, M.; Villette, S.; Pan, J.; Brettel, K.; Vos, M. H. **Role of the Middle Residue in the Triple tryptophan Electron Transfer Chain of DNA Photolyase: Ultra Fast Spectroscopy of a Trp→Phe Mutant**. *J. Phys. Chem. B* **2006**, *110*, 15654-15658.

Malfoy, B.; Reynaud, J. A. **Electrochemical Investigations of Amino Acids at Solid Electrodes: Part II. Amino Acids Containing no Sulfur Atoms: Tryptophan, Tyrosine, Histidine and Derivatives**. *J. Electroanal. Chem.* **1980**, *114*, 213-223.

Mamedov, F.; Sayre, R. T.; Styring, S. **Involvement of Histidine 190 on the D1 Protein in Electron/Proton Transfer Reactions on the Donor Side of Photosystem II**. *Biochemistry* **1998**, *37*,14245–14256.

Mao, S. S.; Holler, T. P.; Yu, G. X.; Bollinger Jr., J. M.; Booker, S.; Johnston, M. I.; Stubbe, J. **A Model for the Role of Multiple Cysteine Residues Involved in Ribonucleotide Reduction: Amazing and Still Confusing**. *Biochemistry* **1992**, *31*, 9733-9743.

Marcus, R. A. **Chemical and Electrochemical Electron-Transfer Theory**. *Annu. Rev. Phys. Chem*. **1964**, *15* 155-196.

Marcus, R. A. **On the Theory of Oxidation-Reduction Reactions Involving Electron Transfer. V. Comparison and Properties of Electrochemical and Chemical Rate Constants**. *J. Phys. Chem.* **1963**, *67*, 853-857.

Markovitch, O.; Agmon, N. **Structure and Energetics of the Hydronium Hydration Shells**. *J. Phys. Chem. A* **2007**, *111*, 2253-2256.

Marx, D.; Tuckerman, M. E.; Hutter, J.; Parrinello, M. **The Nature of the Hydrated Proton in Water**. *Nature* **1999**, *397*, 601-604.

Mayer, J. M. **Proton-Coupled Electron Transfer: A Reaction Chemist's View.** *Annu. Rev. Phys. Chem.* **2004**, *55*, 363-390.

Merényi, G.; Lind, J.; Shen, X. **Electron Transfer from Indoles, Phenols and Sulfite (SO_3^{2-}) to Chlorine Dioxide ($ClO_2^{\bullet}$)**. *J. Phys. Chem.* **1988**, *92*, 134–137.

Meyer, T. J.; Meyer, G. J.; Pfennig, B. W.; Schoonover, J. R.; Timpson, C. J.; Wall, J. F.; Kobusch, C.; Chen, X. H.; Peek, B. M.; Wall, C. G.; Ou, W.; Erickson, B. W.; Bignozzi, C. A. **Molecular-Level Electron Transfer and Excited State Assemblies on Surfaces of Metal Oxides and Glass**. *Inorg. Chem*. **1994**, *33*, 3952-3964.

Meyer, T. J.; Huynh, M. H. V. **The Remarkable Reactivity of High Oxidation State Ruthenium and Osmium Polypyridyl Complexes**. *Inorg. Chem.,* **2003**, *42*, 8140-8160.

Meyer, T. J.; Huynh, M.-H. V.; Thorp, H. H. **The Possible Role of Proton-Coupled Electron Transfer (PCET) in Water Oxidation by Photosystem II**. *Angew. Chem. Int. Ed*. **2007**, *46*, 5284-5304.

Miller, A.; Padmakumar, K.; Sorkin, D. L.; Karapetian, A.; Vance, C. K. **Proton-Coupled Electron Transfer in Fe-superoxide Dismutase and Mn-superoxide Dismutase**. *J. Inorg. Biochem.* **2003**, *93*, 71-83.

Minnihan, E. C.; Seyedsayamdost, M. R.; Stubbe, J. **Use of 3-Aminotyrosine to Examine the Pathway Dependence of Radical Propagation in *Escherichia coli* Ribonucleotide Reductase**. *Biochemistry* **2009**, *48*, 12125-12132.

Mohammed, O. F.; Pines, D.; Dreyer, J.; Pines, E.; Nibbering, E. T. J. **Sequential Proton Transfer Through Water Bridges in Acid-Base Reactions**. *Science* **2005**, *310*, 83-86.

Moyer, B. A.; Meyer, T. J. **Oxobis(2,2′-bipyridine)pyridineruthenium(IV) Ion, $[(bpy)_2(py)Ru{=}O]^{2+}$**. *J. Am. Chem. Soc.* **1978**, *100*, 3601-3603.

Nakagawa, T.; Beasley, C. A.; Murray, R. W. **Efficient, Electro-Oxidation of Water near Its Reversible Potential by a Mesoporous IrO_x Nanoparticle Film**. *J Phys. Chem. C* **2009**, *113*, 12958-12961.

Nekrassova, O.; Allen, G. D.; Lawrence, N. S.; Jiang, L.; Jones, G. I.; Compton, R. G. **The Oxidation of Cysteine by Aqueous Ferricyanide: A Kinetic Study**. *Chem. Phys. Phys. Chem.* **2004**, *6*, 1316-1320.

Nekrassova, O.; Allen, G. D.; Lawrence, N. S.; Jiang, L.; Jones, T. G. J. Compton, R. G. **The Oxidation of Cysteine by Aqueous Ferricyanide: A Kinetic Study using a Boron Doped Diamond Electrode Voltammetry**. *Electroanalysis* **2002**, *14,* 1464-1469.

Nguyen, N. T.; Wrona, M. Z.; Dryhurst, G. **Electrochemical Oxidation of Tryptophan**. *J. Electroanal. Chem.* **1986**, *199*, 101-126.

Offenbacher, A. R.; Vassiliev, I. R.; Seyedsayamdost, M. R.; Stubbe, J.; Barry, B. A. **Redox Linked Structural Changes in Ribonucleotide Reductase**. *J. Am. Chem. Soc.* **2009**, *131*, 7496-7497.

Ogata, N. **Denaturation of Protein by Chlorine Dioxide: Oxidative Modification of Tryptophan and Tyrosine Residues**. *Biochemistry* **2007**, *46*, 4898-4911.

Park, S.-Y.; Lee, Y.-S.; Kwon, O.-H.; Jang, D.-J. **Transport of Water in Acid-Base Reactions of 7-hydroxyquinoline**. *Chem. Commun.* **2009**, 926-928.

Pecci, L.; Montefoshi, G.; Musci, G.; Cavallini, D. **Novel Findings on the Copper Catalyzed Oxidation of Cysteine**. *Amino Acids* **1997**, *13*, 355-367.

Persson, A. L.; Erikson, M.; Katterle, B.; Pötsch, S.; Sahlin, M.; Sjöberg, B. **A New Mechanism-based Radical Intermediate in a Mutant R1 Protein Affecting the Catalytically Essential Glu^{441} in Escherichia coli Ribonucleotide Reductase**. *J. Biol. Chem*. **1997**, *272*, 31533-31541.

Posener, M. L.; Adams, G. E.; Wardman, P.; Cundall, R. B. **Mechanism of Tryptophan Oxidation by some Inorganic Radical-Anions: A Pulse Radiolysis Study**. *J. Chem. Soc. Farad. Trans. 1* **1976**, 72, 2231-2239.

Prigogine, I.; Rice, S. A. *Adv. Chem. Phys.* **2000** *Vol 111;* Zundel, G. **Hydrogen Bonds with Large Proton Polarizability and Proton Transfer Processes in Electrochemistry and Biology**. Pp 1-218.

Rappaport, F.; Guergova-Kuras, M.; Nixon, P. J.; Diner, B. A.; Lavergne, J. **Kinetics and Pathways of Charge Recombination in Photosystem II**. *Biochemistry* **2002**, *41*, 8518-8527.

Reece, S. Y.; Hodgkiss, J. M.; Stubbe, J.; Nocera, D. G. **Proton-Coupled Electron Transfer: The Mechanistic Underpinning for Radical Transport and Catalysis in Biology.** *Philos. Trans. R. Soc. B* **2006**, *361*, 1351-1364.

Reece, S.; Hodgkiss, J. M.; Stubbe, J.; Nocera, D. G. **Proton-Coupled Electron Transfer: The Mechanistic Underpinning for Radical Transport and Catalysis in Biology**. *Philos. Trans. R. Soc. B* **2006**, *361*, 1351-1364.

Reece, S. Y.; Nocera, D. G. **Direct Tyrosine Oxidation Using the MLCT Excited States of Rhenium, Polypyridyl Complexes**. *J. Am. Chem. Soc.* **2005**, *127*, 9448-9458.

Reece, S. Y.; Nocera, D. G. **Proton-Coupled Electron Transfer in Biology: Results from Synergistic Studies in Natural and Model Systems**. *Annu. Rev. Biochem*. **2009**, *78*, 673-699.

Reece, S. Y.; Seyedsayamdost, M. R.; Stubbe, J.; Nocera, D. G. **Direct Observation of a Transient Tyrosine Radical Competent for Initating Turnover in a Photochemical Ribonucleoride Reductase**. *J. Am. Chem. Soc.* **2007**, *129*, 13828-13830.

Reece, S. Y.; Seyedsayamdost, M. R.; Stubbe, J.; Nocera, D. G. **Electron Transfer Reactions of Fluorotyrosyl Radicals**. *J. Am. Chem. Soc.* **2006**, *128*, 13654-13655.

Rickert, K. W.; Klinman, J. P. **Nature of Hydrogen Transfer in Soybean Lipoxygenase 1: Separation of Primary and Secondary Isotope Effects**. *Biochemistry* **1999**, *38*, 12218–12228.

Roffey, R. A.; Kramer, D. M.; Govindjee; Sayre, R. T. **Lumenal Side Histidine Mutations in the D1 Protein of Photosystem II Affect Donor Side Electron Transfer in *Chlamydornonas reinhardtii***. *Biochim. Biophys. Acta Bioenerg*. **1994**, *1185*, 257–270.

Rudolph, M.; Reddy, D. P.; Feldberg, S. W. **A Simulator for Cyclic Votammetric Responces**. *Anal. Chem*. **1994**, *66*, 598A-600A.

Sancar, A.; **Structure and Function of DNA Photolyase and Cryptochrome Blue-Light Photoreceptors**. *Chem. Rev.* **2003**, *103*, 2203-2237.

Savige, W. E. **Isolation and Identification of Some Photo-oxidation Products of Tryptophan.** *Aust. J. Chem.* **1971**, *24*, 1285–1293.

Savige, W. E. **New Oxidation Products of Tryptophan**. *Aust. J. Chem.* **1975**, *28*, 2275-2287.

Seyedsayamdost, M. R.; Yee, C. S.; Reece, S. Y.; Nocera, D. G.; Stubbe, J. **pH Rate Profiles of F_nY_{356}-R2s (n = 2, 3, 4) in *Escherichia coli* Ribonucleotide Reductase: Evidence that Y356 Is a Redox-Active Amino Acid along the Radical Propagation Pathway**. *J. Am. Chem. Soc.* **2006**, *128*, 1562-1568.

Shih, C.; Museth, A. K.; Abrahamsson, M.; Blnco-Rodriguez, A. M.; Di, Bilio, A. J.; Sudhamsu, J.; Crane, B. R.; Ronayne, K. L.; Towrie, M.; Vlček Jr. A.; Richards, J. H.; Winkler, J. R.; Gray, H. B. **Tryptophan-Accelerated Electron Flow Through Proteins**. *Science* **2008**, *320*, 1760-1762.

Sjödin, M.; Irebo, T.; Utas, J. E.; Lind, J.; Merényi, G.; Åkermark, B.; Hammarström, L. **Kinetic Effects of Hydrogen Bonds on Proton-Coupled Electron Transfer from Phenols**. *J. Am. Chem. Soc.* **2006**. *128*, 13076-13083.

Sjödin, M.; Stenbjörn, S.; Åkermark, B.; Sun, L.; Hamarström, L. **Proton-Coupled Electron Transfer from Tyrosine in a Tyrosine−Ruthenium−tris-Bipyridine Complex: Comparison with $Tyrosine_z$ Oxidation in Photosystem II**. *J. Am. Chem. Soc.* **2000**, *122*, 3932-3936.

Sjödin, M.; Styring, S.; Wolpher, H.; Xu, Y.; Sun, L.; Hammarström, L. **Switching the Redox Mechanism: Models for Proton-Coupled Electron Transfer from Tyrosine and Tryptophan**. *J. Am. Chem. Soc*. **2005**, *127*, 3855-3863.

Solar, S.; Getoff, N.; Surdhar, P. S.; Armstrong, D. A.; Singh, A. **Oxidation of Tryptophan and N-Methylindole by $N_3^{\bullet}$, $Br_2^{\bullet-}$ and $(SCN)_2^{\bullet-}$ Radicals in Light- and Heavy- Water Solutions: A Pulse Radiolysis Study**. *J. Phys. Chem.* **1991**, *95*, 3639-3643.

Song, N.; Stanbury, D. M.; **Proton-Coupled Electron Transfer Oxidation of Phenols by Hexachloroiridate(V)**. *Inorg. Chem*. **2008**, *47*, 11458-11469.

Stewart, D. J.; Napolitano, M. J.; Bakhmutova-Albert, E. V.; Margerum, D. W. **Kinetics and Mechanisms of Chlorine Dioxide Oxidation of Tryptophan**. *Inorg. Chem*. **2008**, *47*, 1639-1647.

Stubbe, J.; Nocera, D. G.; Yee, C. S.; Chang, M. C. Y. **Radical Initiation in the Class I Ribonucleotide Reductase: Long-Range Proton-Coupled Electron Transfer**. *Chem. Rev*. **2003**, *103*, 2167-2201.

Stubbe, J.; van der Donk, W. A. **Protein Radicals in Enzyme Catalysis**. *Chem. Rev*. **1998**, *98*, 705-762.

Svensson, B.; Etchebest, C.; Tuffery, P.; van Kan, P.; Smith, J.; Styring, S. **A Model for the Photosystem II Reaction Center Core Including the Structure of the Primary Donor P_{680}**. *Biochemistry* **1996**, *35*, 14486–14502.

Tommos, C.; Babcock, G. T. **Oxygen Production in Nature: A Light-Driven Metalloradical Enzyme Process**. *Accts. Chem. Res.* **1998**, *31*, 18-25.

Tommos, C.; Hoganson, C. W.; Di Valentin, M.; Lydakis-Simantiris, N.; Dorlet, P.; Westphal, K.; Chu, H.-A.; McCracken, J.; Babcock,G. T. **Manganese and Tyrosyl Radical Function in Photosynthetic Oxygen Evolution**. *Curr. Opin. Chem. Biol.* **1998**, *2*, 244-252.

Trammell, S. A.; Meyer, T. J. **Diffusional Mediation of Surface Electron Transfer on TiO_2**. *J. Phys. Chem. B* **1999**, *103*, 104-107.

Vuilleumier, R.; Borgis, D. **Transport and Spectroscopy of the Hydrated Proton: A Molecular Dynamics Study**. *J. Chem. Phys.* **1999**, *111*, 4251-4266.

Weaver, M. J.; Tyma, P. D.; Nettles, S. M. **Solvent Isotope Effects upon the Kinetics of some Simple Electrode Reactions**. *J. Electroanal. Chem*. **1980**, *114*, 53-72.

Weinberg D. W.; Gagliardi, C. J.; Hull, J. F.; Murphy, C. F.; Kent, C. A.; Westlake, B.; Paul, A.; Ess, D. H.; McCafferty, D. G.; Meyer, T. J. **Proton-Coupled Electron Transfer**. *Chem. Rev.* **2012**, *112*, 4016-4093.

Westphal, K. L.; Lydakis-Simantiris, N.; Cukier, R. I.; Babcock, G. T. **Effects of Sr^{2+}-Substitution on the Reduction Rates of $Y_z^{\bullet}$ in PSII Membranes-Evidence for Concerted Hydrogen Atom Transfer in Oxygen Evolution**. *Biochemistry* **2000**, *39*, 16220-16229.

Westphal, K. L.; Tommos, C.; Cukier, R. I.; Babcock, G. T. **Concerted Hydrogen-Atom Abstraction in Photosynthetic Water Oxidation**. *Curr. Opin. Plant Biol.* **2000**, *3*, 236-242.

Willit, J. L.; Bowden, E. F. **Adsorption and Redox Thermodynamics of Strongly Adsorbed Cytochrome *c* on Oxide Electrodes**. *J. Phys. Chem.* **1990**, *94*, 8241-8245.

Xu, J.; Voth, G. A. **Redox-coupled Proton Pumping in Cytochrome *c* Oxidase: Further Insights from Computer Simulation**. *Biochim. Biophys. Acta Bioenerg.* **2008**, *1777*, 196-201.

Young, R. C.; Keene, F. R.; Meyer, T. J. **Measurement of Rates of Electron Transfer Between $Ru(bpy)_3^{3+}$ and $Fe(phen)_3^{2+}$ and Between $Ru(phen)_3^{3+}$ and $Ru(bpy)_3^{2+}$ by Differential Excitation Flash Photolysis**. *J. Am. Chem. Soc.* **1977**, *99*, 2468-2473.

Zhang, M.-T.; Hammarström, L. **Proton Coupled Electron Transfer from Tryptophan: A Concerted Mechanism with Water as Proton Acceptor**. *J. Am. Chem. Soc*. **2011**, *133*, 8806-8809.

Zhou, Y.; Yu, B.; Levon, K. **Potentiometric Sensor for Dipicolinic Acid**. *Biosensors and Bioelectronics.* **2005**, *20,* 1851-1855.

Zouni, A. Z.; Witt, H.; Kern, J.; Fromme, P.; Krauss, N.; Saenger, W.; Orth, P. **Crystal Structure of Photosystem II from *Synechococcus elongatus* at 3.8 Å Resolution**. *Nature* **2001**, *409*, 739-743.